

**“SYNTHESIS AND SPECTRAL STUDIES OF THE
LANTHANIDE COMPLEXES
WITH PYRIDINE AND SOME AMINO ACIDS:
KINETIC AND THERMODYNAMIC APPROACH”**

Thesis

Submitted to

NAGALAND UNIVERSITY

In partial fulfilment of requirements for the Degree

Of

DOCTOR OF PHILOSOPHY IN CHEMISTRY



By

JULIANA SANCHU

Ph.D. Registration No. 788/2017

DEPARTMENT OF CHEMISTRY

SCHOOL OF SCIENCES

NAGALAND UNIVERSITY

LUMAMI-798627

NAGALAND, INDIA

2022

**“Every accomplishment begins with the
decision to try.”**

- Anonymous

Specially dedicated to

My Mom, Brothers and Husband.



NAGALAND UNIVERSITY

(A Central University Estd. By the Act of Parliament No. 35 of 1989)

Headquarters: Lumami – 798627, Nagaland, India

Department of Chemistry

DECLARATION

I, **Mrs. Juliana Sanchu** bearing Ph.D. Registration No. **788/2017** with effect from **30th August 2016**, hereby declare that the subject matter of my Ph.D. thesis entitled “**Synthesis and Spectral Studies of the Lanthanide Complexes with Pyridine and Some Amino Acids: Kinetic and Thermodynamic approach**” is the record of original work done by me and the contents of this thesis did not comprise of the basis for the award of any previous degree/ diploma to me or to anybody else in any other University/Institute to the best of my knowledge.

This Ph.D. thesis is submitted in compliance with the UGC Regulation 2016 dated May 05, 2016 (Minimum Standard and Procedure for Award of M. Phil. /Ph.D. Degree) to the Nagaland University for the degree of Doctor of Philosophy in Chemistry.

Juliana

(Juliana Sanchu)

Upalav
19/12/22

Head

Department of Chemistry
Nagaland University

विभागाध्यक्ष / Head

रसायन विज्ञान विभाग / Department of Chemistry

Nagaland University

Lumami-798627

M. Indira Devi
19/12/2022

(Prof. M. Indira Devi)

Supervisor
Professor

Dept. of Chemistry
Nagaland University
Lumami-798627

NAGALAND UNIVERSITY



(A Central University Estd. By the Act of Parliament No. 35 of 1989)

Headquarters: Lumami – 798627, Nagaland, India

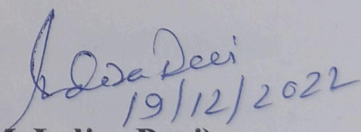
Prof. Mayanglambam Indira Devi
Professor, Department of Chemistry

e-mail:cam_indira@yahoo.co.in

CERTIFICATE

This is to certify that **Mrs. Juliana Sanchu**, a registered Research Scholar for Ph.D. degree in Chemistry under Nagaland University has carried out her research work under my guidance and supervision. Her thesis entitled “**Synthesis and Spectral Studies of the Lanthanide Complexes with Pyridine and Some Amino Acids: Kinetic and Thermodynamic approach**” embodies the original research work and has fulfilled all the requirements according to the rules/ regulations of Nagaland University.

Further, to the best of my knowledge, the research work has not been submitted to any University/ Institution for the award of any degree or diploma.


(Prof. M. Indira Devi)

Supervisor

ACKNOWLEDGEMENTS

On this much awaited moment of accomplishment, above all I wish to give thanks to Almighty God for all the blessings bestowed in my life and for always enlightening my path.

First and foremost, my heartiest gratitude to my supervisor Professor Mayanglambam Indira Devi for accepting me as her student and letting me experience this journey of research. I am extremely indebted to her for all her invaluable guidance, wisdom, encouragement, and constructive discussions we had throughout the research and without her I wouldn't have been able to complete this thesis.

I would like to express my sincere thanks to Prof. Upasana Bora Sinha, HoD for the Department of Chemistry for her support throughout my research. I am also thankful to Prof. M.S Rawat, Dean School of Sciences and Prof. Sangyu Yaden for their encouragement during assessment of my pre-submission seminar of this thesis. I am also grateful to other faculty members of Chemistry Department, Prof. Dipak Sinha, Dr. I. Tovishe Phucho, Dr. Prabakhar, Dr. Nurul and Dr. Dushila for sharing their valuable knowledge and advice towards my research.

A big thanks to my dear friends as well as labmates Zevivonii Thakro and Punazungba Imsong for all the help they had extended during my research work. Also, I am thankful to my lab mates Mhasiriekho Ziekhrii, Chubazungba Imsong and Sentienla Imsong for their help and support. I also thank my fellow scholars of the Department, for their support.

I sincerely appreciate Prameshwari Takhellambam, Niriezonuo, Mridhushmita Baruah, Takhe Yaba, Lobeno Mozhui, Keviphruonuo Kuotsu, Lydia and Gloria for their good company during the last few years of my research. My special thanks goes to my dearest friend Asikho Kiso who has dragged me into this whirl of research which actually turned out to be a beautiful and knowledgeable experience. She has always been there for me to cherish and motivate.

My deepest gratitude to Sir Bendangtemsü for coming forward to help me in hour of need. Also, my sincere appreciation to Miss Sunepjungla, Miss Temsuienla, Miss Lovitoli and Mr Pyobemo for their constant help.

I am privileged to thank UGC NON-NET fellowship for the financial support granted to me during my research work. I would also like to thank, NIT Chumukedima, Nagaland as well as Mizoram University, Aizawl for allowing me to do characterization.

Finally, I would like to thank my parents and brothers for their never-ending love, support, encouragement and for believing in me. Last yet most important, I want to thank my beloved husband Vilhouzhalie Sopfunuo for always being there for me, patiently dealing with my frustrations and mood-swings and for sending me positive energy throughout this entire journey of my research. I really do appreciate it.

-Juliana Sanchu

NAGALAND UNIVERSITY



(A Central University Estd. By the Act of Parliament No. 35 of 1989)

Headquarters: Lumami – 798627, Nagaland, India

Prof. Mayanglambam Indira Devi
Professor, Department of Chemistry

e-mail: cam_indira@yahoo.co.in

CERTIFICATE

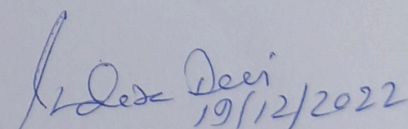
This is to certify that **Mrs. Juliana Sanchu**, a registered Research Scholar for Ph.D. degree in Chemistry under Nagaland University, bearing Ph.D. Registration No. **788/2017**, has satisfactorily completed all the courses offered in the Pre-Ph.D Course Work Programme in the Department of Chemistry, Nagaland University, Hqrs. Lumami.

The course includes:

CHEM-601 Research Methodology

CHEM-602 (D) Advance in Chemistry

CHEM-603 Literature Review, Report Writing and Presentation.


(Prof. M. Indira Devi)

Supervisor



Sl. No. : 16- 59076

NAGALAND UNIVERSITY

STATEMENT OF MARKS Ph. D COURSE WORK EXAMINATION, 2017

DEPARTMENT OF CHEMISTRY

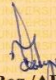
The following are the marks secured by Juliana Sanchu
Roll No. 03/16 of Ph.D Course Work Examination held in 2017

Subject(s)/Paper(s)	Max. Marks	Minimum Qualifying Marks	Marks Secured
Paper No. Chem-601 Research Methodology	100	35	87
Paper No. Chem-602 (D) Advance in Chemistry	100	35	79
Paper No. Chem-603 Literature Review, Report Writing and Presentation	100	35	68
Total Aggregate Marks			234
Average Pass Mark – 55 %			

Result	Division	Percentage
Passed	I Division	78 %

Marks compared by 

H.Q. LUMAMI



COE/Dy. Reg./AR (Exams)

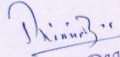
NAGALAND UNIVERSITY

HEAD QUARTERS : LUMAMI

Ph. D COURSE WORK EXAMINATION

This is to certify that Mr/Ms. Juliana Sanchu
of Nagaland University bearing Roll No. 3/16 is qualified in the Ph.D Course Work Examination
in the Department of Chemistry Nagaland University held in the Year 2017


Head of Department
Head
Department of Chemistry
Nagaland University


Dean
School of Science
Nagaland University
Hqs. Lumami Nagaland

LIST OF FIGURES

Figure 1.1.	The periodic table of elements. The lanthanide series is given at the bottom of the periodic table.	2
Figure 1.2.	Graphical plot of the ionic radius of trivalent lanthanide ions versus number of f electrons.	5
Figure 1.3.	Energy levels splitting for the lanthanide ions with $4f^N$ configuration.	14
Figure 1.4.	Energy level diagram adapted from Dieke's diagram of some trivalent lanthanide ions.	14
Figure 1.5.	Structure of an amino acid.	15
Figure 1.6.	Structure of L-Aspartic acid.	16
Figure 1.7.	Structure of L-Histidine.	17
Figure 1.8.	Structure of L-Valine.	19
Figure 1.9.	Structure of Isonicotinic acid.	20
Figure 1.10.	Proposed Structures of the Complexes.	24
Figure 1.11.	Structure of the Lanthanide(III) Complexes.	25
Figure 1.12.	Synthesis of Lanthanide(III) Complexes.	26
Figure 1.13.	Possible Structures of Lanthanide(III) Complexes.	26
Figure 1.14.	Schematic Structures of Lanthanide Complexes.	27
Figure 1.15.	Synthesis of Earth Metal Complexes.	28
Figure 1.16.	Suggested Molecular Structure of the Lanthanide Complexes.	28
Figure 1.17.	Schematic Representations of Lanthanide(III) Complexes.	29
Figure 1.18.	Molecular Structures of the Complexes.	30
Figure 1.19.	Structure of Lanthanide Metal Complexes.	31
Figure 1.20.	Synthesis of Acesulfame Lanthanide Metal Complexes.	32
Figure 1.21.	Synthesis of Lanthanide Monoborohydrate from Lanthanide Monochloride Complexes.	32
Figure 1.22.	Effect of temperature on the rate of reaction.	33
Figure 1.23.	The concept of activation energy.	34
Figure 2.1.	Basic components of a FT-IR spectrometer.	53
Figure 2.2.	Optical diagram of a Michelson interferometer in FT-IR.	54
Figure 2.3.	Illustration of Bragg's law.	55

Figure 2.4.	Effect of particle size on diffraction curve.	56
Figure 2.5.	Schematic representation of a Spectrofluorometer.	58
Figure 2.6.	Schematic diagram of thermogravimetric analyzer.	60
Figure 2.7.	Block diagram of thermobalance.	62
Figure 2.8.	Bouguer–Beer Rule.	63
Figure 2.9.	Schematic diagram of UV–Visible Spectrophotometer.	64
Figure 2.10.	Gaussian curve analysis on an expanded single peak of Pr(III) spectrum.	68
Figure 3.1.	Probable Chemical Reaction for the synthesized Praseodymium (III): Ligands [(i) Aspartic acid, (ii)Histidine (iii) Valine] Complexes.	78
Figure 3.2.	The FT-IR spectra of the ligands (L-Aspartic acid, L-Histidine and L-Valine) and Pr(III): Ligands complexes. *Red are the complexes and black are the ligands.	81
Figure 3.3.	(a) Emission spectra and (b) Excitation spectra of Praseodymium(III) and Praseodymium complexes.	84
Figure 3.4.	XRD spectrum of Praseodymium: Ligands (a) L-Aspartic acid, (b) L-Histidine and (c) L-Valine complexes.	86
Figure 3.5.	TGA of the three synthesized Praseodymium: Ligands (a) L-Aspartic acid, (b) L-Histidine and (c) L-Valine complexes.	87
Figure 4.1.	The zwitterions of L-Aspartic acid.	98
Figure 4.2.	Chemical reaction pathway of Praseodymium(III) with L-Aspartic acid complex in aquated medium.	98
Figure 4.3.	UV-vis spectra of Praseodymium(III) and Praseodymium(III):L-Aspartic acid complex in aquated DMF solvent.	103
Figure 4.4.	UV-vis absorption spectra of Praseodymium(III):L-Aspartic acid complex in various aquated organic solvents.	103
Figure 4.5.	Absorption spectrum for Praseodymium (III): L-Aspartic acid complex in DMF medium at different time intervals of 25°C, 30°C, 35°C, 40°C and 45°C.	107
Figure 4.6.	Graph for oscillator strength vs. time (in hrs) for $^3H_4 \rightarrow ^3P_2$ transition for Praseodymium (III): L-Aspartic acid complex in	113

	DMF solvent at various temperatures 25°C, 30°C, 35°C, 40°C & 45°C.	
Figure 4.7.	Plot of Log k versus $1/T \times 10^3$ for Praseodymium (III): L-Aspartic acid complex in DMF at different temperatures	114
Figure 5.1.	Chemical representation of L-Histidine in its isoelectronic point pH 7.6 (zwitter ion form).	127
Figure 5.2.	The Possible chemical reaction for Praseodymium(III): L-Histidine complex in solution.	127
Figure 5.3.	The absorption spectra for Praseodymium(III) and Praseodymium(III):L-Histidine complex in aqueous solution.	132
Figure 5.4.	The absorption spectra for Praseodymium(III):L-Histidine complex in aqueous solution.	132
Figure 5.5.	Absorption spectra for the complexation of Pr(III):L-Histidine at 298°K, 303°K, 308°K, 313°K and 318°K in aqueous DMF solvent.	136
Figure 5.6.	Plot of oscillator strength Vs time (in hrs) for $^3H_4 \rightarrow ^3P_2$ transition for Pr(III):L-Histidine complex in aqueous DMF solvent at five different temperatures (i.e., 298°K, 303°K, 308°K, 313°K and 318°K).	142
Figure 5.7.	Plot of Log k versus $1/T \times 10^3$ for Pr (III): L-Histidine complex in aqueous DMF solvent at different temperatures.	143
Figure 6.1.	Structure of L-Valine in its free state and zwitterion form.	155
Figure 6.2.	Absorption spectra of Pr(III) and Pr(III): L-Valine complex in aqueous DMF solvent.	158
Figure 6.3.	Absorption spectra of Pr(III) and Pr(III): L-Valine complex in various aqueous organic solvents.	158
Figure 6.4.	Absorption spectra for the interaction of Pr(III): L-Valine at various temperatures 298°K, 303°K, 308°K, 313°K and 318°K in DMF solvent.	162
Figure 6.5.	Plot of oscillator strength vs. time (in hrs) for $^3H_4 \rightarrow ^3P_2$ transition for Pr (III): L-Valine complex in DMF solvent at different temperatures 298°K, 303°K, 308°K, 313°K and 318°K.	168

Figure 6.6.	Graph of Log k versus $1/T \times 10^3$ for the complexation of Pr (III): L-Valine in DMF at various temperatures	169
Figure 6.7.	The reaction pathway for nona-coordinated Pr(III): L-Valine complex in an aquated organic solvent.	172
Figure 7.1.	Probable Chemical Reaction for the synthesized Praseodymium (III): Ligands (Isonicotinic acid) complex	181
Figure 7.2.	The FT-IR spectra of the ligands (Isonicotinic acid) and Pr(III): Ligands complex. *Red is the complex and black is the ligand.	183
Figure 7.3.	(a) Emission spectra of Praseodymium(III) and Praseodymium(III):Isonicotinic acid complex. (b) Excitation spectra of Praseodymium(III) and Praseodymium(III):Isonicotinic acid complex.	184 185
Figure 7.4.	XRD spectrum of Praseodymium:Isonicotinic acid complex.	187
Figure 7.5.	TGA of the the synthesized Praseodymium: Isonicotinic acid complex.	187
Figure 7.6.	Absorption spectra of Pr(III) and Pr(III):Isonicotinic acid complex in aquated DMF (50% v/v)	190

LIST OF TABLES

Table 1.1	Selection rules for lanthanide f-f transitions.	10
Table 2.1.	The zero order energies and partial derivatives with respect to F_k and ξ_{4f} parameters with Pr(III)	69
Table 2.2.	Matrix Element for Pr(III)	70
Table 3.1.	Analytical data and other details of the lanthanide (III) complexes (Asp. =Aspartic Acid, His=Histidine and Val=Valine); calculated values are given in brackets.	80
Table 3.2.	FT-IR wavenumbers with functional groups assigned to the Pr:L(L-Aspartic acid, L-Histidine and L-Valine) complexes.	83
Table 3.3.	Antibacterial activity of lanthanide complex, metal ion as negative control, commercial drug as positive control, here A is [Pr(Aspartic acid) ₃ NO ₃], B is [Pr(Histidine) ₃ NO ₃] and C is [Pr(Valine) ₃ NO ₃]	88
Table 3.4.	Minimum Inhibitory Concentration assay of Lanthanide (III) complexes against bacterial pathogens.	89
Table 3.5.	Antifungal Activity of Lanthanide (III) complexes, here A is [Pr(Aspartic acid) ₃ NO ₃], B is [Pr(Histidine) ₃ NO ₃] and C is [Pr(Valine) ₃ NO ₃].	89
Table 4.1.	Comparative studies of energy interaction values- Slater–Condon (F_k), Lande (ξ_{4f}), Racah energy (E^k), Nephelauxetic ratio (β), bonding ($b^{1/2}$), and covalency (δ) factors of Praseodymium(III) and Praseodymium(III):L-Aspartic acid complex in various aqueous medium.	104
Table 4.2.	Comparative studies of energies (cm^{-1}) values as well as RMS values for Praseodymium(III) and Praseodymium(III):L-Aspartic acid in various aqueous medium.	105
Table 4.3.	Comparative studies of Oscillator strengths and Judd–Ofelt parameters for Praseodymium(III) and Praseodymium(III):L-Aspartic acid complex in various aqueous medium.	106
Table 4.4.	Oscillator Strengths and Judd-Ofelt parameters for Praseodymium(III):L-Aspartic acid complex at different time intervals of 298 K (25°C).	108

Table 4.5.	Oscillator Strengths and Judd-Ofelt parameters for Praseodymium(III):L-Aspartic acid complex at different time intervals of 303 K (30°C).	109
Table 4.6.	Oscillator Strengths and Judd-Ofelt parameters for Praseodymium(III):L-Aspartic acid complex at different time intervals of 308 K (35°C).	110
Table 4.7.	Oscillator Strengths and Judd-Ofelt parameters for Praseodymium(III):L-Aspartic acid complex at different time intervals of 313 K(40° C).	111
Table 4.8.	Oscillator Strengths and Judd-Ofelt parameters for Praseodymium(III):L-Aspartic acid complex at different time intervals of 318 K (45°C).	112
Table 4.9.	Rate Constants of Praseodymium (III): L-Aspartic acid complex in DMF solvent.	114
Table 4.10.	Thermodynamic parameters, activation energy and rate constants for Praseodymium(III):L-Aspartic acid complex.	114
Table 5.1.	Comparison of energy interaction values- Slater–Condon (F_k), Lande (ξ_{4f}), Racah energy (E^k), Nephelauxetic ratio (β), bonding ($b^{1/2}$), and covalency (δ) factors of Pr(III) and Pr(III):L-Histidine complex in aqueous solution.	133
Table 5.2.	Comparison of energies (cm^{-1}) values as well as RMS values for Pr(III) and Pr(III):L-Histidine complex in aqueous solution.	134
Table 5.3.	Comparison of Oscillator strengths and Judd–Ofelt parameters for Pr(III) and Pr(III):L-Histidine complex in aqueous solution.	135
Table 5.4.	Observed and calculated oscillator strengths and Judd-Ofelt intensity parameters for the complexation of Pr(III):L-Histidine at 298K (25°C) in various time intervals(hr).	137
Table 5.5.	Observed and calculated oscillator strengths and Judd-Ofelt intensity parameters for the complexation of Pr(III):L-Histidine at 303K (30°C) in various time intervals (hr).	138
Table 5.6.	Observed and calculated oscillator strengths and Judd-Ofelt intensity parameters for the complexation of Pr(III):L-Histidine at 308K (35°C) in various time intervals (hr).	139

Table 5.7.	Observed and calculated oscillator strengths and Judd-Ofelt intensity parameters for the complexation of Pr(III):L-Histidine at 313K (40°C) in various time intervals(hr).	140
Table 5.8.	Observed and calculated oscillator strengths and Judd-Ofelt intensity parameters for the complexation of Pr(III):L-Histidine at 318K (45°C) in various time intervals(hr).	141
Table 5.9.	Rate constant k ($\text{Mol L}^{-1} \text{s}^{-1}$) and activation energy, E_a values for the complexation of Pr(III):L-Histidine at various temperatures.	143
Table 5.10.	Thermodynamic parameters for Pr(III):L-Histidine complex at different temperatures and activation energy for the complexation reaction.	143
Table 6.1.	Comparison of energy interaction values- Slater–Condon (F_k), Lande (ξ_{4f}), Racah energy (E^k), Nephelauxetic ratio (β), bonding ($b^{1/2}$), and covalency (δ) factors of Pr(III) and Pr(III): L- Valine complex in different aquated solvents.	159
Table 6.2.	Comparison of energies (cm^{-1}) values as well as RMS values for Pr(III) and Pr(III): L- Valine in different aquated solvents.	160
Table 6.3.	Comparison of Oscillator strengths and Judd–Ofelt parameters for Pr(III) and Pr(III): L- Valine complex in different aquated solvents.	161
Table 6.4.	Computed oscillator strengths and Judd-Ofelt intensity parameter for Pr(III): L-Valine complex at 298°K (25°C) in various time (hr) intervals.	163
Table 6.5.	Computed oscillator strengths and Judd-Ofelt intensity parameter for Pr(III): L-Valine complex at 303°K (30°C) in various time (hr) intervals.	164
Table 6.6.	Computed oscillator strengths and Judd-Ofelt intensity parameter for Pr(III): L-Valine complex at 308°K (35°C) in various time (hr) intervals.	165
Table 6.7.	Computed oscillator strengths and Judd-Ofelt intensity parameter for Pr(III): L-Valine complex at 313°K (40°C) in various time (hr) intervals.	166

Table 6.8.	Computed oscillator strengths and Judd-Ofelt intensity parameter for Pr(III): L-Valine complex at 318 ^o K (45 ^o C) in various time (hr) intervals.	167
Table 6.9.	Rate constant and activation energy for the complexation of Pr(III): L-Valine at various temperatures.	169
Table 6.10.	The activation energy and thermodynamic features for Pr(III): L-Valine complex at various temperatures.	169
Table 7.1.	Analytical data and other details of the Praseodymium (III):Isonicotinic acid complex; calculated values are given in brackets	183
Table 7.2.	FT-IR wavenumbers with functional groups assigned to the Pr:Isonicotinic acid complex.	184
Table 7.3.	Antibacterial activity of Pr(III):Isonicotinic acid complex, metal ion as negative control, commercial drug as positive control.	188
Table 7.4.	Minimum Inhibitory Concentration assay of Pr(III):Isonicotinic acid complex against bacterial pathogens.	188
Table 7.5.	Antifungal Activity of Pr(III):Isonicotinic acid complex.	189
Table 7.6.	Computed value of energy interaction parameters Slater-Condon F_k (cm ⁻¹), Spin Orbit Interaction ζ_{4f} (cm ⁻¹), Nephelauxetic ratio (β), bonding ($b_{1/2}$), and covalency (δ) parameters of Pr(III) and Pr(III) with Isonicotinic acid in aquated (N,N Dimethylformamide) solvent.	190
Table 7.7.	Observed and calculated P and T_λ (T_λ , $\lambda= 2, 4, 6$) intensity parameter of Pr(III) with Isonicotinic acid in aquated DMF solvent.	191

CONTENTS

List of figures	i - iv
List of tables	v – viii
<hr/>	
CHAPTER 1	
<hr/>	
Introduction	
1.1. General introduction to lanthanides	2 - 3
1.1.1. Lanthanide chemistry	3 - 4
1.1.2. Lanthanide coordination chemistry	4 - 7
1.1.3. Magnetic and Spectroscopic Properties of Lanthanides	7 - 9
1.1.4. Selection Rules	9 - 11
1.1.5. Related terms and properties	11 - 15
1.2. General properties and structures of the Ligands	15 - 20
1.2.1. Amino Acid	15 - 19
1.2.2. Pyridine	19 - 20
1.3. Antimicrobial Activity	20 - 21
1.4. Applications	21 - 23
1.4.1. Biological	21 - 22
1.4.2. Physical	22 - 23
1.5. Synthesis and Importance of Lanthanide Complexes	23 - 33
1.6. Chemical Kinetics	33 - 34
1.7. Scope and Aim of the study	34 - 35
References	

CHAPTER 2

Experimental methods and techniques	
2.1. Materials employed	51
2.1.1. Lanthanide	51
2.1.2. Amino Acids	51
2.1.3. Solvents	51
2.1.4. Pyridine	51

2.2. EXPERIMENTAL	51
2.2.1. Synthesis of lanthanide complexes	51
2.3. INSTRUMENTATION	51 - 65
2.3.1. Elemental analysis	51
2.3.2. Estimation of metal	52
2.3.3. Molar conductance measurements	52
2.3.4. Fourier Transform Infrared Spectroscopy (FT-IR)	52 - 54
2.3.5. Powdered X-ray Diffraction (XRD) studies	54 - 57
2.3.6. Spectrofluorometer	57 - 59
2.3.7. Thermogravimetric (TGA)	59 - 62
2.3.8. UV–Visible Spectroscopy	62 - 65
2.3.9. Biocidal studies	65
2.4. Spectral analysis of 4f-4f transition of Pr(III) with some selected amino acid and pyridine ligands	65 - 71
2.4.1. Theoretical background	66 - 71
2.5. Kinetic studies	71
2.5.1. Rate of the reactions	71
References	

CHAPTER 3

Synthesis, spectral and antimicrobial studies of Praseodymium (III): Ligands (L-Aspartic acid, L-Histidine and L-Valine) Complexes

3.1. Introduction	76 - 77
3.2. Materials and methods	77 - 80
3.2.1. Synthesis of lanthanide complexes [Pr(III):Ligands (L-Aspartic acid, L-Histidine and L-Valine) complexes]	77 - 78
3.2.2. Biological Activity	78 - 80
3.3. Results and discussion	80 - 90
3.4. Conclusions	90 - 91
References	

CHAPTER 4

Absorption spectral study for the interaction of Pr(III) with L-Aspartic acid in various aquated organic solvents through *4f-4f* transition spectra: Analysis of reaction pathways and thermodynamic parameters.

4.1. Introduction	96 - 97
4.2. Materials and methods	97 - 98
4.3. Theoretical	99 - 102
4.3.1. Energy interaction parameters	99 - 100
4.3.2. Intensity Parameters	100 - 101
4.3.3. Rate of the reactions	101 - 102
4.4. Figures and tables	103 - 114
4.5. Results and discussion	114 - 118
4.6. Conclusion	118 - 119
References	

CHAPTER 5

Computation of spectral parameters for the complexation of Pr(III) with L-Histidine through *4f-4f* transition spectra: Further analysis of its kinetic and thermodynamic parameters.

5.1. Introduction	125 - 126
5.2. Materials and methods	126 - 127
5.3. Theoretical	128 - 131
5.3.1. Energy interaction parameters	128 - 129
5.3.2. Intensity Parameters	129 - 130
5.3.3. Rate of the reactions	130 - 131
5.4. Figures and tables	132 - 143
5.5. Results and discussion	144 - 147
5.6. Conclusion	147 - 148
References	

CHAPTER 6

4f-4f transition spectral study of the interaction of Pr(III) with L-Valine in solution: Further analysis of its kinetics and thermodynamic parameters

6.1. Introduction	154 - 155
-------------------	-----------

6.2. Materials and methods	155
6.3. Theoretical	156 - 157
6.3.1. Energy interaction and Intensity parameters	156
6.3.2. Evaluation of thermodynamic parameters	157
6.4. Figures and tables	158 - 169
6.5. Results and discussion	170 - 173
5.6. Conclusion	173
References	

CHAPTER 7

Synthesis, spectral and antimicrobial studies of Praseodymium (III): Isonicotinic acid complex.

7.1. Introduction	179 - 180
7.2. Materials and methods	180 - 182
7.2.1. Synthesis of Pr(III):Isonicotinic acid complex	180 - 181
7.2.2. Biological Activity	181 - 182
7.3. Results and discussion	182 - 193
7.4. Conclusions	193
References	

CHAPTER 8

Summary and Conclusion	198 - 202
-------------------------------	------------------

APPENDIX – 1 Ph.D. Thesis Certificate on Plagiarism check

APPENDIX – 2 Publications

APPENDIX - 3 Conferences/Seminars/Workshops Presented/Attended

INTRODUCTION

This chapter presents a brief introduction on the lanthanides and ligands (L-Aspartic acid, L-Histidine, L-Valine and Isonicotinic acid) used for the synthesis of the complexes. The chemistry, spectral, magnetic, unique and intriguing characteristics of lanthanides were discussed. The importance and applications of lanthanides complexes and their counterparts was presented. A brief explanation on chemical kinetic, activation energy and the effect of temperature on the rate of reaction and activation energy are also presented. Finally, the aim and scope of the study was discussed.

1.1. General introduction to lanthanides

A set of 15 elements with atomic numbers ranging from lanthanum (atomic number 57) to lutetium (atomic number 71) make up the lanthanide series in the periodic table of elements (figure 1.1). Due to the gradual filling of the final electron in the antepenultimate shell's f-orbitals, these elements are known as f-block elements. With the addition of the lanthanide-like elements scandium ($Z = 21$) and yttrium ($Z = 39$), the lanthanide series can be expanded to include these elements, which are referred to as rare earth. Contrary to what their name suggests, rare earth is just as common in nature as tin or silver.

1 H																	2 He
3 Li	4 Be											5 B	6 C	7 N	8 O	9 F	10 Ne
11 Na	12 Mg											13 Al	14 Si	15 P	16 S	17 Cl	18 Ar
19 K	20 Ca	21 Sc	22 Ti	23 V	24 Cr	25 Mn	26 Fe	27 Co	28 Ni	29 Cu	30 Zn	31 Ga	32 Ge	33 As	34 Se	35 Br	36 Kr
37 Rb	38 Sr	39 Y	40 Zr	41 Nb	42 Mo	43 Tc	44 Ru	45 Rh	46 Pd	47 Ag	48 Cd	49 In	50 Sn	51 Sb	52 Te	53 I	54 Xe
55 Cs	56 Ba		72 Hf	73 Ta	74 W	75 Re	76 Os	77 Ir	78 Pt	79 Au	80 Hg	81 Tl	82 Pb	83 Bi	84 Po	85 At	86 Rn
87 Fr	88 Ra		104 Rf	105 Db	106 Sg	107 Bh	108 Hs	109 Mt	110 Ds	111 Rg	112 Cn	113 Uut	114 Fl	115 Uup	116 Lv	117 Uus	118 Uuo
Lanthanides	57 La	58 Ce	59 Pr	60 Nd	61 Pm	62 Sm	63 Eu	64 Gd	65 Tb	66 Dy	67 Ho	68 Er	69 Tm	70 Yb	71 Lu		
Actinides	89 Ac	90 Th	91 Pa	92 U	93 Np	94 Pu	95 Am	96 Cm	97 Bk	98 Cf	99 Es	100 Fm	101 Md	102 No	103 Lr		

Figure 1.1. The periodic table of elements. The lanthanide series is given at the bottom of the periodic table.

The absorption and photoluminescence of lanthanide ions are essential properties. Several lanthanide ions exhibit luminescence when exposed to ultraviolet light, typically in the visible or near-infrared spectral range. As an illustration, Sm^{3+} produces orange light, Eu^{3+} red light, Tb^{3+} green light, and Tm^{3+} blue light. Other lanthanide ions (Pr^{3+} , Sm^{3+} , Dy^{3+} , Ho^{3+} , and Tm^{3+}) exhibit transitions in the near-infrared range. Nd^{3+} , Er^{3+} , and Yb^{3+} are widely recognised for their near-infrared luminescence. It is particularly desirable for applications that the emitted lanthanide ions have good colour purity. Trivalent lanthanides exhibit unique sharp, relatively weak absorption bands, mostly detected in the visible near UV part of the spectrum. Lanthanide ions line-like absorption and emission, which produces exceptionally high colour purity for the produced light, is an intriguing property of these particles. The luminous lanthanide ions are crucial for many applications because of their intriguing spectroscopic characteristics. In addition to being

used to create optical fibres for telecommunications¹, organic light emitting diodes (OLEDs)², contrast agents for magnetic resonance imaging³, and biological investigations^{4,5}, they are also utilised to create lamp phosphors⁶. Lasers use near-infrared emitting ions, which are also crucial to telecommunications and optical amplifiers^{7,8}. In order to ascertain the natural frequencies of lanthanides, absorption and luminescence spectroscopy are crucial techniques in the study of lanthanide systems.

1.1.1. Lanthanide chemistry

In the whole series, the stable oxidation state for lanthanide elements is +3. Due to the presence of an empty, partially filled, or fully filled 4f shell, Ce⁴⁺, Eu²⁺, Sm²⁺, Yb²⁺, and Tb⁴⁺ are the sole exceptions. The xenon core effectively shields the 4f orbitals, turning them into "inner orbitals" for the valence 4f orbitals. The lanthanide metal ions' chemical and spectroscopic characteristics can be explained by this phenomenon.

Ionic radii of the lanthanide series elements decline from atomic number 58, cerium, to atomic number 71, lutetium, resulting in smaller than predicted ionic radii for the following elements. This effect, known as lanthanide contraction, occurs when 6s electrons are attracted nearer to the nucleus as a result of poor 4f electron shielding of the nuclear charge, resulting in a decreased atomic radius. Trivalent lanthanide ions have a binding preference for the often-employed donor atoms (O > N > S), which are hard Lewis's acids. In their complexes, the bonds are electrostatic in nature. As a result, the coordination geometry of lanthanide complexes is determined by steric considerations. Only ligands with donor groups containing negatively charged oxygens (such as carboxylate, sulfonate, phosphonate, and phosphinate, etc.) may successfully bind to the lanthanide ion in an aqueous solution because water molecules and hydroxide ions are particularly potent ligands for Ln³⁺. The trivalent lanthanide ions (Ln³⁺) exhibit coordination numbers ranging from 6 to 12, with 8 and 9 being the most frequent, and share a number of other common coordination features.

Due to their ionic nature, Ln³⁺ ions have varying coordination numbers and geometries due to their weak stereochemical preferences and labile coordination sphere.

The most prevalent coordination geometries for Ln³⁺ complexes in solid state include square anti-prismatic, dodecahedral, tricapped trigonal prismatic, monocapped square anti-prismatic, bicapped square anti-prismatic, and bicapped dodecahedral.

The solution prediction for the coordination numbers is more challenging⁹. When the ligand's electronic density or a number of donating atoms is insufficient, the

lanthanide ions use anions such as water, chloride, or hydroxide to complete their coordination sphere.

The coordination characteristics of the ligand are dependent on the type of donor atoms. Because of their hard acid nature, lanthanide ions preferentially bond to hard bases. As a result, stronger bonds are formed by ligands using negatively charged -O or -N donor atoms. Due to its strong acidic nature and the predominance of ionic bonding interactions, Ln^{3+} prefers hard bases. In aqueous solutions, ligands with negatively charged oxygen coordinating moieties produce complexes with high thermodynamic stability that are resistant to hydrolysis^{10,11}. Even though they are softer, nitrogen donors in anhydrous environments can more effectively coordinate lanthanides, even in the presence of minute amounts of water⁹.

1.1.2. Lanthanide coordination chemistry

The $4f^n 5d^1 6s^2$ configuration of lanthanides makes the +3 oxidation state by far the most stable (although +2 and +4 oxidation states exist for some lanthanide elements). This is due to the low electronegativity of lanthanides and the increasing stabilisation of the 4f, 5d and 6s orbitals ($4f > 5d > 6s$) caused by successive removals of electrons from the neutral Ln metal. As a result, their trivalent cations Ln(III) play a nearly crucial role in lanthanide coordination chemistry.

The term "lanthanide (or lanthanoidic) contraction" refers to the continuous and smooth decrease in the atomic and ionic radii that results from the steady filling of the 4f orbitals with 14 electrons over the lanthanide series. Some important changes in the chemical behaviour of certain elements are the result of this tendency (and, of course, on the properties of the following third-row transition elements that are smaller than what would be normally expected in the absence of the f-block).

The gradual filling of the 4f orbitals with 14 electrons over the lanthanide series leads to a continuous and smooth decrease in the atomic and ionic radii, a phenomenon is known as "lanthanide (or lanthanoidic) contraction." This trend is to blame for some significant changes in the chemical behaviour of these elements (and, of course, on the properties of the following third-row transition elements that are smaller than what would be normally expected in the absence of the f-block). From 1.061 for La(III) to 0.848 for Lu(III), the trivalent lanthanide ionic radius declines, with a relative maximum (cusp) in the graph corresponding to the partially full $4f^7$ shell of Gd(III) (figure 1.2). When transitioning

from La(III) to Lu(III), the amount of this contraction is only around 15%, but the difference in ionic radius between the two successive lanthanides is just about 1%.

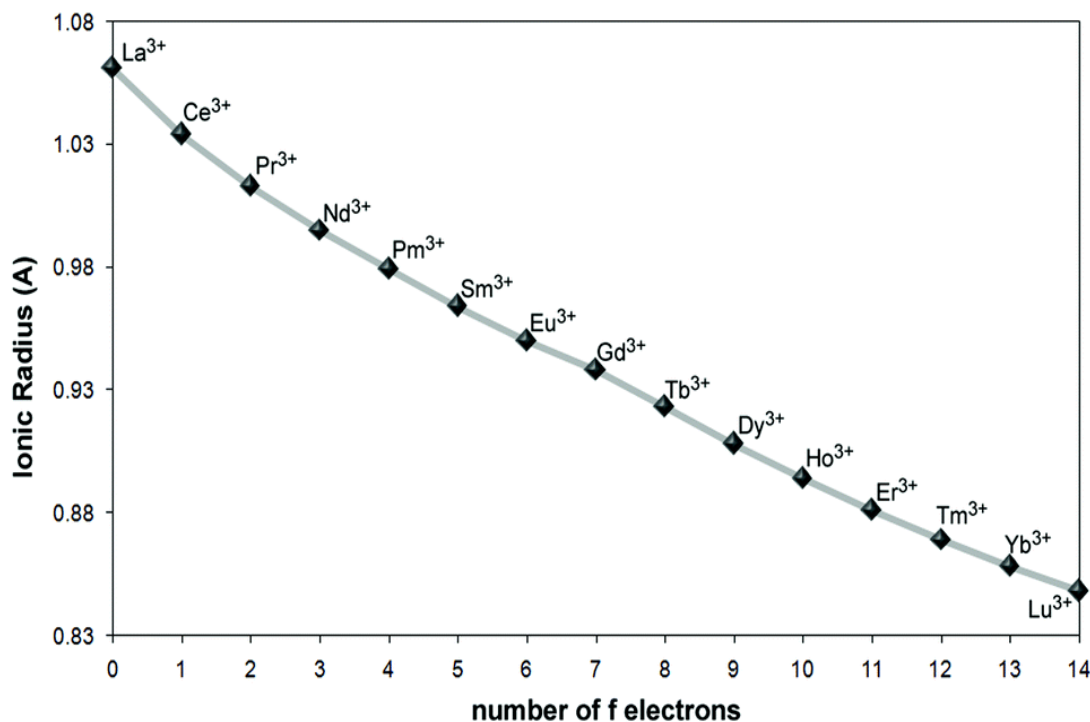


Figure 1.2. Graphical plot of the ionic radius of trivalent lanthanide ions versus number of f electrons.

Since the outward-filled $5s^2p^6$ shell effectively shields 4f electrons, the latter is often referred to as "core-like electrons." Since the coordination characteristics of lanthanide ions change quite a little across the lanthanide family, lanthanide ions exhibit a relatively comparable chemical behaviour (but this variability is much less pronounced than that found among transition-metal ions)¹².

Coordination primarily occurs through ionic interactions, with covalence playing a minor role in Ln-ligand dative bonds. Since 4f electrons are contracted into the core, they rarely engage in bonding. Because of this, there can be no π -back bonding, and the chemistry of the M_0 state is almost non-existent (i.e., carbonyls). Thus, a complicated interplay between interligand steric restraints and electrostatic interactions (i.e., minimization of repulsive terms, particularly ligated atoms-ligated atom repulsions) determines the shape of the complex^{13,14}.

The coordination geometry of the lanthanide complexes, and most likely that of the d-block transition components, is not at all controlled by orbital directionality, as is further demonstrated by the wide radial dispersion of the core-like f orbitals. Actually, ligand

steric hindrance and cation size play a major role in determining it. Large lanthanide ions have a great ability to reach high coordination numbers, with the lowest being C.N.=6 (which is extremely rare and only occurs with ligands that have a certain steric hindrance) and the highest being C.N.=12. The heavier (and smaller) lanthanide ions (Gd-Lu) prefer to achieve octa-coordination, whereas the earlier terms of the lanthanide series (La-Nd) frequently favour C.N.=9. Even though there are numerous examples of coordination equilibria in solution (especially for mid-term lanthanides), this can be simply explained on the basis of lanthanide contraction. This is because the size variation along the series is so smooth that it is impossible to make a precise estimation of the lanthanide coordination sphere in advance¹⁵.

In any event, as stated by Byrne and Li¹⁶, the mid-term lanthanide element Gd (and, to a lesser extent, Eu) exhibits a coordination behaviour that is rather "anomalous" and midway between that of the lighter and heavier lanthanide elements. The lanthanide series was previously divided into two groups, "of cerium" (La-Pr) and "of yttrium" (Sm-Lu), but this division does not seem to adequately reflect the chemical trend of the series.

Last but not least, because lanthanides are strong Lewis' acids with a-class (hard) characteristics, they have a strong preference for hard donors, especially negatively charged donor groups^{14,15}. Along the lanthanide series, this hard-acid behaviour and, consequently, the ionic character of the bonding increase, with the heavier lanthanide ions having smaller ionic radii having greater effectiveness. Although N-based ligands also form stable complexes with lanthanides, O-donors are still the most successful at coordinating them. Lanthanides' coordination chemistry with S-donors and other chalcogens is still fairly limited. There are various instances of Ln-complexes with monodentate or multidentate neutral ligands that are based on -O or -N, with the strength of the metal-ligand bond rising as the dipolarity of the ligand increases. It is practically impossible to remove complexes from aqueous solutions without directly Ln-bonded H₂O molecules because water molecules, in particular, have a significant attraction for lanthanide ions and provide strong coordination to the lanthanide centre, frequently filling the metal coordination sphere (lanthanide ions possess very high hydration energies). Since water is the most efficient luminescence deactivator, this is regrettably extremely detrimental to lanthanide emission, especially in the near-infrared. Consequently, this is a drawback that needs to be taken into account while attempting to create Ln complexes with higher brightness.

The synthesis of lanthanide complexes from aqueous solutions (or even typical hydrated lanthanide salts) is typically an entropy-driven process due to the strong attraction for H₂O molecules. With a positive entropy change (chelating impact), complexation with a chelating ligand will cause a decrease in the hydration of lanthanide ions, which is somewhat offset by the strongly endothermic dehydration reaction. In order to take advantage of the increase in entropy, it is necessary to choose ligands that have great coordinating properties or, at the very least, those that can provide a lot of binding sites (i.e., macrocyclic ligands) during the formation of complexes¹⁷.

1.1.3. Magnetic and Spectroscopic Properties of Lanthanides

In 1906, Becquerel investigated the absorption of lanthanide ions and observed strong absorption lines¹⁸. Before Bethe, Kramers, and Becquerel proposed that the lines may be caused by intraconfigurational 4fⁿ - 4fⁿ transitions, it was impossible to understand why these lines are so sharp¹⁹⁻²¹. Since the filled 5s and 5p shells protect the electrons in the 4f shell, they are unable to participate in the chemical interaction between the ligands and lanthanide ions. Because of this, the spectra of lanthanide ions resemble sharp lines made by unbound atoms or ions. Each lanthanide ion exhibits a distinctive absorption and emission spectrum and can emit in the near-UV, visible, near-infrared, and infrared parts of the electromagnetic spectrum. The Laporte selection rule makes this intraconfigurational 4fⁿ - 4fⁿ transitions parity prohibited. According to this, the spectral lines connected to the electric-dipole transition must originate from the opposing parity states. Charge transfer states and the mixing of opposite-parity configurations like 4f^{N-1}-5d¹ can produce electric dipole transitions in noncentrosymmetric systems²². Magnetic dipole transitions are allowed in the lanthanide ions. Their intensity may be determined with ease and is essentially independent of the surrounding matrix. The ⁵D₀ → ⁷F₁ emission line of Eu³⁺ serves as an illustration of a transition that is solely magnetic in nature. The ligand field induces electric dipolar transitions in lanthanide ions, and the strength of these transitions is highly dependent on the coordinating environment. Thus, the ligand field is the only factor affecting their intensity. A hypersensitive transition of the Eu³⁺ emission line from ⁵D₀ → ⁷F₂ is one illustration of such a transition.

The spectroscopic characteristics of the trivalent lanthanide ions are distinct. Because the 5s² and 5p⁶ subshells are filled, the 4f orbitals of the Ln(III) cations are shielded, giving them their peculiar spectroscopic characteristics. The ions of trivalent lanthanides display highly distinct bands of absorption in the ultraviolet, visible, and

infrared, with the exception of lanthanum and lutetium, which do not absorb light²³. These bands, which are unique to each ion, have the same wavelength in both the solid and liquid states of matter. Their compounds spectra exhibit substantially stronger f-f transition-related absorption bands that are linked with smaller, more distinct absorption bands. Deep inside the atom, the 4f orbital is highly insulated by the 5s and 5p electrons. Since the complex formation has almost no effect on the f electrons, the colour of a given ion is mostly unaffected by the ligands. The f-f transition bands are sharp compared to the large d-d transition bands. The bands' narrow line width and peak position show the electrical structure (of a portion) of the 4fⁿ arrangement. The coordination polyhedron's structure and the symmetry of the rare earth site are revealed by the crystal field splitting²⁴.

Due to the prohibited transitions, both magnetic and electric dipolar transitions in lanthanides are feeble. Their lengthy lives and narrow emission lines define their luminosity (in the order of milliseconds). Because of the prohibited transitions, the lanthanide ions absorb energy less effectively. This makes it challenging to directly photoexcite lanthanide ions. This can be avoided by utilising the organic chromophores wide absorption cross sections and the antenna effect, which transfers energy from organic chromophores to lanthanide ions. Lanthanide ions can combine with organic ligands such as pyridines, calixarenes, polyaminopolycarboxylic acids, and β -diketones to create complexes. By creating ligands with appropriate photophysical characteristics, highly luminous lanthanide complexes can be created.

In solution or in glasses, the absorption spectra of single crystals doped with lanthanides exhibit a group of narrow lines; nevertheless, the lines within the group widen to form a single absorption band. These bands must be attributed to the 4f-electronic shell's transition. Every group or band represents the change in $^{2S+1}L_J$ free ion levels (or J-manifolds). Because they don't involve a configuration change, they are known as intra-configurational transitions. For the understanding of the observed transitions, three mechanisms must be taken into account²⁵, namely:

- (i) Magnetic-Dipole Transition.
- (ii) Induced Electric Dipole Transition.
- (iii) Electric Quadrupole Transition.

(i) *Magnetic-Dipole Transition*

The interaction of a spectroscopic active ion with the magnetic field component of light passing through a magnetic dipole result in the magnetic dipole transition. The rotational

displacement of charge can alternatively be thought of as magnetic dipole radiation. A magnetic dipole transition has even parity because the sense of rotation is not reversed under inversion through a point (or inversion centre). Consequently, between states of equal parity, a magnetic dipole operator has even transformation properties (or intra-configurational transition).

(ii) Induced Electric Dipole Transition

The bulk of lanthanide optical transitions that have been recorded are induced electric dipole transitions, which are the result of the lanthanide ion's interaction with the electric field vector via an electric dipole. The development of an electric dipole requires a linear transition of charge that has an odd parity. Therefore, under inversion with respect to the inversion centre, the electric dipole operator exhibits peculiar transformation features. The Laporte Selection Rules prohibit intra-configurational electric dipole transfer. Judd-Ofelt's theory^{26,27} provided a thorough explanation of the induced electric dipole transition.

(iii) Electric Quadrupole Transition

The displacement with a quadrupole nature leads to the electric quadrupole transition. Four-point charges make create an electric quadrupole, which has an overall zero dipole moment and zero charge. It can be described as the arrangement of two dipoles so as to cancel out each other's dipole moment. The parity of an electric quadrupole is even. Transitions between an electric quadrupole and magnetic dipole are substantially weaker than those between induced electric dipole and an electric quadrupole. Hypersensitive transitions, however, are regarded as pseudoquadrupole transitions because they adhere to the quadrupole transitions' selection rules.

1.1.4. Selection Rules

When interpreting atomic and molecular spectra, a selection rule is essential since it predicts when a spectral transition might happen. The multiplet terms of the Ln^{3+} ions under the Russell-Saunders Coupling Scheme are denoted by the notation $^{2s+1}\text{L}_J$, where S stands for Total Electron Spin, L for Total Orbital Angular Momentum, and J for Total Momentum. Only under rigorous conditions are selection criteria valid, albeit they may be reduced in some cases. Only the Russell Saunders Coupling Scheme is subject to the selection criteria for ΔL and ΔS . Due to the fact that L and S are undesirable numbers in the intermediate coupling scheme, these selection rules are relaxed. The selection rules on ΔJ are tougher to break down since J still functions as a decent quantum number in the

intermediate coupling scheme; J-mixing is the sole weak impact that can loosen these rules. On the point group symmetry of the rare earth site, the selection procedures for ΔM depend²⁸. Table 1.1 lists the selection criteria for transitions using induced electric dipoles and magnetic dipoles.

Table 1.1: Selection rules for lanthanide f-f transitions. S represents total spin angular momentum, L the total atomic orbital angular momentum and J the total angular momentum.

Magnetic Dipole Transitions (MD)	Induced Electric Dipole Transition(ED)
$\Delta J = \Delta S = \Delta L = 0$	$\Delta L = \pm 1, \Delta J = 0, \Delta S = 0, \Delta L \leq 6$
$\Delta J = 0, 1$ but $0 \leftrightarrow 0$ is forbidden	$ \Delta J \leq 6 ; \Delta L = 2, 4, 6$ if $J = 0$ and $J' = 0$
$M' - M = -P$, where $P = \pm 1$	$M' - M = - (q + p)$

The selection criteria for lanthanide ion intraconfigurational optical transitions between $^{2S+1}L_J$ levels are $L=1$ or $J=1$. Magnetic Dipole and Electric Quadrupole transitions are among the permitted 4fn-4fn electronic transitions. Only the oscillating magnetic vector of the radiation interacts with the 4f electrons of Ln^{3+} ions during magnetic dipole intraconfigurational electronic transitions, not the oscillating electric vector. Even though the oscillator strengths of these transitions are roughly 10⁻⁶ times lower than those of a transition that is fully permitted, they can nevertheless be helpful for particular lanthanides²⁹. The occurrence of $^7F_0 \rightarrow ^5D_0$ and $^5D_0 \rightarrow ^7F_0$ transitions in some Eu(III) complexes³⁰⁻³³ is a well-known illustration of how Judd-Ofelt theory's selection principles can break down. The selection rules disallow the $^7F_0 \rightarrow ^5D_0$ transitions because $J (0 \leftrightarrow 0)$ is prohibited. Tanaka et al.^{34,35} attributed this anomalous behaviour as the reason for the collapse of closure approximation in Judd-Ofelt. Wybourne³⁶ has demonstrated that the second-order matrix element $U^{(0)}$ is zero, demonstrating that no intensity can result from this mechanism. Wybourne postulated a method in which the spin selection rule is weakened by scalar third-order contribution involving spin-orbit interaction acting within higher-lying perturbing states. Burdick³⁷⁻⁴⁰ created this model. Lanthanide electric and magnetic dipolar transitions are weak due to forbidden transitions. Their luminous properties include narrow emission lines and lengthy lifetimes (in the order of milliseconds). Because of the prohibited transitions, lanthanide ion absorption is weaker. Direct photo-excitation of lanthanide ions is so problematic. This

can be addressed by utilising the organic chromophores' wide absorption cross-section and energy transfer from organic chromophores to lanthanide ions via the antenna effect. Lanthanide ions have the ability to form complexes with organic ligands such as β -diketones, polyaminopolycarboxylic acids, pyridines and calixarenes. Designing ligands with adequate photophysical characteristics yields highly luminous lanthanide complexes. Lanthanide ions that emit visible light are Eu^{3+} (red), Eu^{2+} (blue), Tb^{3+} (green), Sm^{3+} (orange), and Tm^{3+} (blue). Nd^{3+} , Er^{3+} and Yb^{3+} are examples of lanthanide ions that emit near-infrared light

1.1.5. Related terms and properties

a) Hypersensitivity

The environment has little impact on the induced electric dipole transition intensities in lanthanides. The lanthanide (III) ion's specific transition dipole strength in various matrices does not change by more than a factor of two or three. A few transitions, however, are substantially stronger in lanthanide complexes than in lanthanide (III) aquo ion complexes and are particularly sensitive to the environment⁴¹⁻⁴³. Much earlier than Judd-Ofelt's theory, Moeller et al.⁴⁴⁻⁴⁶ first noted the remarkable phenomena of the high sensitivity of spectrum intensities for ligand environment. They did this for the β -diketonate and EDTA complexes of Nd^{3+} , Ho^{3+} and Er^{3+} . These transitions adhered to the selection rules $|\Delta S|=0$; $|\Delta L|\leq 2$; $|\Delta J|\leq 2$ and were referred to as "HYPERSENSITIVE" by Jorgensen and Judd. the selection criteria for pure quadrupole transitions are the same as these criteria. However, computations showed that the intensities had a quadrupole character; as a result, hypersensitive transitions were referred to as having a pseudoquadrupole character^{47,48}. In order to gather data on the co-ordinating ligands' binding characteristics, the relative binding power of various binding sites, the degree of outer and inner sphere coordination, and the identification of the immediate coordination environment in complex species⁴⁹⁻⁵³, the hypersensitive transition has been widely used as a probe.

In order to understand how the coordination number affects the intensity and fine structure of the spectra, Karraker⁵⁴ studied the hypersensitive transitions of Nd^{3+} , Ho^{3+} and Er^{3+} and took into account the absorption spectra of six, seven, and eight coordinated β -diketonates in non-aqueous conditions. The β -diketonate ligands were chosen because they all attach to lanthanides (III) in a bidentate fashion, resulting in a six member chelate ring and involving two oxygen donor atoms. Coordination number and the shape of the

bound ligands were the two primary factors. Low polarity solvents were chosen in order to minimise the solvent effect on the lanthanide ion's crystal field splitting. His thorough research demonstrated that the lanthanide ion's coordination and symmetry were reflected in changes in the hypersensitive transitions. The following findings formed the basis of the conclusion:

- i) For sensitivity transitions between coordinated lanthanide ions six, seven, and eight, the appearance of the absorption bands varies.
- ii) When an unidentate ligand is added to a solution containing six or seven coordinated complexes, the spectra are altered to resemble those of seven or eight coordinated complexes.
- iii) The spectra of hydrated complexes change to spectra that resemble the spectra of lower coordination lanthanides when the water is removed from the solution.
- iv) The degree of the hypersensitive transition and the lanthanide's coordination number are correlated.

Karraker⁵⁵ examined the impact of strong aqueous chloride on perchlorate solution on hypersensitive transitions in his later paper. Changes in the band's form were thought to be diagnostic indicators of changes in the coordination number of lanthanides.

In terms of lanthanide complexes' absorption spectrum intensities in solutions, Chopin et al.⁵⁶ have made excellent contributions. While methodically examining Ln(III) complexes with Poly (amino carboxylic) acids, they proposed a different sequence for oscillator strength of hypersensitive transitions for Nd³⁺ and Ho³⁺ but were unable to provide an explanation for the varied behaviours of the two ions. On the other hand, Fellow and Choppin⁵⁶ and Choppin⁵⁷ discovered a strong link between the oscillator strength and the total ligand pK_a for dibasic acid. Regarding the degree of hypersensitive transitions, these researchers offered three generalisations:

- i) Increased ligand absorption intensity is correlated with increased basic character of the coordination ligand.
- ii) Intensity is increased by shortening the distance between the metal and ligand, and
- iii) The degree of higher intensity increases as the number of more fundamental ligands increases.

The hypersensitivity can be extended to several additional transitions that typically do not exhibit it in the presence of a ligand. The transitions that weren't hypersensitive were typically thought to be nearly insensitive. The hypersensitive transition for Pr(III) has

been observed to be the ${}^3\text{H}_4 \rightarrow {}^3\text{P}_2$ transition occurring at roughly $5,200\text{ cm}^{-1}$, but for Nd(III), the ${}^4\text{I}_{9/2} \rightarrow {}^4\text{G}_{5/2}$ transition, which takes place at about $17,300\text{ cm}^{-1}$, is thought to act in a similar manner. The transitions ${}^3\text{H}_4 \rightarrow {}^3\text{P}_2$, ${}^3\text{P}_1$, ${}^3\text{P}_0$, and ${}^1\text{D}_2$ of Pr(III) and ${}^4\text{I}_{9/2} \rightarrow {}^4\text{G}_{7/2}$, ${}^4\text{F}_{7/2}$, and ${}^4\text{F}_{5/2}$ of Nd(III) are examples of these transitions that do not adhere to the selection rules and as a result, cannot be regarded as hypersensitive transitions, but have been discovered to exhibit significant sensitivity towards even small changes in the nearby coordination environment around Pr(III) and Nd(III)⁵⁸⁻⁶⁰. Choppin et al. also noted hypersensitivity in the ${}^4\text{G}_{7/2} \rightarrow {}^4\text{K}_{13/1}$ transition of Nd(III), although Peacock⁶¹ only noted it in the ${}^4\text{I}_{9/2} \rightarrow {}^4\text{G}_{5/2}$ transition of Nd(III). In their series of investigations with N(III) complexes, Misra and colleagues⁶²⁻⁶⁴ discovered unexpected sensitivity in ${}^4\text{I}_{9/2} \rightarrow {}^4\text{F}_{7/2}$ and ${}^4\text{F}_{5/2}$ transitions that displayed different binding properties depending on the ligands utilised. "Ligand Mediated Pseudohypersensitive Transitions" is the name they gave these transitions. For the development of such pseudohypersensitivity, ligand denticity bite coordination and the type of chelate ring created by the ligand are crucial factors.

b) Energy levels in the lanthanide ions

The 4f-shell can contain 0 to 14 electrons in the lanthanide series, which runs from La^{3+} to Lu^{3+} . The 4f electrons have limited contact with the chemical environment of the ion and are not involved in chemical bonding because they are protected by the outer 5s and 5p shells. The three configurations $4f^0$ (an empty f-shell), $4f^7$ (a half-filled f-shell), and $4f^{14}$ are the most stable (filled-f-shell).

The various energy levels for the same configuration are caused by various interactions inside the lanthanide ion. Electron-electron repulsions within the 4f orbitals are the strongest of these interactions and produce terms with spacing on the order of 10^4 cm^{-1} . The spin-orbit connection then causes this to divide into many J levels (figure 1.3). This is the result of the interaction between the electron's spin magnetic moment and the field produced by its travel around the nucleus. The $(2S+1)L_J$ terms at the free ion level provide the energy states for lanthanide ions. S = total spin angular momentum; L = total atomic orbital angular momentum; and J = total angular momentum. The ions' spherical symmetry is disrupted when they are combined with ligands, which prevents them from being free. Additionally, the 4f electrons and the ligands' electric fields interact electrostatically as a result. This is known as the crystal field.

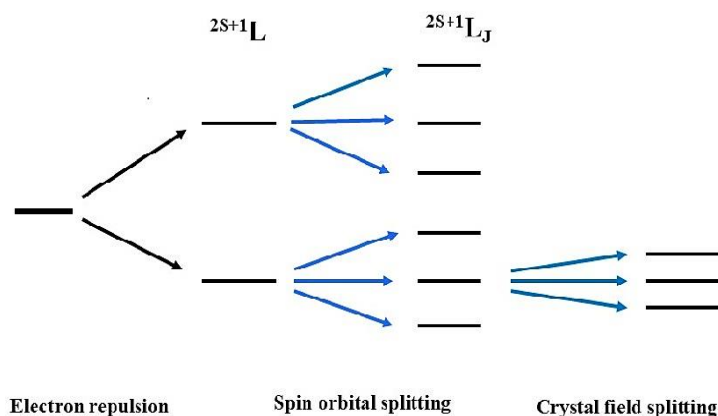


Figure 1.3. Energy levels splitting for the lanthanide ions with $4f^N$ configuration.

Figure 1.4 displays the energy level diagram for some trivalent lanthanide ions. This diagram can be used to illustrate the absorption and luminescent characteristics of the given trivalent lanthanide ions

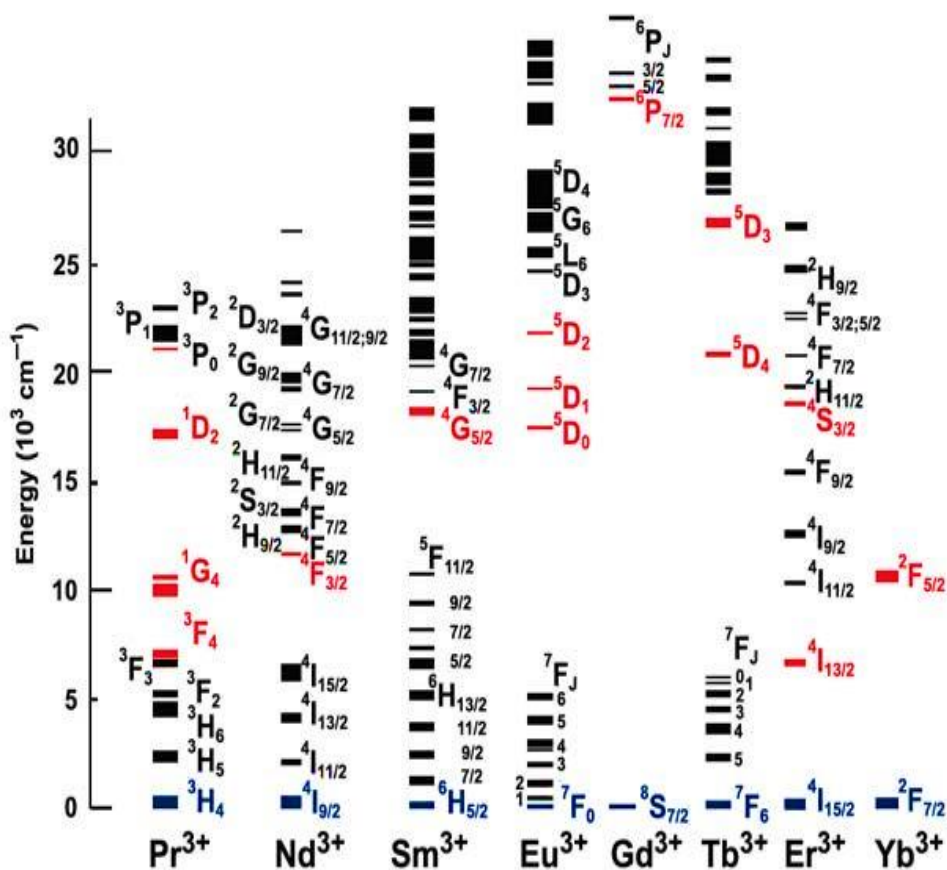


Figure 1.4. Energy level diagram adapted from Dieke's diagram of some trivalent lanthanide ions.

c) *Non radiative decay*

Radiative decay does not completely destroy excited lanthanide ion states. Luminescence will compete with non-radiative decay of the excited state if the energy difference between the excited state and the following lower state is small. Multiphonon relaxation is the process of allowing matrix vibrations to dissipate electronic excitation energy⁶⁵. The coupling of lanthanide energy levels with the vibrational modes in the lanthanide ion's immediate environment may be the cause. Because high energy O-H vibrations are particularly effective at quenching lanthanide luminescence, water molecules are kept out of the first coordination sphere of lanthanide complexes.

1.2. General properties and structures of the Ligands

1.2.1. Amino Acid

All living things need amino acids as fundamental building blocks to create proteins. They can also combine with carbohydrates and lipids⁶⁶. Through the condensation of amino groups and carboxylic groups, which results in the loss of water, ribosomes catalyse the polymerization of amino acids to produce proteins. The amino N- and a carboxy C terminus of the corresponding terminal amino acids give peptides their directionality. As the fundamental components of the widest range of biological substances, amino acids have a distinctive structure. All twenty amino acids—aside from proline—have an amino group, a carboxyl group, and a functional group covalently attached to the alpha carbon. The functional groups are used to categorise the side chains of the essential amino acids into polar, non-polar, or basic side chains⁶⁷.

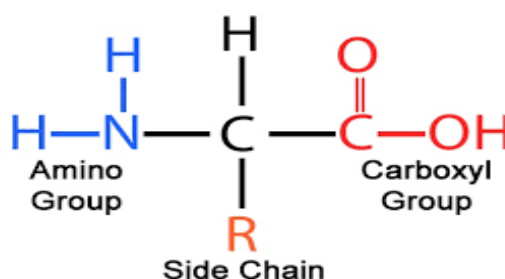


Figure 1.5. Structure of an amino acid.

Most amino acids have chiral carbons connected to a carboxylic acid, an amino group, an alpha hydrogen, and a distinctive side chain (R-group) as given in figure 1.5. Only one amino acid, glycine, is achiral, meaning it lacks a side chain in favour of a hydrogen atom. Some amino acids are considered essential amino acid as they cannot be produced by the

body in sufficient quantities; as a result, they must be obtained through food and supplements. Amino acids have important functions in biological and metabolic processes⁶⁸, such as stress resistance, nitrogen storage etc.

Amino acids exist as zwitterions with the carboxyl group deprotonated and the amino group protonated at neutral pH. The pK_a of the various side chains functional groups has a significant impact on the charge and, consequently, the reactivity of amino acids which are affected by pH changes. pH value of amino acids where its net charge value is zero is known as its isoelectric point (pI). The side chain chemistry in this situation plays a major role in determining the specific reactivity. For example, the sulphur atom in the side chains of methionine and cysteine can both be oxidised to SO_x or, in the case of cysteine, can create disulphide bonds with other cysteine sites in the same or different proteins, a process known as cross-linking. Histidine, Lysine, Cysteine, and Serine are nucleophilic amino acids that have side chains that contain atoms with a free pair of electrons that can attack electron-deficient atoms. Leucine and phenylalanine are two examples of amino acids having hydrophobic side chains, or side chains that contain either aliphatic or aromatic groups; these amino acids are less reactive. Amino acids that are basic or acidic are charged at neutral pH and have a high reactivity in ionic interactions as a result.

Essential amino acids not only play critical functions in enzymes and other proteins, but they also serve as precursors for a variety of crucial nitrogen-containing compounds in physiology. Hormones, nucleotide bases, and neurotransmitters are a few of the particular products. In the fields of respiratory physiology, cardiology, renal failure, neurological illnesses, and congenital abnormalities, essential amino acid therapy has drawn a lot of interest. The relative abundance and affordability of these physiologically active molecules are what make exogenous essential amino acid treatment beneficial⁶⁹

a) L- Aspartic acid

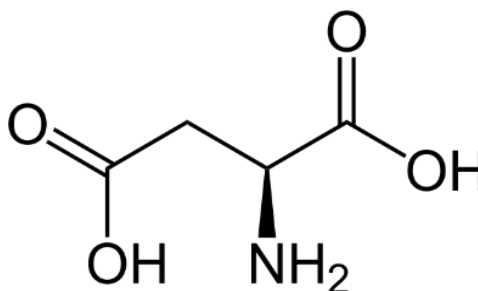


Figure 1.6. Structure of L-Aspartic acid.

Chemical properties: Acidic

Physical properties: Polar (Charged)

Aspartic acid is a non-essential amino acid. It is asymmetric, and exists in two mirror-image forms. Only one form, denoted by the L, occurs naturally in proteins, however.

L- Aspartic acid and Glutamic acid play important roles as general acids in enzyme active centers, as well as in maintaining the solubility and ionic character of proteins. Aspartic acid is alanine with one of the β - hydrogens replaced by a carboxylic group. It has an α - keto homolog, oxaloacetate, just as pyruvate is the α - keto homolog of alanine. It stimulates a neural receptor called the NMDA receptor, which plays a role in memory and cognition. Finally, it has an important role in gluconeogenesis, which is the process of making glucose, or sugar, when the supply is low⁷⁰.

b) Histidine

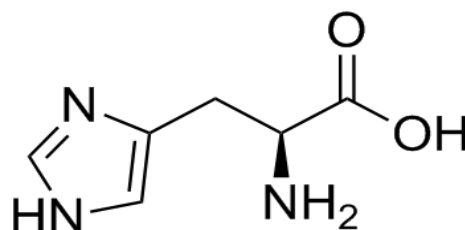


Figure 1.7. Structure of L-Histidine.

Histidase converts histidine into N-formiminoglutamate (FIGlu), which adds the formimino group to tetrahydrofolate and creates glutamate⁷¹. The rationale for the FIGlu excretion test is an enhanced urine elimination of FIGlu caused by a dietary folic acid deficit^{72,73}. One carbon metabolism heavily depends on tetrahydrofolic acid (THF), a metabolite of histidine and the active form of folic acid. With the addition of two protons (H^+) and two molecules of NADPH, dihydrofolate reductase changes the inactive form of folic acid into its active form. In order to synthesise methionine, thymidine, purine-C8, and purine-C2, several types of THF are required. Some microorganisms directly manufacture folic acid, in contrast to humans. Methotrexate is an effective treatment for people with acute lymphocytic leukaemia because it prevents folic acid in humans from being converted to its active form⁷⁴.

Numerous living things and physiological systems are affected by histidine. Histidine quenches hydroxyl and hydrogen peroxide, but not superoxide anions, in its capacity as a free radical scavenger. As the adenine nucleotide pool rises after histidine injection, the total free energy of cells increases⁷⁵.

The control of oxidative DNA breakdown involves histidine significantly. Histidine loses its ability to control the oxidative degradation of DNA when its imidazole component is protonated⁷⁶. Evidence suggests that the protective effect of histidine at low hydrogen peroxide levels may be due to its capacity to bind hydroxyl free radicals. In isolated perfused rat hearts, histidine also lessens the ischemia brought by myocardial damage.

The chemical messenger histamine is a significant metabolite of histidine. This potent ingredient is created by decarboxylating histidine, which is a common trigger for allergic and inflammatory reactions. Numerous cellular processes, including gastric acid secretion, vasodilation and allergy reactions, are mediated by histamine. Additionally, histamine has been proposed as a potential brain neurotransmitter. Histamine is not employed in medicine; however, histamine antagonists serve vital medicinal purposes.

The mediator of numerous inflammatory and allergic responses, histamine, is produced from histidine. Additionally, histidine is a good scavenger of oxygen-free radicals. According to research on the antioxidative effects of the amino acid in heart myocardial injury in rats, it was found that histidine protected postischemic reperfusion injury. Histidine-treated hearts recovered more functionally and had higher levels of high-energy phosphates. Hydrogen peroxide and hydroxyl radicals were demonstrated to be quenched by histidine, but not superoxide anions. The effects of histidine on cerebral vasospasm were demonstrated in a different investigation using subarachnoid haemorrhage in rabbits. In a rat investigation on the effects of histidine on brain edoema and cardiac function following thrombotic ischemia, it was discovered that reduced histidine decreased brain water content and improved left ventricular performance.

Carnosine and anserine, two histidine-containing dipeptides, displayed anti-inflammatory properties and might be helpful in the healing of wounds⁷⁷. These dipeptides are thought to interact with lipid peroxidation products and oxygen radicals to prevent membrane deterioration.

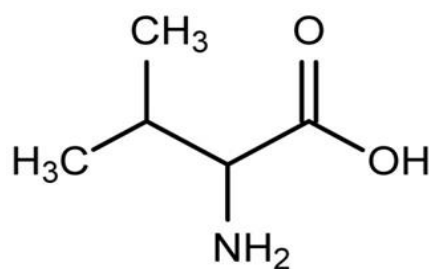
c) Valine

Figure 1.8. Structure of L-Valine.

It has been demonstrated that diets low in valine cause chicks' urinary calcium excretion to increase and their bone mass to decrease. Diets lacking in BCAAs have been researched for potential anti-tumor applications⁷⁸. These researchers have shown that diets lacking in valine and leucine had the best results in reducing tumour growth with the least amount of mass loss. However, tumour growth inhibition was less effective and host development was adversely affected in diets lacking in all three BCAA. This shows that limiting the intake of specific amino acids might be more advantageous for tumour therapy and cause less weight loss than cutting out all three BCAAs. If untreated, vitamin B12 deficiency results in neurological decline. In a study group of B12 deficient bats, the injection of valine and isoleucine—two precursors in the propionic acid pathway—protected against brain impairment⁷⁹. According to this research, valine and isoleucine managed to get around this by promoting the propionic acid pathway.

1.2.2. Pyridine

Pyridine (py) is a significant heterocyclic substance that is present in many different natural products. To treat a variety of human illnesses, there are numerous medications with pyridine ring systems. The chemical compound pyridine and its derivatives have many essential uses in a wide range of industries. Both medical and non-medical applications exist for pyridine derivatives. Numerous biological actions of pyridine derivatives have been documented, and several of the compounds are being used in medicine. Additionally, the use of pyridine derivatives in contemporary medicine is growing⁸⁰.

Observing the pharmaceutical industry, Omeprazole has been a popular pyridine-based medication since 1998. Since 2014, the antiemetic medicine netupitant has been used in combination with another medication to prevent immediate and delayed nausea and

vomiting brought on by cancer chemotherapy, paving the way for the creation of anticancer treatments. On the basis of these developments, pyridine research is an ongoing field with higher expectations for addressing a number of disease-related problems.

a) Isonicotinic acid

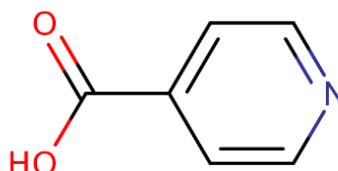


Figure 1.9. Structure of Isonicotinic acid.

In addition to its many other uses as a plant growth regulator, herbicide, pesticide, and corrosion regulator, isonicotinic acid (4-picolinic acid) has derivative applications as an antibacterial medicine for treating psoriasis, arthritis, and tuberculosis.

1.3. Antimicrobial Activity

A substance that kills or prevents the growth of microorganisms like bacteria, fungi, or protozoans is known as an anti-microbial. Antimicrobial medications either eradicate microorganisms or stop them from proliferating. The majority of the metal complexes have antibacterial properties. Chelation and coordination have been theorised to lessen the polarity of the metal ion by partially sharing its positive charge with the donor group throughout the entire chelate ring system^{81,82}. Thus, during the process of chelation, the central metal atom becomes more lipophilic, which in turn favours its ability to pass through the lipid layer of the membrane. This increases the metal complex's ability to penetrate the bacterial membrane, which in turn raises the activity of the complexes. In addition, a number of additional elements, including solubility, dipole moments and conductivity affected by metal ions, may also play a role in the outstanding anti-microbial activity of metal complexes⁸³. It has also been noted that some moiety introduced into such compounds, such as azomethine or heteroaromatic nucleus, exhibit extensive biological activity, which may be the cause of the increase in hydrophobic character and liposolubility of the molecules in crossing the microorganism's cell membrane and the

enhancement of complexes' biological activity and utilisation ratio⁸⁴. The metal complexes inhibit protein synthesis by disrupting cell respiration, which limits the organism's ability to expand further⁸⁵.

At certain concentrations, metal complexes are poisonous to the majority of microorganisms and frequently cause severe disruptions in biological processes. While some metal ions impede the growth of many bacteria at larger concentrations, other metal complexes are necessary for the growth of microorganisms at extremely low concentrations. The type of the metal ion, the ligands, and their quantities are the key determinants of the metal complexes toxicity⁸⁶.

It has been discovered that Schiff bases and their metal complexes have significant biological activity. Azomethines are an important class of physiologically active ligands that serve as models for the metal ligand binding sites in a number of enzymes. Azomethines bind to the metal ions through nitrogen, oxygen or sulphur atoms. It is known that these ligands and their metal complexes have antibacterial, antimalarial, anticancer and antileukemic properties^{87,88}.

1.4. Applications

Lanthanide complexes have a variety of prospective and existing uses in both solution and solid states because of their intriguing characteristics.

1.4.1. Biological

By taking advantage of their similar chemical characteristics, the Ln^{3+} ions have been employed as spectroscopic probes for Ca^{2+} ions in bioinorganic chemistry. They are both hard cations with a preference for O and N donors, have similar coordination numbers, are similar in size to Ca^{2+} at 1.1 Å, and the biological system is not considerably perturbed when Ca^{2+} ions are replaced by Ln^{3+} ions⁸⁹.

Similar applications for lanthanides can be seen in fluoroimmunoassay systems, an immunology technique for detecting biomolecules. The procedure is more sensitive and specific than those that use radioactive materials. Fluoroimmunoassays take advantage of the long-lasting luminescence of Ln ions⁹⁰⁻⁹³ in this process; the Ln^{3+} ion attaches to the biological species of interest, which is subsequently excited and some of the energy can be transferred to the Ln^{3+} excited state. By prolonging the duration between the excitation pulse and the measurement of emission, the luminescence emerging from the Ln^{3+} ion can be preferentially recorded because the fluorescence

arising from the biological species (commonly referred to as autofluorescence) is brief in comparison.

It has been shown that luminous lanthanide complexes can be utilised as pH, hydroxide, halide and oxygen sensors⁹⁰. The oxygen sensor makes use of the fact that energy is transferred back from the excited Ln^{3+} state to the chromophore's T_1 state, which is susceptible to O_2 deactivation.

The potential health benefits of Ln^{3+} complexes and their application as potential medications have been investigated in recent review papers⁹⁴. Biochemists are currently interested in studies of novel chemotherapeutic Schiff bases. Some medications reportedly had more activity as metal complexes than as organic molecules. Their inclusion as anti-cancer medicines are one of the intriguing potential advantageous uses. Ln^{3+} ions are hypothesised to raise intracellular Ca^{2+} concentration, which is crucial for mediating DNA cleavage, which is the chemical process underlying how they increase the mortality rate of cancer cells. Ln^{3+} ions can be utilised to analyse medicines as well as used as potential drugs⁹⁵. It was discovered that certain medications that are present in solution cause sensitised emission from Eu^{3+} and Tb^{3+} ions bound to organic ligands, enabling the identification of the former.

Complexes are utilised as shift reagents in NMR spectroscopy to take advantage of the magnetic behaviour of the Ln^{3+} ions in solution⁹⁶, and the paramagnetic properties of gadolinium are utilised since Gd(III) complexes are frequently used as in vivo contrast agents for magnetic resonance imaging (MRI)⁹⁷⁻⁹⁹.

1.4.2. Physical

Recently, a possible use for triboluminescent substances (such as Eu^{3+} and Tb^{3+} complexes) has been emphasised¹⁰⁰. Triboluminescent Ln^{3+} materials, which release light only when damaged, can be utilised to detect damage to the composite material's structural integrity in bridges, aeroplanes and other structures. Numerous applications, including as phosphors for fluorescent lighting, display monitors and x-ray imaging, utilise solid-state Ln^{3+} ions doped into insulating hosts^{33,101}.

In optical fibres, Er^{3+} and Nd^{3+} are utilised to amplify light through stimulated emission. It has been demonstrated that numerous crystalline hosts containing Ln^{3+} ions can generate effective lasers. Nd is employed in hosts like YAG or YLF in one of the most popular lasers. It is possible to build effective lasers to the line-like emission band at about 1064 nm, which has a substantially stimulated emission cross-section. Solid-state lasers

have all used Yb^{3+} , Eu^{3+} , Tm^{3+} and Ho^{3+} . Heller studied many Ln^{3+} ions in solution in 1968 with the eventual goal of incorporating them into liquid lasers¹⁰²⁻¹¹².

The synthesis of lanthanide compounds for electroluminescent (EL) displays is a newer topic of research that has received progress. Device studies have demonstrated that the EL emission from the Eu^{3+} (red) and Tb^{3+} (green) complexes is effective. High charge carrier mobility, high thermal stability and photoluminescence (PL) efficiency are characteristics of good EL materials. Semiconducting (conjugated) polymers, which make up the majority of the materials used in EL displays today, have difficulty emitting pure colour. Since polymers (and small organic compounds) produce broadband emission that is rarely pure in one colour, filters must be used. Full-color displays (red, green, and blue) are the ideal requirement. It is common for β -diketonates to be present in the Ln^{3+} electroluminescent complexes that have been examined, and this is especially true of the Eu^{3+} complexes¹¹³⁻¹¹⁷. This is due to the extreme hypersensitive $\Delta J = 2$ emission that Eu^{3+} β -diketonates exhibit, which appears as monochromatic radiation in the red area.

1.5. Synthesis and Importance of Lanthanide Complexes

Numerous investigations and research projects have made significant advancements in the field of the chemistry of lanthanides. They have made advancements in the fields of coordination chemistry¹¹⁸, inorganic chemistry¹¹⁹, applications in industries and agriculture¹²⁰, medical and biological applications¹²¹, magnetic resonance imaging agents (MRI)^{122,123}, bio-imaging, lighting devices¹²⁴ and telecommunications⁸. The use of Lanthanides is also noticeably expanding as an excellent diagnostic and prognostic probe in biological and clinical aspects¹²⁵. Because of the unique electronic configuration of lanthanides, they are considered to have remarkable physical and chemical characteristics¹²⁶.

Since they exhibit a variety of reactions in both their ground state and excited state, lanthanide complexes in organic and aqueous solutions have been attracting a significant amount of interest for the past 20 years¹²⁵. The majority of lanthanides are ionic salts, making them hard acceptors. Lanthanide ions create 9 or 8 coordinations by forming stable complexes with oxygen and nitrogen donor ligands. Due to the chelate effect, Lanthanide complexes that are synthesized using chelated ligands result in stronger complexes than those that are made with monodentate ligands¹²⁷. Lanthanide ions are used to form coordination compounds and supramolecular systems such as helicate, grids, interlock, and bundle molecules because they have smaller atomic radii and a high

positive charge, which meet the ideal conditions for producing a higher coordination number^{128–130}. These structures cannot be formed using commonly used templating ions (ligand-based reactions on the coordination site of the metal), and so using the Lanthanide ions is necessary¹³¹. Lanthanide complexes in solution display a wide range of characteristics, and they typically show a narrow emission band, significant Stokes shifts, and extended excited lifetimes. They also typically emit in the red and green regions of the spectrum^{132,133}.

The Lanthanide ions prefer to coordinate to oxygen, sulphur, and nitrogen donor atoms of the ligand due to their high charge density, Lewis's acid and reactivity. The ligands, which serve as transmitters for complexation, are used to transport energy in order to achieve a consistent excitation state^{134–137}. Lanthanide ions can work as a substitute for other elements like calcium and magnesium and act as a probe in place of these metals when examining the structural roles played by bimolecular processes because they share similar properties with these other elements^{138–140}.

P. R. Maravalli et al. (1999) synthesized a series of Lanthanide (III) complexes using 3-N-methyl piperidion-4-salicylidene amino- 5- mercapto- 1, 2, 4-trazole ligand with Ln (III) nitrate; where Ln = La, Ce, Pr, Nd, Sm, Gd, Tb, Dy, ER, Yb and Y by direct reaction method (figure 1.10). The complexes synthesized were characterized by different methods and suggested the structure of the complexes. The spectral studies show that the coordination bonding between the metal and the ligand is a bidentate one and proposed the complexes to have coordination number six¹⁴¹.

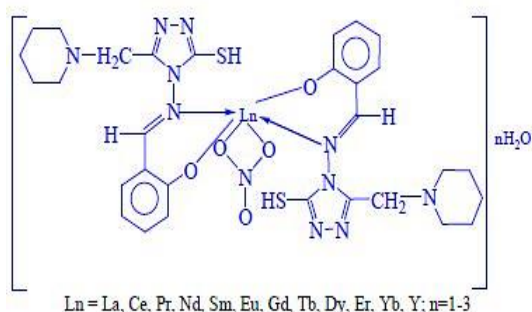


Figure 1.10. Proposed Structures of the Complexes.

I. P. Kostova et al.(2001) reported the synthesized Lanthanide(III) complexes with 4-methyl-7-hydrocoumarin ligand and studied their thermal analysis and the various spectral properties using different spectroscopic methods. The synthesized complexes were identified and characterized by elemental analysis, IR, NMR, conductivity, Mass

spectroscopy, DTA and TGA¹⁴². Irena Kostova and group (2005) synthesized some of the Lanthanide complexes and disclosed its antineoplastic activity and its cytotoxic effect. The complexes were found to have metal-ligand coordination through hydroxyl group^{143,144}.

As Lanthanide(III) complexes were used as a detector of natural sugar and as a cancer biomarker at a certain pH, O. Alpturk and co-workers in 2006 designed complexes of Lanthanide which shows a successful detection of natural sugar and exhibits enhanced fluorescence emission¹⁴⁵.

B. S. Kumari et al. (2009) synthesized a series of Lanthanide(III) chloride complexes with heterocyclic Schiff base (2-(N-salicylideneamino)-3-carboxyethyl-4,5-dimethylthiophene) base under microwave irradiation in solid state (figure 1.11). The spectral studies showed that the metals were coordinated at the ONO donor site of the ligand acting as a neutral tridentate and studies shown from the X-ray diffraction of the lanthanide (III) complexes results in orthorhombic. The synthesized complexes were also reported to be a promising antimicrobial agent¹⁴⁶.

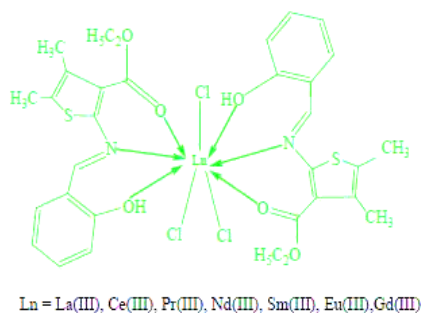


Figure 1.11. Structure of the Lanthanide(III) Complexes.

T. Moaienla and co-workers (2009) studied the comparative absorption spectra of Lanthanide with L-phenylalanine, L-glycine, L-alanine, and L-aspartic in the presence and absence of Ca^{2+} in organic solvents. The investigation shows that 4f-4f transition Lanthanides can be utilized to study the binding nature of biologically important ligands. From the different studies and evaluated parameters (Slator-Condon F_k , Racah E^k , spin-orbit coupling constant ξ_{4f} , Nephelauxetic β , oscillator strength and Judd-Ofelt T_λ) it is found that the absorption spectra of Lanthanide complexes in DMF solvent was the most favorable one among the organic solvents used¹⁴⁷.

N. V.S. Rao and co-workers (2010) synthesized new Lanthanide complexes, Tb(III), Dy(III), and Gd(III) of N-aryl base showing mesomorphism (figure 1.12); all the

synthesized complexes were characterized and it is observed that electronic properties are dominated by the donor-acceptor of the organic chromophore ligand and the emission maxima shows a ligand-driven strong fluorescence with large Stokes shift. The nature of the interaction (Vander Waals interaction, electrostatic interaction) between the coordinated ligand and the Lanthanide ions leads to an increase transition temperature and thermal stability¹⁴⁸.

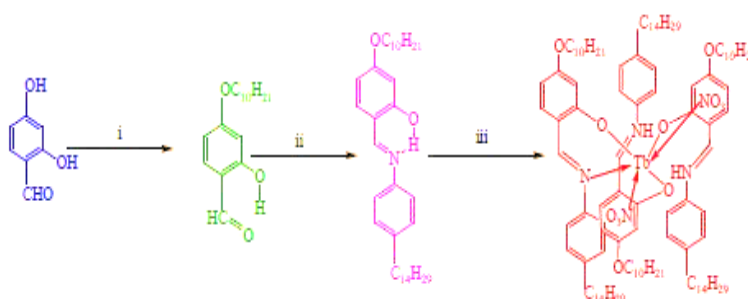


Figure 1.12. Synthesis of Lanthanide(III) Complexes.

M. R. Anoop et al. (2011), reported the synthesis, thermal and spectral study of 1,2-diphenyl-4-butyl-3,5-pyrazolidione(phenylbutazone) Lanthanide(III) complexes which were characterized by elemental analysis, IR, molar conductance, Uv-Vis and NMR spectra. In their study the spectra show that the phenylbutazones act as a bidentate and mono-ionic ligand coordinating at the carbonyl oxygen of the ligand ring. TGA analysis showed the thermal stability of the complex and the kinetic and thermodynamic parameters were also evaluated for the dehydration and decomposition state of the complexes. From the different spectral characterizations analysis data they have given the possible structure of the complexes¹⁴⁹ which is shown in figure 1.13.

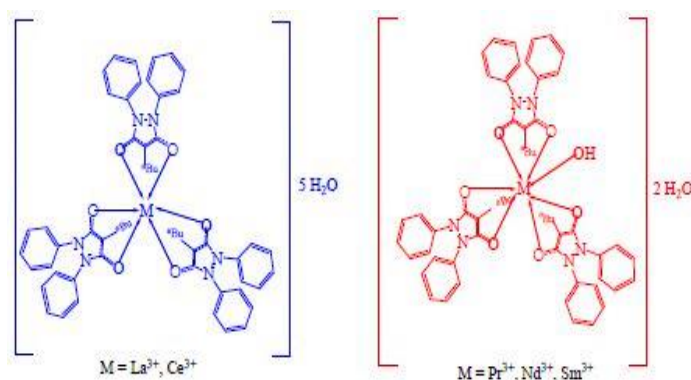


Figure 1.13. Possible Structures of Lanthanide(III) Complexes.

R. Gupta and his group (2012) synthesized a biologically active La(III), Sm(III), Gd(III) and Dy(III) complexes with furan-2-carboxylic acid as ligand and their spectra were characterized and reported. The synthesized complexes were found to have more promising activity than that of the ligand itself¹⁵⁰.

A. Hussain et al. (2012) synthesized Lanthanide(III) complexes (figure 1.14) with 4-phenyl-2,2,6,2-terpyridine, curcumin and diglucosylcurcumin and studied their DNA photocleavage and photocytotoxicity activity. The coordination between the ligands and the Ln³⁺ ions increase the hydrolytic stability and photocytotoxicity of the ligands. This study made a way for the Lanthanide(III) complexes to the field of photochemotherapeutic applications as the synthesized complexes were found to be suitable for photochemotherapeutic applications as it doesn't show any hydrolytic DNA cleavage activity and it also show photocytotoxicity in HeLa cancer cells¹⁵¹.

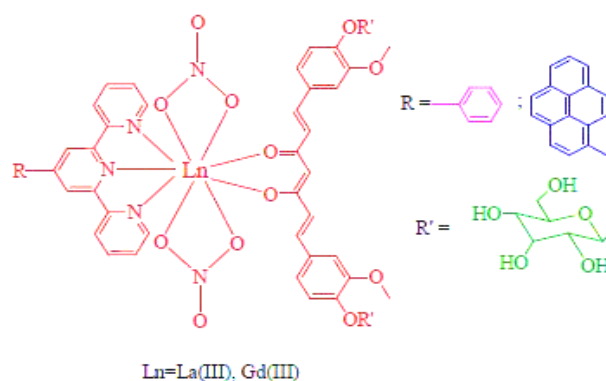


Figure 1.14. Schematic Structures of Lanthanide Complexes.

X. Hu et al. (2013) successfully synthesized series of Lanthanide amidate complexes by direct protonolysis and studied its structural diversity. The characterization data show that the complexes possessed abundant and different structures with varying coordination mode. Coordinations at the carbonyl oxygen site of the ligand both in the anionic and neutral with rare earth metal complexes, high molecular weight and low distributions of molecular weight of heterotactic-rich polymers and the ability for the ring opening polymerization of rac-lactide using lanthanide amidate complexes as a catalyst were also reported in this study¹⁵².

L. Zhao et al. (2014) by simple silylamine elimination prepared two novel amidate rare-earth metal amide of Ln[SiMe₃]₂]₃ and proligand N-(2,6-diisopropylphenyl) benzamide (figure 1.15), both the complexes were reported to have two chelating amidate; coordinated tetrahydrofuran and amino group molecule. Complexes were also found to

have an excellent catalytic activity for aldehydes and a moderate activity for inactivated ketones¹⁵³.

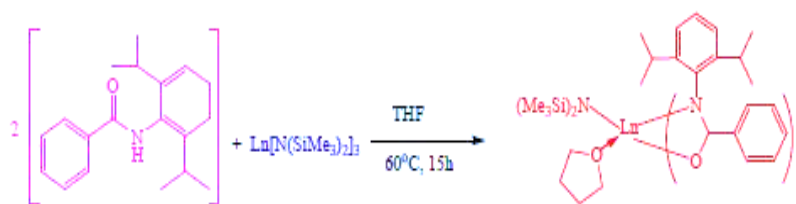


Figure 1.15. Synthesis of Earth Metal Complexes.

S. M. A. Barody and H. Ahmad, (2015) synthesized four Ln (III) complexes [where Ln=La(III), Ce(III), Sm(III) and Gd(III)]. The ligand used was a new mesogen Schiff base name N-N-di-(pentyloxybenzoate) salicylidene-1,3-diamino propane which was prepared by 1:2 reaction of 4-pentyloxy(4'-formyl-3'-hydroxy)-benzoate and 1,3-diaminopropane. The complexes are characterized by FT-IR, elemental analysis, NMR, Mass, magnetic susceptibility and molar conductivity. Investigation of the data collected shows that two of the ligands is bonding to the metal in stereochemistry: one deprotonated phenolic oxygen and the other bidentate through phenolic oxygen (figure 1.16). From the studies of thermal stability TGA/DSC curve of the complexes, it was found to be very stable thermally¹⁵⁴.

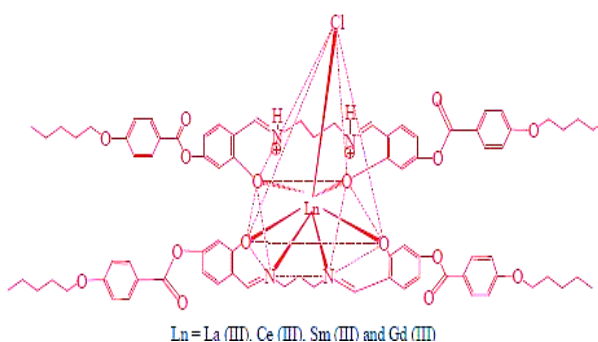


Figure 1.16. Suggested Molecular Structure of the Lanthanide Complexes.

R. Su et al. (2016), reported a Lanthanide polymer nanostructure by templatefree solvothermal methods using DMF as a solvent and ligand 2-methyl benzoic acid. The outcome of the reaction was characterized by elemental analysis, powder X-ray diffraction, scanning electron microscopy and downward luminescence which give a characteristic transitions¹⁵⁵.

Berezhnytska et al. (2017), synthesized a series of polycomplexes of Neodymium(III) nitrate with 2-methyl-5-phenylpenten-1-3,5-dione and allyl-3-oxo-

butanoate. The nature and the structure of the coordination were found to be dependent on the ligand and they remain constant on polymerization which was important for the investigation of the coordination and the structure of the polyhydra¹⁵⁶.

C. Lian et al. (2017), reported a synthesized and characterized novel coordinated polymer of Ln(III) (Ln=Pr(III), Gd(III) and Yb(III)) and 1,1-(2,4,6-trimethylbenzene-1,3,5-triyl(methylene))- tris (pyridine-4-carboxylic acid) and N,N-dimethylacetamide as ligand. Examining the polymer, they are found to be isomorphous and iso-structural exhibiting the cavate 14- membered cages which gives infinite 1D metallic chain through two COO- groups that later interlinks to polymerize into 3D porous scaffold. The study also shows that they can be used as a luminescent probe toward Pd²⁺ ions¹⁵⁷.

I. Olyshevets et al. (2018) synthesized Lanthanide(III) complexes using dimethyl[(4-methylphenyl)sulfonyl] amido phosphate as a ligand and single-crystal to single-crystal phase transition phase of the newly anion (figure 1.17), characterized, studied and reported. The study leads to a highly thermal stability, red luminescence dominated by ⁵D₀ - ⁷F₄ transition and a longer emission decay period which support the complexes for further application in light-emitting diode¹⁵⁸.

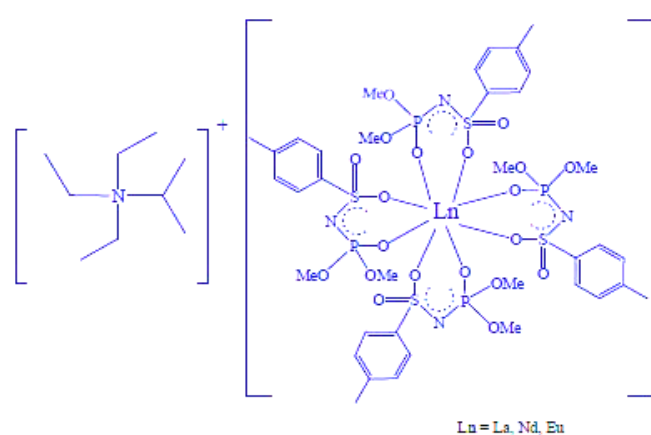


Figure 1.17. Schematic Representations of Lanthanide(III) Complexes.

M. P. C. Campello et al. (2019), reported a series of Lanthanide (III) complexes which were stabilized by a mixed ligand of three β -diketonate units and a phenanthroline derivative (figure 1.18). Using DMSO and PBS as a solvent UV-Vis and florescent spectra were recorded exhibiting absorption and emission bands at 350 nm and 520 nm respectively. The complexes show a similar cytotoxic activity towards ovarian cancer cells and the effect of the complexes, particularly the Eu (III) complex in the mitochondria and lysosome which were determined through Transition Electron Microscopy (TEM).

These studies pointed out the potentiality of the complexes as an anticancer agents which could challenge future investigations¹⁵⁹.

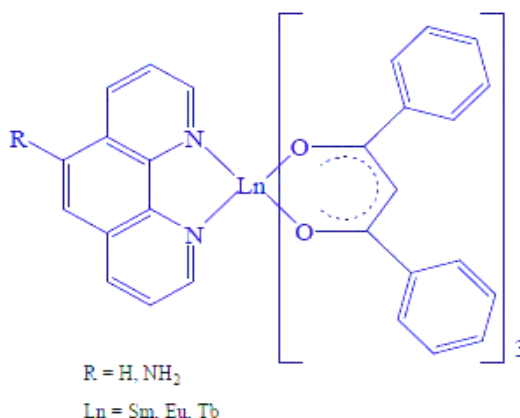


Figure 1.18. Molecular Structures of the Complexes.

Lanthanide complexes are making a remarkable way into synthetic clay as they exhibit a charismatic trait. Y. Wang et al. (2019), outline the development of the luminescent organic-inorganic material using Lanthanide complexes as the host. The study provides excellent aqueous solubility, a hydrogel with self-sustaining, and thin, flexible and independent films of the hybrid material. The luminescent properties of the Lanthanide complexes were retained even on the impact of the clay and so, it boosted the luminescence of the hybrid material which was used for the chemical molecule and the sensing of metal ions luminescent. In view of the different traits that the hybrid exhibit, its novel material was reported to be auspicious in the field of biology, therapeutic, security and solar cells¹⁶⁰.

In 2020, R. Li et al. reported the synthesis of Lanthanide(III) complexes as a suitor for the photoluminescence device and a photo-magnetic functional using Ln(III), Sm(III), Dy(III) and 2,2'-bipyridine-6,6'-dicarboxylic acid. Their magnetic properties, florescent properties and crystallography of the compounds were examined; showing a long-lasting luminescence, excellent quantum capability and a strong f-f transition. Dy(III) complex shows a single magnetic manner and were moderate in magnetization, which can be served as the photo-magnetic activity¹⁶¹.

R. Fouad (2020) set-forth unique potential biological agents of Lanthanide(III) complexes that were synthesized through a reaction between two biologically active molecules 2-carbaldehyde thiophene and salicylic acid hydrazide, and Sm(NO₃)₃.6H₂O, Eu(NO₃)₃.6H₂O, Dy(NO₃)₃.6H₂O, and LaCl₃.6H₂O. On exploring the complexes, it was disclosed that the coordination was at the OONS site of the donor ligand (figure 1.19) and

characterization was done through different methods such as the FT-IR, Mass, H^1 NMR, molar conductance and elemental analysis for further studies. The complexes were also reported to exhibit promising anti-tumour, anti-microbial, anti-oxidant agents and anti-microbial agents against bacteria which are more convincing than that of the reference drug¹⁶².

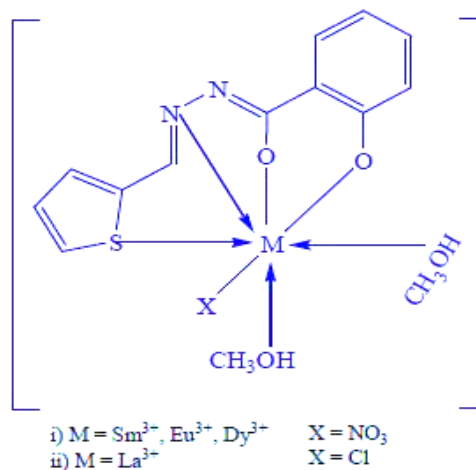


Figure 1.19. Structure of Lanthanide Metal Complexes.

T.D. Nguyen and group (2020) synthesized a highly-purified f-element nitrate using Lanthanides as there is a struggle to obtain it in a pure form which mostly preferred sophisticated apparatus with high temperatures. Using an aqueous reaction, the lanthanide complexes were prepared by combining Lanthanide salts (Lanthanum, Cerium, Praseodymium, Neodymium and Europium) and a ligand which holds high nitrogen (5,5'-bis(tetrazolato)amine monohydrate). Nano-structural lanthanide nitrate, formed were obtained on dehydration of the synthesized complexes as under an inert environment, they have the ability to go through self-extension burning reaction. The study shows that the Ln^{3+} ions possessed a very low reduction potential, so they must react with the nitrogen to give Ln(III) nitrate rather than Lanthanide itself. This new way of producing authentic Lanthanides/Actinides nitrate may provide a way into the application in nuclear fuels in the coming days¹⁶³.

L. Zeybel and D. A. Köse (2021) reported a hydrothermal synthesis of Lanthanide cations (Eu, Tb, Ho, Er, Yb) with acesulfame-K (figure 1.20). The synthesized complexes were analyzed and characterized through Mass, NMR, IR, Solid state UV-Vis and elemental analysis. On examining the TGA curve shows that the hydrated water coordinates outside the coordination sphere. The coordination of the complexes was found to be six coordinates¹⁶⁴.

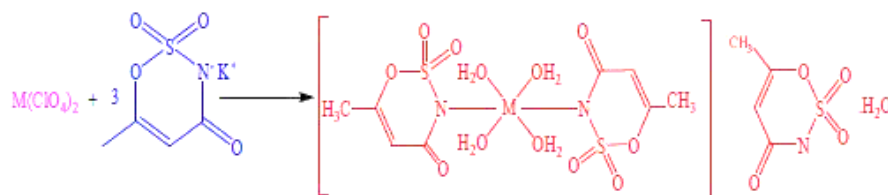


Figure 1.20. Synthesis of Acesulfame Lanthanide Metal Complexes.

Lanthanide complexes have drawn the interest of many researchers to synthesize, characterize and investigate their applications, and with it L. Zhu et al. (2021) reported satisfactory coordination for stabilizing Lanthanide monochloride and monoborohydrate using β -diketiminato as the ligand (figure 1.21). On the investigation of the ring-opening polymerization in lactide, Lanthanide monoborohydrate was found to have an efficient capability for L-lactide and rac-lactide to give the α,ω -telechelic poly lactide diols with high molecule weight and moderate molecular weight distribution¹⁶⁵.

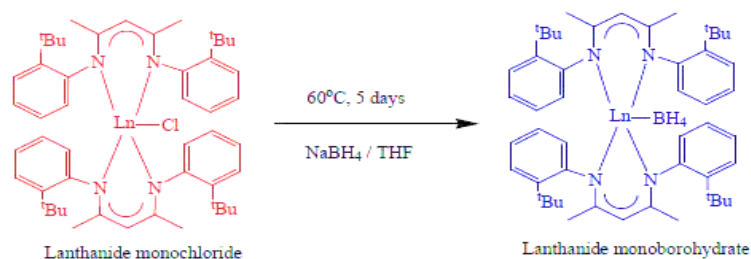


Figure 1.21. Synthesis of Lanthanide Monoborohydrate from Lanthanide Monochloride Complexes.

Lanthanide complexes have many other implementations in different fields. Complexes of Lanthanides have made its way into the field of nano science and technology as the complexes can decompose to oxide molecule of nano size¹⁶⁶. Lanthanide complexes were also found to have DNA cleaving ability and with increase in time the potentiality of the complexes also increases due to the change in the DNA strain on the insertion of the complex into the DNA^{167,168}. The complexes of Lanthanides were found to have capability to act as antibacterial agents to fight pathogenic strains that causes urinary tract infections¹⁶⁹. Currently hydrolysis is securing a lot of interest in biotechnology and as the lanthanide ions have been discovered to obtain phosphodiesterolytic activity with increasing pH, they made a way into biotechnology province¹⁷⁰. As Lanthanides hold a long lifetime period of emission, they applied as

luminescent biolabeling. They can be found in the market as Lanthanide label kit which can be utilized for the labeling¹⁷¹.

1.6. Chemical Kinetics

Chemical kinetics is the area of chemistry that deals with understanding the mechanism and rate of chemical reactions. It is a positive number that expresses how a reactant's or product's concentration changes throughout the course of a reaction. The concentration of the reactants steadily falls while that of the products gradually increases as a reaction progresses. When the temperature changes, a reaction's pace changes significantly. Every 10° degree rise in temperature has been found to result in an increase in the rate of reaction 2 to 3 times. This is caused by an increase in the number of molecules that exceed the threshold energy (E_T) due to an increase in the number of collisions that actually occur as temperature rises¹⁷².

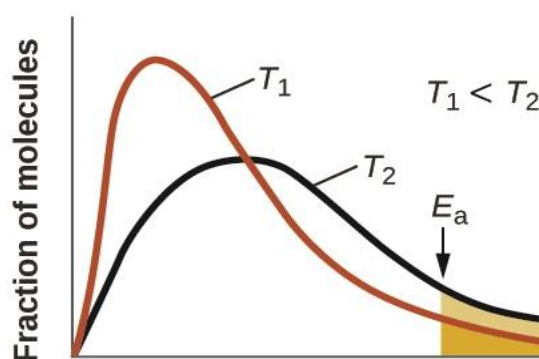


Figure 1.22. Effect of temperature on the rate of reaction.

Change of activation energy with temperature The activation energy is discovered to be almost constant over a constrained temperature range. But accurate measurements across a large temperature range reveal that the activation energy rises as the temperature falls, i.e., it tends to rise at lower temperatures.

Concept of activation energy (E_a)

In 1897, Arrhenius put forth the idea of activation energy (E_a). Arrhenius asserted that the process of turning the reactant into the product is not one of a downward slope (process taking place of its own). Instead, before the interacting molecules transform to products, they must pass an energy barrier. An idealised high energy state between the reactants and products is the energy-barrier. Threshold energy is the quantity of energy that corresponds to the top of the energy barrier (E_T). The reacting molecules must obtain this amount of energy at a minimum before they may react. Activated molecules are those

responding molecules whose energy is greater than or equal to the threshold energy, which is located at the top of the energy barrier.

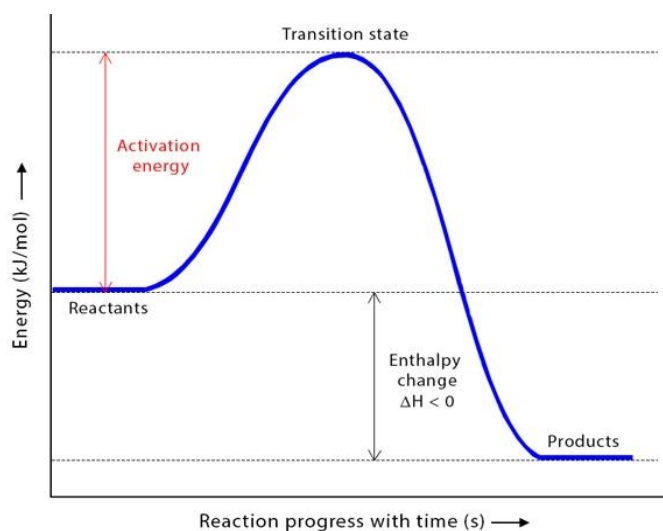


Figure 1.23. The concept of activation energy

The activation energy is the additional energy that the molecules that are reacting must receive in addition to their normal energy in order to react.

Thus, Activation energy = Threshold energy – Average energy of the reactant molecules.

Or, $E_a = E_T - E_R$

Depending upon the magnitude of the activation energy, the following three cases are possible:

- i) When the activation energy (E_a) is small, the reaction is fast.
- ii) When the activation energy (E_a) is large, the reaction is slow.
- iii) When the activation energy (E_a) is zero (0), the reaction is very fast or instantaneous.

1.7. Scope and Aim of the study

Over the past few decades, Lanthanide complexes have gained a lot of attention in various research due to their implementation in Inorganic chemistry, Organometallic, Industries, Agriculture, Biotechnology, Biomolecular, Lighting Device, Imaging, Labeling and nano-sciences. Currently one of the most needed magnetic and luminescent materials for LEDs, Bio-medical, NMR shift reagent, MRI contrast agent, telecommunication and lasers need to be synthesized with Lanthanide ions which have a unique magnetic and photophysical properties that could offer a charm and attraction to many researcher's interests. Lanthanide ions are known to be one of the best non-

enzymatic agents for DNA and RNA hydrolysis; they can also interact with peroxide and free radicals without forming into radicals.

Because of the vast applications and importance of Lanthanide complexes our interest was to synthesize a series of Lanthanide complexes using Praseodymium and some selected amino acids and pyridine as ligands and the spectral studies were carried out using UV-visible spectrophotometer through which the energy interaction and intensity parameters were computed. Elemental analysis, FT-IR, powdered XRD, photoluminescence spectrophotometer, molar conductometry and TGA were used for the characterization of the synthesized complexes. The characterization was used for conformations of the complexation, phase identification, cell parameters, thermal stability and to analyse the mode of coordination of the metal with ligands. The solubility of the synthesized complexes was recorded and their antimicrobial activities were also studied. The reaction pathway of the complexation is further studied through chemical kinetics and thermodynamic parameters were evaluated.

The present work will play a vital role in the forthcoming studies on the interaction of lanthanides with biomolecules in the field of biological chemistry. The synthesized complexes show good luminescence characteristics and could be useful in various photochemical applications. The complexes also exhibit good antimicrobial properties as compared to that of the metal and ligand alone and can be used in various therapeutic fields.

REFERENCES

1. Kido, J. & Okamoto, Y. Organo lanthanide metal complexes for electroluminescent materials. *Chem. Rev.* **102**, 2357–2368 (2002).
2. Reyes, R., Cremona, M., Teotonio, E. E. S., Brito, H. F. & Malta, O. L. Voltage color tunable OLED with (Sm,Eu)- β -diketonate complex blend. *Chem. Phys. Lett.* **396**, 54–58 (2004).
3. Faulkner, S. & Matthews, J. L. Fluorescent Complexes for Biomedical Applications. *Compr. Coord. Chem. II* **9**, 913–944 (2003).
4. Yam, V. W. W. & Lo, K. K. W. Luminescent polynuclear d 10 metal complexes. *Chem. Soc. Rev.* **28**, 323–334 (1999).
5. Sigel, H. *Metal Ions in Biological Systems : Volume 40: The Lanthanides and Their Interrelations with Biosystems*. vol. 40 (CRC Press, 2003).
6. Yamamoto, H., Shionoya, S. & Yen, W. M. *Phosphor Handbook. Phosphor Handbook* (CRC Press, 2007). doi:10.1201/9781315222066.
7. Kuriki, K., Koike, Y. & Okamoto, Y. Plastic optical fiber lasers and amplifiers containing lanthanide complexes. *Chem. Rev.* **102**, 2347–2356 (2002).
8. Bünzli, J. C. G. & Eliseeva, S. V. Lanthanide NIR luminescence for telecommunications, bioanalyses and solar energy conversion. *J. Rare Earths* **28**, 824–842 (2010).
9. Bünzli, J. C. G. & Milicic-Tang, A. Chapter 145 Solvation and anion interaction in organic solvents. *Handb. Phys. Chem. Rare Earths* **21**, 305–366 (1995).
10. Caravan, P., Ellison, J. J., McMurry, T. J. & Lauffer, R. B. Gadolinium(III) Chelates as MRI Contrast Agents: Structure, Dynamics, and Applications. *Chem. Rev.* **99**, 2293–2352 (1999).
11. Vandevyver, C. D. B., Chauvin, A. S., Comby, S. & Bünzli, J. C. G. Luminescent lanthanide bimetallic triple-stranded helicates as potential cellular imaging probes. *Chem. Commun.* 1716–1718 (2007) doi:10.1039/B701482A.
12. Cotton, S. A. Scandium, yttrium, the lanthanides. *Annu. Reports Sect. 'A' (Inorganic Chem.* **106**, 276–285 (2010).
13. Tsukube, H. & Shinoda, S. Lanthanide complexes in molecular recognition and chirality sensing of biological substrates. *Chem. Rev.* **102**, 2389–2403 (2002).
14. Bünzli, J. C. G. & Piguet, C. Lanthanide-containing molecular and supramolecular polymetallic functional assemblies. *Chem. Rev.* **102**, 1897–1928 (2002).
15. Greenwood N.N. & Earnshaw A. *Chemistry of the Elements*. vol. 55 (Elsevier

- Science, 2012).
16. Byrne, R. H. & Li, B. Comparative complexation behavior of the rare earths. *Geochim. Cosmochim. Acta* **59**, 4575–4589 (1995).
 17. Bünzli, J. C. G. & Piguet, C. Taking advantage of luminescent lanthanide ions. *Chem. Soc. Rev.* **34**, 1048–1077 (2005).
 18. Becquerel, J. Sur les variations des bandes d'absorption d'un crystal dans un champ magnétique. *Comp. rend Hebd. Acad. Sci.* **142**, (1906).
 19. Bethe, H. Zur Theorie des Zeemaneffektes an den Salzen der seltenen Erden. *Zeitschrift für Phys.* 1930 603 **60**, 218–233 (1930).
 20. Kramers, H. Théorie générale de la rotation paramagnétique dans les cristaux. *Proc. K. Akad. Wet. C* **33**, 959–972 (1930).
 21. Becquerel, J. Einleitung in eine Theorie der magneto-optischen Erscheinungen in Kristallen. *Zeitschrift für Phys.* 1929 583 **58**, 205–216 (1929).
 22. Van Vleck, J. H. On the Anisotropy of Cubic Ferromagnetic Crystals. *Phys. Rev.* **52**, 1178 (1937).
 23. Moeller, T. & Brantley, J. C. Observations on the Rare Earths. LVIII. Reaction between Neodymium and Ethylenediaminetetraacetate Ions in Aqueous Solution. *J. Am. Chem. Soc.* **72**, 5447–5451 (1950).
 24. Görller-Walrand, C. & Binnemans, K. Chapter 155 Rationalization of crystal-field parametrization. *Handb. Phys. Chem. Rare Earths* **23**, 121–283 (1996).
 25. Broer, L. J. F., Gorter, C. J. & Hoogschagen, J. On the intensities and the multipole character in the spectra of the rare earth ions. *Physica* **11**, 231–250 (1945).
 26. Ofelt, G. S. Intensities of Crystal Spectra of Rare-Earth Ions. *J. Chem. Phys.* **37**, 511 (2004).
 27. Judd, B. R. Optical Absorption Intensities of Rare-Earth Ions. *Phys. Rev.* **127**, 750 (1962).
 28. Görller-Walrand, C. & Binnemans, K. Chapter 167 Spectral intensities of f-f transitions. *Handb. Phys. Chem. Rare Earths* **25**, 101–264 (1998).
 29. Tanner, P. A. Spectra, Energy Levels and Energy Transfer in High Symmetry Lanthanide Compounds. 167–278 (2012) doi:10.1007/B96863.
 30. Blasse, G. Vibronic transitions in rare earth spectroscopy. <http://dx.doi.org/10.1080/01442359209353266> **11**, 71–100 (2008).
 31. Blasse, G. & Bril, A. Structure and Eu³⁺-fluorescence of lithium and sodium lanthanide silicates and germanates. *J. Inorg. Nucl. Chem.* **29**, 2231–2241 (1967).

-
32. Blasse, G. The influence of charge-transfer and rydberg states on the luminescence properties of lanthanides and actinides. *Spectra Chem. Interact.* 43–79 (1976) doi:10.1007/BFB0116577.
 33. Blasse, G. & Grabmaier, B. C. A General Introduction to Luminescent Materials. *Lumin. Mater.* 1–9 (1994) doi:10.1007/978-3-642-79017-1_1.
 34. Tanaka, M. & Kushida, T. J-mixing effect on the vibronic spectra of Eu³⁺ ions. *J. Alloys Compd.* **193**, 183–185 (1993).
 35. Tanaka, M., Nishimura, G. & Kushida, T. Contribution of J mixing to the 5D₀-7F₀ transition of Eu³⁺ ions in several host matrices. *Phys. Rev. B. Condens. Matter* **49**, 16917–16925 (1994).
 36. Wybourne, B. G. *Optical Properties of Ions in Crystals.* vol. 35 (Wiley Interscience, 1996).
 37. Downer, M. C., Burdick, G. W. & Sardar, D. K. A new contribution to spin-forbidden rare earth optical transition intensities: Gd³⁺ and Eu³⁺. *J. Chem. Phys.* **89**, 1787 (1998).
 38. Downer, M. C. The puzzle of two-photon rare earth spectra in solids. 29–75 (1989) doi:10.1007/3540501541_2.
 39. Burdick, G. W. & Downer, M. C. The role of linear crystal-field terms in hypersensitive Eu³⁺ optical transition intensities. *Eur. J. Solid State Inorg. Chem.* **28**, 217–220 (1991).
 40. Burdick, G. W. & Reid, M. F. Many-body perturbation theory calculations of two-photon absorption in lanthanide compounds. *Phys. Rev. Lett.* **70**, 2491 (1993).
 41. GRUEN, D. M., DEKOCK, C. W. & MCBETH, R. L. Electronic Spectra of Lanthanide Compounds in the Vapor Phase. 102–121 (1967) doi:10.1021/BA-1967-0071.CH008.
 42. Gruen, D. M. & Dekock, C. W. Absorption Spectra of Gaseous NdBr₃ and NdI₃. *J. Chem. Phys.* **45**, 455 (2004).
 43. Katzin, L. I. Absorption and circular dichroic spectral studies of europium(III) complexes with sugar acids and amino acids, with remarks on “hypersensitivity”. *Inorg. Chem.* **8**, 1649–1654 (1969).
 44. Moeller, T. & Brantley, J. C. Observations on the Rare Earths. LVIII. Reaction between Neodymium and Ethylenediaminetetraacetate Ions in Aqueous Solution. *J. Am. Chem. Soc.* **72**, 5447–5451 (1950).
 45. Moeller, T. & Jackson, D. E. The rare earths. *Anal. Chem.* **22**, 1393–1397 (1950).
-

-
46. Moeller, T. *Inorganic Syntheses. Inorganic Syntheses* vol. 5 (Wiley Blackwell, , 1957).
 47. Chrysochoos, J. & Evers, A. Effect of the primary and secondary solvation spheres of Eu^{3+} upon the electric-quadrupole transitions ($\Delta J = 2$). *Chem. Phys. Lett.* **18**, 115–119 (1973).
 48. Chrysochoos, J. Dependence of the intensity of the absorption bands of Eu^{3+} in solution upon the anions present. *J. Chem. Phys.* **60**, 1110 (2003).
 49. Sinha, S. P. Structure and bonding in highly coordinated Lanthanide complexes. 69–149 (1977) doi:10.1007/3-540-07508-9_3.
 50. Henrie, D. E., Fellows, R. L. & Choppin, G. R. Hypersensitivity in the electronic transitions of lanthanide and actinide complexes. *Coord. Chem. Rev.; (Netherlands)* **18**, 199–224 (1976).
 51. Mason, S. F. Lanthanide(III) f-f transition probabilities. *J. Indian Chem. Soc.* **63**, 73–79 (1986).
 52. Mason, S. F., Peacock, R. D. & Stewart, B. Ligand-polarization contributions to the intensity of hypersensitive trivalent lanthanide transitions. <http://dx.doi.org/10.1080/00268977500103321> **30**, 1829–1841 (2006).
 53. Misra, S. N. Energy interaction parameters and intensity analysis of praseodymium and neodymium complexes. *J. Sci. Res.* **44**, (1985).
 54. Karraker, D. G. Hypersensitive Transitions of Six-, Seven-, and Eight-Coordinate Neodymium, Holmium, and Erbium Chelates. *Inorg. Chem.* **6**, 1863–1868 (1967).
 55. Karraker, D. G. The Hypersensitive Transitions of Hydrated Nd^{3+} , Ho^{3+} , and Er^{3+} Ions. *Inorg. Chem.* **7**, 473–479 (1968).
 56. Choppin, G. R. & Fellows, R. L. HYPERSENSITIVITY IN COMPLEXES OF $\text{Nd}(\text{III})$ AND $\text{Ho}(\text{III})$ WITH MONOBASIC LIGANDS. <http://dx.doi.org/10.1080/00958977408073815> **3**, 209–215 (2006).
 57. Choppin, G. R. Speciation of trivalent f elements in natural waters. *J. Less-Common Met.* **126** p. **307**, (1986).
 58. Richardson, F. S. Selection Rules for Lanthanide Optical Activity. *Inorg. Chem.* **19**, 2806–2812 (1980).
 59. Devlin, M. T., Stephens, E. M. & Richardson, F. S. Comparison of Electric-Dipole Intensity Parameters for a Series of Structurally Related Neodymium, Holmium, and Erbium Complexes in Aqueous Solution. Theory and Experiment. *Inorg. Chem.* **27**, 1517–1524 (1988).
-

-
60. Misra, S. N. Interaction of some fluorinated nucleic acid components with praseodymium: an absorption spectral approach. *Indian J. Biochem. Biophys.* **27**, 284–290 (1990).
 61. Peacock, R. D. The intensities of lanthanide $f \leftrightarrow f$ transitions. *Rare Earths* 83–122 (1975) doi:10.1007/BFB0116556.
 62. Misra, S. N., Mehta, S. B., Chaudhari, K. G. & Suveerkumar, C. M. Electric dipole intensity parameters for a series of structurally related Nd(III) complexes and oscillator strengths of multiplet to multiplet electronic transitions. *Indian J. Chem. Sect. A Inorganic, Phys. Theor. Anal.* **33**, 893–897 (1994).
 63. Misra, S. N. & Mehta, S. B. Ligand-Mediated Pseudohypersensitivity of Some $4f-4f$ Transitions in Neodymium(III) Interaction with Fluorinated Nucleic Acid Components. <https://doi.org/10.1246/bcsj.64.3653> **64**, 3653–3658 (2006).
 64. Misra, S. N., Anjaiah, K., Joseph, G. & Abdi, S. H. Interactions of praseodymium and neodymium with nucleosides and nucleotides: absorption difference and comparative absorption spectral study. *Indian J. Biochem. Biophys.* **29**, 70–76 (1992).
 65. Blasse, G. & Grabmaier, B. C. *Luminescent Materials*. (Springer Berlin Heidelberg, 1994).
 66. Tester, R. F. & Karkalas, J. CARBOHYDRATES | Classification and Properties. *Encycl. Food Sci. Nutr.* 862–875 (2003) doi:10.1016/B0-12-227055-X/00166-8.
 67. Geiger, O., González-Silva, N., López-Lara, I. M. & Sohlenkamp, C. Amino acid-containing membrane lipids in bacteria. *Prog. Lipid Res.* **49**, 46–60 (2010).
 68. Vranova, V., Rejsek, K., Skene, K. R. & Formanek, P. Non-protein amino acids: Plant, soil and ecosystem interactions. *Plant Soil* **342**, 31–48 (2011).
 69. Zurita, J. Amino acids with relevance to health, climate and the environment Development of mass spectrometric methods. (2018).
 70. Howland, J. *Biochemistry: By D Voet and J G Voet*. pp 1223. John Wiley and Sons, New York. 1990 ISBN. *Biochem. Educ.* **18**, 212–212 (1990).
 71. Martin, D. W., Mayes, A. P. and & Rodwell, V. W. *Harper's Review of Biochemistry, Lange Medical Publications*. (Lange Medical Publications, 1983).
 72. Armstrong, P. W. *et al.* Fibrinolysis or primary PCI in ST-segment elevation myocardial infarction. *N. Engl. J. Med.* **368**, 1379–1387 (2013).
 73. Koblin, D. D. *et al.* Effect of Nitrous Oxide on Folate and Vitamin B12 Metabolism in Patients. *undefined* **71**, 610–617 (1990).
-

-
74. Gökbuget, N. & Hoelzer, D. High-dose methotrexate in the treatment of adult acute lymphoblastic leukemia. *Ann. Hematol.* **72**, 194–201 (1996).
 75. Cai, Q., Takemura, G. & Ashraf, M. Antioxidative properties of histidine and its effect on myocardial injury during ischemia/reperfusion in isolated rat heart. *J. Cardiovasc. Pharmacol.* **25**, 147–155 (1995).
 76. Ouzou, S., Deflandre, A. & Giacomoni, P. U. Protonation of the imidazole ring prevents the modulation by histidine of oxidative DNA degradation. *Mutat. Res.* **316**, 9–16 (1994).
 77. Boldyrev, A. A. & Severin, S. E. The histidine-containing dipeptides, carnosine and anserine: distribution, properties and biological significance. *Adv. Enzyme Regul.* **30**, 175–188 (1990).
 78. Nishihira, T., Takagi, T. & Mori, S. Amino acid imbalance and intracellular protein synthesis. *undefined* (1993).
 79. Vieira-Makings, E., van der Westhuyzen, J. & Metz, J. Both valine and isoleucine supplementation delay the development of neurological impairment in vitamin B12 deficient bats. *Int. J. Vitam. Nutr. Res.* **60**, 41–46 (1990).
 80. Henry, G. D. De novo Synthesis of Substituted Pyridines. *ChemInform* **35**, no-no (2004).
 81. Chohan, Z. H., Supuran, C. T. & Scozzafava, A. Metal binding and antibacterial activity of ciprofloxacin complexes. <http://dx.doi.org/10.1080/14756360310001624948> **20**, 303–307 (2008).
 82. Chohan, Z. H., Scozzafava, A. & Supuran, C. T. Unsymmetrical 1,1'-disubstituted Ferrocenes: Synthesis of Co(ii), Cu(ii), Ni(ii) and Zn(ii) Chelates of Ferrocenyl -1-thiadiazolo-1'-tetrazole, -1-thiadiazolo-1'-triazole and -1-tetrazolo-1'-triazole with Antimicrobial Properties. <http://dx.doi.org/10.1080/1475636021000006261> **17**, 261–266 (2008).
 83. Chohan, Z. H., Arif, M., Akhtar, M. A. & Supuran, C. T. Metal-based antibacterial and antifungal agents: Synthesis, characterization, and in vitro biological evaluation of Co(II), Cu(II), Ni(II), and Zn(II) complexes with amino acid-derived compounds. *Bioinorg. Chem. Appl.* **2006**, (2006).
 84. Singh, K., Singh, D. P., Singh Barwa, M., Tyagi, P. & Mirza, Y. Antibacterial Co(II), Ni(II), Cu(II) and Zn(II) Complexes of Schiff bases Derived from Fluorobenzaldehyde and Triazoles. <http://dx.doi.org/10.1080/14756360600642131> **21**, 557–562 (2008).
-

-
85. Singh, K., Kumar, Y., Puri, P. & Singh, G. Spectroscopic, thermal, and antimicrobial studies of Co(II), Ni(II), Cu(II), and Zn(II) complexes derived from bidentate ligands containing N and S donor atoms. *Bioinorg. Chem. Appl.* **2012**, (2012).
 86. Fasina, T. M., Ejia, F. N., Dueke-Eze, C. U. and Idika, N. Substituent Effect on the Antimicrobial Activity of Schiff Bases Derived from 2-aminophenol and 2-aminothiophenol. *Int. J. Biol. Chem.* **7**, 79–85 (2013).
 87. Sumrta, S. H., Habiba, U., Zafar, W., Imran, M. & Chohan, Z. H. A review on the efficacy and medicinal applications of metal-based triazole derivatives. <https://doi.org/10.1080/00958972.2020.1839751> **73**, 2838–2877 (2020).
 88. Ndagi, U., Mhlongo, N. & Soliman, M. E. Metal complexes in cancer therapy – An update from drug design perspective. *Drug Des. Devel. Ther.* **11**, 599–616 (2017).
 89. Bünzli, J. Claude G. The europium(III) ion as spectroscopic probe in bioinorganic chemistry. *Inorganica Chim. Acta* **139**, 219–222 (1987).
 90. Parker, D., Kanthi Senanayake, P. & Gareth Williams, J. A. Luminescent sensors for pH, pO₂, halide and hydroxide ions using phenanthridine as a photosensitizer in macrocyclic europium and terbium complexes. *J. Chem. Soc. Perkin Trans. 2* **0**, 2129–2140 (1998).
 91. Beltyukova, S. V. & Egorova, A. V. Terbium chelates for fluoroimmunoassays. *J. Pharm. Biomed. Anal.* **18**, 267–270 (1998).
 92. Elbanowski, M. & Mąkowska, B. The lanthanides as luminescent probes in investigations of biochemical systems. *J. Photochem. Photobiol. A Chem.* **99**, 85–92 (1996).
 93. Hemmilä, I., Mikkilä, V. M. & Takalo, H. Development of luminescent lanthanide chelate labels for diagnostic assays. *J. Alloys Compd.* **249**, 158–162 (1997).
 94. Wang, K., Li, R., Cheng, Y. & Zhu, B. Lanthanides—the future drugs? *Coord. Chem. Rev.* **190–192**, 297–308 (1999).
 95. Beltyukova, S. V., Tselik, E. I. & Egorova, A. V. Use of sensitized luminescence of lanthanides in analysis of drugs. *J. Pharm. Biomed. Anal.* **18**, 261–266 (1998).
 96. Aime, S., Botta, M., Fasano, M. & Terreno, E. Lanthanide(III) chelates for NMR biomedical applications. *Chem. Soc. Rev.* **27**, 19–29 (1998).
 97. Aime, S. *et al.* Non-ionic Ln(III) chelates as MRI contrast agents: Synthesis, characterisation and ¹H NMR relaxometric investigations of bis(benzylamide)diethylenetriaminepentaacetic acid Lu(III) and Gd(III)
-

- complexes. *Inorganica Chim. Acta* **254**, 63–70 (1997).
98. Bligh, S. W. A. *et al.* Synthesis and crystal structure of a gadolinium(III) complex of a tetraimine schiff-base macrocycle: A potential contrast agent for magnetic resonance imaging. *Polyhedron* **11**, 2571–2573 (1992).
99. Smirnova, T. I., Smirnov, A. I., Belford, R. L. & Clarkson, R. B. Lipid Magnetic Resonance Imaging Contrast Agent Interactions: A Spin-Labeling and a Multifrequency EPR Study. *J. Am. Chem. Soc.* **120**, 5060–5072 (1998).
100. Bushby, L. M. Photochemistry and photophysics of lanthanide complexes. (2001).
101. Tissue, B. M. Synthesis and Luminescence of Lanthanide Ions in Nanoscale Insulating Hosts. *Chem. Mater.* **10**, 2837–2845 (1998).
102. Slooff, L. H. *et al.* Optical properties of erbium-doped organic polydentate cage complexes. *J. Appl. Phys.* **83**, 497 (1998).
103. Zhang, Q. J. *et al.* Amplified spontaneous emission of an Nd³⁺-doped poly(methyl methacrylate) optical fiber at ambient temperature. *Appl. Phys. Lett.* **72**, 407 (1998).
104. Heller, A. Liquid lasers—Fluorescence, absorption and energy transfer of rare earth ion solutions in selenium oxychloride. *J. Mol. Spectrosc.* **28**, 208–232 (1968).
105. Andrews, D. L. Lasers in Chemistry. 232 (1997).
106. Kanellopoulos, A. J. Laser cataract surgery: A prospective clinical evaluation of 1000 consecutive laser cataract procedures using the Dodick photolysis Nd:YAG system. *Ophthalmology* **108**, 649–654 (2001).
107. Quade, M. *et al.* Neodymium:YAG 30-W cw laser side pumped by three diode laser bars. *Appl. Opt. Vol. 37, Issue 12, pp. 2361-2364* **37**, 2361–2364 (1998).
108. Payne, S. A. *et al.* Ytterbium-doped apatite-structure crystals: A new class of laser materials. *J. Appl. Phys.* **76**, 497 (1998).
109. Samelson, H., Lempicki, A., Brecher, C. & Brophy, V. ROOM-TEMPERATURE OPERATION OF A EUROPIUM CHELATE LIQUID LASER. *Appl. Phys. Lett.* **5**, 173 (2004).
110. Bernard, J. E., Whitford, B. G. & Madej, A. A. A Tm:YAG laser for optical frequency measurements: mixing 148 THz light with CO₂ laser radiation. *Opt. Commun.* **140**, 45–48 (1997).
111. Pratisto, H., Ith, M., Frenz, M. & Weber, H. P. Infrared multiwavelength laser system for establishing a surgical delivery path through water. *Appl. Phys. Lett.* **67**, 1963 (1998).
112. Heller, A. Liquid lasers—Design of neodymium-based inorganic ionic systems. *J.*

- Mol. Spectrosc.* **28**, 101–117 (1968).
113. Miyamoto, Y., Uekawa, M., Ikeda, H. & Kaifu, K. Electroluminescent properties of a Eu-complex doped in phosphorescent materials. *J. Lumin.* **81**, 159–164 (1999).
114. Okada, K. *et al.* Bright red light-emitting organic electroluminescent devices based on a novel thiophene-containing europium complex as an emitting layer. *J. Mater. Chem.* **9**, 3023–3026 (1999).
115. Christou, V. *et al.* New molecular lanthanide materials for organic electroluminescent devices. *Synth. Met.* **111–112**, 7–10 (2000).
116. Moses, D., Dogariu, A. & Heeger, A. J. Mechanism of carrier generation and recombination in conjugated polymers. *Synth. Met.* **116**, 19–22 (2001).
117. Huang, Y. J. *et al.* Excitation Energy-Transfer Processes in the Sensitization Luminescence of Europium in a Highly Luminescent Complex. *ChemistryOpen* **8**, 388–392 (2019).
118. Ribeiro Da Silva, M. D. M. C. *et al.* Three N₂O₂ ligands derived from the condensation of 1,2-cyclohexanediamine with salicylaldehyde, acetylacetone and benzoylacetone: A new contribution to the energetical characterization of Schiff bases. *J. Therm. Anal. Calorim.* **87**, 291–296 (2007).
119. KOSTOVA, I. P., MANOLOV, I. I. & RADULOVA, M. K. Stability of the complexes of some lanthanides with coumarin derivatives. I. Cerium(III)-4-methyl-7-hydroxycoumarin. *Acta Pharm.* **54**, 37–47 (2004).
120. Gonzalez, V., Vignati, D. A. L., Leyval, C. & Giamberini, L. Environmental fate and ecotoxicity of lanthanides: Are they a uniform group beyond chemistry? *Environ. Int.* **71**, 148–157 (2014).
121. Zhang, C. X., Qiao, X. M., Chen, H. W. & Zhang, Y. Y. Syntheses and Biological Activities of Lanthanide Metal Complexes with Nitronly Nitroxide. <http://dx.doi.org/10.1080/15533174.2013.819914> **45**, 145–150 (2014).
122. Na, H. B. *et al.* Development of a T1 Contrast Agent for Magnetic Resonance Imaging Using MnO Nanoparticles. *Angew. Chemie* **119**, 5493–5497 (2007).
123. Tóth, É., Helm, L. & Merbach, A. Relaxivity of Gadolinium(III) Complexes: Theory and Mechanism. *Chem. Contrast Agents Med. Magn. Reson. Imaging Second Ed.* 25–81 (2013) doi:10.1002/9781118503652.CH2.
124. Osawa, M., Hoshino, M., Wada, T., Hayashi, F. & Osanai, S. Intra-complex energy transfer of europium(III) complexes containing anthracene and phenanthrene moieties. *J. Phys. Chem. A* **113**, 10895–10902 (2009).

-
125. Misra, S. N., Gagnani, M. A., Indira, D. M. & Shukla, R. S. Biological and Clinical Aspects of Lanthanide Coordination Compounds. *Bioinorg. Chem. Appl.* **2**, 155 (2004).
126. Zapała, L., Kosińska, M., Woźnicka, E., Byczyński, Ł. & Zapała, W. Synthesis, spectral and thermal study of La(III), Nd(III), Sm(III), Eu(III), Gd(III) and Tb(III) complexes with mefenamic acid. *J. Therm. Anal. Calorim.* **124**, 363–374 (2016).
127. Burgess, J. Kinetic aspects of chemical speciation. *Analyst* **117**, 605–611 (1992).
128. Agarwal, R. K., Arora, K. & Dutt, P. Some high coordination compounds of thorium(IV) and dioxouranium(VI) derived from hydrazones of isonicotinic acid hydrazide. *Polyhedron* **13**, 957–964 (1994).
129. Agarwal, R. K., Garg, R. & Sindhu, S. K. SYNTHESIS, SPECTRAL AND THERMAL PROPERTIES OF SOME HIGH COORDINATED COMPLEXES OF THORIUM(IV) AND DIOXOURANIUM(VI) DERIVED FROM 4[N-(2'-HYDROXY-1'-NAPHTHALIDENE)AMINO] ANTIPYRINETHIOSEMICARBAZONE. *Bull. Chem. Soc. Ethiop.* **19**, 185–195 (2005).
130. Singh, L., Tyagi, N. & Dhaka, N. P. Synthesis and physico-chemical characteristics of some dioxouranium (VI) complexes of N-isonicotinamido-3-methoxy-4-hydroxy benzalaldimine and n-isonicotinamidocinnamalaldimine. *Asian J. Chem.* **10**, (1998).
131. Barry, D. E., Caffrey, D. F. & Gunnlaugsson, T. Lanthanide-directed synthesis of luminescent self-assembly supramolecular structures and mechanically bonded systems from acyclic coordinating organic ligands. *Chem. Soc. Rev.* **45**, 3244–3274 (2016).
132. Parker, D., Dickins, R. S., Puschmann, H., Crossland, C. and Howard, J. A. K. Being Excited by Lanthanide Coordination Complexes: Aqua Species, Chirality, Excited-State Chemistry, and Exchange Dynamics. *Chem. Rev.* **102**, 1977–2010 (2002).
133. Roy, B. C., Santos, M., Mallik, S. & Campiglia, A. D. Synthesis of metal-chelating lipids to sensitize lanthanide ions. *J. Org. Chem.* **68**, 3999–4007 (2003).
134. Gusev, A. N. *et al.* Synthesis, structure and luminescence studies of Eu(III), Tb(III), Sm(III), Dy(III) cationic complexes with acetylacetone and bis(5-(pyridine-2-yl)-1,2,4-triazol-3-yl)propane. *Inorganica Chim. Acta* **406**, 279–284 (2013).
135. El-Ansary, A. L. & Abdel-Kader, N. S. Synthesis, Characterization of La(III),
-

- Nd(III), and Er(III) Complexes with Schiff Bases Derived from Benzopyran-4-one and Their Fluorescence Study. *Int. J. Inorg. Chem.* **2012**, 1–13 (2012).
136. Carac, A., Boscencu, R., Carac, G. & Bungau, S. Spectral Study of Some Lanthanides Complexes with Quaternary Pyridinium Ligands. *researchgate.net*.
137. Alghool, S., Abd El-Halim, H. F., Abd El-Sadek, M. S., Yahia, I. S. & Wahab, L. A. Synthesis, thermal characterization, and antimicrobial activity of lanthanum, cerium, and thorium complexes of amino acid Schiff base ligand. *J. Therm. Anal. Calorim.* **112**, 671–681 (2013).
138. Wang, X. L. *et al.* Synthesis, crystal structure and DNA cleavage activities of copper(II) complexes with asymmetric tridentate ligands. *J. Inorg. Biochem.* **98**, 423–429 (2004).
139. XU, D., MA, S., DU, G., HE, Q. & SUN, D. Synthesis, characterization, and anticancer properties of rare earth complexes with Schiff base and o-phenanthroline. *J. Rare Earths* **26**, 643–647 (2008).
140. Easmon, J. *et al.* Synthesis, cytotoxicity, and antitumor activity of copper(II) and iron(II) complexes of 4N-azabicyclo[3.2.2]nonane Thiosemicarbazones derived from acyl diazines. *J. Med. Chem.* **44**, 2164–2171 (2001).
141. Maravalli, P. B. & Goudar, T. R. Thermal and spectral studies of 3-N-methyl-morpholino-4-amino-5-mercapto-1,2,4-triazole and 3-N-methyl-piperidino-4-amino-5-mercapto-1,2,4-triazole complexes of cobalt(II), nickel(II) and copper(II). *Thermochim. Acta* **325**, 35–41 (1999).
142. Kostova, I., Manolov, I., Nicolova, I., Konstantinov, S. & Karaivanova, M. New lanthanide complexes of 4-methyl-7-hydroxycoumarin and their pharmacological activity. *Eur. J. Med. Chem.* **36**, 339–347 (2001).
143. Kostova, I., Trendafilova, N. & Momekov, G. Theoretical and spectroscopic evidence for coordination ability of 3,3'-benzylidenedi-4-hydroxycoumarin. New neodymium (III) complex and its cytotoxic effect. *J. Inorg. Biochem.* **99**, 477–487 (2005).
144. Kostova, I., Kostova, R., Momekov, G., Trendafilova, N. & Karaivanova, M. Antineoplastic activity of new lanthanide (cerium, lanthanum and neodymium) complex compounds. *J. Trace Elem. Med. Biol.* **18**, 219–226 (2005).
145. Alptürk, O. *et al.* Lanthanide complexes as fluorescent indicators for neutral sugars and cancer biomarkers. *Proc. Natl. Acad. Sci. U. S. A.* **103**, 9756–9760 (2006).
146. Kumari, B. S., Rijulal, G. & Mohanan, K. Microwave Assisted Synthesis,

- Spectroscopic, Thermal and Biological Studies of Some Lanthanide(III) Chloride Complexes with a Heterocyclic Schiff Base. <http://dx.doi.org/10.1080/15533170802679550> **39**, 24–30 (2011).
147. Moaienla, T., Singh, T. D., Singh, N. R. & Devi, M. I. Computation of energy interaction parameters as well as electric dipole intensity parameters for the absorption spectral study of the interaction of Pr(III) with l-phenylalanine, l-glycine, l-alanine and l-aspartic acid in the presence and absence of Ca²⁺. *Spectrochim. Acta Part A Mol. Biomol. Spectrosc.* **74**, 434–440 (2009).
148. Rao, N. V. S. *et al.* Fluorescent lanthanide complexes of Schiff base ligands possessing N-aryl moiety: influence of chain length on crossover (calamitic to discotic) phase behaviour. <http://dx.doi.org/10.1080/02678292.2010.517328> **37**, 1393–1410 (2010).
149. Anoop, M., Binil, P., Jisha, K. & Suma, S. Synthesis, spectral and thermal studies of lanthanum (III) complexes of phenylbutazone. *J. Korean* (2011).
150. Gupta, R. & Gupta, K. C. Synthesis, IR spectral studies and antimicrobial studies of some rare earth metal complexes with meso 2,3-dimercaptosuccinic acid. *Natl. Acad. Sci. Lett.* **35**, 249–252 (2012).
151. Hussain, A. *et al.* Enhancing the photocytotoxic potential of curcumin on terpyridyl lanthanide(III) complex formation. *Dalt. Trans.* **42**, 182–195 (2012).
152. Hu, X. *et al.* Synthesis and structural diversity of lanthanide amidate complexes and their catalytic activities for the ring-opening polymerization of rac-lactide. *J. Organomet. Chem.* **732**, 92–101 (2013).
153. Zhao, L., Ding, H., Zhao, B., Lu, C. & Yao, Y. Synthesis and characterization of amidate rare-earth metal amides and their catalytic activities toward hydrophosphonylation of aldehydes and unactivated ketones. *Polyhedron* **83**, 50–59 (2014).
154. science, S. A.-B.-J. of university of A. for P. & 2021, undefined. Novel Ester Monomers and Its Transition Metal Polychelates and Their Photovoltaic Application On Dye Sensitized Solar Cells. *iasj.net*.
155. Su, R. R., Tao, P., Han, Y., Zeng, C. H. & Zhong, S. L. Lanthanide Coordination Polymer Nanosheet Aggregates: Solvothermal Synthesis and Downconversion Luminescence. *J. Nanomater.* **2016**, (2016).
156. Berezhnytska, O. *et al.* Synthesis, Characterization, and Luminescent Properties of Polymer Complexes of Nd(III) with β -Dicarbonyl Ligands. *Nanoscale Res. Lett.*

-
- 12, 1–8 (2017).
157. Lian, C. *et al.* Synthesis and characterization of lanthanide-based coordination polymers for highly selective and sensitive luminescent sensor for Pb²⁺ over mixed metal ions. *J. Alloys Compd.* **702**, 303–308 (2017).
158. Olyshevets, I. *et al.* Synthesis and Characterization of Anionic Lanthanide(III) Complexes with a Bidentate Sulfonylamidophosphate (SAPh) Ligand. *Inorg. Chem.* **59**, 76–85 (2020).
159. Campello, M. P. C. *et al.* Lanthanide complexes with phenanthroline-based ligands: insights into cell death mechanisms obtained by microscopy techniques. *Dalt. Trans.* **48**, 4611–4624 (2019).
160. Wang, Y., Li, P., Wang, S. & Li, H. Recent progress in luminescent materials based on lanthanide complexes intercalated synthetic clays. *J. Rare Earths* **37**, 451–467 (2019).
161. Li, R. F., Li, R. H., Liu, X. F., Chang, X. H. & Feng, X. Lanthanide complexes based on a conjugated pyridine carboxylate ligand: structures, luminescence and magnetic properties. *RSC Adv.* **10**, 6192–6199 (2020).
162. Fouad, R. Synthesis and characterization of lanthanide complexes as potential therapeutic agents. *J. Coord. Chem.* **73**, 2015–2028 (2020).
163. Nguyen, T. A. D. *et al.* Lanthanide Complexes of Bis(tetrazolato)amine: A Route to Lanthanide Nitride Foams. *Inorg. Chem.* **59**, 16109–16116 (2020).
164. Zeybel, L. & Köse, D. A. Acesulfame complex compounds of some lanthanide group metal cations. Synthesis and characterization. *J. Mol. Struct.* **1226**, 129399 (2021).
165. Zhu, L., Xu, Y., Yuan, D., Wang, Y. & Yao, Y. Synthesis and structural characterization of lanthanide monoborohydride complexes supported by 2-tertbutylphenyl substituted β -diketiminato, and their application in the ring-opening polymerization of lactide. *J. Organomet. Chem.* **934**, 121662 (2021).
166. Devipriya, S., Arunadevi, N. & Vairam, S. Synthesis and thermal characterization of lanthanide(III) complexes with mercaptosuccinic acid and hydrazine as ligands. *J. Chem.* (2013) doi:10.1155/2013/497956.
167. Subhan, M. A., Alam, K., Rahaman, M. S., Rahman, M. A. & Awal, R. Synthesis and Characterization of Metal Complexes Containing Curcumin and Study of their Anti-microbial Activities and DNA-binding Properties. *J. Sci. Res.* **6**, 97–109 (2013).
-

-
168. Chu, L. F. *et al.* Synthesis and Biological Studies of Some Lanthanide Complexes of Schiff Base. <http://dx.doi.org/10.1080/15533174.2015.1031048> **45**, 1617–1626 (2015).
169. More, G., Bootwala, S., Shenoy, S., Mascarenhas, J. & Aruna, K. Synthesis, characterization and in vitro antitubercular and antimicrobial activities of new aminothiophene schiff bases and their Co(II), Ni(II), Cu(II) and Zn(II) metal complexes. *Orient. J. Chem.* **34**, 800–812 (2018).
170. Torres, J. *et al.* Phosphodiesterolytic activity of lanthanide (III) complexes with α -amino acids. *Inorganica Chim. Acta* **358**, 3320–3328 (2005).
171. MOTSON, G. R., FLEMING, J. S. & BROOKER, S. POTENTIAL APPLICATIONS FOR THE USE OF LANTHANIDE COMPLEXES AS LUMINESCENT BIOLABELS. *Adv. Inorg. Chem.* **55**, 361–432 (2004).
172. Laidler Keith J. *Chemical Kinetics* . (Pergamon Press, 1965).

CHAPTER 2

EXPERIMENTAL METHODS AND TECHNIQUES

This chapter outlines the materials employed, solvents used, experimental techniques adopted and analytical procedures used in the current research work. A brief discussion of the various instrumentation techniques used for the characterization of synthesized complexes is also presented in this chapter. Theoretically on how the intensity, energy interaction parameters and thermodynamic parameters are computed have also been discussed in detail

2.1. MATERIALS EMPLOYED

2.1.1. Lanthanide

Praseodymium (III) nitrate hexahydrate $[\text{Pr}(\text{NO})_3 \cdot 6\text{H}_2\text{O}]$ of 99.9% purity was purchased from Sigma Aldrich and was used as received.

2.1.2. Amino Acids

L-Aspartic acid, L-Histidine and L-Valine were obtained from HIMEDIA and were used as received.

2.1.3. Solvents

Acetonitrile, N,N-Dimethylformamide, 1,4-Dioxane, Methanol, Ethanol and Ether of 99.5% purity was purchased from Merck and used as received.

2.1.4. Pyridine

Pyridine derivative Isonicotinic acid was purchased from HIMEDIA and was used as received

2.2. EXPERIMENTAL

2.2.1. Synthesis of lanthanide complexes [Pr(III):Ligands (L-Aspartic acid, L-Histidine, L-Valine and Isonicotinic acid) complexes]:

All of the praseodymium(III) complexes were synthesized using the general method outlined below. 20 ml of 0.01 mol aquated solution of the ligand was added to 20 ml of hot alcoholic solution of praseodymium(III) nitrate hexahydrate and refluxed. The refluxing procedure was carried out for 24-36 hours while the pH of the solution was kept at its isoelectric point. The solution was taken and kept in a water bath until it had been concentrated to half of its original volume. The solution was allowed to cool, filtered and the filtrate was kept. After a few days, the crystals were collected at the bottom of the beaker which was washed with modest amounts of distilled water, alcohol and ether. The collected crystals were dried in a desiccator.

2.3. INSTRUMENTATION

2.3.1. Elemental analysis

The carbon, hydrogen, oxygen and nitrogen contents of the newly prepared Schiff base metal complexes were performed at Mizoram University.

2.3.2. Estimation of metal

The percentage of metal in the Schiff base metal complexes was estimated gravimetrically as their oxides by fusion with AnalaR ammonium oxalate. In a typical experiment, about 0.3 g of the dried complex was accurately taken in a previously weighed silica crucible. AnalaR ammonium oxalate, roughly 3 parts by weight of the complex was added and the mixture was incinerated slowly at first and then strongly using a Bunsen burner for 3 hrs. It was then cooled in a desiccator and weighed. The procedure was repeated till the final oxide weight was constant. From this, the percentage of metal in the complex was calculated.

2.3.3. Molar conductance measurements

Conductance measurements are useful in determining the electrolytic nature of the complexes. Conductance values of the complexes were obtained on a Systronics Model-304 digital conductivity meter using ethanol as solvent. The molar conductivity of the complexes was determined using the formula:

$$\lambda_m = \frac{(1000 \times \text{Conductance} \times \text{Cell constant})}{\text{Concentration}}$$

The conductance values were compared with the standard values from the literature¹ to find out the electrolytic nature of the complexes.

2.3.4. Fourier Transform Infrared Spectroscopy (FT-IR)

Spectroscopy is the study of the emission and absorption of electromagnetic radiation due to vibrations of atoms or molecules. Infrared spectroscopy is one of the most widely used spectroscopic techniques for chemical analysis and characterization of both organic and inorganic compounds which is also known as vibrational spectroscopy. Vibrational spectroscopy detects the vibrational energies of molecules by the absorption of infrared radiation or by the inelastic scattering of light by a molecule associated with solid, gas, or liquid. It is considered to be an easy way to detect the certain impurities and functional groups present in a molecule and also the absorption spectra confirm the identity of a pure compound.

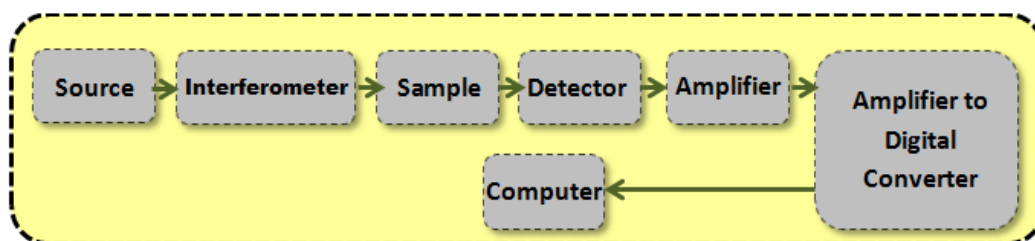


Figure 2.1. Basic components of a FT-IR spectrometer.

Fourier transform infrared spectroscopy (FT-IR) is the most commonly used vibrational spectroscopic technique for the characterization of various materials. The FT-IR spectroscopy is based on the principle of the interference of IR radiation between two beams to produce an interferogram or a signal as a function of optical path difference between the beams. The basic components of the FT-IR spectrometer are illustrated schematically in Fig. 2.1. The two commonly used IR light sources are Nernst glower and Globar which generate infrared radiation energy by heating the solid materials using electric current to incandescence. The radiation beam generated by the source enters an interferometer then to the sample. Michelson interferometer is the most commonly used interferometer which is the key component in FT-IR spectrometer where the spectral encoding takes place. The Michelson interferometer consists of one beam-splitter bisecting the planes of two mirrors as shown in Fig. 2.2. The beam-splitter transmits half of the incident beam from the source to one of the fixed mirrors and reflects the other half to the other moving mirror. These two transmitted and reflected beams returns from both the mirrors and recombine into one beam at the beam-splitter which exits and irradiates the sample. In a Michelson interferometer the two beams reflected from the fixed and moving mirrors interfere as follows:

$$A_f = A_1 + A_2 \quad (1)$$

where A_f , A_1 and A_2 are the amplitude of the final, fixed mirror, and moving mirror beam respectively. If A_f is greater than A_1 or A_2 the two beams are said to undergo constructive interference and if A_f is less than A_1 or A_2 it is said to be destructive interference. Also, the square of the amplitude of a light beam is proportional to its intensity. The moving mirror functions to create an optical path difference between the two split beams to produce the light interference which is termed an interferogram. These interferogram signals are received by the FT-IR detector which is then transmitted to or reflected from the sample. To interpret the produced interferogram signal, a mathematical technique called the Fourier transformation is used as a means to convert the interferogram into an

infrared spectrum. This transformed spectrum is a plot of the light intensity versus wavenumber. This is performed by a computer using a fast Fourier transform (FFT) algorithm equipped with FT-IR which constructs the infrared spectrum which results in a substantial reduction of computation time.² The final Fourier transform infrared spectrum is ready for interpretation.

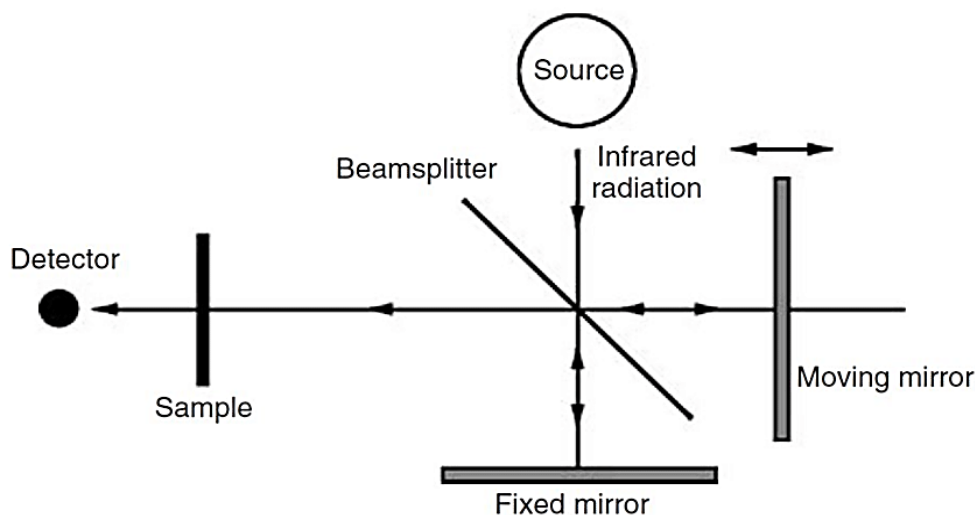


Figure 2.2. Optical diagram of a Michelson interferometer in FT-IR.

Infrared spectra (IR) are highly useful in identifying the nature of coordination sites, particularly in Schiff base complexes involving multidentate ligands. Most of the assignments of IR absorption frequencies have been based on the concept of group frequency. The important vibrating group in free Schiff bases is naturally the functional group. IR spectra of the Schiff bases and their complexes in the range of $400\text{--}4000\text{ cm}^{-1}$ were recorded on a Shimadzu FT-IR spectrophotometer (spectrum two) using KBr pellets.

2.3.5. Powdered X-ray Diffraction (XRD) studies

The structural characterization of the crystalline material can be accomplished using the significant and widely applied analytical technique known as X-ray diffraction. It is generally used for phase identification, determining crystallite size, finding unit cell parameters, sample purity, an atomic position as well as arrangement in the crystal. The basis of the X-ray diffraction method is the interaction of a monochromatic X-ray beam with a crystalline sample. X-rays are electromagnetic radiation $\sim 1\text{ \AA}$ wavelength range. X-rays are generated when electrically charged particles having a sufficient level of

kinetic energy, $KE = eV = \frac{1}{2} mv^2$ are instantly decelerated by a heavy metal target such as molybdenum or copper. These X-rays are used to study the crystallographic nature of the crystals following Bragg's law. The concept of Bragg's law can be illustrated in Fig. 2.3. The group of black dots in the figure represent the periodic atomic arrangement forming a given set of planes A, B, and C separated by an inter-planar distance d . Two perfectly monochromatic and parallel X-ray beams 1 and 2 of wavelengths λ are incident on the atoms S and Q on the adjacent planes within the crystal making an angle θ . This is also called Bragg's angle of reflection which is equal to the incident angle θ . From the figure, it can be seen that the path difference between X-ray beam 1S1' and beam 2Q2' is

$$PQ+QR = d \sin\theta+d \sin\theta \quad (2.1)$$

These X-ray beams will be in phase if their path difference differs by a whole number 'n' of wavelengths, therefore:

$$n\lambda = PQ+QR \quad (2.2)$$

$$n\lambda = d \sin\theta+d \sin\theta \quad (2.3)$$

[Since $PQ = QR$]

$$n\lambda = 2d \sin\theta \quad (2.4)$$

This expression is known as Bragg's law.

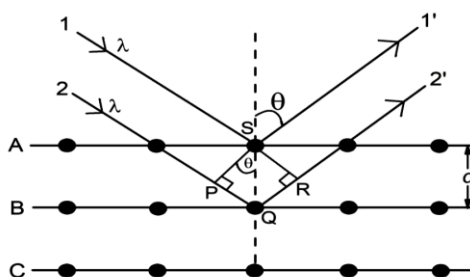


Figure 2.3. Illustration of Bragg's law.

From the corresponding 2θ values of the diffraction peak, the phase of the nanomaterials can be found by comparing with JCPDS (Joint Committee on Powder Diffraction Standards) powder diffraction file. If the d -spacing with corresponding hkl planes are known, the lattice parameters can be determined using the following formulae:

(a) For monoclinic phase: $\frac{1}{d^2} = \frac{1}{\sin^2\beta} \left(\frac{h^2}{a^2} + \frac{k^2 \sin^2\beta}{b^2} + \frac{l^2}{c^2} - \frac{2hl \cos\beta}{ac} \right)$ (2.5)

(b) For cubic phase: $\frac{1}{d^2} = \frac{h^2+k^2+l^2}{a^2}$ (2.6)

(c) For tetragonal phase: $\frac{1}{d^2} = \frac{h^2+k^2}{a^2} + \frac{l^2}{c^2}$ (2.7)

$$(d) \text{ For hexagonal phase: } \frac{1^2}{d^2} = \frac{4}{3} \left(\frac{h^2 + hk + k^2}{a^2} \right) + \frac{l^2}{c^2} \quad (2.8)$$

Where, a , b and c are the lattice parameters and β is Bragg's angle.

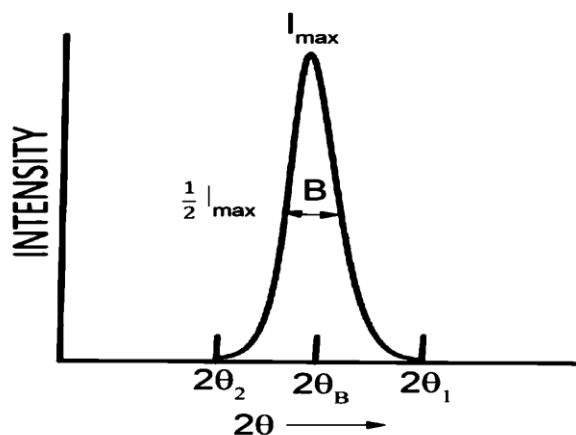


Figure 2.4. Effect of particle size on diffraction curve.

By measuring the width (in radians) of the diffraction curves, one can determine the average particle size 'r' of a very small crystal. As crystal size decreases, the diffraction curve's width widens. Half of the highest intensity of the diffraction curve is used to measure the width B. It is the deviation from the two angles where the intensity is zero, assuming the diffraction curve to be triangular. From Fig. 2.4

$$B = \frac{1}{2} (2\theta_1 - 2\theta_2) = \theta_1 - \theta_2 \quad (2.9)$$

Equations of path difference for the two angles are

$$2r \sin \theta_1 = (m+1)\lambda \quad (2.10)$$

$$\text{and } 2r \sin \theta_2 = (m-1)\lambda \quad (2.11)$$

By subtraction we get

$$r(\sin \theta_1 - \sin \theta_2) = \lambda, \quad (2.12)$$

$$2r \cos \frac{\theta_1 + \theta_2}{2} \sin \frac{\theta_1 - \theta_2}{2} = \lambda \quad (2.13)$$

But θ_1 and θ_2 are both very nearly equal to θ_B , so that

$$\theta_1 + \theta_2 = 2\theta_B \text{ and } \sin \frac{\theta_1 - \theta_2}{2} = \frac{\theta_1 - \theta_2}{2} \text{ (approx.)} \quad (2.14)$$

Therefore

$$2r \frac{\theta_1 - \theta_2}{2} \cos \theta_B = \lambda, \quad (2.15)$$

$$r = \frac{\lambda}{B \cos \theta_B} \quad (2.16)$$

A more exact treatment of the problem gives

$$r = \frac{0.9\lambda}{BCos\theta_B} \quad (2.17)$$

which is known as the Scherrer formula.

The diffracted X-rays are detected and recorded by an X-ray diffractometer which consists of three basic components: (i) An X-ray tube, (ii) sample holder, and (iii) a detector. X-ray spectra $K\alpha$ and $K\beta$ are generated by heating a filament in a cathode ray tube to produce electrons which are accelerated by applying voltage and allowed to bombard with the target material (Cu, Fe, Mo, Cr). These collimated X-rays are directed towards the sample at an angle θ while the intensity of the X-ray is scanned at twice the angle of the incident (2θ) by the detector. When the incident X-rays impinge the sample satisfying the Bragg's law, constructive interference is produced and an intensity of peak occurs. The detector records the diffracted signal and converts them to a count rate with a distinct pattern which is then sent to an output device such as computer or printer.³⁴

Crystal and molecular structure determination by X-ray diffraction technique is probably the ultimate in structural elucidation in the solid state. The powder X-ray diffraction (XRD) patterns were recorded with Rigaku Ultima IV X-ray diffractometer with Cu $K\alpha$ radiation ($\lambda=1.540\text{\AA}$) from 10° to 80° (2θ) at room at NIT, Chumukedima; Dimapur temperature and match with JCPDS data from P-Analytical - X'pert highscore software. All samples were single-phase to XRD.

2.3.6. Spectrofluorometer

Photoluminescence bands can be either fluorescence or phosphorescence depending on the average lifetime of the excited state which is much longer for phosphorescence than fluorescence. The emission of the luminophore is monitored in luminescence spectroscopy which is one of the most sensitive and selective methods of analysis for measuring the energy levels between the two electronic states of the luminescence centres in many inorganic and organic compounds. Two different types of luminescence spectra can be scanned i.e., excitation and emission spectra using a spectroscopic technique called spectrofluorometer. It is an analytical instrument used to monitor and record the fluorescence of a sample. Spectrofluorometer contains both an excitation monochromator and an emission monochromator. A schematic representation of the main elements of the spectrofluorometer is displayed in Fig 2.5.

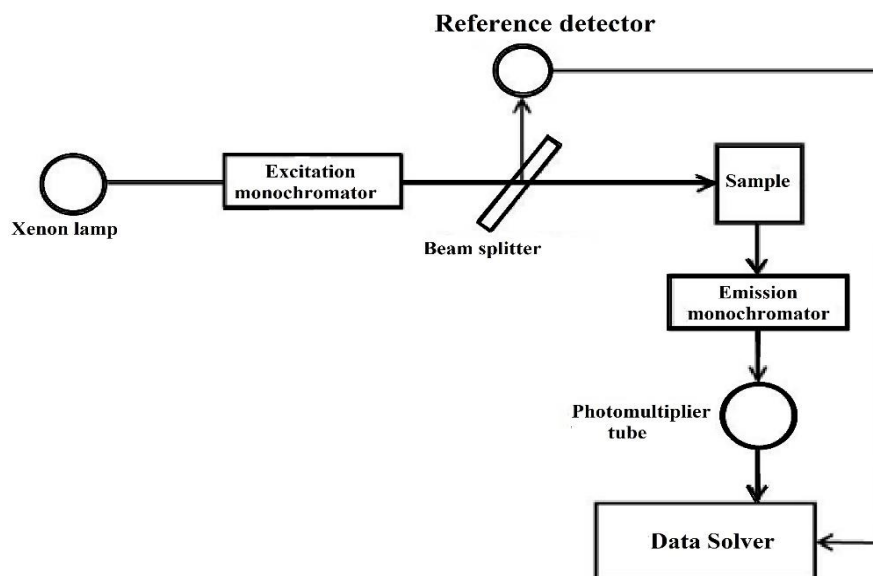


Figure 2.5. Schematic representation of a Spectrofluorometer

The sample is excited with a light source such as lasers, xenon arcs or mercury-vapor lamps, etc. which are then focused on the entrance slit of the monochromator (the excitation monochromator). The emitted light is collected by a focusing lens and analysed utilizing a second monochromator (the emission monochromator). These monochromators maintain high resolution over the entire spectral range and minimize spherical aberrations and re diffraction by using all its reflective optics. It contains two detectors: a Signal detector and a reference detector. The signal detector is a photon-counting detector that uses a photomultiplier tube to send the signal to a photon counting module. The reference detector monitors the xenon lamp to correct the wavelength and time-dependent output of the lamp. A suitable detector is connected to a computer that records two kinds of spectra, (i) emission spectra and (ii) excitation spectra. During the emission spectra measurement, the excitation wavelength is fixed and the emission monochromator is scanned. The excitation is usually fixed at a wavelength at which the sample has significant absorbance. Emission spectra give information on the energetic position of the optical transitions that are involved in the emission of light. On the other hand, in excitation spectra, the emission wavelength is fixed and the excitation monochromator is scanned. The emission is normally fixed at a wavelength that corresponds to the emission peak of the sample. In contrast to an absorption spectrum, an excitation spectrum gives information on the energetic position of absorption bands that lead to the emission of the chosen wavelength.^{5,6}

Photoluminescence is the emission of light from any form of matter irradiated by any light source under optical excitation. The emitted light can be measured and analysed spectrally, spatially, and transiently. These factors of photoluminescence can be a direct measure of various important material properties. The photoluminescence spectra were recorded with SHIMADZU Fluorescence Spectrophotometer Model No. RF – 6000.

2.3.7. Thermogravimetric (TGA)

Basic Principle

It is a simple analytical technique that measures the amount and rate of change in the weight of a material as a function of temperature or time in a controlled atmosphere. Measurements are used primarily to determine the composition of materials and to predict their thermal stability at temperatures up to 1000 °C. It is the most widely used thermal method as shown in fig. 2.6. which can characterize materials that exhibit weight loss or gain due to decomposition, oxidation, or dehydration. As materials are heated, they can lose weight from a simple process such as drying, or from chemical reactions that liberate gases. Some materials can gain weight by reacting with the atmosphere in the testing environment. Since weight loss and gain are disruptive processes to the sample material, knowledge of the magnitude and temperature range of those reactions are necessary in order to design adequate thermal ramps and holds during those critical reaction periods. Such analysis relies on a high degree of precision in three measurements: weight, temperature, and temperature change.

A plot of weight change versus temperature is referred to as the thermogravimetric curve (TGA curve) which helps in revealing the extent of purity of analytical samples and determining the mode of their transformations within specified range of temperature. As many weight loss curves look similar, the weight loss curve may require transformation before results may be interpreted. A derivative weight loss curve can be used to tell the point at which weight loss is most apparent.

Therefore, TGA curves can provide information about the composition of multi component systems, thermal stability, oxidative stability of materials, decomposition kinetics of materials, the effect of reactive or corrosive atmospheres on materials and moisture content of materials.

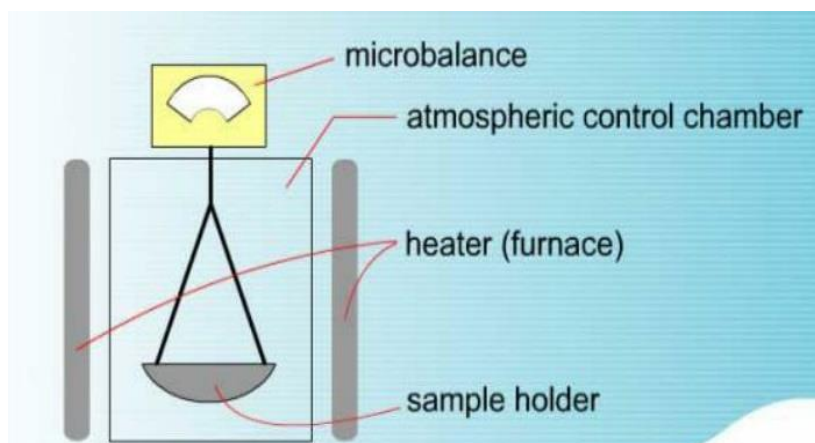


Figure 2.6. Schematic diagram of thermogravimetric analyzer.

Experimental Set Up

The instrument used in thermogravimetry (TGA) is called a thermobalance. It consists of a sample pan that is supported by a precision balance. That pan resides in a furnace and is heated or cooled during the experiment. The mass of the sample is monitored during the experiment and a purge gas controls the sample environment. This gas may be inert or a reactive gas that flows over the sample to prevent oxidation or other undesired reactions and exits through an exhaust. The whole arrangement shown in fig. 2.7. with block diagram provides the flexibility necessary for the production of useful analytical data in the form of TGA curve. Basic components of a typical thermobalance are listed below:

1. Balance
2. Furnace: heating device
3. Unit for temperature measurement and control (Programmer)
4. Recorder: automatic recording unit for the mass and temperature changes

The basic requirement of an automatic recording balance are includes accuracy, sensitivity, reproducibility, and capacity. Recording balances are of two types, null point and deflection type. The null type balance, which is more widely used, incorporates a sensing element which detects a deviation of the balance beam from its null position. A sensor detects the deviation and triggers the restoring force to bring the balance beam back to the null position. The restoring force is directly proportional to the mass change. Deflection balance of the beam type involve the conversion of the balance beam deflection about the fulcrum into a suitable mass change trace by (a) photographic recoding i.e. change in path of a reflected beam of light available of photographic

recording, (b) recording electrical signals generated by an appropriate displacement measurement transducer, and (c) using an electrochemical device. The different balances used in TGA instruments are having measuring range from 0.0001mg to 1g depending on sample containers used.

The furnace and control system must be designed to produce linear heating at over the whole working temperature range of the furnace and provision must be made to maintain any fixed temperature. A wide temperature range generally 150 °C to 2000 °C of furnaces is used in different instruments manufacturers depending on the models. The range of furnace basically depends on the types of heating elements are used. In our instrument, temperature can vary from 25 °C to 900 °C isothermally and the maximum temperature range is 1000 °C. Sample weight can range from 1 mg to 150 mg but sample weights of more than 25 mg are preferred and sometimes excellent results are obtained with 1mg of material.

Temperature measurement are commonly done using thermocouples, chromal–alumel thermocouple are often used for temperature up to 1100 °C whereas Pt–Rh thermocouple is employed for temperature up to 1750 °C. Temperature may be controlled or varied using a program controller with two thermocouple arrangement, the signal from one actuates the control system whilst the second thermocouple is used to record the temperature.

Graphic recorders are preferred to meter type recorders. X–Y recorders are commonly used as they plot weight directly against temperature. The present instrument facilitates microprocessor-controlled operation and digital data acquisition and processing using personal computer with different types recorder and plotter for better presentation of data.

The whole of the balance system is housed in a glass to protect it from dust and provide inert atmosphere. There is a control mechanism to regulate the flow of inert gas to provide inert atmosphere and water to cool the furnace. The temperature sensor of furnace is linked to the programme to control heating rates, etc. The balance output and thermocouple signal may be fed to recorder to record the TGA Curve.⁷⁻¹⁴

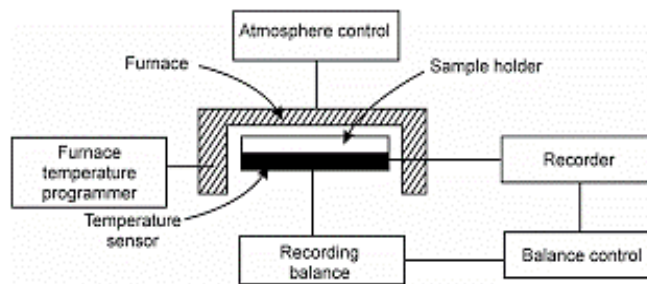


Figure 2.7. Block diagram of thermobalance.

2.3.8. UV–Visible Spectroscopy

Basic Principle The instrument used in ultraviolet–visible spectroscopy is called a UV–Visible Spectrophotometer. A spectrophotometer provides a means for analyzing liquids, gases and solids through the use of radiant energy in the far and near ultraviolet and visible regions of the electromagnetic spectrum.

The instrument operates by passing a beam of light through a sample and measuring the wavelength of light reaching a detector. The wavelength gives valuable information about the chemical structure and the intensity is related to the number of molecules, which means quantity or concentration. Analytical information can be revealed in terms of transmittance, absorbance or reflectance of energy in the wavelength range between 160 and 3500 mill microns.¹⁵

Light is quantized into tiny packets called photons, the energy of which can be transferred to an electron upon collision. However, the transfer occurs only when the energy level of the photon equals the energy required for the electron to get promoted onto the next energy state, for example from the ground state to the first excitation state. This process is the basis for absorption spectroscopy. Generally, light of a certain wavelength and energy is illuminated on the sample, which absorbs a certain amount of energy from the incident light. The energy of the light transmitted from the sample afterwards is measured using a photo detector, which registers the absorbance of the sample. A spectrum is a graphical representation of the amount of light absorbed or transmitted by matter as a function of wavelength. A UV–Visible spectrophotometer measures absorbance or transmittance from the UV range to which the human eye is not sensitive to the visible wavelength range to which the human eye is sensitive. Bouguer–Beer law as shown in fig. 2.8. is a basic principle of quantitative analysis, is

also called the Lambert–Beer rule. The following relationship is established when light with intensity I_0 is directed at a material and light with intensity I is transmitted.

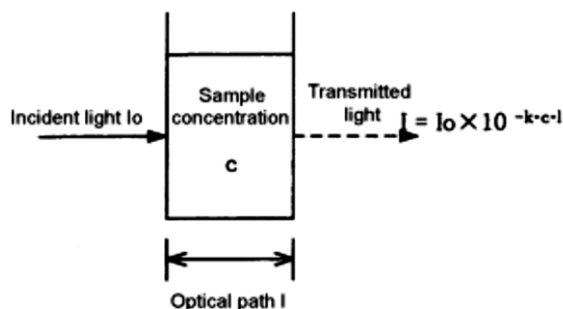


Figure 2.8. Bouguer–Beer Rule.

In this instance the value I/I_0 is called transmittance (T) and the value $I/I_0 \times 100$ is called transmission rate ($T\%$). The value $\log(1/T) = \log(I_0/I)$ is called absorbance (Abs).

$$T = I/I_0 = 10^{-kcl}$$

$$Abs = \log(1/T) = \log(I_0/I) = -kcl$$

Here k is proportionality constant and l = length of light path through the cuvette in cm. As can be seen from the above formulas, transmittance is not proportional to sample concentration. However, absorbance is proportional to sample concentration (Beer's law) along with optical path (Bouguer's law). In addition, when the optical path is 1cm and the concentration of the target component is 1mol/l, the proportionality constant is called the molar absorption coefficient and expressed using the symbol ϵ . The molar absorption coefficient is a characteristic value of a material under certain, specific conditions. Finally, stray light, generated light, scattered light, and reflected light must not be present in order for the Bouguer–Beer rule to apply.

Experimental Set Up

Spectrophotometers consist of a number of fundamental components: Light Sources (UV and VIS), monochromator (wavelength selector), sample holder, a detector, signal processor and readout. The radiation source used is often a tungsten filament, a deuterium arc lamp which is continuous over the ultraviolet region, and more recently light emitting diodes (LED) and xenon arc lamps for the visible wavelengths. The detector is typically a photodiode or a CCD. Photodiodes are used with monochromators, which filter the light so that only light of a single wavelength reaches the detector. When measuring absorbance at the UV spectrum, the other lamp has to be turned off. The same goes when

measuring visible light absorbance. Fig. 2.9. shows schematic diagram of UV–Visible Spectrophotometer.

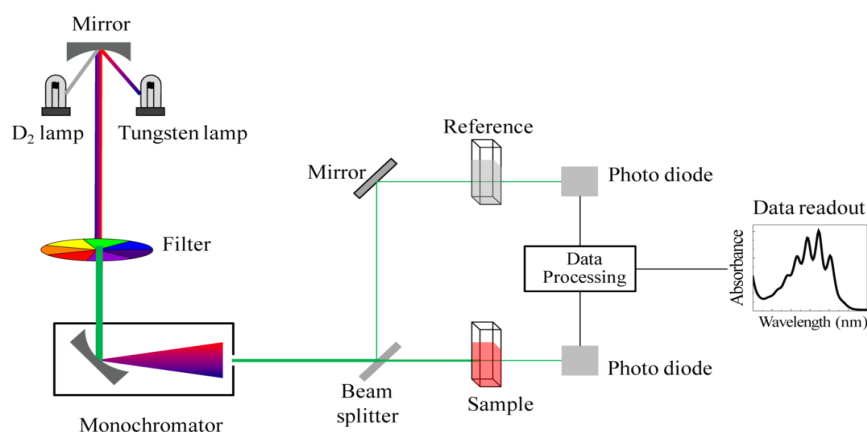


Figure 2.9. Schematic diagram of UV–Visible Spectrophotometer.

The light source is a monochromator; the light is split into two equal intensity beams by a half-mirrored device before it reaches the sample. One beam, the sample beam, passes through a small transparent container (cuvette) containing a solution of the compound being studied in a transparent solvent. The other beam, the reference, passes through an identical cuvette containing only the solvent. The containers for the sample and reference solution must be transparent to the radiation which will pass through them. Quartz or fused silica cuvettes are required for spectroscopy in the UV–Vis–NIR region. The light sensitive detector follows the sample chamber and measures the intensity of light transmitted from the cuvettes and passes the information to a meter that records and displays the value to the operator on an LCD screen. The intensities of these light beams are then measured by electronic detectors and compared. Some UV–Visible spectrophotometry has two detectors the phototube and the photomultiplier tube. The sample and reference beam are measured at the same time. The intensity of the reference beam, which should have suffered little or no light absorption, is defined as I_0 . The intensity of the sample beam is defined as I . Over a short period of time, the Spectrometer automatically scans all the component wavelengths in the manner described.

The ultraviolet (UV) region scanned is normally from 200 to 400 nm, and the visible portion is from 400 to 800 nm. Therefore, this method is excellent to both determine the concentration and identify the molecular structure or the structural changes. Spectrophotometer is also useful to study the changes in the vibration and conformation

energy levels after and before an interaction with a substrate, or another molecule.¹⁶ The spectral data have been recorded on Perkin Elmer Lambda-35 UV-Vis Spectrophotometer with computer attached, high resolution. The temperatures of all the observations were maintained using water circulating HAAKE DC 10 thermostat.

2.3.9. Biocidal studies

The *in vitro* biological activity of the investigated Schiff base metal complexes were tested against bacteria Gram-positive *Staphylococcus aureus* and *Bacillus subtilis* were utilised in addition to Gram-negative *Escherichia coli* and *Klebsiella pneumonia* by disc diffusion method¹⁷ using Muller Hinton agar as nutrient and ampicillin as control. Antifungal activities against *Fusarium oxysporum*, *Penicillium italicum*, *Aspergillus niger* and *Candida albicans* were determined in sabour dextrose agar medium using nystatin as control. Filter paper discs of 6.0 mm diameter were charged with solutions of appropriate metal complexes in DMSO. The discs were stored dry in the cold. The broth culture of the test bacterium was flooded on the surface of Muller Hinton plate and inoculated. After drying the plates at 37° C for 30 minutes, the filter paper discs containing the metal complexes were incubated at 36° C for a period of 24 hrs. The degree of sensitivity was determined by measuring the zone of inhibition of growth around the discs.

2.4. Spectral analysis of 4f-4f transition of Pr(III) with some selected amino acid and pyridine ligands

The dimensions of lanthanide coordination chemistry in solutions becomes a new age with the increasing use of lanthanides as probes in the exploration of the structural functions of biomolecular reactions.¹⁸ The paramagnetic nature and the presence of a quite detailed internal f- electron transition spectra in easily accessible spectral region of lanthanide ions have been utilized as an absorption spectral probe in various biomolecular reactions. The 4f–4f transition spectra of lanthanide have been found to exhibit significant sensitivity towards even minor changes in the immediate coordination environment around lanthanide ion through variation in the absorption spectral pattern, degree of red shift and intensification of 4f–4f bands, which makes absorption spectral spectroscopy involving 4f–4f transitions an extremely powerful tool for studying lanthanide chemistry particularly in solutions both in aqueous and non-aqueous media.^{19,20} Comparative and differential absorption spectral study involving 4f-4f transitions is therefore one of the

most effective techniques to reveal the interaction of biologically active ligands with Ln(III).²¹ The Comparative Absorption Spectral Analysis of the complexation of Lanthanides with biological ligands (Amino acids/Pyridine) involves:

a) Evaluation of Energy Interaction Parameters, i.e

- (i) Nephelauxetic Ratio (β)
- (ii) Slater- Condon (F_k)
- (iii) Lande Factor/Spin-Orbit Coupling Constant (ξ_{4f})
- (iv) Bonding Parameter ($b^{1/2}$)
- (v) Percentage Covalency (δ)

b) Evaluation of Electric Dipole Intensity Parameters, which includes

- (i) Oscillator Strength (P)
- (ii) Judd- Ofelt Parameter (T_λ)

2.4.1. Theoretical background

The energy of $4f-4f$ transitions is composed of two main components, viz the electrostatic and spin orbit interaction between $4f$ electrons i.e.,

$$E = \sum \int_k^k F_k + A_{SO} \xi_{4f} \dots\dots\dots (1)$$

where F_K and A_{SO} are the angular part of electrostatic and spin orbit interaction respectively and their values can be calculated by applying tensor operator technique; F_K and ξ_{4f} are radial integrals. Thus, to define energy level scheme of $4fn$ configuration, four radial integrals F_2, F_4, F_6 and ξ_{4f} are required which had been evaluated by the Hartee Fock Method.^{22,23}

Using Taylor Expansion Series, the energy level structure of lanthanides can be expressed in the first order approximation. Then, the energy E_j of the j^{th} energy level is given by:

$$E_j(F_k, \xi_{4f}) = E_{oj}(F_k^0, \xi_{4f}^0) + \sum_{k=2,4,6} \frac{\partial E_j}{\partial F_k} \Delta F_k + \frac{\partial E_j}{\partial \xi_{4f}} \Delta \xi_{4f} \dots (2)$$

where E_{oj} is the zero-order energy of the j^{th} level. The values of F_K and ξ_{4f} are given by,

$$F_k = F_k^0 + \Delta F_k \dots\dots\dots (3)$$

$$\xi_{4f} = \xi_{4f}^0 + \Delta \xi_{4f} \dots\dots\dots (4)$$

$$\text{When } \Delta F_k \ll F_k^0 \text{ and } \Delta \xi_{4f} \ll \xi_{4f}^0 \dots\dots\dots (5)$$

$$\Delta E_j = \sum_{k=2,4,6} \frac{\partial E_j}{\partial F_k} \Delta F_k + \frac{\partial E_j}{\partial \xi_{4f}} \Delta \xi_{4f} \dots\dots\dots (6)$$

The observable changes leading to intensification of peaks in the spectral region is due to the red shift on all the electronic transitions, indicating the expansion of the metal orbital

radius which results in the decrease of the inter-electronic repulsion parameters (Slater-Condon, F_K 's). This phenomenon is known as nephelauxetic effect, which measures the change in F_K with respect to free ion and expressed by a nephelauxetic ratio ' β ' and is given as:

$$\beta_1 = \frac{F_k^0}{F_k^f}; \beta_2 = \frac{\xi_{4f}^0}{\xi_{4f}^f} \text{ and } \dots\dots\dots (7)$$

$$\beta = \left[\frac{\beta_1 + \beta_2}{2} \right]$$

Where F_k^0 and F_k^f ($k=2,4,6$) refers to parameters in complex and free ion respectively.

The amount of mixing of $4f$ orbital and ligand orbital can be given by another bonding parameter i.e., ' $b^{1/2}$ ', which is related to nephelauxetic effect and given as:

$$b^{1/2} = \left[\frac{1-\beta}{2} \right]^{1/2} \dots\dots\dots (8)$$

Sinha²⁴, introduced another parameter known as the percentage covalency parameter, which can be expressed as:

$$\delta\% = \left[\frac{1-\beta}{\beta} \right] \times 100 \dots\dots\dots (9)$$

The intensity of the absorption band is measured by the oscillator strength (P), which is directly proportional to the area under the absorption curve. It can be expressed in terms of molar extinction coefficient (ϵ_{max}), energy of the transition in wave number ($\bar{\nu}$) and the refractive index (η) of the medium by the following relationship:

$$P = 4.31 \times 10^{-9} \left[\frac{9\eta}{(\eta^2 + 1)^2} \right] \int \epsilon_{max}(\bar{\nu}) d\bar{\nu} \dots\dots (10)$$

The experimental values of oscillator strength (P_{exp}) of the absorption bands were calculated by performing Gaussian curve analysis of the curves [Fig.4.1].

By Gaussian Curve analysis. The half band width is given by

$$\bar{\nu}^{1/2} = \left[\frac{1}{P} - \frac{1}{Q} \right] \times 10^7 \dots\dots\dots (11)$$

Now, Oscillator strength (P_{exp}) can be found out from the equation,

$$P = 4.60 \times 10^{-9} \times \epsilon_m \times \Delta\nu_{1/2} \dots\dots\dots (12)$$

where the molar extinction co-efficient ϵ_{max} is given by the equation,

$$\epsilon_m = \frac{\text{Absorbance}}{\text{Concentration} \times 1}$$

Where 1 = path length of the cell in cm = 1 cm

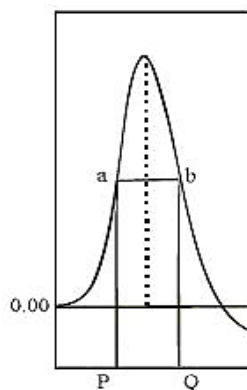


Figure 2.10. Gaussian curve analysis on an expanded single peak of Pr(III) spectrum

In order to define the energy parameters, we have to calculate four terms i.e, F_2 , F_4 , F_6 and ξ_{4f} which can be solved using the following equation,

$$\Delta E_{obs} = \sum_{k=2,4,6} \frac{\partial E_j}{\partial F_k} \Delta F_k + \frac{\partial E_j}{\partial \xi_{4f}} \Delta \xi_{4f} \dots (13)$$

Considering F_k 's and ξ_{4f} as empirical, derived from least square fit of the experimental energy level of the Pr^{3+} ion, which is either free or complexes, the solution of the equation taking into account, the difference in energy and calculating the energy terms using Wong's values and practical differential co-efficient for F_2^0 , F_4^0 , F_6^0 and ξ_{4f}^0 for Praseodymium gave parameters of Slater-Condon integrals, in some cases, higher than those observed for the aqueous ion. In our complexes, we expect the metal ion to expand so that the bonding parameters become positive and subsequently the Slater-Condon integrals should be lower than that for the aqueous ion. Thus, the values, which yield from the above method, are not realistic. Because of the above shortcomings, a pure solution of the four equations with four unknown is ruled out. Another method known as the partial and multiple regression method²⁵⁻²⁹, yield the values of only two parameters F_2 and ξ_{4f} . Equation (13) can now be written as,

$$\Delta E_{obs} = E_{oj} + \frac{\partial E_j}{\partial F_2} \Delta F_2 + \frac{\partial E_j}{\partial \xi_{4f}} \Delta \xi_{4f} \dots (14)$$

and it can be again expressed as,

$$\frac{E_{obs} - E_{oj}}{\delta E_j / \xi_{4f}} = \Delta \xi_{4f} + \frac{\delta E_j / \delta F_2}{\delta \xi_{4f} / \delta \xi_{4f}} \Delta F_2 \dots (15)$$

The reported values for the Zero Order Energies and Partial Derivatives with respect to F_k and ξ_{4f} parameters for Pr (III) ion are given in Table 4.1a on making the following substitutions in equation (3).

Table 2.1. The zero order energies and partial derivatives with respect to F_k and ξ_{4f} parameters with Pr(III).

Level	$E_{oj}^{(a)}$	$\frac{\partial E_j}{\partial F_2}$	$\frac{\partial E_j}{\partial F_4}$	$\frac{\partial E_j}{\partial F_6}$	$\frac{\partial E_j}{\partial \xi_{4f}}$
1D_2	16972	45.97	-37.63	510	2.906
3P_0	20412	70.17	81.81	-1253	1.905
3P_1	20990	70.07	80.66	-1278	3.974
3P_2	22220	67.56	68.42	-1077	5.029

a) $F_2^0 = 305.0 \text{ cm}^{-1}$, $F_4^0 = 51.88 \text{ cm}^{-1}$, $F_6^0 = 5.321 \text{ cm}^{-1}$ and $\xi_{4f}^0 = 730.5 \text{ cm}^{-1}$

* *E.Y. Wong, J. Chem. Phys., 38 (1963) 976.*³⁰

$$Y = \frac{E_{obs} - E_{oj}}{\delta E_j / \delta \xi_{4f}}, \quad a = \Delta \xi_{4f}$$

$$X = \frac{\delta E_j / \delta F_k}{\delta E_j / \delta \xi_{4f}}, \quad b = \Delta F_2$$

Hence the equation (15) can be written in the form,

$$Y = a + Xb \dots\dots\dots (16)$$

Considering the four bands of Pr^{3+} , the above equation becomes the set of equation which can be represented as:

$$Y_1 = a + X_1b$$

$$Y_2 = a + X_2b$$

$$Y_3 = a + X_3b \dots\dots\dots (17)$$

$$Y_4 = a + X_4b$$

Where each equation corresponds to an observed band in praseodymium.

On solving the above equation (17) by statistical method, we get;

$$b = \frac{\Sigma XY}{\Sigma X^2} \quad \text{and} \quad a = \bar{Y} - \bar{bx} \dots\dots\dots (18)$$

where,

$$E\Sigma XY = \Sigma XY - \frac{\Sigma X \Sigma Y}{4}$$

$$\Sigma X^2 = \Sigma X^2 - \frac{(\Sigma X)^2}{4}$$

$$\bar{Y} = \frac{\Sigma Y}{4} \quad \text{and} \quad \bar{X} = \frac{\Sigma X}{4}$$

The values obtained yield approximate solutions for F_2 and ξ_{4f} . Approximate values for F_4 and F_6 are then found from the following relation:

$$\frac{F_4}{F_2} = 0.13805 \quad \text{and} \quad \frac{F_6}{F_2} = 0.0151$$

In order to get more accurate values of F^k 's and ξ_{4f} , their initial values are slightly perturbed so that the roots mean square deviation denoted by

$$\text{R.M.S} = \left[\frac{\sum (E_{cal} - E_{obs})^2}{4} \right]^{1/2} \quad \text{for Pr (III)}$$

is reduced. Care is to be taken that the values of F^k 's and ξ_{4f} don't exceed those reported for the aqueous Pr^{3+} system. Mathematically correct solution is the one which makes the weighted difference between the squares of observed and calculated values (i.e, r.m.s value minimum) have the minimum values, with N denoting the number of observations as:

$$\text{R.M.S} = \left[\frac{\sum (E_{cal} - E_{obs})^2}{N} \right]^{1/2}$$

The observed oscillator strength (P_{obs}) of the transition energies were expressed in terms of parameters defined by Judd and Ofelt known as the T_2 , T_4 and T_6 parameters which are given by the following equation.

$$\frac{P_{obs}}{\nu} = [(U^2)]^2 T_2 + [(U^4)]^2 T_4 + [(U^6)]^2 T_6 \dots \dots \dots (19)$$

These values are procured using Carnall's co-efficient for aquo system.

For praseodymium complexes, four equations exist for the observed values of the four bands. Since $[(U^2)]^2$ and $[(U^6)]^2$ has zero value for the 3P_1 and 3P_0 levels, the ordinary simultaneous equation gave the values of T_2 , T_4 and T_6 by simple calculation. Matrix elements for Pr(III) are given in Table 4.2a.

Table 2.2. Matrix Element * for Pr(III)

Level	$[(U^2)]^2$	$[(U^4)]^2$	$[(U^6)]^2$
1D_2	0.0026	0.0170	0.052
3P_0	0	0.1728	0
3P_1	0	0.1707	0
3P_2	0	0.0362	0.1355

*W.T. Carnall, P.R. Fields and K. Rajnak, *J. Chem. Phys.*, 49 (1968) 4424. ³¹

Carnall's formation envisages intensities for the 3P_1 and 3P_0 bands, whereas in reality these values differ by a factor of nearly two. Hence the derived T_4 value is approximate, not accurate. However, this does not introduce much error in T_6 , though one would accept that this T_6 value is not exactly correct. The calculation of T_2 involves T_4 and T_6 and suffer from disadvantage that its value is affected by inaccuracies incurred in both T_4 and T_6 . In some cases, it turns out a negative value, a physically unacceptable solution. However,

we believe that our conclusions about structure derived from T_4 and T_6 do have some meaning.

For Pr^{3+} , ${}^3\text{H}_4 \rightarrow {}^3\text{F}_2$ transition occurring around 5200 cm^{-1} shows hypersensitivity, however, the ${}^3\text{H}_4 \rightarrow {}^3\text{P}_2$, ${}^3\text{H}_4 \rightarrow {}^3\text{P}_1$, ${}^3\text{H}_4 \rightarrow {}^3\text{P}_0$ and ${}^3\text{H}_4 \rightarrow {}^1\text{D}_2$ transitions also have been found minor changes in the immediate coordination environment around Pr(III) ^{32,33}, though this transition cannot be regarded as hypersensitive as these do not obey selection rules.

2.5. Kinetic studies

2.5.1. Rate of the reactions

Based on the concept of activation energy. Arrhenius described the temperature dependence of the rate constant (k) by the equation,

$$k = Ae^{\frac{-E_a}{RT}} \dots\dots\dots (5)$$

This equation is known as the Arrhenius rate equation.

Where A stands for frequency factor. The factor $\exp(-E_a/RT)$ is a measure of the likelihood of a molecule being in an activated state.

Plotting graph $\log k$ (rate constant) versus $1/T$ yields the Arrhenius rate equation, which is used to determine the activation energy for the $\text{Pr(III):L-Aspartic acid}$ complex in DMF solvent.^{34,35} The equation (5) may be expressed as follows:

$$\begin{aligned} \ln k &= \ln A - \frac{E_a}{RT} \\ \text{or, } 2.303 \log k &= 2.303 \log A - \frac{E_a}{RT} \\ \text{or, } \log k &= \log A - \frac{E_a}{2.303RT} \dots\dots\dots (6) \end{aligned}$$

where, A = pre-exponential factor, often known as the frequency factor.

As a result, plotting $\log k$ versus $1/T$ should provide a straight line with a negative slope.

Slope = $\frac{E_a}{2.303R}$ and Intercept = $\log A$; R is the universal gas constant.

The activation energy E_a is calculated from the slope as

$$E_a = -\text{Slope} \times 2.303 \times R \dots\dots\dots (7)$$

The complexation's thermodynamic characteristics were established using a Van't Hoff plot of $\log k$ versus $1/T \times 10^3$, which was provided as

$$\begin{aligned} \log k &= -\frac{\Delta H^\circ}{R} \left[\frac{1}{T} \right] + \frac{\Delta S^\circ}{R} \dots\dots\dots (8) \\ \text{Or } \log k &= -\frac{\Delta G^\circ}{RT} \end{aligned}$$

REFERENCES

1. Geary, W. J. The use of conductivity measurements in organic solvents for the characterisation of coordination compounds. *Coord. Chem. Rev.* **7**, 81–122 (1971).
2. Smith, B. C. Fundamentals of Fourier Transform Infrared Spectroscopy. (2011) doi:10.1201/B10777.
3. Cullity, B. D. *Elements of X-ray Diffraction*. (Addison-Wesley Publishing Company, 1978). doi:10.1088/0031-9112/29/12/034.
4. Guinebretière, R. X-ray Diffraction by Polycrystalline Materials. *X-ray Diffr. by Polycryst. Mater.* (2010) doi:10.1002/9780470612408.
5. Solé, J. G., Bausá, L. E. & Jaque, D. An Introduction to the Optical Spectroscopy of Inorganic Solids. *An Introd. to Opt. Spectrosc. Inorg. Solids* 1–283 (2005) doi:10.1002/0470016043.
6. Pelant, I. & Valenta, J. Luminescence Spectroscopy of Semiconductors. *Lumin. Spectrosc. Semicond.* **9780199588**, 1–560 (2012).
7. Daniels T.C. *Thermal analysis*. (John Wiley & Sons, 1973).
8. Wendlandt Wesley Wm. *Thermal Methods of Analysis* . (John Wiley & Sons, Incorporated, 1964).
9. Duval Clement. *Inorganic Thermogravimetric Analysis* . (Elsevier Publishing Company, 1953).
10. Keatch Cyril Jack & Dollimore David. *An Introduction to Thermogravimetry*. (John Wiley & Sons Incorporated, 1975).
11. Brown, M. E. Introduction to thermal analysis : techniques and applications. 264 (2001).
12. Haines, P. J. Principles of thermal analysis and calorimetry. 220 (2002).
13. Earnest, C. M. Compositional Analysis by Thermogravimetry. *Compos. Anal. by Thermogravim.* (1988) doi:10.1520/STP997-EB.
14. Garn D. Paul. *Thermoanalytical Methods of Investigation* . (Academic Press, 1965).
15. Sibilía, J. P. A Guide to materials characterization and chemical analysis. 318 (1988).
16. Chatwal R. Gurdeep & Anand K. Sham. *Instrumental Methods of Chemical Analysis* (Himalaya Publishing House, 1979).
17. Pelczar Michael J., Chan E.C.S. & Reid N. R. *Microbiology*. (Tata McGraw-Hill, 1988).
18. Evans C.H. *Biochemistry of the Lanthanides*. (Plenum Press, 1990).
19. Wybourne, B. G. & Meggers, W. F. Spectroscopic Properties of Rare Earths. *Phys.*

- Today* **18**, 70 (2009).
20. Nugent, L. J., Baybarz, R. D., Burnett, J. L. & Ryan, J. L. Electron-transfer and $f \rightarrow d$ absorption bands of some lanthanide and actinide complexes and the standard (III–IV) oxidation potentials for each member of the lanthanide and actinide series. *J. Inorg. Nucl. Chem.* **33**, 2503–2530 (1971).
 21. Mehta, J. P., Bhatt, P. N. & Misra, S. N. An absorption spectral study of Nd (III) with glutathione (reduced), GSH in aqueous and aquated organic solvent in presence and absence of Zn (II). *J. Solid State Chem.* **171**, 175–182 (2003).
 22. Brian R. Judd. *Operator Techniques in Atomic Spectroscopy*. (McGraw-Hill, 1963).
 23. Carnall, W. T., Fields, P. R. & Rajnak, K. Spectral Intensities of the Trivalent Lanthanides and Actinides in Solution. II. Pm^{3+} , Sm^{3+} , Eu^{3+} , Gd^{3+} , Tb^{3+} , Dy^{3+} , and Ho^{3+} . *J. Chem. Phys.* **49**, 4412 (2003).
 24. Sinha, S. P. Spectroscopic investigations of some neodymium complexes. *Spectrochim. Acta* **22**, 57–62 (1966).
 25. Kothari, A. & Misra, S. N. Electronic spectral study of amino-acid complexes of Nd(III). <https://doi.org/10.1139/v83-304> **61**, 1778–1783 (2011).
 26. Kothari, A. & Misra, S. N. Electronic spectral study of amino-acid complexes of Nd(III). *Can. J. Chem.* **61**, 1778–1783 (1983).
 27. Kothari, A., Jain, R., Ahmed, A., Nuclear, S. M.-J. of I. and & 1981, undefined. A study of ternary complexes of praseodymium with cysteine and diols. *Elsevier*.
 28. Joshi, G., Singh, M. & Misra, S. Spectrophotometric Study of Some Praseodymium (III) Schiff Base Complexes. (1984).
 29. Misra, S., Joshi, G., Chemistry, M. S.-J. of I. and N. & 1981, undefined. Study of some anhydrous praseodymium fluoro β -diketonates interelectronic repulsion, spin-orbit interaction bonding electronic energy levels and IR. *Elsevier*.
 30. Wong, E. Y. Configuration Interaction of the Pr^{3+} Ion. *J. Chem. Phys.* **38**, 976 (2004).
 31. Carnall, W. T., Fields, P. R. & Rajnak, K. Electronic Energy Levels in the Trivalent Lanthanide Aquo Ions. I. Pr^{3+} , Nd^{3+} , Pm^{3+} , Sm^{3+} , Dy^{3+} , Ho^{3+} , Er^{3+} , and Tm^{3+} . *J. Chem. Phys.* **49**, 4424 (2003).
 32. Borina, A. F. The central ion effect on the complex formation process in aqueous organic solvents. The Jahn-Teller effect in the Cu^{2+} solutions. *Russ. J. Coord. Chem.* 2007 3311 **33**, 831–837 (2007).
 33. Devlin, M. T., Stephens, E. M. & Richardson, F. S. Comparison of Electric-Dipole

Intensity Parameters for a Series of Structurally Related Neodymium, Holmium, and Erbium Complexes in Aqueous Solution. Theory and Experiment. *Inorg. Chem.* **27**, 1517–1524 (1988).

34. Laidler Keith J. *Chemical Kinetics*. (Pergamon Press, 1965).
35. Ross, P. D. & Subramanian, S. Thermodynamics of protein association reactions: forces contributing to stability. *Biochemistry* **20**, 3096–3102 (1981).

Synthesis, spectral and antimicrobial studies of Praseodymium (III): Ligands (L-Aspartic acid, L-Histidine and L-Valine) Complexes.

In this chapter, three new Praseodymium (III) complexes were synthesized using some selected amino acids (L-Aspartic acid, L-Histidine and L-Valine) as ligands. These complexes, the metal ions and the ligands were characterized through various physicochemical, spectral and TGA studies. The elemental and IR studies revealed that the ligand is coordinated to the metal ion in a bidentate fashion through the oxygen atom of the carboxylic acid and nitrogen atom of the amine. The powder XRD of Praseodymium (III) complexes was studied. The photoluminescent properties of the metal ion and the metal complexes were evaluated, and it was observed that the metal complexes show enhancement of intensities compared to the free metal ion. TGA studies show that all the complexes were thermally stable, and the antimicrobial properties of the complexes could also be detected.

3.1. Introduction

Lanthanide chemistry has just been intensively investigated in the last two decades, when it was discovered that these elements had distinctive chemical features, such as fluorescence and powerful magnetic capabilities, due to their peculiar 4f electrons¹. Lanthanides are being rapidly and efficiently incorporated by chemists into a wide range of substances and materials for advanced uses. Because they are necessary for so many technical products, such as computers, smartphones, solar cells, batteries, optical glasses, wind turbines, lasers² etc, lanthanides are sometimes referred to as "the seeds of technology." It is often believed that lanthanide (III) complexes with ligands are the most crucial elements in the search for novel materials because of the sharp f-f transitions. The motivation to keep researching novel lanthanide complexes came from these characteristics of lanthanide compounds and their prospective uses¹.

As the fundamental components of proteins, amino acids also act as the nitrogenous basis for molecules like neurotransmitters and hormones. An amino acid is a type of organic chemical that, as defined by chemistry, possesses both a carboxylic acid (-COOH) and an amino (-NH₂) functional group. The distinctive characteristics of each amino acid depend on the variation in the side-chain group or R-group. Strong Lewis's acids, such as lanthanides, coordinate with hard bases (carboxylates) and strongly electronegative donors like N or O³. Similar to biological complexes [i.e., protein-lanthanide interactions], the formation of many lanthanide complexes depends on the Lewis acid reactivity of these elements. The generation of novel structure of Lanthanide (III): Amino acids complex is formed through the oxygen donor atom of the carboxylate group, and via the nitrogen atom of the amino group. They are frequently utilised in the synthesis of complexes to produce unique structures. This kind of ligand can generate coordination compounds that have a wide range of uses⁴. Numerous coordination compounds of this sort may have antibacterial, antioxidant, anti-tumour, and anti-diabetic activities. The lanthanide chemistry that underpins our contemporary technologies is crucial, and as a result, the scientific community is making significant contributions to comprehending the mechanistic specifics of the interaction between lanthanides and ligands, allowing for the development of direct applications of these concepts.

In this paper, we synthesized three praseodymium (III): amino acid complexes. Characterization of the complexes were performed based on the following techniques of

elemental analysis, IR, XRD, Fluorescence studies and TGA. We also made an attempt to study the antimicrobial properties of the Pr (III): amino acids complexes.

3.2. Materials and methods

The ligands L-Aspartic acid, L-Histidine and L-Valine were acquired from HIMEDIA, while praseodymium (III) nitrate hexahydrate $[\text{Pr}(\text{NO})_3 \cdot 6\text{H}_2\text{O}]$ of 99.9% purity was purchased from Sigma Aldrich. Nutrient Agar, Nutrient Broth and Sabouraud dextrose agar was purchased from HIMEDIA. Elemental Analyzers CHNS-O EuroVector were used to analyse the elemental analyses for C, H, O, and N. Using the oxalate-oxide technique, the metal content was determined. Using a Systronic direct reading conductometer and 10^{-3} M solutions of the complexes in a suitable solvent, measurements of molar conductance were performed. The infrared spectra were recorded using KBr pellets on the Perkin Elmer FT-IR spectrophotometer (Spectrum two) over the range of 400-4000 cm^{-1} . Luminescence studies was carried out using fluorescence spectrophotometer SHIMADZU model no. RF – 6000. Powder X-Ray diffraction studies were carried out using the X-Ray Diffraction Rigaku Ultima IV using $\text{Cu}_{\text{K}\alpha}$ radiation of wavelength $\lambda = 1.5406 \text{ \AA}$ from 10° to 80° (2θ) at room temperature. With a heating rate of 20° C/min and nitrogen environment, thermal analysis was performed using the SDT Q600V20.9 Build 20 thermal analyzer.

3.2.1. Synthesis of lanthanide complexes [Pr(III):Ligands (L-Aspartic acid, L-Histidine and L-Valine) complexes]: All of the praseodymium(III) complexes were synthesized using the general method outlined below. 20 ml of 0.01 mol aquated solution of the ligand was added to 20 ml of hot alcoholic solution of praseodymium(III) nitrate hexahydrate and refluxed. The refluxing procedure was carried out for 24-36 hours while the pH of the solution was kept at its isoelectric point. The solution was taken and kept in a water bath until it had been concentrated to half of its original volume. The solution was allowed to cool, filtered and the filtrate was kept. After a few days, the crystals were collected at the bottom of the beaker which was washed with modest amounts of distilled water, alcohol and ether. The collected crystals were dried in a desiccator.

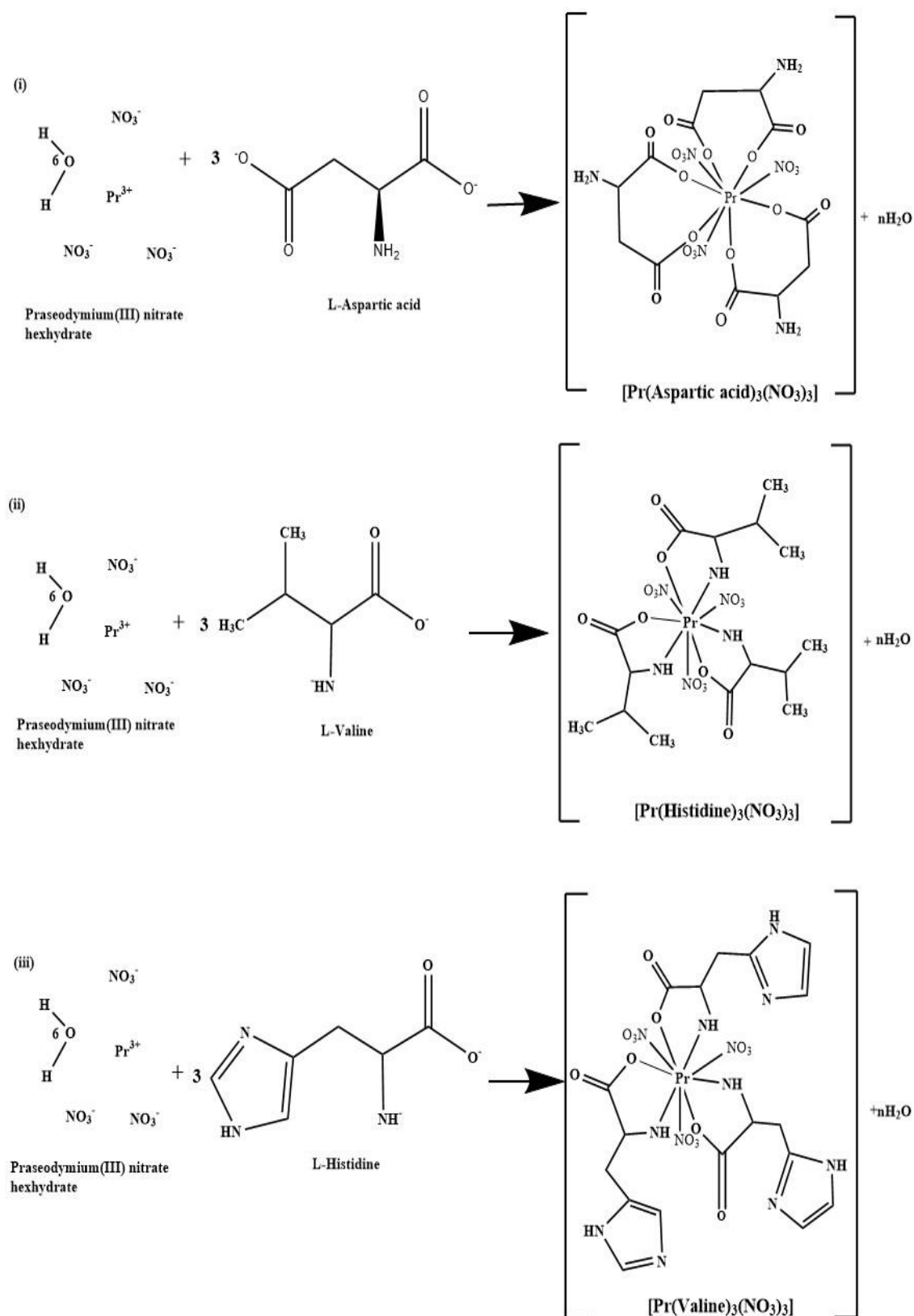


Figure 3.1. Probable Chemical Reaction for the synthesized Praseodymium (III): Ligands [(i) Aspartic acid, (ii)Histidine (iii) Valine] Complexes.

3.2.2. Biological Activity

Source of Microorganism: For the purpose of evaluating the antimicrobial activities, organisms such as Gram-positive *Staphylococcus aureus* and *Bacillus subtilis* were utilised in addition to Gram-negative *Escherichia coli* and *Klebsiella pneumoniae*. The fungal culture *Fusarium oxysporum*, *Penicillium italicum*, *Aspergillus niger* and *Candida albicans* were used.

Preparation of Bacterial Pathogens: The overnight cultures (0.2ml) of each bacterium were divided into 20ml of sterile nutrient broth and incubated for around 3-5 hours in order to standardise the culture. The standard cultures were employed in a loop for the antibacterial test.

Antibacterial Assay: Nutrient Agar was sterilised and prepared. In Petriplates, 20 ml of medium were added and left to solidify. The sterile cotton swab used to create the bacterial grass culture was labelled. With the use of a metallic borer with centres at least 24 mm in diameter, the wells were drilled into the medium. 50 µl of the test sample, diluted to the necessary concentration of 1 mg/ml, were added to the appropriate wells. Reference antimicrobial medication is added to additional wells⁵. The plates are immediately incubated for 24 hours at 37°C. By measuring the diameter of zones exhibiting total inhibition, activity was calculated (mm). The medication was contrasted with growth inhibition.

Minimum Inhibitory Concentration: The minimum inhibitory concentration was determined using the tube dilution method by preparing different concentration of metal complex solution (i.e., 300 µg/ml, 500 µg/ml, 600 µg/ml, 800 µg/ml and 1 mg/ml)⁶. Cleaned test tubes were taken and different concentration of metal complex such as 300 µl/ml, 500 µl/ml, 600 µl/ml, 800 µl/ml and 1 mg/ml was poured in the cleaned test tubes respectively and the volume of the medium was made upto 2 ml with nutrient broth. 2ml of the prepared control was put into the test tubes and autoclave at 121°C temperature and 15 lbs pressure for 15 minutes. After sterilization, the medium was allowed to cool and 0.2ml of overnight cultures of each organism was dispensed into sterile medium and incubated for 24 hours. The activity was measured by turbidity in the broth⁷.

Antifungal Assay: The antifungal activity of metal complex was studied against four fungal cultures, *Aspergillus niger*, *Penicillium italicum*, *Candida albicans* and *Fusarium oxysporum*. Sabouraud dextrose agar was prepared and sterilized. The culture plates were prepared with the same method as that of the antibacterial assay. After the media was solidified, respective fungal spore suspensions were transferred in the petri plates. With the help of a sterile metallic borer, the wells were made in the centers at least 24 mm of the media. Recommended concentration 50 μ l of the test sample 1 mg/ml in water was introduced in the wells. The plates were incubated at 30°C for 72 hours. The results were recorded as zones of inhibition in mm⁸.

3.3. Results and discussion

According to analytical data, Praseodymium (III) complexes were synthesized with a metal-ligand stoichiometry of 1:3 and had good storage properties. The complexes are non-hydroscopic solids and are soluble in common organic solvents, such as methanol, ethanol, ACN and DMF. The analytical values of the complexes are in good agreement with their formation and the elemental analysis and metal composition of the complex are given in table 3.1. The molar conductance values of the complexes, given in table 3.1. were in the range of 10-13.1 $\Omega^{-1}\text{cm}^2\text{mol}^{-1}$ in DMF solution at room temperature. These values indicated that the complexes were non-electrolytes in nature⁹.

Table 3.1. Analytical data and other details of the lanthanide (III) complexes (Asp.=Aspartic Acid, His=Histidine and Val=Valine); calculated values are given in brackets.

Sl. no	Complexes	%Yield	Colour	M	C	H	N	O	Molar conductance (DMF) $\Omega^{-1}\text{cm}^2\text{mol}^{-1}$
1	[Pr(Asp.) ₃ (NO ₃) ₃] PrC ₁₅ H ₂₂ N ₆ O ₂₁	83	Greenish white	18.46 (18.51)	23.60 (23.58)	2.91 (2.88)	11.01 (11.05)	44.02 (43.98)	12.6
2	[Pr(His.) ₃ (NO ₃) ₃] PrC ₂₁ H ₂₈ N ₁₂ O ₁₅	80	Brown	16.99 (16.96)	30.40 (30.42)	3.41 (3.39)	20.27 (20.31)	28.93 (28.91)	12.9
3	[Pr(Val) ₃ (NO ₃) ₃] PrC ₁₈ H ₃₄ N ₆ O ₁₅	77	Green	19.69 (19.72)	30.21 (30.19)	4.80 (4.81)	11.75 (11.69)	33.35 (33.40)	11.5

IR Spectra

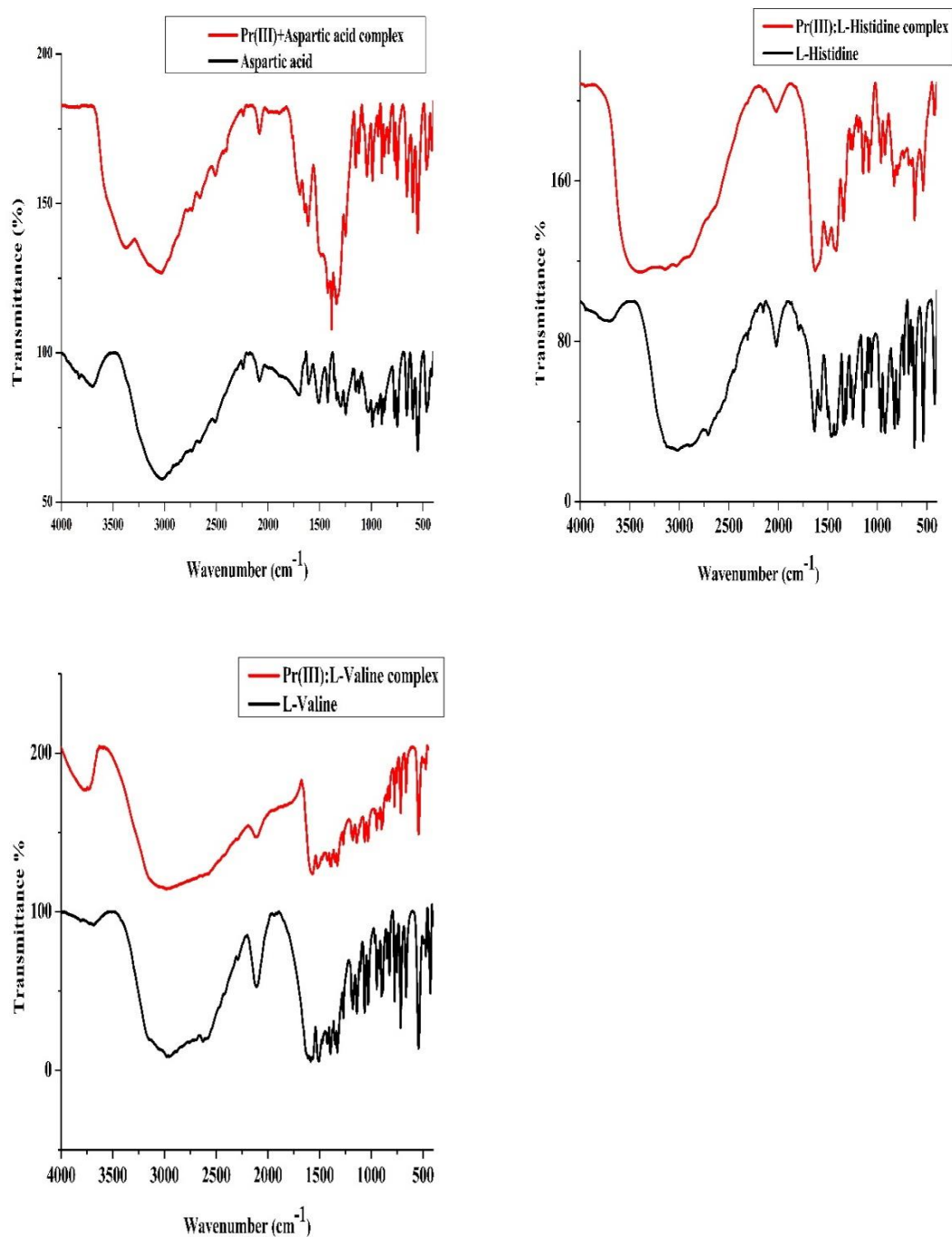


Figure 3.2. The FT-IR spectra of the ligands (L-Aspartic acid, L-Histidine and L-Valine) and Pr(III): Ligands complexes. *Red are the complexes and black are the ligands.

The infrared spectra of Pr(III):L complexes (L-Aspartic acid, L-Histidine and L-Valine) and pure ligands are shown in figure 3.2. The characteristic infrared absorption frequencies of these complexes in solid state are tabulated in Table 3.2. Analysing the characteristic infrared absorption frequencies of the L-Aspartic acid complex with Pr^{3+}

ion, we could observe the representative -OH (carboxylic acids) and -NH (amine) stretching vibrations in the spectrum of the complex at 3104.30 cm^{-1} and 3437.03 cm^{-1} . We have also observed the characteristic bands of the carboxyl group at 1712 cm^{-1} and 1338.84 cm^{-1} . The peak at 1614.52 cm^{-1} corresponds to the bending vibration of the NH_2 group. The peaks at around 492.37 cm^{-1} and 406.62 cm^{-1} leads to M-O strong coordination bond^{10,11}. Whereas, the peak at 1566.61 cm^{-1} represents the presence of NO_3 in the complex.

However, analysing the characteristic infrared absorption frequencies of the Pr : L-Histidine complex, we could observe the -NH (amine) stretching vibration in the spectrum of the complex at 3383.52 cm^{-1} . We have also observed the characteristic bands of the carboxyl group at 1192.09 cm^{-1} and 1145.13 cm^{-1} . The peak at 1621.92 cm^{-1} corresponds to the bending vibration of the NH_2 group, which leads to the vibrations in the ring at 624.24 cm^{-1} . However, the other two types of vibrations such as twisting and wagging of the NH_2 group appeared at 830.15 cm^{-1} and 624.24 cm^{-1} , respectively. The different modes of vibrations of the existing -COO group in the complex gave rise to the peaks at 1192.09 cm^{-1} and 1145.13 cm^{-1} , which may correspond to its wagging, bending and rocking. The peaks at around 536.93 cm^{-1} and 419.55 cm^{-1} may lead to coordinating sites such as oxygen and nitrogen; M-O and M-N, respectively¹². The peak at high energy (536.93 cm^{-1}) may correspond to M-O coordination if we consider the electronegativity, availability of lone pair of electrons and opposite charges on praseodymium (III) and oxygen ions that form strong bonding as compared to that of M-N. The peak at 419.55 cm^{-1} is though may due to the coordination of nitrogen atom with praseodymium (III). The other peaks at 2024.39 cm^{-1} , 1269.71 cm^{-1} , 1247.35 cm^{-1} , 1086.03 cm^{-1} , 794.70 cm^{-1} , 722.81 cm^{-1} , 682.84 cm^{-1} , and 655.80 cm^{-1} may represent -C-H bending, -C=N and -C=C stretching, --CH wagging, and -CH rocking vibrations, respectively¹³. However, the peak at 1340.63 cm^{-1} represents NO_3 counter ion.

Similarly, the Pr: L-Valine complex are analysed and -N-H (Amine) and -O-H (carboxylic acid) stretching vibration spectrum were found at 3727.80 cm^{-1} (medium), 2110.54 cm^{-1} (weak and broad) and 3136.56 cm^{-1} . We have also observed the characteristic bands of the carboxyl group at 1191.22 cm^{-1} , 1176.39 cm^{-1} and 1140.20 cm^{-1} . The peak at 1564.65 cm^{-1} corresponds to the bending vibration of the NH_2 group, which leads to the wagging of -N-H at 889.16 cm^{-1} . The peaks at 1521.59 cm^{-1} and 1352.14 cm^{-1} represents the presence of NO_3 ion in the complex. The peaks at around 541.76 cm^{-1} and 470 cm^{-1} may

lead to coordinating sites such as oxygen and nitrogen respectively. The peak at high energy (541.76 cm^{-1}) leads to M–O coordination and the peak at 470 cm^{-1} praseodymium (III) is coordinated to nitrogen atom.

Table 3.2. FT-IR wavenumbers with functional groups assigned to the Pr:L(L-Aspartic acid, L-Histidine and L-Valine) complexes.

Assignments (Functional groups)	Wavenumbers (cm^{-1})		
	Pr(III):Aspartic acid complex	Pr(III):Histidine complex	Pr(III):Valine complex
-N-H stretching (amines)	3437.03	3383.52	3727.80(m), 2110.54 (w, b)
-O-H stretching (carboxylic acid)	3104.30,		3136.56(b)
-COO stretching	2414.49		
-C-H bending (aromatic compounds)		2024.39	
-C=O stretching (carboxylic acid)	1712.59		
-N-H bending	1614.52	1621.92	1564.65
Ring		1596	
-N-O asymmetric stretching (nitro compound)	1566.61		1521.59
-C-C stretching (in ring)		1497.86	
-C-H bending	1413.27, 1487.38		1474.17, 1424.95, 1384.72
-N-O symmetric stretching (nitro compounds)		1340.63	1352.14
-C-H rocking		722.81(s)	1329.44
-C-N stretching (aromatic amine)		1269.71	
-C-H wagging	1233.10, 1026.42	1247.35	1271.68
-C-O stretching (carboxylic acid)	1338.84	1192.09, 1145.13	1191.22, 1176.39, 1140.20
-C-N stretching (amine)		1086.03	1065.14, 1033.45
-O-H bending (carboxylic acid)		921.52	948.72, 903.10
-N-H wagging	857.34, 761.53	830.15, 624.24	889.16
=C-H bending	697.03, 673.55	794.70, 682.84, 655.80	775.39, 665.01

Luminescence studies

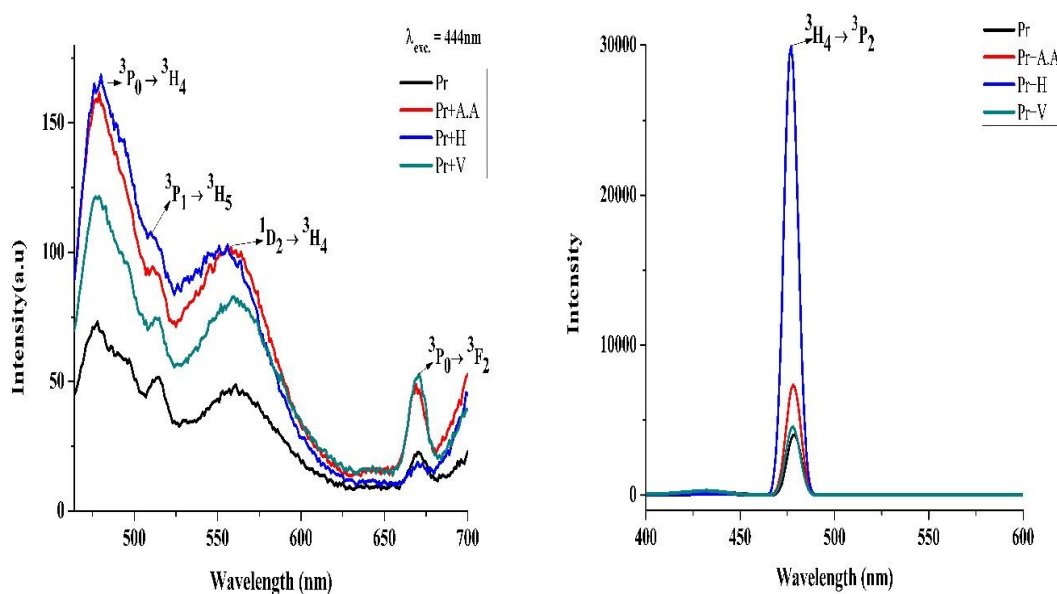


Figure 3.3. (a) Emission spectra and (b) Excitation spectra of Praseodymium(III) and Praseodymium complexes.

Figure 3.3. (a) and (b) shows the emission spectra of Pr^{3+} ions and Pr(III) complexes in the spectral region 430–700 nm obtained by 444 nm excitation corresponding to the ${}^3\text{H}_4 \rightarrow {}^3\text{P}_2$ transition. The emission bands centred at 479, 510, 556 and 671 nm are assigned to ${}^3\text{P}_0 \rightarrow {}^3\text{H}_4$, ${}^3\text{P}_1 \rightarrow {}^3\text{H}_5$, ${}^1\text{D}_2 \rightarrow {}^3\text{H}_4$ and ${}^3\text{P}_0 \rightarrow {}^3\text{F}_2$ transition, respectively. Upon 444 nm excitation, the excited Pr^{3+} ion decay non-radiatively from the ${}^3\text{P}_1$ and ${}^1\text{D}_2$ excited state to the lower lying ${}^3\text{H}_4$, ${}^3\text{H}_5$ and ${}^3\text{F}_4$ energy states^{14,15}. The luminescence intensity of the emission transitions depends on the population of the complexes and Pr ion in the excited levels. However, the intensity of the ${}^3\text{P}_0 \rightarrow {}^3\text{H}_4$ transition is high due to the fast nonradiative decay from the higher lying ${}^3\text{P}_{2,1,0}$ levels. The inset of Figure 3.3. describes the emission channels of Pr^{3+} ions in Pr(III):amino acid complexes. From the emission spectra it is clear that the emission intensity of the ${}^3\text{P}_0 \rightarrow {}^3\text{H}_4$ transition is almost constant for the Pr(III):amino acid complexes due to the increase in the energy transfer among the excited complexes ions. Moreover, the free metal ion and lanthanide complex of the emission bands ${}^3\text{P}_0 \rightarrow {}^3\text{F}_4$ transition overlap each other whereas for ${}^3\text{P}_0 \rightarrow {}^3\text{H}_4$, ${}^3\text{P}_1 \rightarrow {}^3\text{H}_5$ and ${}^1\text{D}_2 \rightarrow {}^3\text{H}_4$, they are well resolved. Significant red shift has been observed for the ${}^3\text{P}_0 \rightarrow {}^3\text{H}_4$, ${}^3\text{P}_1 \rightarrow {}^3\text{H}_5$ and ${}^1\text{D}_2 \rightarrow {}^3\text{H}_4$ emission transition whereas, ${}^3\text{P}_0 \rightarrow {}^3\text{F}_2$ emission transition shows blue shift. Observation of the emission

transitions shows that the emission band ${}^3P_0 \rightarrow {}^3H_4$ occurs peaked at ~476 nm, ~ 478 nm, ~ 479 nm and ~480 nm while, ${}^3P_1 \rightarrow {}^3H_5$ peaks occurs at ~510 nm, ~511 nm, ~513 and ~514 nm whereas, for ${}^3P_0 \rightarrow {}^3H_5$ peaks occurs at ~556 nm, ~558 nm, ~560 nm and ~561 nm respectively. This red shift may be due to the distribution of excited ions in the vicinity of ligand fields at complexation¹⁶. The intensities of all the observed emission bands increase with the increase of functional groups in the ligands of the complexes. This may be mainly due to the phenomenon of quenching through the energy transfer between the excited state of the Pr(III) ion. The emission dominates from the 3P_0 state which is populated by fast multiphonon non-radiative relaxation from the higher lying ${}^3P_{2,1,0}$ levels. As the complexation of the Pr^{3+} ion with the ligands takes place, the energy transfer process becomes more predominant and fast quenching in emission intensity takes place¹⁷. At lanthanide (III): Ligands complexes red emission quenches significantly but quenching of blue emission is less. All the lanthanide complexes show enhancement in the emission intensity compared to that of the metal ion. The enhancement of luminescence intensity of the lanthanide ion and the metal complexes was in the order $Pr(III):Histidine > Pr(III):Aspartic\ acid > Pr(III):Valine > Pr(III)$. The enhancement of the emission intensity of all metal complexes was clear evidence of metal-ligand complexation. The quantum yield for $Pr(III):L\text{-}Aspartic\ acid$ complex was 0.0505, $Pr(III):L\text{-}Histidine$ complex was 0.0741 and $Pr(III):L\text{-}Valine$ complex was 0.0449 and for $Pr(III)$ was 0.0441 respectively. Compared to the metal ion, which served as their precursor, the metal complexes displayed significant fluorescence intensities. The addition of a metal ion to the complex may have made the ligand more rigid in its conformation, which would have raised the fluorescence intensities of the complexes. These findings indicate that the created complexes could be useful in photochemical application¹⁸⁻²⁰.

X-Ray Diffraction

Praseodymium (III):ligand complexes' X-ray diffraction pattern was observed (figure 3.4.). The unit cell parameters and Miller indices were used to connect the Bragg angles and the set of interplanar spacing to these values, which were then applied to the individual reflections using formulas using $\sin 2\theta$ ²¹. The reflections between 2θ in the diffractogram of the complexes ranged from 10 to 60° , with a maxima at $2\theta = 23.772$, 19.029 and 29.676.

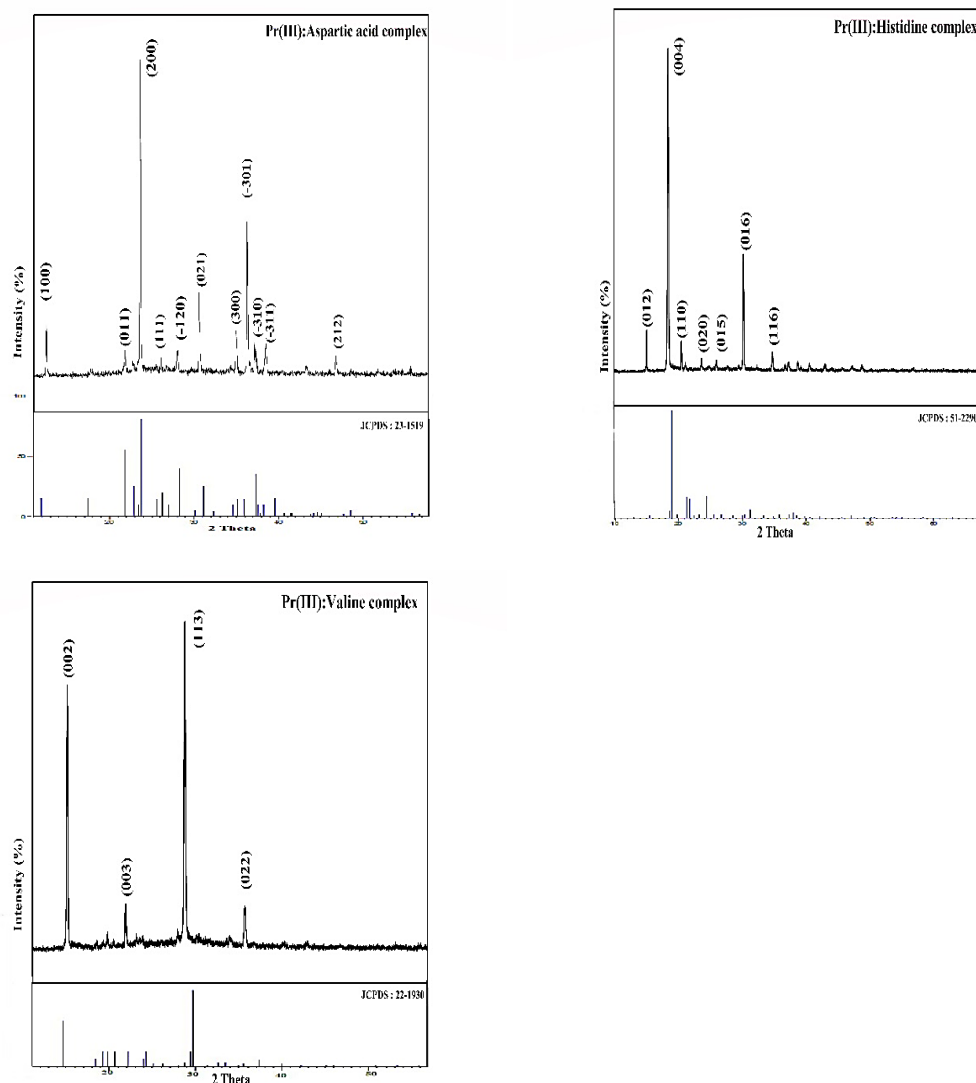


Figure 3.4. XRD spectrum of Praseodymium: Ligands ((a) L-Aspartic acid, (b) L-Histidine and (c) L-Valine) complexes.

The lattice parameters calculated for the unit cell value of Pr (III):L-Aspartic acid complex are; $a = 7.6080$ (Å), $b = 6.9660$ (Å), $c = 5.1220$ (Å) and cell volume of cell = 267.55 (Å)³ with space group P21. The lattice parameters for Pr(III):L-Histidine complex was found to be $a = 5.1430$ (Å), $b = 7.2940$ (Å), $c = 18.6740$ (Å) and cell volume of cell = 700.52 (Å)³ with space group P212121. And finally, The lattice parameters calculated for the unit cell value of Pr(III):L-Valine complex are; $a = 9.6470$ (Å), $b = 5.2550$ (Å), $c = 12.0100$ (Å) and cell volume of cell = 608.67 (Å)³ with space group P21. However, the three observed diffraction pattern corresponds to monoclinic, orthorhombic and monoclinic phases which matches with the JCPDS PDF No. 00-023-1519, 00-051-2290

and 00-022-1930 respectively. The presence of possible phases such as PrO_3 is not observed. This confirms the lattice substitution of Pr^{3+} in $(\text{C}_4\text{H}_6\text{NO}_4)_3^-$, Pr^{3+} in $(\text{C}_6\text{H}_8\text{N}_3\text{O}_2)_3^-$ and Pr^{3+} in $(\text{C}_5\text{H}_{10}\text{NO}_2)_3^-$ sites respectively. The crystal size was estimated using the Scherrer formula's,

$$d_{\text{XRD}} = \frac{\kappa\lambda}{\beta \cos \theta}$$

where k is the shape factor (≈ 0.9), β is the full width at half maximum of the reflection peak, θ is Bragg's angle, and λ is the wavelength of $\text{Cu } k_\alpha$ radiation. The average crystal size (d_{XRD}) was found to be 40.11 nm, 15.78 nm and 25.20 nm respectively.

Thermal analysis

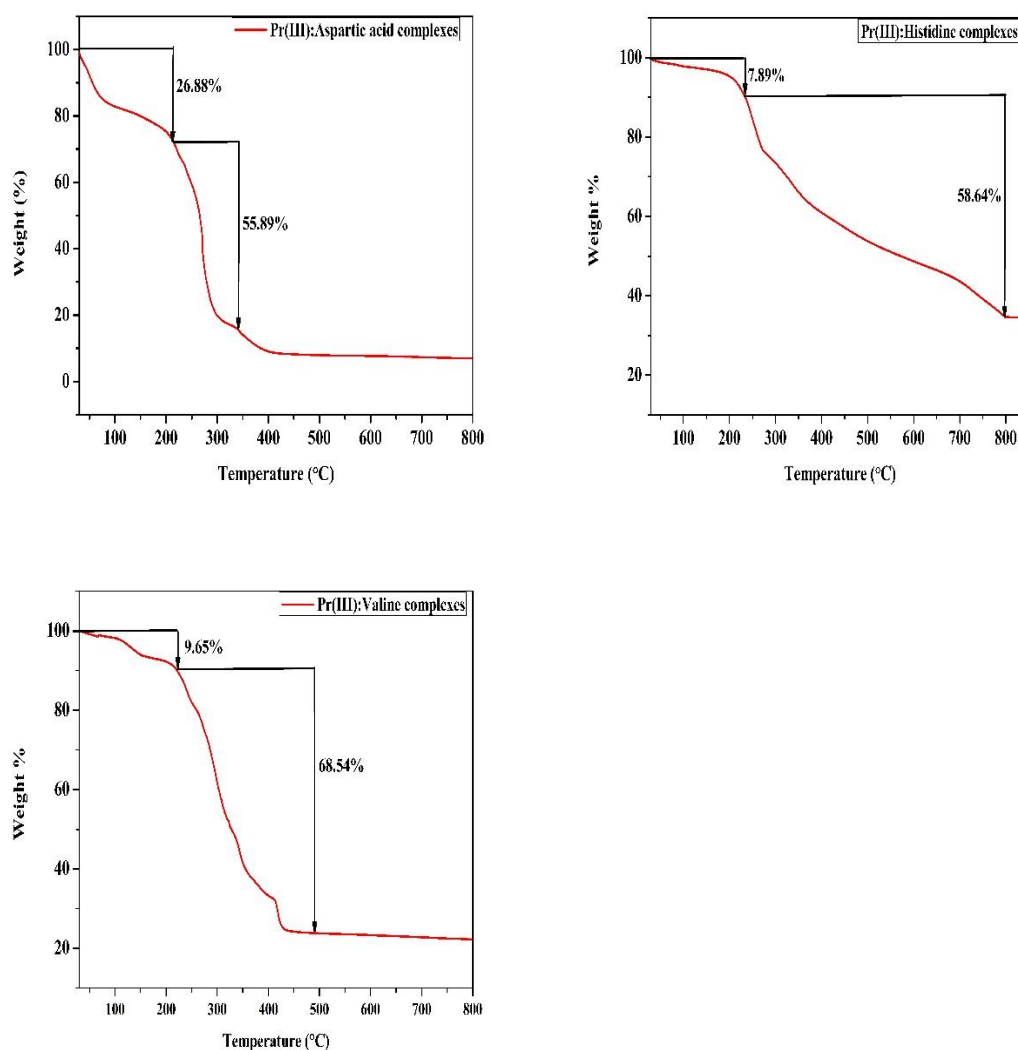


Figure 3.5. TGA of the three synthesized Praseodymium: Ligands (a) L-Aspartic acid, (b) L-Histidine and (c) L-Valine complexes.

The TGA measurements of the complexes were measured in dynamic air while being heated at a rate of 20°C/min. From figure 3.5., it has been found that the Praseodymium (III): Aspartic acid complex thermally decomposes in two stages, in the first stage three molecules of nitrate molecules decomposes and in the second stage three molecules of aspartic acid decomposes leaving Pr(III) as the final residue. Also, the Praseodymium (III):Histidine acid complex decomposes thermally in two stages, in the first stage a single molecule of nitrate decomposes and in the second stage the three molecules of ligand and two molecules of nitrate decomposes leaving PrO as the final residue. Finally, the Praseodymium (III):Valine complex thermally decomposes in two stages, similarly as that of the Pr:L-Aspartic acid complex where in the first stage three molecules of nitrate decomposes and in the second stage the three molecules of Valine decomposes leaving Pr(III) as the final residue. The stages of decomposition of the synthesized complexes are quite in agreement when compared to the elemental analysis result as given in table 3.1. Among the three synthesized complexes, The stability of praseodymium (III):Histidine complex is greatest as it start decomposes ~250°C in room temperature, whereas praseodymium(III):Aspartic acid complex is lowest as it start decomposition at ~210°C and praseodymium(III):Valine complex starts at ~230°C. Following is the stability order of the three complexes in dynamic air.

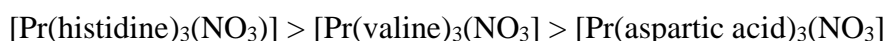


Table 3.3. Antibacterial activity of lanthanide complex, metal ion as negative control, commercial drug as positive control, here A is [Pr(Aspartic acid)₃NO₃], B is [Pr(Histidine)₃NO₃] and C is [Pr(Valine)₃NO₃].

Sl. No.	Name of bacterial pathogens	Zone of inhibition(mm)				
		Lanthanide complex			Negative control	Positive control (Ampicillin)
		A	B	C		
1	<i>Escherichia coli</i>	32	32	32	No zone	37
2	<i>Klebsiella pneumonia</i>	23	25	22	No zone	20
3	<i>Staphylococcus aureus</i>	22	24	21	No zone	26
4	<i>Bacillus subtilis</i>	14	14	13	No zone	10

Table 3.4. Minimum Inhibitory Concentration assay of Lanthanide (III) complexes against bacterial pathogens.

Sl. No.	Name of the bacterial pathogens	Observation of Growth				
		300 µg/ml	500 µg/ml	600 µg/ml	800 µg/ml	1 mg/ml
[Pr(Aspartic acid) ₃ (NO ₃) ₃]						
1	<i>Klebsiella pneumonia</i>	+	-	-	-	-
2	<i>Bacillus subtilis</i>	+	+	-	-	-
[Pr(Histidine) ₃ (NO ₃) ₃]						
1	<i>Klebsiella pneumonia</i>	+	-	-	-	-
2	<i>Bacillus subtilis</i>	+	-	-	-	-
[Pr(Valine) ₃ (NO ₃) ₃]						
1	<i>Klebsiella pneumonia</i>	+	+	-	-	-
2	<i>Bacillus subtilis</i>	+	-	-	-	-

Note: + = Growth of bacteria, - = No growth of bacteria

Table 3.5. Antifungal Activity of Lanthanide (III) complexes, here A is [Pr(Aspartic acid)₃NO₃], B is [Pr(Histidine)₃NO₃] and C is [Pr(Valine)₃NO₃].

Sl. No.	Name of Fungal Pathogens	Zone of inhibition (mm)		
		A	B	C
1	<i>Candida albicans</i>	45	48	40
2	<i>Aspergillus niger</i>	34	31	33
3	<i>Penicillium italicum</i>	21	18	20
4	<i>Fusarium oxysposum</i>	15	13	10

Antibacterial Activity of Lanthanide (III) Complex: Antibacterial activity of Lanthanide (III) complex with positive control commercial drugs (Ampicillin) and negative control as metal ion²² were studied against four bacterial pathogens such as *Escherichia coli*, *Klebsiella pneumonia*, *Staphylococcus aureus* and *Bacillus subtilis*. Lanthanide complex has shown better result in the form, zone of inhibition in culture plates rather than commercial drugs against two pathogens such as *Klebsiella pneumonia* and *Bacillus subtilis*. The zone of inhibition (mm) of Lanthanide metal complex in the culture plates were 23, 25 and 22 mm against *Klebsiella pneumonia* and 14, 14 and 13 mm against *Bacillus subtilis* respectively. Whereas negative control (metal ion) did not

show any zone of inhibition (Table 3.5.). The present finding shows the antibacterial activity of the three synthesized Lanthanide (III) complexes.

Minimum Inhibitory Concentration Assay: *Klebsiella pneumonia* and *Bacillus subtilis* were checked for the Minimum inhibitory concentration. Minimum inhibitory concentrations of bacterial pathogens were observed such as *Bacillus subtilis* (300 µg/ml) and *Klebsiella pneumonia* (500 µg/ml) (Table 3.6.). This result is similar to the finding of Chohan *et al*²³.

Antifungal Activity of Praseodymium (III) Complex: The inhibitory activity of Lanthanide (III) complexes was observed in fungal pathogens. Among the three fungal pathogens *Candida albicans* was highly susceptible (45 mm, 48 mm and 40 mm) followed by *Aspergillus niger* (34 mm, 31 mm and 33 mm), *Penicillium italicum* (21 mm, 18 mm and 20 mm) and *Fusarium oxysporum* (15mm, 13 mm and 10 mm). The results are presented in Table 3.7.

3.4. Conclusions

Three new Praseodymium (III): Amino acids complexes were synthesized which is verified by the characterization and they were non hydroscopic solid and soluble in water and most of the organic solvents. Their molar conductance was in the range from 10-13.1 $\Omega^{-1}\text{cm}^2\text{mol}^{-1}$ in DMF solution at room temperature which indicated that the complexes were non-electrolytes in nature⁹. Amino acid coordinates with Praseodymium (III) by its oxygen anion of deprotonated carboxyl group and the nitrogen atom of NH_2 group. The metal to oxygen and metal to nitrogen coordination has been justified by our IR data. The synthesized complexes were crystalline in nature and they match the JCPDS PDF No. 00-023-1519, 00-051-2290 and 00-022-1930. The Pr(III):Aspartic acid complex and Pr(III):Valine complex have monoclinic phase and average crystal size (d_{XRD}) are 40.11nm and 15.78nm respectively. Whereas, Pr(III):Histidine complex have Orthorhombic phase and average crystal size (d_{XRD}) is 25.20nm. The lattice parameters calculated for the unit cell value of Pr (III):L-Aspartic acid complex are; $a = 7.6080$ (Å), $b = 6.9660$ (Å), $c = 5.1220$ (Å) and cell volume of cell = 267.55 (Å)³ with space group P21. The lattice parameters for Pr(III):L-Histidine complex was found to be $a = 5.1430$ (Å), $b = 7.2940$ (Å), $c = 18.6740$ (Å) and cell volume of cell = 700.52 (Å)³ with space

group P212121. And finally, The lattice parameters calculated for the unit cell value of Pr (III):L-Valine complex are; $a = 9.6470$ (Å), $b = 5.2550$ (Å), $c = 12.0100$ (Å) and cell volume of cell = 608.67 (Å)³ with space group P21.

The metal ion and the complexes were excited at 444 nm and the excited metal ion and complexes decay non-radiatively from the ³P_J and ¹D₂ excited state to the lower lying ³H₄, ³H₅ and ³F₄ energy states. The quantum yield for Pr(III) is 0.0335, Pr(III):Aspartic acid complex was 0.0505, Pr(III):Histidine complex was 0.0741 and Pr(III):Valine complex was 0.0449 respectively. The synthesized complexes possess high thermal stability in air at room temperature as they start decomposition above 200°C and they have good antimicrobial properties. The findings indicates that it can be useful for photochemical and therapeutic applications.

REFERENCES

1. Martinez-Gomez, N. C., Vu, H. N. & Skovran, E. Lanthanide Chemistry: From Coordination in Chemical Complexes Shaping Our Technology to Coordination in Enzymes Shaping Bacterial Metabolism. *Inorg. Chem.* **55**, 10083–10089 (2016).
2. Cotruvo, J. A. The Chemistry of Lanthanides in Biology: Recent Discoveries, Emerging Principles, and Technological Applications. *ACS Cent. Sci.* **5**, 1496–1506 (2019).
3. Sanchu, J., Thakro, Z., Imsong, C. & Devi, M. I. Computation of spectral parameters for the complexation of Pr(III) with L-Histidine through 4f-4f transition spectra: Further analysis of its kinetic and thermodynamic parameters. *Chem. Phys. Impact* **5**, 100127 (2022).
4. Simal, A. L. & Martinelli Catelli De Souza Adriana. Composites based on poly(ethylene terephthalate) fibers with polyaniline. II. The effect of the growth of the polyaniline molecules during the polymerization in the morphology of the PET substrate. *J. Appl. Polym. Sci.* **77**, 2346–2362 (2000).
5. Shelke, V. A., Jadhav, S. M., Shankarwar, S. G., Munde, A. S. & Chondhekar, T. K. Synthesis, characterization, antibacterial and antifungal studies of some transition and rare earth metal complexes of N-benzylidene-2-hydroxybenzohydrazide. *Bull. Chem. Soc. Ethiop.* **25**, 381–391 (2011).
6. Balasankar, T., Gopalakrishnan, M. & Nagarajan, S. Synthesis and antibacterial activity of some 5-(4-biphenyl)-7-Aryl[3,4-d]-1,2,3-benzoselenadiazoles. <http://dx.doi.org/10.1080/14756360601051365> **22**, 171–175 (2008).
7. Mohanan, K., Aswathy, R., Nitha, L. P., Mathews, N. E. & Kumari, B. S. Synthesis, spectroscopic characterization, DNA cleavage and antibacterial studies of a novel tridentate Schiff base and some lanthanide(III) complexes. *J. Rare Earths* **32**, 379–388 (2014).
8. Kadam, M. S., Khiste, S. A., Dake, S. A. & Khade, B. C. Studies on X-Ray Diffraction, Thermogravimetric Stability, Antibacterial- Antifungal Activity of Fe(II), Ni(II), Cu(II) Metal Chloroquine Complexes Against Bacterial Strains and Fungal Spore. *Anti-Infective Agents* **18**, 339–351 (2019).
9. Geary, W. J. The use of conductivity measurements in organic solvents for the characterisation of coordination compounds. *Coord. Chem. Rev.* **7**, 81–122 (1971).
10. Hu, H. *et al.* Synthesis of a BiOIO₃/Bi₂O₄ heterojunction that can efficiently

- degrade rhodamine B and ciprofloxacin under visible light. *Opt. Mater. (Amst)*. **133**, 112893 (2022).
11. Sharma, K. V., Sharma, V. & Tripathi, U. N. Synthesis, spectral and biological investigations of 5(2'-hydroxyphenyl)-3-(4-substituted-phenyl) pyrazolines of cobalt(II) and their addition complexes with N, P donor ligands. <http://dx.doi.org/10.1080/00958970802233110> **62**, 506–518 (2009).
 12. Devi, P. P., Chipem, F. A. S., Singh, C. B. & Lonibala, R. K. Complexation of 2-amino-3-(4-hydroxyphenyl)-N'-[(2-hydroxyphenyl) methylene] propane hydrazide with Mn(II), Co(II), Ni(II), Cu(II) and Zn(II) ions: Structural characterization, DFT, DNA binding and antimicrobial studies. *J. Mol. Struct.* **1176**, 7–18 (2019).
 13. Nazir, M. & Naqvi, I. I. Synthesis and characterization of uranium (IV) complexes with various amino acids. *J. Saudi Chem. Soc.* **14**, 101–104 (2010).
 14. Herrera, A. & Balzaretto, N. M. Effect of High Pressure in the Luminescence of Pr³⁺-Doped Ge₂O-PbO Glass Containing Au Nanoparticles. *J. Phys. Chem. C* **122**, 27829–27835 (2018).
 15. Liu, C. *et al.* Excitation wavelength dependent luminescence of LuNbO₄:Pr³⁺- Influences of intervalence charge transfer and host sensitization. *J. Phys. Chem. C* **120**, 26044–26053 (2016).
 16. Rajesh, D., Balakrishna, A., Seshadri, M. & Ratnakaram, Y. C. Spectroscopic investigations on Pr³⁺ and Nd³⁺ doped strontium–lithium–bismuth borate glasses. *Spectrochim. Acta Part A Mol. Biomol. Spectrosc.* **97**, 963–974 (2012).
 17. Jamalajah, B. C. *et al.* Optical absorption, fluorescence and decay properties of Pr³⁺-doped PbO–H₃BO₃–TiO₂–AlF₃ glasses. *J. Lumin.* **129**, 1023–1028 (2009).
 18. Liu, C. *et al.* Host-sensitized luminescence of Dy³⁺ in LuNbO₄ under ultraviolet light and low-voltage electron beam excitation: energy transfer and white emission. *J. Mater. Chem. C* **5**, 9012–9020 (2017).
 19. Sasi Kumar, M. V *et al.* Thermal, structural and spectroscopic properties of Pr³⁺-doped lead zinc borate glasses modified by alkali metal ions. <https://doi.org/10.1016/j.jtusci.2016.04.004> **11**, 593–604 (2018).
 20. Kamal, R. & Hafez, H. Novel Down-converting single-phased white light Pr³⁺-doped BaWO₄ Nanophosphors material for DSSC applications. *Opt. Mater. (Amst)*. **121**, 111646 (2021).

-
21. Mathews, S., Kumari, B. S., Rijulal, G. & Mohanan, K. Synthesis, Characterization and Antibacterial Activity of Some Transition Metal Complexes of 2-N-(isatinamino)-3-carboxyethyl-4,5,6,7-tetrahydrobenzo[b]thiophene. <http://dx.doi.org/10.1080/00387010802007981> **41**, 154–161 (2008).
 22. Omar, M. M., Abd El-Halim, H. F. & Khalil, E. A. M. Synthesis, characterization, and biological and anticancer studies of mixed ligand complexes with Schiff base and 2,2'-bipyridine. *Appl. Organomet. Chem.* **31**, e3724 (2017).
 23. Chohan, Z. H., Supuran, C. T., Ben Hadda, T., Nasim, F. U. H. & Khan, K. M. Metal based isatin-derived sulfonamides: Their synthesis, characterization, coordination behavior and biological activity. <http://dx.doi.org/10.1080/14756360802447636> **24**, 859–870 (2009).

Absorption spectral study for the interaction of Pr(III) with L-Aspartic acid in various aquated organic solvents through $4f-4f$ transition spectra: Analysis of reaction pathways and thermodynamic parameters.

In this chapter the interaction of Praseodymium (III) with L-Aspartic Acid has been analysed theoretically through $4f-4f$ transition in various aquated organic solvents (DMF, ACN, Dioxane and methanol). Spectral parameters such as: Energy interaction parameters like Slater–Condon (F_k 's), Lande factor (ζ_{4f}), Racah energy (E^k), nephelauxetic effect (β), bonding ($b^{1/2}$) and percent covalency (δ), as well as intensity parameters: oscillator strength ' P ' and Judd–Ofelt T_λ ($\lambda=2,4,6$) were evaluated. The degree of outer and inner sphere coordination, the level of metal $4f-4f$ orbital involvement in the complexation, defining the immediate coordination environment around the metal Pr(III), and the coordination number of the complex formed could be revealed through the analysis of these spectral parameters. The rate of complexation for Pr(III) with L-Aspartic acid and consequently its thermodynamic parameters have been evaluated through $4f-4f$ transition spectra.

4.1. Introduction

In recent decades Lanthanide chemistry has received a lot of attention. Lanthanides are used as structural and functional probes to understand biomolecule structures, conformations and properties[1–3]. Many concepts and hypotheses have been amended or abandoned as the science of coordination chemistry progresses. Complex formation processes are a "key" in several research fields like analytical, bioinorganic, clinical and biochemical aspects of coordination chemistry has an emerging research area[4][5][6][7]. Under certain experimental and physiological circumstances, lanthanide (III) ions are hard metal ions, preferring hard donor ligands such as oxygen, halogen and nitrogen. In multidentate large biological molecules, many ligands contain oxygen, nitrogen, sulphur, halogen and phosphorous donor atoms in the form of functional groups[8]. While analysing the comparison in the absorption spectra of Pr(III): amino acids complex quantitatively, we discovered some interesting structural information about the amino acid molecule, including its coordinating sites[9]. When Pr(III) binds to amino acids, the energies of $4f-4f$ bands shifts, reducing the energy interaction parameters such as F_k , ζ_{4f} and E^k of $4f-4f$ electronic transitions[10]. Amino acids contain amine and carboxylic acid functional groups and can modify the form and size of buoyant materials while maintaining the -R group (side chains) [11]. Amino acids are essential to our general health since they play a critical role in enzyme and protein synthesis and contribute significantly to human health, the brain system, hormone secretion and muscle construction. They are also required for the proper functioning of vital cellular and organ networks[12,13]. It has been thoroughly examined how different lanthanides interact with a wide spectrum of proteins, amino acids, and polypeptides [14]. In complexation, lanthanides favour donor atoms in the following order: O>N>S and F>Cl. This indicates that the lanthanide ion has a strong preference for 'O' donor atoms. There is strong evidence of the bonding of Ln (III) ions with amino acids; Ln(III) ion is bonded with the carboxylate group's oxygen atom and the amine group's nitrogen atom [15]. Amino acids exist in a neutral state when they are in the solid phase. As seen in figure 4.1., if their isoelectric point is preserved, they exist as zwitterions in aquated solution. [16]

The inner structure of the lanthanide (III) complex can be revealed by examining the $4f-4f$ transition spectra. Using $4f-4f$ transition spectra recorded in various aquated organic solvents, the energy interaction and intensity parameters for the complexation of Pr (III) with amino acids, other ligands and polypeptides including O, N, and S donors were examined [13–15]. The spectroscopic characteristics of trivalent lanthanide ions are

*The text of this chapter has been published as:

96

¹Juliana Sanchu, Chubazenba Imsong, Zevivonü Thakro, Mhasiriekho Ziekhrü and M. Indira Devi, "Absorption spectral study for the interaction of Pr(III) with L-Aspartic acid in various aquated organic solvents through $4f-4f$ transition spectra: Analysis of reaction pathways and thermodynamic parameters", Journal of Pharmaceutical Negative Results, Volume 13(S01) (2022).

unusual. Because the overlaying $5s^2$ and $5p^6$ shells shelter the $4f$ electrons from external forces, the electron cloud of the Ln (III) ion is mostly unaffected by the ligand environment.[20] The $f-f$ transitions spectra are responsible for the absorption spectra of trivalent lanthanide ions. As a result, the absorption spectra of lanthanide complexes are often sharp and line-like, in contrast to transition metal's broad absorption bands. The $f-f$ bands' intensity is affected by the nature of the coordination sphere in a quantitative way [21].

Comparative absorption spectroscopy was used in this study to estimate the energy interaction and intensity parameters for the complexation of praseodymium (III) with L-aspartic acid in various aqueous organic solvents. The fluctuation in spectral characteristics could reveal the mechanism of binding in terms of inner and outer-sphere complexation, degree of covalency, and $4f$ -orbital involvement. The simultaneous coordination of Pr(III): L-Aspartic acid complex at various temperatures in DMF medium was investigated using reaction rate and thermodynamic parameters to investigate reaction rate, pre-exponential factors, and thermodynamic parameters.

4.2. Materials and methods

Praseodymium (III) chloride hydrate was purchased from Sigma Aldrich with 99.9% purity, and L-Aspartic acid from HIMEDIA are used for spectral and kinetic studies. The solvents used DMF, ACN, Dioxane and MeOH are of A/R grade from E. Merck. The concentrations of Pr(III):L-Aspartic acid complex were kept at 0.01 M and the pH was maintained to 2.77. In all the preparations, binary mixtures (50% v/v) of water in four different organic solvents (Acetonitrile, Dioxane, Dimethylformamide & Methanol) were used. The absorption spectra were recorded using a UV-Vis spectrophotometer (Perkin Elmer Lambda 365).

For kinetic experiments, equimolar quantities of Pr(III):L-Aspartic acid complex was added to aquated DMF solvent and the resulting mixture was agitated in an inert atmosphere generated to form the complex in solution. All spectra were taken using a Perkin Elmer Lambda-35 UV-Visible Spectrophotometer with a connected kinetic assembly that was temperature-controlled. Water flowing HAAKE DC 10 thermostat is used to maintain the desired temperature.

Praseodymium (III) with Amino acids form Metal Complex

Praseodymium (III) are "hard acids" and hard acceptors, they prefer to form complexes with "hard bases" and hard donor ligands. Coordination numbers typically range from 6 to 12, the physiologically significant being 8 or 9. Therefore, the complexes can take on a variety of geometrical forms. In their solid-state, amino acids are neutral. However, when they are dissolved in an aqueous medium and their isoelectric point is maintained, they exist as zwitterions as shown in figure 4.1. [22–24].

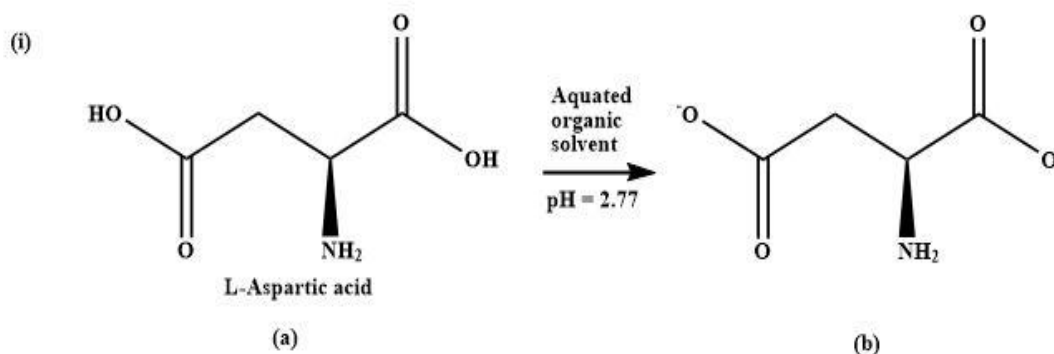


Figure 4.1. The zwitterions of L-Aspartic acid.

When the value of the pH is less than 7, only the 'O' atom bind to the metal ion; but when the pH value is above 7, both 'O' atom and 'N' atom bind with the metal ion [25]. Since the isoelectric point of L-aspartic acid is pH 2.77 the metal ion interacts with only the oxygen atoms of the L-Aspartic acid and acts as bidentate, forming a complex with the praseodymium(III) as given in figure 4.2.

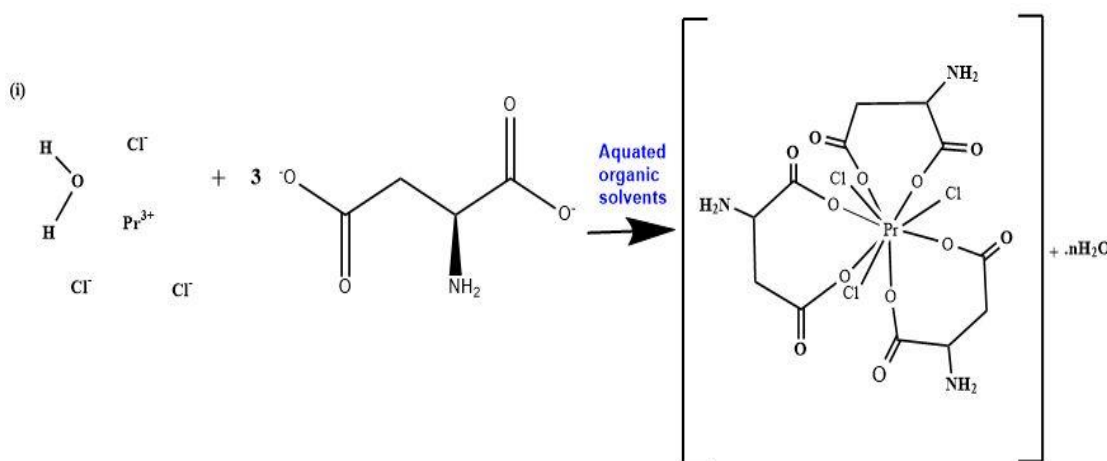


Figure 4.2. Chemical reaction pathway of Praseodymium(III) with L-Aspartic acid complex in aquated medium.

4.3. Theoretical

4.3.1. Energy interaction parameters

The Nephelauxetic ratio is determined by the covalency, as illustrated below.

$$\beta = \frac{F_K^C}{F_K^f} \text{ or } \frac{E_C^K}{E_f^K}$$

For complex and free ions, Slater–Condon parameters are written as F_K while Racah parameters are expressed as E^K . Covalent percentage and bonding parameter are calculated using the equations given below;

$$b^{1/2} = \left[\frac{1-\beta}{2} \right]^{1/2}$$

$$\delta = \left[\frac{1-\beta}{\beta} \right] \times 100$$

The Electrostatic term E_0 was stated as, using the Slater radial integral and the Slater–Condon parameter.

$$E_0 = \sum_{k=0}^{k=6} K^k F_k$$

Where K^k is the angular coefficient.

The direct-integrals, or Slater–Condon parameters (F^k), are a decreasing function of K with the relationship given as,

$$F_1^k = \int_0^\infty \int_0^\infty \frac{r_{<}^k}{r_{>}^{k-1}} R_i^2(r_i) R_j^2(r_j) r_i^2 r_j^2 dr_i dr_j$$

The near and distant electron radii are ' $r_{<}$ & ' $r_{>}$ ', the 4f-radial wave function is ' R_i ' and the i^{th} & j^{th} electrons are ' i & ' j '. Condon and Shortley reformulated the Slater–Condon parameter (F^k) integrals in terms of reduced integrals (F_k).

$$F_k = \frac{F^k}{D_k}$$

Combining the above two relations, the reduced Slater–Condon integral is given by an equation,

$$F_k = \frac{1}{D_k} \int_0^\infty \int_0^\infty \frac{r_{<}^k}{r_{>}^{k-1}} R_i^2(r_i) R_j^2(r_j) r_i^2 r_j^2 dr_i dr_j$$

The linear combinations of F_k are given as the energy interaction parameter Racah E^{ki} ,

$$E^1 = \frac{70F_2 + 231F_4 + 20.02F_6}{9}$$

$$E^2 = \frac{F_2 - 3F_4 + 7F_6}{9}$$

$$E^3 = \frac{5F_2 + 6F_4 - 9F_6}{3}$$

The energy (E_{so}) in 4f–4f electronic transition is known to come from a significant magnetic contact, but the spin-orbit interactions may be written as,

$$E_{so} = A_{so} \xi_{4f}$$

where ' ξ_{4f} ' denotes the radial integral and ' A_{so} ' denotes the angular component of spin-orbit interaction. By first-order approximation, the energy E_j of the j^{th} level is represented as,

$$E_j(F_k, \xi_{4f}) = E_{0j}(F_k^0, \xi_{4f}^0) + \frac{\partial E_j}{\partial F_k} \Delta F_k + \frac{\partial E_j}{\partial \xi_{4f}} \Delta \xi_{4f}$$

where ' E_{0j} ' denotes the j th level's zero-order energy. The equivalent values of F_k and ξ_{4f} are provided in the equations below.

$$F_k = F_k^0 + \Delta F_k$$

$$\xi_{4f} = \xi_{4f}^0 + \Delta \xi_{4f}$$

The zero-order ΔE_j and the observed value of E_j are expressed by the given equation,

$$\Delta E_j = \sum_k \frac{\partial E_j}{\partial F_k} + \frac{\partial E_j}{\partial \xi_{4f}} \Delta \xi_{4f}$$

The following problem may be solved using the least square approach to determine the values of ΔF_2 & $\Delta \xi_{4f}$.

The following is the formula for determining the estimated values of F_4 and F_6 :

$$\frac{F_4}{F_2} = 0.1380 \text{ and } \frac{F_6}{F_2} = 0.0150$$

4.3.2. Intensity Parameters

Judd[26] and Ofelt[27] established a theoretical technique for calculating band intensities. They thought the transitions are essentially electric dipole transitions, and that the oscillator strength corresponding to the induced electric dipole transition $\Psi J \rightarrow \Psi' J'$ as given by

$$\sum_{\lambda=2,4,6} T_{\lambda} \sigma(f^N \psi J \| U^{\lambda} \| f^N \psi' J')^2 \dots \dots \dots (1)$$

The rank matrix element is denoted by $U^{(\lambda)}$. The three numbers T_2 , T_4 , and T_6 are associated with the radial components of the $4f^N$ wave functions, the closest of which is $4f^{N-1}5d$.

The expression connects the measured intensity of an absorption band to the probability (P) of radiant energy absorption (oscillator strength):

$$P = \frac{2303mc^2}{N\pi e^2} \int \epsilon_i(\sigma) d\sigma$$

$$P = 4.318 \times 10^{-9} \int \epsilon_i(\sigma) d\sigma \dots\dots\dots (2)$$

The intensity of the absorption band is determined by the experimentally observed oscillator strength (P_{obs}), which is directly proportional to the area under the absorption curve and is estimated using Gaussian curve analysis:

$$P = 4.60 \times 10^{-9} \times \epsilon_{max} \times \Delta\nu_{\frac{1}{2}} \dots\dots\dots (3)$$

The molar extinction coefficient is given by ϵ_{max} .

The T_2 , T_4 and T_6 values supplied by Judd and Ofelt were utilised to represent the computed oscillator strength (P_{obs}) of the transition energies, as derived by the equation below.

$$\frac{P_{obs}}{\nu} = [(U^2)]^2 T_2 + [(U^4)]^2 T_4 + [(U^6)]^2 T_6 \dots\dots\dots (4)$$

Carnall[26] gave the matrix elements of Pr(III) system as $U^{(\lambda)}$.

4.3.3. Rate of the reactions

Based on the concept of activation energy. Arrhenius described the temperature dependence of the rate constant (k) by the equation,

$$k = Ae^{\frac{-E_a}{RT}} \dots\dots\dots (5)$$

This equation is known as the Arrhenius rate equation.

Where A stands for frequency factor. The factor $\exp(-E_a/RT)$ is a measure of the likelihood of a molecule being in an activated state.

Plotting graph $\log k$ (rate constant) versus $1/T$ yields the Arrhenius rate equation, which is used to determine the activation energy for the Pr(III):L-Aspartic acid complex in DMF solvent. [29,30]

The equation (5) may be expressed as follows:

$$\ln k = \ln A - \frac{E_a}{RT}$$

$$\text{or, } 2.303 \log k = 2.303 \log A - \frac{E_a}{RT}$$

$$\text{or, } \log k = \log A - \frac{E_a}{2.303RT} \dots\dots\dots (6)$$

where, A = pre-exponential factor, often known as the frequency factor.

As a result, plotting $\log k$ versus $1/T$ should provide a straight line with a negative slope.

$$\text{Slope} = \frac{E_a}{2.303R} \quad \text{and Intercept} = \log A$$

The activation energy E_a is calculated from the slope as

$$E_a = -\text{Slope} \times 2.303 \times R \dots\dots\dots (7)$$

Where R is the universal gas constant

The complexation's thermodynamic characteristics were established using a Van't Hoff plot of $\log k$ versus $1/T \times 10^3$, which was provided as

$$\log k = -\frac{\Delta H^\circ}{R} \left[\frac{1}{T} \right] + \frac{\Delta S^\circ}{R} \dots\dots\dots (8)$$

$$\text{Or } \log k = -\frac{\Delta G^\circ}{RT}$$

4.4. Figures and tables

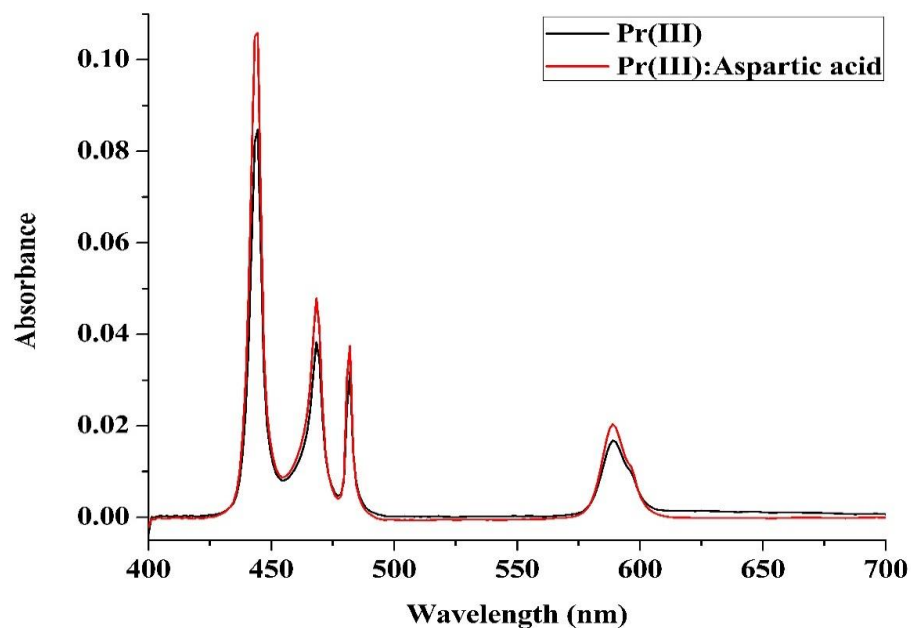


Figure 4.3. UV-vis spectra of Praseodymium(III) and Praseodymium(III):L-Aspartic acid complex in aquated DMF solvent.

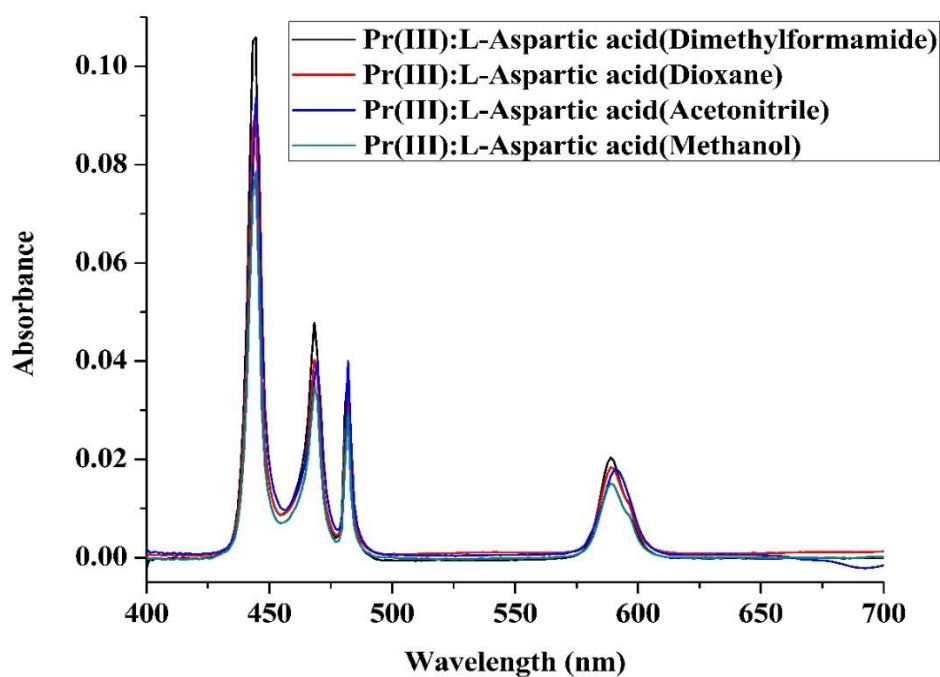


Figure 4.4. UV-vis absorption spectra of Praseodymium(III):L-Aspartic acid complex in various aquated organic solvents.

Table 4.1. Comparative studies of energy interaction values- Slater–Condon (F_k), Lande (ξ_{4f}), Racah energy (E^k), Nephelauxetic ratio (β), bonding ($b^{1/2}$), and covalency (δ) factors of Praseodymium(III) and Praseodymium(III):L-Aspartic acid complex in various aqueous medium.

Systems	F_2	F_4	F_6	ξ_{4f}	E^1	E^2	E^3	β	$b^{1/2}$	δ
ACETONITRILE										
Pr(III)	309.523	44.534	6.691	724.72	3612.55	25.327	589.34	0.947	0.1616	5.612
Pr(III)+Aspartic Acid	309.294	44.512	6.672	724.49	3612.34	25.311	588.96	0.948	0.1628	5.634
DIMETHYLFORMAMIDE										
Pr(III)	309.043	44.572	6.759	725.33	3613.21	25.376	589.78	0.946	0.1631	5.703
Pr(III)+Aspartic Acid	309.020	44.537	6.731	724.94	3612.92	25.298	589.34	0.949	0.1642	5.741
1,4-DIOXANE										
Pr(III)	309.196	44.493	6.654	724.52	3612.32	25.318	589.21	0.947	0.1609	5.609
Pr(III)+Aspartic Acid	309.173	44.469	6.633	724.25	3612.15	25.294	588.83	0.948	0.1619	5.627
METHANOL										
Pr(III)	309.323	44.474	6.639	724.48	3612.09	25.274	589.05	0.945	0.1589	5.594
Pr(III)+Aspartic Acid	309.305	44.427	6.613	724.12	3611.85	25.248	588.77	0.947	0.1611	5.621

Table 4.2. Comparative studies of energies (cm^{-1}) values as well as RMS values for Praseodymium(III) and Praseodymium(III):L-Aspartic acid in various aqueous medium.

Systems	$^3\text{H}_4 \rightarrow ^3\text{P}_2$		$^3\text{H}_4 \rightarrow ^3\text{P}_1$		$^3\text{H}_4 \rightarrow ^3\text{P}_0$		$^3\text{H}_4 \rightarrow ^1\text{D}_2$		RMS
	E_{obs}	E_{cal}	E_{obs}	E_{cal}	E_{obs}	E_{cal}	E_{obs}	E_{cal}	
ACETONITRILE									
Pr(III)	22626.84	22543.21	22247.33	22185.47	21763.55	21649.72	18945.34	19146.05	102.56
Pr(III)+Aspartic Acid	22626.63	22527.66	22229.14	22170.89	21741.29	21621.43	18925.11	19120.52	102.33
DIMETHYLFORMAMIDE									
Pr(III)	22627.13	22575.31	22273.67	22199.15	21789.23	21689.43	18968.61	19178.63	102.81
Pr(III)+Aspartic Acid	22626.63	22556.63	22251.61	22183.09	21763.75	21643.09	18947.07	19151.23	102.46
1,4-DIOXANE									
Pr(III)	22626.72	22529.71	22231.09	22152.76	21736.43	21626.21	18923.14	19125.72	102.32
Pr(III)+Aspartic Acid	22626.51	22505.37	22213.65	22129.41	21717.79	21603.76	18901.51	19101.34	102.12
METHANOL									
Pr(III)	22626.69	22513.58	22207.82	22135.72	21719.65	21638.26	18921.56	19104.62	102.14
Pr(III)+Aspartic Acid	22626.39	22498.27	22185.62	22094.56	21689.23	21612.87	18889.23	19092.13	102.05

Table 4.3. Comparative studies of Oscillator strengths and Judd–Ofelt parameters for Praseodymium(III) and Praseodymium(III):L-Aspartic acid complex in various aqueous medium.

Systems	$^3H_4 \rightarrow ^3P_2$		$^3H_4 \rightarrow ^3P_1$		$^3H_4 \rightarrow ^3P_0$		$^3H_4 \rightarrow ^1D_2$		T ₂	T ₄	T ₆
	Pobs	Pcal	Pobs	Pcal	Pobs	Pcal	Pobs	Pcal			
ACETONITRILE											
Pr(III)	17.265	17.265	5.321	4.428	2.265	3.067	2.197	2.197	-253.2	10.127	54.321
Pr(III)+Aspartic Acid	21.735	21.735	5.721	4.699	3.595	4.321	3.765	3.765	-350.4	11.893	67.853
DIMETHYLFORMAMIDE											
Pr(III)	19.042	19.042	5.542	4.456	2.367	4.256	3.623	3.623	-321.7	12.153	53.428
Pr(III)+Aspartic Acid	20.098	20.098	5.921	4.761	2.972	4.541	4.035	4.035	-465.1	13.239	62.653
1,4- DIOXANE											
Pr(III)	17.623	17.623	5.278	4.165	2.231	3.967	2.978	2.978	-209.5	10.078	49.152
Pr(III)+Aspartic Acid	19.326	19.326	5.567	4.539	3.389	4.349	3.436	3.436	-312.9	12.217	55.294
METHANOL											
Pr(III)	15.723	15.723	5.123	4.067	1.725	3.721	2.749	2.749	-189.3	10.026	52.236
Pr(III)+Aspartic Acid	17.265	17.265	5.434	4.478	2.328	4.167	2.967	2.967	-232.5	12.518	57.447

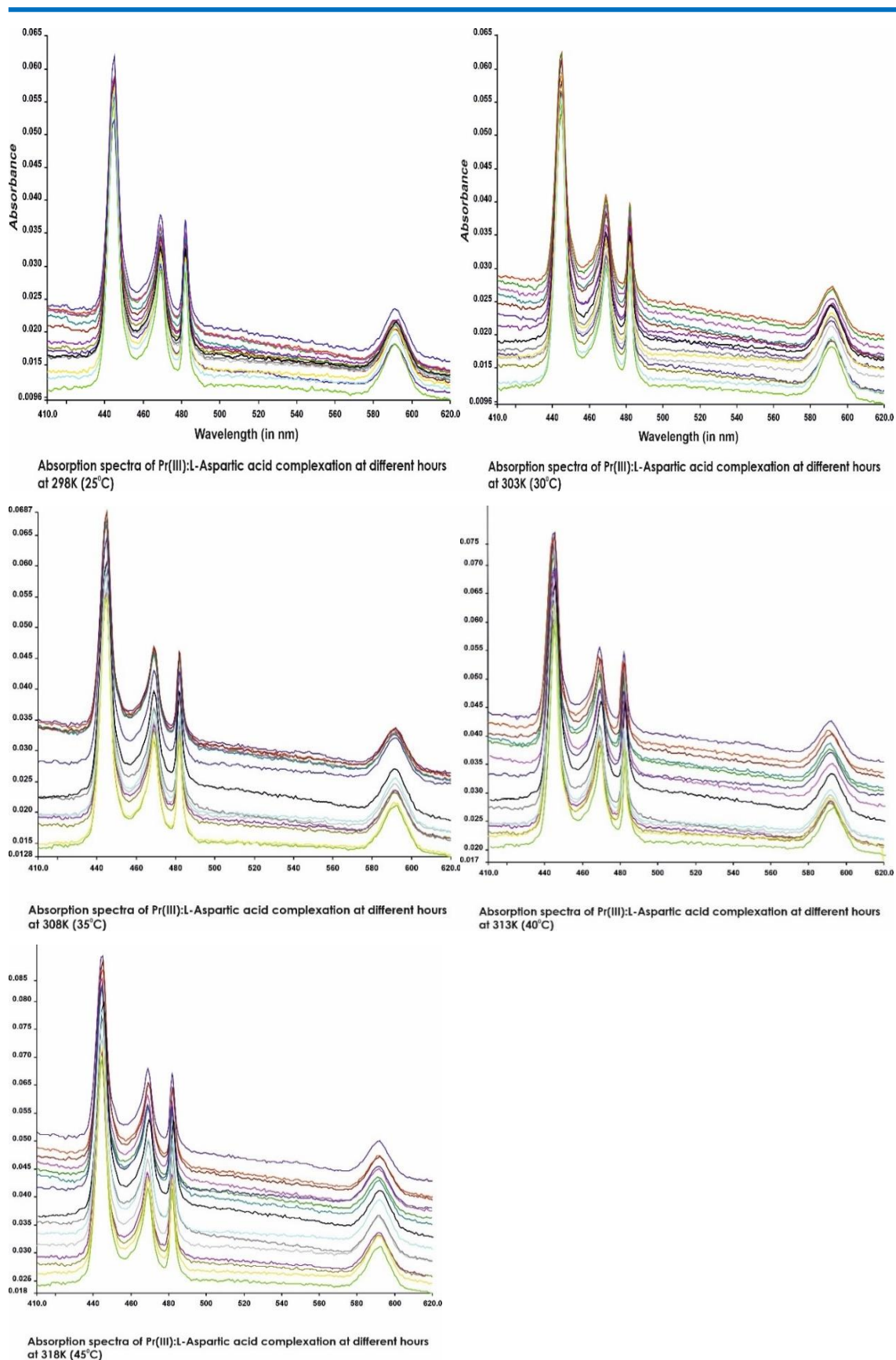


Figure 4.5. Absorption spectrum for Praseodymium (III): L-Aspartic acid complex in DMF medium at different time intervals of 25°C, 30°C, 35°C, 40°C and 45°C.

Table 4.4: Oscillator Strengths and Judd-Ofelt parameters for Praseodymium(III):L-Aspartic acid complex at different time intervals of 298 K (25°C).

System	${}^3\text{H}_4 \rightarrow {}^3\text{P}_2$		${}^3\text{H}_4 \rightarrow {}^3\text{P}_1$		${}^3\text{H}_4 \rightarrow {}^3\text{P}_0$		${}^3\text{H}_4 \rightarrow {}^1\text{D}_2$		T_2	T_4	T_6
	P_{obs}	P_{cal}	P_{obs}	P_{cal}	P_{obs}	P_{cal}	P_{obs}	P_{cal}			
0	4.711	4.711	2.612	1.865	1.181	1.911	1.804	1.804	79.023	4.187	14.460
2	4.921	4.921	2.623	1.932	1.234	1.894	1.775	1.775	79.245	4.398	14.945
4	5.131	5.131	2.645	1.966	1.265	1.933	1.815	1.815	81.923	4.821	15.332
6	5.223	5.223	2.665	1.992	1.279	1.967	1.921	1.921	88.921	4.943	15.873
8	5.407	5.407	2.763	2.067	1.355	2.036	2.113	2.113	91.231	5.466	16.231
10	5.545	5.545	2.846	2.097	1.367	2.099	2.267	2.267	171.431	5.687	16.436
12	5.672	5.672	2.883	2.133	1.396	2.128	2.345	2.345	202.321	5.977	16.643
14	5.723	5.723	2.925	2.185	1.411	2.165	2.431	2.431	208.562	6.056	16.851
16	5.851	5.851	2.966	2.212	1.485	2.197	2.546	2.546	210.214	6.167	18.176
18	5.915	5.915	3.038	2.279	1.513	2.265	2.672	2.672	211.875	6.269	18.598
20	6.149	6.149	3.125	2.334	1.554	2.329	2.754	2.754	270.137	6.559	18.784
22	6.246	6.246	3.236	2.451	1.620	2.435	2.918	2.918	273.751	6.749	18.904
24	6.355	6.355	3.376	2.545	1.767	2.523	3.075	3.075	276.920	6.921	19.123
26	6.429	6.429	3.534	2.631	1.823	2.646	3.156	3.156	285.706	7.063	19.334
28	6.541	6.541	3.625	2.756	1.891	2.727	3.227	3.227	308.334	7.137	19.525
30	6.653	6.653	3.768	2.867	1.908	2.816	3.454	3.454	345.413	7.285	19.667
32	6.718	6.718	3.838	2.952	1.976	2.881	3.523	3.523	359.202	7.564	19.843
34	6.823	6.823	3.974	3.066	2.026	2.935	3.741	3.741	401.576	7.758	20.266

*The text of this chapter has been published as:

¹Juliana Sanchu, Chubazenba Imsong, Zevivonü Thakro, Mhasiriekho Ziekhru and M. Indira Devi, "Absorption spectral study for the interaction of Pr(III) with L-Aspartic acid in various aquated organic solvents through 4f-4f transition spectra: Analysis of reaction pathways and thermodynamic parameters", Journal of Pharmaceutical Negative Results, Volume 13(S01) (2022).

Table 4.5. Oscillator Strengths and Judd-Ofelt parameters for Praseodymium(III):L-Aspartic acid complex at different time intervals of 303 K (30°C).

System	${}^3\text{H}_4 \rightarrow {}^3\text{P}_2$		${}^3\text{H}_4 \rightarrow {}^3\text{P}_1$		${}^3\text{H}_4 \rightarrow {}^3\text{P}_0$		${}^3\text{H}_4 \rightarrow {}^1\text{D}_2$		T_2	T_4	T_6
	P_{obs}	P_{cal}	P_{obs}	P_{cal}	P_{obs}	P_{cal}	P_{obs}	P_{cal}			
0	5.523	5.523	1.195	1.079	1.075	1.091	1.342	1.342	215.230	3.731	17.845
2	5.756	5.756	1.366	1.147	1.091	2.046	1.557	1.557	204.312	4.145	19.361
4	5.921	5.921	3.154	2.187	1.165	2.147	1.107	1.107	187.542	5.817	20.056
6	6.156	6.156	3.232	2.247	1.223	2.246	1.168	1.168	175.527	6.231	20.189
8	6.325	6.325	2.756	1.985	1.241	1.953	1.227	1.227	163.606	5.326	20.556
10	6.562	6.562	2.768	2.023	1.263	1.995	1.338	1.338	149.805	5.535	20.609
12	6.735	6.735	2.742	2.071	1.304	2.007	1.447	1.447	137.163	5.656	20.665
14	6.967	6.967	2.797	2.056	1.389	2.114	1.545	1.545	140.427	5.723	21.314
16	7.008	7.008	3.121	2.265	1.411	2.239	1.768	1.768	133.712	6.217	21.452
18	7.167	7.167	3.245	2.361	1.447	2.341	1.969	1.969	36.274	6.467	21.942
20	7.245	7.245	3.411	2.439	1.502	2.412	2.073	2.073	16.434	6.752	22.324
22	7.573	7.573	3.485	2.531	1.585	2.491	2.139	2.139	21.507	6.959	22.954
24	7.761	7.761	3.513	2.572	1.614	2.522	2.371	2.371	9.318	7.043	23.125
26	7.827	7.827	3.647	2.663	1.659	2.607	2.463	2.463	45.164	7.353	23.641
28	7.914	7.914	3.721	2.725	1.692	2.675	2.529	2.529	58.173	7.463	23.743
30	8.168	8.168	4.429	3.086	1.714	3.146	2.783	2.783	65.239	8.556	25.068
32	8.382	8.382	5.047	3.371	1.783	3.447	2.912	2.912	66.428	9.571	25.487
34	8.582	8.582	3.634	2.962	1.828	2.849	3.065	3.065	121.135	7.917	25.891

Table 4.6. Oscillator Strengths and Judd-Ofelt parameters for Praseodymium(III):L-Aspartic acid complex at different time intervals of 308 K (35°C).

System	${}^3\text{H}_4 \rightarrow {}^3\text{P}_2$		${}^3\text{H}_4 \rightarrow {}^3\text{P}_1$		${}^3\text{H}_4 \rightarrow {}^3\text{P}_0$		${}^3\text{H}_4 \rightarrow {}^1\text{D}_2$		T_2	T_4	T_6
	P_{obs}	P_{cal}	P_{obs}	P_{cal}	P_{obs}	P_{cal}	P_{obs}	P_{cal}			
0	6.521	6.521	2.635	1.711	0.646	1.669	1.121	1.121	78.145	4.643	20.421
2	6.643	6.643	2.741	1.823	0.723	1.729	1.357	1.357	78.341	4.862	20.569
4	6.755	6.755	2.852	1.936	0.845	1.841	1.573	1.573	66.705	5.497	20.656
6	6.813	6.813	2.942	2.008	0.898	1.967	1.636	1.636	76.187	5.775	20.832
8	6.962	6.962	3.017	2.145	0.904	2.085	1.742	1.742	38.428	5.887	21.362
10	7.039	7.039	3.165	2.263	0.947	2.138	1.838	1.838	42.276	5.945	21.672
12	7.183	7.183	3.273	2.352	0.993	2.253	1.916	1.916	44.456	5.997	22.019
14	7.234	7.234	3.361	2.476	1.006	2.321	2.058	2.058	40.745	6.019	22.345
16	7.341	7.341	3.446	2.531	1.018	2.392	2.148	2.148	132.415	6.096	22.567
18	7.475	7.475	3.573	2.619	1.038	2.425	2.363	2.363	37.543	6.287	22.876
20	7.681	7.681	3.690	2.755	1.092	2.489	2.481	2.481	47.458	6.372	23.471
22	7.767	7.767	3.756	2.838	1.114	2.556	2.546	2.546	66.371	6.463	23.535
24	7.943	7.943	3.829	2.953	1.146	2.678	2.661	2.661	48.169	6.548	24.323
26	8.006	8.006	3.992	3.009	1.192	2.742	2.734	2.734	66.321	6.749	24.573
28	8.216	8.216	4.051	3.156	1.236	2.837	2.826	2.826	86.538	6.992	24.729
30	8.473	8.473	4.193	3.231	1.288	2.907	2.969	2.969	91.376	7.418	25.468
32	8.567	8.567	4.258	3.312	1.316	2.989	3.013	3.013	100.464	7.587	26.352
34	8.748	8.748	4.385	3.476	1.371	3.069	3.145	3.145	99.276	7.276	26.867

Table 4.7. Oscillator Strengths and Judd-Ofelt parameters for Praseodymium(III):L-Aspartic acid complex at different time intervals of 313 K(40° C).

System	${}^3\text{H}_4 \rightarrow {}^3\text{P}_2$		${}^3\text{H}_4 \rightarrow {}^3\text{P}_1$		${}^3\text{H}_4 \rightarrow {}^3\text{P}_0$		${}^3\text{H}_4 \rightarrow {}^1\text{D}_2$		T_2	T_4	T_6
	P_{obs}	P_{cal}	P_{obs}	P_{cal}	P_{obs}	P_{cal}	P_{obs}	P_{cal}			
0	6.532	6.532	1.812	1.623	1.417	1.623	2.645	2.645	212.561	4.537	20.175
2	6.641	6.641	1.983	1.836	1.631	1.743	2.734	2.734	234.323	5.117	20.365
4	6.867	6.867	2.043	1.917	1.678	1.865	2.846	2.846	251.635	5.350	20.735
6	7.037	7.037	2.174	1.987	1.708	1.956	2.951	2.951	269.266	5.832	21.537
8	7.321	7.321	2.231	2.061	1.783	2.043	3.067	3.067	263.437	5.543	22.482
10	7.549	7.549	2.452	2.136	1.882	2.159	3.134	3.134	266.431	5.752	23.368
12	7.811	7.811	2.531	2.251	1.955	2.238	3.265	3.365	45.672	7.291	23.653
14	7.949	7.949	2.672	2.304	1.998	2.376	3.347	3.347	243.435	5.652	24.434
16	8.098	8.098	2.708	2.443	2.008	2.436	3.409	3.409	66.134	6.653	24.842
18	8.213	8.213	2.785	2.567	2.089	2.498	3.574	3.574	270.456	6.762	25.365
20	8.423	8.423	4.084	2.647	2.134	2.505	3.623	3.623	91.532	7.456	25.473
22	8.565	8.565	2.659	2.721	2.235	2.596	3.745	3.745	274.382	6.631	26.267
24	8.677	8.677	2.934	2.836	2.341	2.625	3.813	3.813	315.438	7.264	26.453
26	8.746	8.746	3.521	2.905	2.393	2.677	3.885	3.885	209.367	6.266	26.854
28	8.828	8.828	4.347	3.006	2.427	2.712	3.957	3.957	99.587	7.743	26.987
30	9.453	9.453	2.173	3.113	2.481	2.747	4.007	4.007	299.683	4.365	29.765
32	9.669	9.669	3.856	3.248	2.512	2.793	4.083	4.083	151.374	7.632	29.987
34	10.056	10.056	2.867	3.355	2.678	2.853	4.169	4.169	258.467	7.462	30.644

Table 4.8. Oscillator Strengths and Judd-Ofelt parameters for Praseodymium(III):L-Aspartic acid complex at different time intervals of 318 K (45°C).

System	${}^3\text{H}_4 \rightarrow {}^3\text{P}_2$		${}^3\text{H}_4 \rightarrow {}^3\text{P}_1$		${}^3\text{H}_4 \rightarrow {}^3\text{P}_0$		${}^3\text{H}_4 \rightarrow {}^1\text{D}_2$		T_2	T_4	T_6
	P_{obs}	P_{cal}	P_{obs}	P_{cal}	P_{obs}	P_{cal}	P_{obs}	P_{cal}			
0	6.762	6.762	1.991	1.782	1.543	1.786	2.856	2.856	203.541	4.865	20.376
2	6.945	6.945	2.045	1.866	1.649	1.856	2.967	2.967	209.633	5.345	20.554
4	7.067	7.067	2.168	1.953	1.716	1.941	3.039	3.039	261.458	5.549	20.941
6	7.231	7.231	2.227	2.047	1.789	2.019	3.155	3.155	271.413	5.654	21.482
8	7.459	7.459	2.356	2.231	1.852	2.123	3.226	3.226	265.827	5.861	22.630
10	7.676	7.676	2.473	2.436	1.940	2.185	3.346	3.346	268.623	6.068	23.342
12	7.864	7.864	2.540	2.673	2.017	2.234	2.461	2.461	48.719	6.361	23.558
14	8.057	8.087	2.607	2.721	2.069	2.387	3.589	3.589	246.347	6.543	24.376
16	8.253	8.253	2.745	2.789	2.178	2.453	3.664	3.664	69.381	6.843	24.896
18	8.491	8.491	2.952	2.824	2.221	2.584	3.721	3.721	273.425	6.952	25.469
20	8.653	8.653	3.084	2.876	2.294	2.638	3.855	3.855	94.456	7.267	25.921
22	8.844	8.844	3.254	2.921	2.356	2.679	3.954	3.954	278.309	7.459	26.256
24	8.912	8.912	3.476	2.992	2.432	2.745	3.989	3.989	317.417	7.660	26.864
26	9.058	9.058	3.753	3.043	2.491	2.809	2.345	2.345	212.367	7.857	27.658
28	9.475	9.475	3.905	3.127	2.523	2.876	4.019	4.019	104.285	7.563	28.409
30	9.931	9.931	4.016	3.178	2.568	2.911	4.154	4.154	303.674	8.045	29.377
32	10.168	10.168	4.127	3.227	2.617	2.985	4.275	4.275	155.438	8.129	30.563
34	10.456	10.456	4.187	3.331	2.684	3.059	4.303	4.303	262.382	7.539	31.478

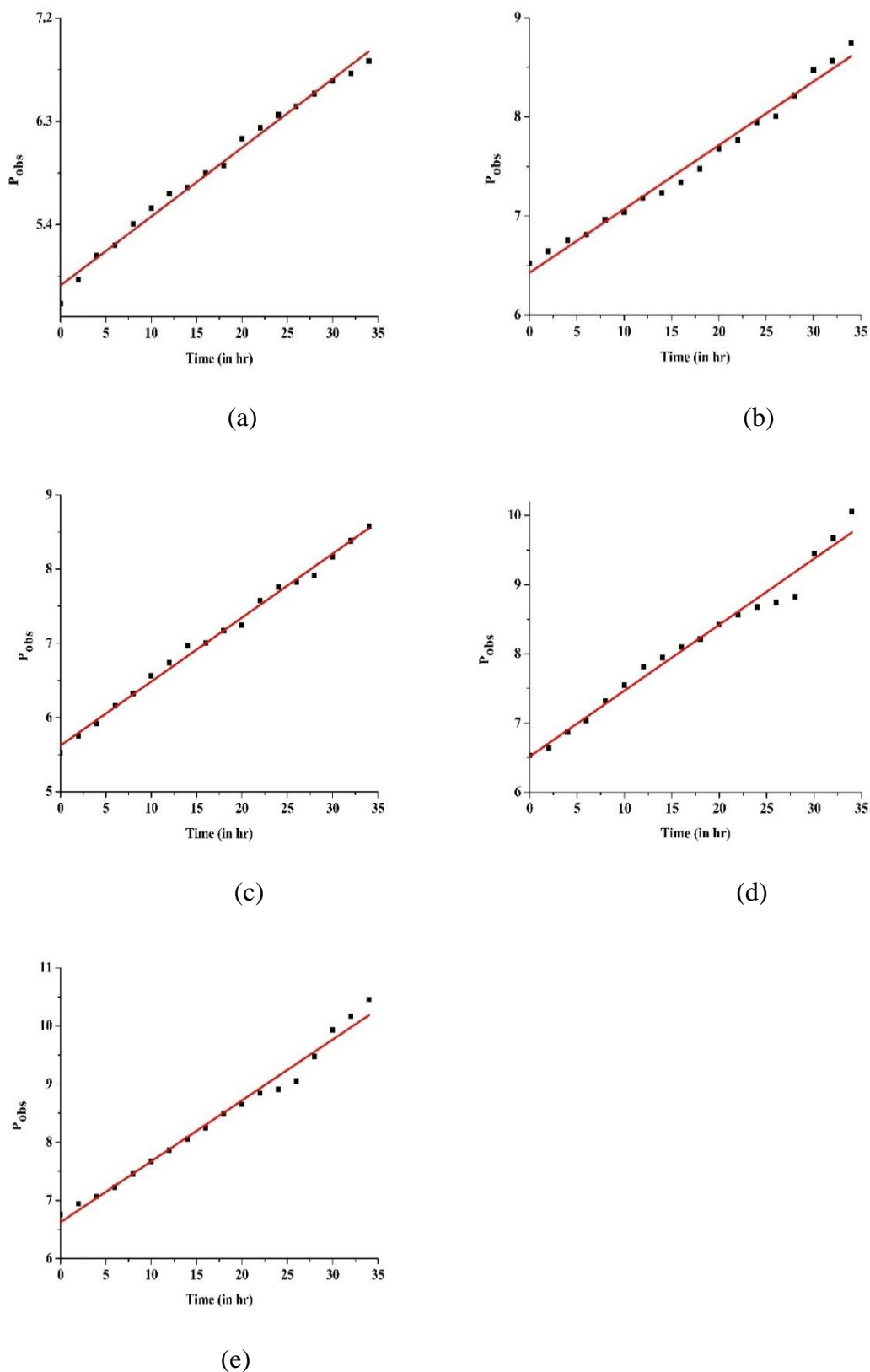
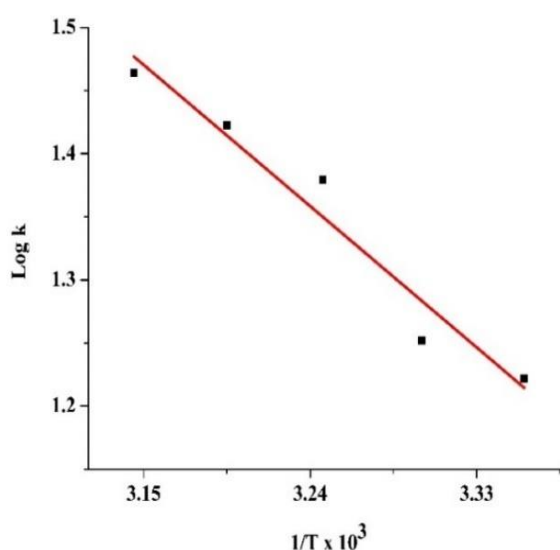


Figure 4.6. Graph for oscillator strength vs. time (in hrs) for ${}^3\text{H}_4 \rightarrow {}^3\text{P}_2$ transition for Praseodymium (III): L-Aspartic acid complex in DMF solvent at various temperatures 25°C , 30°C , 35°C , 40°C & 45°C

Table 4.9. Rate Constants of Praseodymium (III): L-Aspartic acid complex in DMF solvent.

Temperature 'K'	1/T x 10 ³	Rate Constant 'k' (Mol L ⁻¹ hr ⁻¹)	Rate Constant 'k' Mol L ⁻¹ s ⁻¹	Log k	Pre-exponential factor 'A'	Activation Energy 'Ea' (kJ)
298	3.3557	0.05997	16.65833	1.22163	16.81879	0.02382
303	3.3003	0.06430	17.86111	1.25191	18.03067	
308	3.2468	0.08619	23.94167	1.37915	24.16578	
313	3.1949	0.09529	26.46944	1.42275	26.71235	
318	3.1447	0.10476	29.10000	1.46389	29.36339	

**Figure 4.7.** Plot of Log k versus $1/T \times 10^3$ for Praseodymium (III): L-Aspartic acid complex in DMF at different temperatures.**Table 4.10.** Thermodynamic parameters, activation energy and rate constants for Praseodymium(III):L-Aspartic acid complex.

Temperature 'K'	Rate Constant 'k' Mol L ⁻¹ s ⁻¹	ΔH (kJ)	ΔG (kJ)	ΔS (kJ)	Activation Energy 'Ea' (kJ)
298	16.65833	0.02382	-6.97044	0.02347	0.02382
303	17.86111		-7.38291	0.02405	
308	23.94167		-8.00126	0.02649	
313	26.46944		-8.52662	0.02732	
318	29.10000		-8.91332	0.02810	

4.5. Results and discussion

Hypersensitive transitions are those transitions that obeyed the selection principle $|\Delta S|=0$; $|\Delta L|\leq 2$; $|\Delta J|\leq 2$ and are extremely responsive to fluctuations in the coordination environment [27]. The transitions ${}^3\text{H}_4\rightarrow{}^3\text{P}_2$, ${}^3\text{P}_1$, ${}^3\text{P}_0$, and ${}^1\text{D}_2$ of Praseodymium(III) are non-hypersensitive because they do not obey selection principles. They however have shown significant sensitivity to minute changes in the coordination surroundings of Praseodymium(III). Hence, these non-hypersensitive transitions were named Pseudohypersensitive, and such findings were termed 'Ligand Mediated Pseudohypersensitivity'[28,29]. Absorption spectrophotometry is an extremely useful tool for lanthanide coordination chemistry, especially in solution and non-aqueous media, because most lanthanides have detailed internal f -electron transition spectra in the visible spectral region and are sensitive to the metal-ligand coordination environment. Pr(III) has a paramagnetic property. In the visible region, it has $4f-4f$ transition spectra (${}^3\text{H}_4\rightarrow{}^3\text{P}_2$, ${}^3\text{H}_4\rightarrow{}^3\text{P}_1$, ${}^3\text{H}_4\rightarrow{}^3\text{P}_0$, & ${}^3\text{H}_4\rightarrow{}^1\text{D}_2$)[33]. In Pr(III):L-Aspartic acid complex, the intensity of the spectral bands increases dramatically, which could be owing to the ligand involvement in the complexation with Pr (III).

Table 4.1. shows the comparison of energy interaction parameters: Slater-Condon F_k (cm^{-1}), Lande ζ_{4f} (cm^{-1}), Racah energy E^k (cm^{-1}), nephelauxetic ratio (β), bonding ($b^{1/2}$) and covalency (δ) factor for Pr(III) and Pr(III):L-Aspartic acid complex in different aquated MeOH, MeCN, DMF and dioxane solvents. When compared to the free Pr(III) state, the values of energy interaction parameters such as F_k , E_k , and ζ_{4f} for Pr(III):L-Aspartic acid complex decreases, indicating a decrease in interelectronic repulsion and spin-orbit interaction parameters, resulting in a decrease in the metal-ligand bond distance, making complexation possible. The decrease in the values of F_k parameters indicates that ligand affects electrostatic repulsion more than spin-orbit coupling. The order of Slater-Condon parameters is found to be $F_2>F_4>F_6$. According to the nephelauxetic effect, the metal-ligand bond distance must decrease when complexation occurs and its impact depends on the coordination number, according to Jorgensen and Ryan[32]. According to Frey and Dew Horrocks [37], the nephelauxetic effect is connected to the covalency of the metal-ligand bond and the coordination number: the smaller the coordination number, the greater the amplitude of the nephelauxetic effect. In all systems, the nephelauxetic effect is between 0.944-0.948, showing the validity of the study; the positive value of δ could indicate the possibility of a covalent bond formed between the Pr (III) and L-Aspartic acid complex. When complexation occurs between Pr(III) and the L-Aspartic acid, the

values of nephelauxetic effect, bonding parameters and covalency factor increase, resulting in the decrease of effective nuclear charge and the interelectronic repulsion parameters. Due to the nephelauxetic effect, the metal-ligand distance is lowered, implying orbital overlapping is more likely to occur, which is a requirement for improving covalency. The binding parameter, often known as the mixing coefficient, is related to β . It is commonly used to assess the extent of engagement of the metal ligands in binding[33]. In Pr(III) spectra, all three of these parameters (β , δ , and $b^{1/2}$) are utilized to define the degree of covalency. The presence of covalent nature in the metal-ligand bonding is indicated by the positive values of $b^{1/2}$. Because of the tiny value of $b^{1/2}$ and the minor change in its values, $4f$ orbitals are only minimally involved in ligand binding. Sinha's parameter (δ) is usually taken as a measure of covalency.

In table 4.2. except for the ${}^3\text{H}_4 \rightarrow {}^1\text{D}_2$ transition, the observed value of energies for ${}^3\text{H}_4 \rightarrow {}^3\text{P}_2$, ${}^3\text{P}_1$ and ${}^3\text{P}_0$ transitions of Pr (III) and Pr(III):L-Aspartic acid complex are more significant than the calculated value of energies. The precision of different energy interaction parameters: Slater-Condon (F_k), Lande factor (ζ_{4f}), Racah energy (E^k), Nephelauxetic ratio (β), bonding ($b^{1/2}$) and covalency (δ) factors, is shown by the root mean square deviation (RMS) values.

Table 4.3. gives the values of oscillator strength (P) and Judd-Ofelt parameters (T_λ) for Praseodymium(III) and Praseodymium(III):L-Aspartic acid complex under various experimental conditions. The table shows that when Pr(III) was added to L-Aspartic acid there were significant changes in the oscillator strength and Judd Ofelt parameters values, which validates the possibility of binding of L-Aspartic acid to Praseodymium(III) in the solution. T_2 is not considered since it is associated to the ${}^3\text{H}_4 \rightarrow {}^3\text{F}_3$ transition, which is beyond the UV-Visible area and has negative findings. Minor changes in the coordinating environment, on the other hand, had a considerable impact on the values of T_4 and T_6 parameters, which were both positive. Variation in the symmetry characteristics of the complex is connected to both T_4 and T_6 parameters[34]; therefore the significant changes in the values of T_4 and T_6 suggest changes in the symmetry of Pr(III), its complex systems and their immediate coordination environment. Outer-sphere coordination occurs between the ligand and metal ion when there are small variations in the values of oscillator strength and Judd Ofelt parameters, while inner-sphere coordination occurs when there are large variations in P and T_λ ($\lambda=2,4,6$). The change in computed values of P and T_λ

presented in table 4.3. could provide strong evidence of the involvement of inner-sphere coordination between L-Aspartic acid and Praseodymium (III).

From figure 4.3., the absorption bands of Pr (III) complexes shift significantly as compared to Pr (III), demonstrating their sensitivity to small changes in the coordination ambience which induce a wavelength shift towards longer wavelengths, resulting in a redshift and strengthening of the $4f-4f$ transition spectral bands. A red shift is observed leading to the phenomena of the nephelauxetic effect. The nephelauxetic effect causes the metal-ligand bond length to shorten, leading to the intensification of the $4f-4f$ bands, indicating the likelihood of ligand binding to the metal ion. Figure 4.4. shows the comparative spectra of Pr(III) and Pr(III): amino acid complexes in aquated MeOH, MeCN, dioxane and DMF solvents. Variation of solvents brings a significant effect on the oscillator strengths of the $4f-4f$ bands and consequently marked variation in the magnitudes of intensity T_{λ} parameters ($\lambda=2,4,6$). DMF has high polarizability and sensitivity, which means it efficiently enhances $4f-4f$ electric dipole intensity and hence could show the possibility of highest covalency for the complexation of Pr(III): Ligands among the four solvents followed by the solvents MeCN, Dioxane and MeOH.

In particular, ligand properties including ion formation, donor atoms, sizes, and solvation effects influence the coordination numbers and geometries. The coordination number of lanthanides in an aqueous solution is 9 and 8, but it can increase to 12 when a ligand is added [35]. Because of the chelate effect, when praseodymium ions create a complex with ligands that are chelated, the resulting complexes are stronger than when they form a complex with monodentate ligands [36]. When the isoelectric point of an amino acid is preserved, the amino acid exists in solution in its zwitterion form. Amino acids are hard donors, whereas the ionic compound Pr(III) is a hard acceptor. L-Aspartic acid produces zwitterion at pH 2.98 in an aqueous solution because at this pH, Pr(III) and the amino acid's oxygen atom form complex [23–25]. The oxygen donor of L-aspartic acid and the praseodymium ion created a stable complex with a 9-coordination number. For the nona-coordinated Pr(III):L-Aspartic acid combination in an aqueous media, Figure 4.2. depicts potential chemical reaction routes.

Five sets of kinetic experiments were analysed at various temperatures (298K, 303K, 308K, 313K, and 318K) to indicate changes in the value of absorbance over time. The kinetic studies were executed by examining the rising variations in absorbance with time corresponding to four bands in the complexation of Praseodymium(III) with L-Aspartic acid, as illustrated in Figure 4.5. all four bands of the Pr(III): L-Aspartic acid complex are

equally sensitive. The rate constants were calculated by plotting oscillator strength over time in Figure 4.6. and listing them in Tables 4.4.-4.8.; oscillator strength graphs develop linearly with time. The absorbance and oscillator strength of the various absorption transition bands can thus be used to explore the Pr (III) and L-Aspartic acid complexation reaction pathways. Absorption spectrum analysis can be used to investigate the kinetics of Pr (III) complexation with L-Aspartic acid since the strength of 4f- 4f transitions increases over time. Table 4.9. shows the measured rates (k) in terms of the complex formed during the reaction, as well as plots of oscillator intensity of $^3H_4 \rightarrow ^3P_2$ transitions for Pr(III):L-Aspartic acid complex vs. time. We can see from the table that when the temperature rises, the rate constant values of complexation rise as well, which is consistent with the Arrhenius equation's theoretical prediction. Additionally, when the temperature rises, the values of the Pre-exponential factor (A) rise, increasing the probability of molecules collision. The Van't Hoff equation is used to compute the activation energy (E_a) and other thermodynamic parameters (ΔG° , ΔH° and ΔS°); figure 4.7. depicts a plot of $1/T$ against $\ln k$. The rate of complexation has been conclusively proved to increase with increasing temperature, and this is used to compute the activation energy E_a of the complexation. Table 4.10. shows that the values of the thermodynamic parameters ΔH° and ΔS° are positive, indicating that the complexation reaction is endothermic and that entropy is increasing. In addition, because $T\Delta S^\circ > \Delta H^\circ$, the coordinating reaction is entropy-driven. Negative ΔG° values imply that complex formation is favoured and spontaneous, as shown in all of Pr(III) and L-Aspartic acid complex systems. As a result, we can further justify that as the system approaches higher temperatures (increasing ΔS° values), the complexation process between Pr(III) and L-Aspartic acid takes place at a random pace. The activation energy (E_a) for the complexation of Pr(III) with L-Aspartic acid in DMF solvent was found to be 0.02382 kJ, lower values of E_a substantiate recent information about the reaction's spontaneity.

4.6. Conclusion

For Praseodymium(III) complexes, a drop in the Lande factor, Racah energy, and Slater-Condon parameters points to a reduction in interelectronic repulsion and spin-orbit interaction, which in turn causes a reduction in the metal-ligand bond distance. The nephelauxetic effect is found to be between 0.944-0.948, showing the validity of the study and indicating the possibility of a covalent bond formed between the Pr (III) and L-Aspartic acid complex. The increased values of the Nephelauxetic ratio, bonding

parameters and covalency factor as well as the resulting decrease of effective nuclear charge and the interelectronic repulsion parameters signify the formation of complex Pr(III):L-Aspartic acid. The appearance of redshift is caused by the intensification of the absorption bands that arise from complexation between Pr (III) and L-Aspartic acid. A red shift is observed leading to the phenomena of the nephelauxetic effect. The nephelauxetic effect causes the metal-ligand bond length to shorten, leading to the intensification of the $4f-4f$ bands, indicating the possibility of ligand binding to the metal ion. The ligand, L-Aspartic acid's role in the inner-sphere coordination of Pr (III) may be strongly supported by the fluctuations in the estimated values of P and T_{λ} . With the oxygen donor ligands of L-aspartic acid, praseodymium ions form a stable complex, and the inner sphere coordination produces a nona-coordination number. The considerable variations in T_4 and T_6 readings show that the symmetry has changed. DMF has high polarizability and sensitivity, which means it efficiently enhances $4f-4f$ electric dipole intensity and hence could show the possibility of highest covalency for the complexation of Praseodymium (III): Ligands among the four solvents followed by the solvents MeCN, Dioxane and MeOH. The $4f-4f$ band intensities of the organic solvents have sensitivity in the order:



It reveals that the changing oscillator strengths of different $4f-4f$ transitions over time could aid in determining the nature of the reaction pathways for the complexation of L-Aspartic acid with Pr(III) in DMF solvent. The rate of complexation increases with time and temperature confirming the Arrhenius prediction of the reaction rate. The positive values of ΔH° and ΔS° indicate that the complexation reaction is endothermic and that entropy is increasing. Furthermore, negative ΔG° values indicate a favourable and spontaneous complex formation. The rate of the reaction for Pr(III):L-Aspartic acid complex increases with temperature and the activation energy are found to be 0.02382 KJ, the lower values of E_a substantiate information on the reaction's spontaneity. The empirical relation between temperature and reaction rate is provided by the readings of the pre-exponential factor (A), which is dependent on the possibility of how often the molecules collide.

References

- [1] A.J. Amoroso, S.J.A. Pope, Using lanthanide ions in molecular bioimaging, *Chem. Soc. Rev.* 44 (2015) 4723–4742. <https://doi.org/10.1039/C4CS00293H>.
- [2] S. Procházková, J. Hraníček, V. Kubiček, P. Hermann, Formation kinetics of europium(III) complexes of DOTA and its bis(phosphonate) bearing analogs, *Polyhedron*. 111 (2016) 143–149. <https://doi.org/10.1016/J.POLY.2016.03.039>.
- [3] J.A. Cotruvo, *The Chemistry of Lanthanides in Biology: Recent Discoveries, Emerging Principles, and Technological Applications*, ACS Cent. Sci. (2019). <https://doi.org/10.1021/acscentsci.9b00642>.
- [4] S. Philip, P.S. Thomas, K. Mohanan, Synthesis, fluorescent studies, antioxidative and α -amylase inhibitory activity evaluation of some lanthanide(III) complexes, *J. Serbian Chem. Soc.* 83 (2018) 561–574. <https://doi.org/10.2298/JSC180918010P>.
- [5] Y. Zhang, W. Thor, K.L. Wong, P.A. Tanner, Determination of Triplet State Energy and the Absorption Spectrum for a Lanthanide Complex, *J. Phys. Chem. C*. 125 (2021)7022–7033. https://doi.org/10.1021/ACS.JPCC.1C00158/SUPPL_FILE/JP1C00158_SI_001.PDF.
- [6] M.N. Gueye, M. Dieng, I.E. Thiam, D. Lo, A.H. Barry, M. Gaye, P. Retailleau, Lanthanide(III) complexes with tridentate Schiff base ligand, antioxidant activity and X-ray crystal structures of the Nd(III) and Sm(III) complexes, *South African J. Chem.* 70 (2017) 08–15. <https://doi.org/10.17159/0379-4350/2017/V70A2>.
- [7] H. Li, X. Wang, D. Huang, G. Chen, Recent advances of lanthanide-doped upconversion nanoparticles for biological applications, *Nanotechnology*. (2020). <https://doi.org/10.1088/1361-6528/ab4f36>.
- [8] S.N. Misra, M.A. Gagnani, D.M. Indira, R.S. Shukla, Biological and Clinical Aspects of Lanthanide Coordination Compounds, *Bioinorg. Chem. Appl.* 2 (2004) 155. <https://doi.org/10.1155/S1565363304000111>.
- [9] N. Bendangsenla, T. Moainla, J. Sanchu, M.I. Devi, N. Bendangsenla, T. Moainla, J. Sanchu, M.I. Devi, Computation of Energy, Intensity and Thermodynamic Parameters for the Interaction of Ln(III) with Nucleic Acid: Analysis of Structural Conformations, Chemical Kinetics and Thermodynamic Behaviour through 4f-4f Transition Spectra as Probe, *J. Mater. Sci. Chem. Eng.* 6 (2018) 169–183. <https://doi.org/10.4236/MSCE.2018.67018>.
- [10] M. Ziekhri, Z. Thakro, C. Imsong, J. Sanchu, M. Indira Devi, Computation of

*The text of this chapter has been published as:

120

¹Juliana Sanchu, Chubazenba Imsong, Zevivonü Thakro, Mhasiriekho Ziekhri and M. Indira Devi, “Absorption spectral study for the interaction of Pr(III) with L-Aspartic acid in various aquated organic solvents through 4f-4f transition spectra: Analysis of reaction pathways and thermodynamic parameters”, *Journal of Pharmaceutical Negative Results*, Volume 13(S01) (2022).

- energy interaction and intensity parameters for the complexation of Pr(III) with glutathione at different pH in the presence/absence of Mg²⁺: 4f-4f transition spectra as a probe, *Polyhedron*. 200 (2021) 115099. <https://doi.org/10.1016/J.POLY.2021.115099>.
- [11] T. Maruyama, Y. Fujimoto, T. Maekawa, Synthesis of gold nanoparticles using various amino acids, *J. Colloid Interface Sci.* 447 (2015) 254–257. <https://doi.org/10.1016/J.JCIS.2014.12.046>.
- [12] K.K. Gangu, S. Maddila, S.N. Maddila, S.B. Jonnalagadda, Nanostructured Samarium Doped Fluorapatites and Their Catalytic Activity towards Synthesis of 1,2,4-Triazoles., *Molecules*. 21 (2016). <https://doi.org/10.3390/MOLECULES21101281>.
- [13] S. Shankar, J.W. Rhim, Amino acid mediated synthesis of silver nanoparticles and preparation of antimicrobial agar/silver nanoparticles composite films, *Carbohydr. Polym.* 130 (2015) 353–363. <https://doi.org/10.1016/J.CARBPOL.2015.05.018>.
- [14] C.H. Evans, C.H. Evans, The Interaction of Lanthanides with Amino Acids and Proteins, in: *Biochem. Lanthanides*, 1990. https://doi.org/10.1007/978-1-4684-8748-0_4.
- [15] N. Ranjana Devi, H. Bimola, C. Sumitra, N. Rajmuhon Singh, Energy and electric dipole intensity parameters for the 4f-4f transitions for the complexation of Pr III and Nd III with dicyandiamide in different solvents in presence and absence of Ca II to explore the similarities between Ln III and Ca II, *J. Indian Chem. Soc.* (2012).
- [16] C. Victory Devi, N. Rajmuhon Singh, Spectrophotometric study of kinetics and associated thermodynamics for the complexation of Pr(III) with l-proline in presence of Zn(II), *Arab. J. Chem.* 10 (2017) S2124–S2131. <https://doi.org/10.1016/J.ARABJC.2013.07.044>.
- [17] R.S. Naorem, N.P. Singh, N.M. Singh, 4f–4f Spectral Analysis and Solvent Effect for the Interaction of Pr(III) with l-Tryptophan Using Different Aqueated Solvents in the Presence and Absence of Zn(II), *Chem. Africa* 2019 31. 3 (2019) 171–180. <https://doi.org/10.1007/S42250-019-00111-9>.
- [18] N. Bendangsenla, T. Moainla, J. Sanchu, M.I. Devi, N. Bendangsenla, T. Moainla, J. Sanchu, M.I. Devi, Computation of Energy, Intensity and Thermodynamic Parameters for the Interaction of Ln(III) with Nucleic Acid: Analysis of Structural Conformations, Chemical Kinetics and Thermodynamic Behaviour through 4f-4f Transition Spectra as Probe, *J. Mater. Sci. Chem. Eng.* 6 (2018) 169–183.

- <https://doi.org/10.4236/MSCE.2018.67018>.
- [19] T. Moaienla, N. Bendangsenla, M.I. Devi, A Probe into the Kinetics of the Interaction of Pr(III) Ions with Some Selected Amino Acids: A 4f-4f Transition Spectral Study, *Adv. Mater. Sci. Appl.* 3 (2014) 157–163. <https://doi.org/10.5963/AMSA0303007>.
- [20] Y. Hasegawa, Y. Kitagawa, T. Nakanishi, Effective photosensitized, electrosensitized, and mechanosensitized luminescence of lanthanide complexes, *NPG Asia Mater.* 2018 104. 10 (2018) 52–70. <https://doi.org/10.1038/s41427-018-0012-y>.
- [21] A. Carac, R. Boscencu, G. Carac, S.G. Bungau, Spectral study of some lanthanides complexes with quaternary pyridinium ligands, *Rev. Chim.* 68 (2017) 2265–2269. <https://doi.org/10.37358/RC.17.10.5868>.
- [22] M. Remko, D. Fitz, R. Broer, B.M. Rode, Effect of metal Ions (Ni 2+, Cu 2+ and Zn 2+) and water coordination on the structure of L-phenylalanine, L-tyrosine, L-tryptophan and their zwitterionic forms, *J. Mol. Model.* 17 (2011) 3117–3128. <https://doi.org/10.1007/S00894-011-1000-0/TABLES/6>.
- [23] F. Costanzo, R.G. Della Valle, V. Barone, MD simulation of the Na⁺-phenylalanine complex in water: competition between cation- π interaction and aqueous solvation, *J. Phys. Chem. B.* 109 (2005) 23016–23023. <https://doi.org/10.1021/JP055271G>.
- [24] A.L. Sobolewski, D. Shemesh, W. Domcke, Computational studies of the photophysics of neutral and zwitterionic amino acids in an aqueous environment: Tyrosine-(H₂O)₂ and tryptophan-(H₂O)₂ clusters, *J. Phys. Chem. A.* 113 (2009) 542–550. https://doi.org/10.1021/JP8091754/SUPPL_FILE/JP8091754_SI_001.PDF.
- [25] J.C.G. Bünzli, C. Piguet, Lanthanide-containing molecular and supramolecular polymetallic functional assemblies, *Chem. Rev.* 102 (2002) 1897–1928. https://doi.org/10.1021/CR010299J/ASSET/CR010299J.FP.PNG_V03.
- [26] W.T. Carnall, P.R. Fields, B.G. Wybourne, Spectral Intensities of the Trivalent Lanthanides and Actinides in Solution. I. Pr³⁺, Nd³⁺, Er³⁺, Tm³⁺, and Yb³⁺, *J. Chem. Phys.* 42 (2004) 3797. <https://doi.org/10.1063/1.1695840>.
- [27] R.D. Peacock, Hypersensitivity of spectral bands in complexes of praeodymium(III), *Chem. Phys. Lett.* (1970). [https://doi.org/10.1016/0009-2614\(70\)80282-2](https://doi.org/10.1016/0009-2614(70)80282-2).
- [28] S.N. Misra, S.O. Sommerer, The ligand mediated pseudohypersensitivity of the

- 3H4 → 3P2, 3H4 → 3P1, 3H4 → 3P0, and 3H4 → 1D2 transitions of praseodymium(III) complexes in solution media, <https://doi.org/10.1139/V92-009>. 70 (2011) 46–54. <https://doi.org/10.1139/V92-009>.
- [29] S.N. Misra, K. John, Difference and Comparative Absorption Spectra and Ligand Mediated Pseudohypersensitivity for 4f-4f Transitions of Pr(III) and Nd(III), <http://dx.doi.org/10.1080/05704929308018115>. 28 (2006) 285–325. <https://doi.org/10.1080/05704929308018115>.
- [30] W.T. Carnall, P.R. Fields, B.G. Wybourne, Spectral Intensities of the Trivalent Lanthanides and Actinides in Solution. I. Pr³⁺, Nd³⁺, Er³⁺, Tm³⁺, and Yb³⁺, *J. Chem. Phys.* 42 (2004) 3797. <https://doi.org/10.1063/1.1695840>.
- [31] E.Y. Wong, Configuration interaction of the Pr³⁺ ion, *J. Chem. Phys.* (1963). <https://doi.org/10.1063/1.1733794>.
- [32] C. Klíxbüll Jørgensen, R. Pappalardo, H.H. Schmidtke, Do the ‘‘Ligand Field’’ Parameters in Lanthanides Represent Weak Covalent Bonding?, *J. Chem. Phys.* 39 (2004) 1422. <https://doi.org/10.1063/1.1734458>.
- [33] R.B. Martin, F.S. Richardson, Lanthanides as probes for calcium in biological systems, *Q. Rev. Biophys.* 12 (1979) 181–209. <https://doi.org/10.1017/S0033583500002754>.
- [34] J. Sanchu, M. Ziekhru, Z. Thakro, M.I. Devi, 4f-4f Transition Spectra of the Interaction of Pr(III) with L-Valine in Solution: Kinetics and Thermodynamic Studies, *Asian J. Chem.* 34 (2022) 2688–2696. <https://doi.org/10.14233/AJCHEM.2022.23911>.
- [35] A.A. Khan, H.A. Hussain, K. Iftikhar, 4f-4f absorption spectra and hypersensitivity in nine-coordinate Ho(III) and Er(III) complexes in different environments., *Spectrochim. Acta. A. Mol. Biomol. Spectrosc.* 60 (2004) 2087–2092. <https://doi.org/10.1016/J.SAA.2003.10.042>.
- [36] S.P. Sinha, Structure and bonding in highly coordinated Lanthanide complexes, (1977) 69–149. https://doi.org/10.1007/3-540-07508-9_3.

Computation of spectral parameters for the complexation of Pr(III) with L-Histidine through $4f-4f$ transition spectra: Further analysis of its kinetic and thermodynamic parameters.

In this chapter the interaction of Pr(III) with L-Histidine has been analysed through $4f-4f$ transition spectra in different solvents. Mode of binding of Pr(III) with L-Histidine is interpreted considering the variations in evaluated values of intensity parameters like oscillator strength (P) and Judd Ofelt electric dipole intensity parameters ' T_λ ' ($\lambda=2,4,6$). Energy interaction parameters like Slater–Condon (F_k 's), Lande factor (ζ_{4f}), Racah energy (E^k), nephelauxetic effect (β), bonding ($b^{1/2}$) and percent covalency (δ). It is further studied through kinetics, subsequently activation energy (E_a), pre-exponential factor (A), specific rate constant/rate constant (k) and thermodynamic parameters viz, ΔH° , ΔG° , ΔS° etc., has been evaluated from which detailed thermodynamical information for the complexation of Pr(III) with L-Histidine in DMF solvent can be explored. Solution spectral studies through kinetic approach could provide pertinent information about the mechanism, reaction pathways, and also about the mode of chemical bond.

5.1. Introduction

The chemistry of the Lanthanides has been playing an emerging role in the different fields of modern research. They have achievements in the field of coordination chemistry[1], inorganic chemistry[2], application in industries and agriculture[3], medical and biological application[4], magnetic resonance imaging agent (M.R.I)[5,6], bioimaging[7], lighting devices[8], lasers[9], telecommunications[10] and the application of the lanthanides are also remarkably increasing as an excellent diagnostics and prognostic probe in biological and clinical aspects[11]. Lanthanides are also found to have excellent physical and chemical properties due to its special electronic configuration[12]. For the last 20 years, the Lanthanide complexes in the organic solution and aqueous solution is attracting much interest as their ground state and excited state have many activities[11]. Because of its coordination chemistry and application in MRI as contrast agents[13] and ion-selective reagents in analytical chemistry[14], lanthanide (Ln) complexes have sparked a lot of interest in thermodynamic[15] and kinetic[16] investigations. Lanthanides are mostly ionic salts and are hard acceptors. Lanthanide ions form stable complexes with oxygen and nitrogen donor ligands and form 9 or 8 coordination[17,18].

Alpha-amino acid such as histidine has one carboxylic group and holds dibasic properties. If the “R” group of alpha-amino acid is replaced by the imidazole, we obtain histidine. The basicity of histidine comes from the imidazole group. Histidine carries four different groups and that can contribute as bonding sites during complexation with the metal ion. These groups with bonding sites include the prime carboxyl and amino groups within the alpha amino acid. However, the two others are contributed by the imidazole compound such as secondary and tertiary nitrogen atoms[19,20]. Because the structure of amino acids prevents all of their possible binding sites from being coordinated to the same metal ion at the same time, their coordination chemistry is characterised by protonated and polynuclear complexes. Amino acid coordination chemistry particularly L-Histidine is extremely significant, and it's a model system of considerable interest[21]. In this present study, L-Histidine an essential amino acid is used as a ligand to study the mode of binding with Pr(III) in their complexation and also to understand the possible structure, conformation and coordination number of the complex formed. Another reason is to understand the thermodynamic properties of the complexation process of Pr(III) with L-Histidine.

*The text of this chapter has been published as:

¹Juliana Sanchu, Zevivonü Thakro, Chubazenba Imsong and M.I. Devi, “Computation of spectral parameters for the complexation of Pr(III) with L-Histidine through *4f-4f* transition spectra: Further analysis of its kinetic and thermodynamic parameters”, Chemical Physics Impact, Volume 5 100127 (2022).

Chemical kinetics is one of the oldest fields of physical chemistry, with its focus on understanding processes and giving exact rate constants to distinct mechanistic stages. The $4f-4f$ transition spectrum variations in lanthanides have been employed only infrequently for mechanistic and kinetic studies. Our research might be one of the few to look at the kinetics of lanthanide complexation with amino acid ligand. Using comparative and absorption difference spectroscopy, we investigated the energy interaction and intensity parameters were computed theoretically to study the mode of binding between Pr (III) and L-Histidine. The variation in the spectral parameters could provide information on the degree of outer and inner sphere coordination, the level of metal $4f-4f$ orbital involvement in the complexation, defining the immediate coordination environment around the metal Pr(III), and the coordination number of the complex formed. The kinetic study of the interaction for Pr (III) with L-Histidine are investigated at various temperatures in aqueous DMF medium, exploiting the sensitivities of $4f-4f$ transitions of Pr(III) to minor coordination changes. We calculated the rate of reactions by monitoring the variations in the absorbance and intensity of pseudohypersensitive transitions ${}^3H_4 \rightarrow {}^3P_2$ of Praseodymium (III): L-Histidine complex. The activation energy (E_a) for the interaction of Pr (III) with L-Histidine has been examined using the Arrhenius equation. The thermodynamic parameters ΔH^0 , ΔS^0 and ΔG^0 as well as the pre-exponential factor (A), for Pr (III): L-Histidine complex, were calculated using Van't Hoff's plot of $\log k$ Vs. $1/T \times 10^3$.

5.2. Materials and Methods

Praseodymium (III) chloride hydrate of 99.9% purity, purchased from Sigma Aldrich L-Histidine from HIMEDIA are used for spectral and kinetic studies. DMF, ACN, Dioxane and MeOH of A/R grade from E. Merck were used as solvents. The concentrations of Pr(III): L-Histidine complex was kept at 0.01 M. The four different organic solvents (DMF, ACN, Dioxane & MeOH) used were made to pH to 7.6. The spectra from 400 to 700 nm were recorded using a Perkin Elmer Lambda 365 UV-Vis spectrophotometer. For kinetic experiments, equimolar quantities of Pr(III):L-Histidine complex were added to aqueous DMF solvent and the resulting mixture was agitated in an inert atmosphere generated to form the complex in solution. On a temperature-controlled Perkin Elmer Lambda-35 UV-Visible Spectrophotometer with attached kinetic assembly in the range 298K (25⁰C), 303K (30⁰C), 308K (35⁰C), 313K (40⁰C), and 318K (45⁰C), a water flowing HAAKE DC 10 thermostat is used to maintain the desired temperature.

*The text of this chapter has been published as:

¹Juliana Sanchu, Zevivonu Thakro, Chubazenba Imsong and M.I. Devi, "Computation of spectral parameters for the complexation of Pr(III) with L-Histidine through $4f-4f$ transition spectra: Further analysis of its kinetic and thermodynamic parameters", Chemical Physics Impact, Volume 5 100127 (2022).

Metal Complexes of L-Histidine with Praseodymium Ion

As “class A” or “hard” acceptors, Praseodymium (III) prefers “class A” or “hard” donor ligands (in the order $O > N > S$ and $F > Cl$). Coordination numbers typically range from 6 - 12, and the physiologically significant are 8 and 9. The complexes can exhibit a variety of geometrical shapes due to its variations in coordination numbers [20]. When ligands are brought to their isoelectronic state in solution, they exist in their neutral form [21] as shown in figure 5.1.

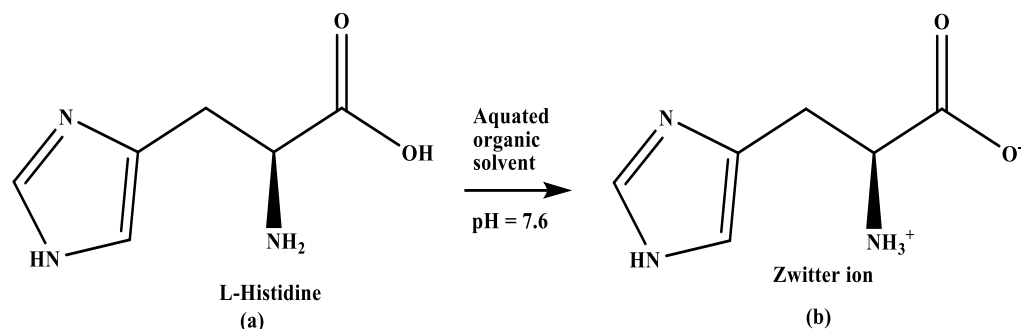


Figure 5.1. Chemical representation of L-Histidine in its isoelectronic point pH 7.6 (zwitterion form).

The pH values affect ligand-metal bonding; for example, when the pH value is less, the metal ion bonds with only the oxygen atom, however when the pH value is high, the metal bonds with both oxygen and nitrogen atoms of the ligand [22-25]. Since the isoelectronic point of L-Histidine is pH 7.6, the Pr(III) binds to the oxygen and nitrogen atoms of L-Histidine as illustrated in figure 5.2.

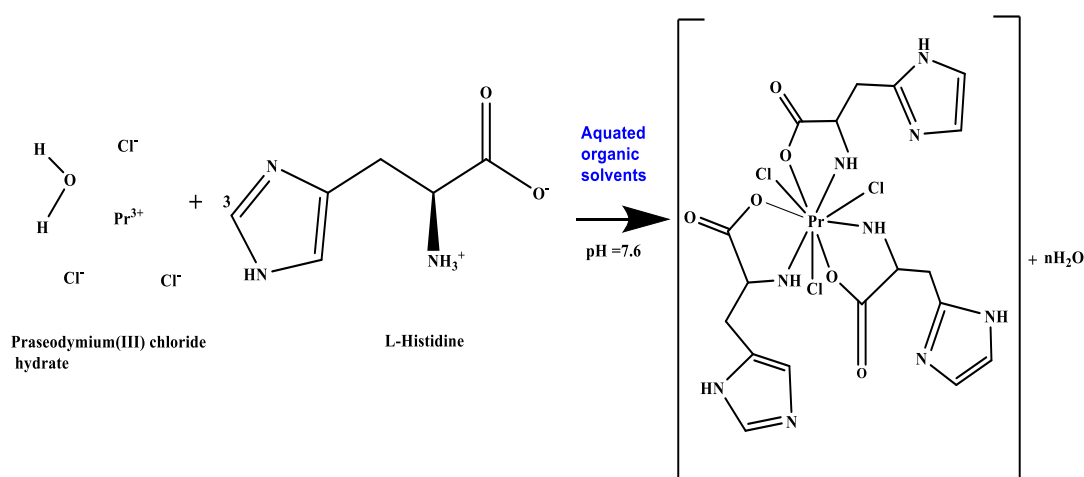


Figure 5.2. The Possible chemical reaction for Praseodymium(III): L-Histidine complex in solution.

5.3. Theoretical

5.3.1. Energy interaction parameters

The covalency is determined by the Nephelauxetic ratio, and that is the ratio of the free ion and complex stated in terms of Racah parameters and Slater–Condon.

$$\beta = \frac{F_K^C}{F_K^f} \text{ or } \frac{E_C^K}{E_f^K}$$

Covalent percentage and bonding parameter are calculated using the equations given below;

$$b^{1/2} = \left[\frac{1-\beta}{2} \right]^{1/2}$$

$$\delta = \left[\frac{1-\beta}{\beta} \right] \times 100$$

The Electrostatic term E_0 was stated as, using the findings of Slater's radial integral, known as the Slater-Condon parameter.

$$E_0 = \sum_{k=0}^{k=6} K^k F_k$$

The angular coefficient is denoted by K^k .

The direct-integrals, or Slater-Condon parameters (F^k), are a decreasing function of K with a relationship given as

$$F_1^k = \int_0^\infty \int_0^\infty \frac{r_{<}^k}{r_{>}^{k=1}} R_i^2(r_i) R_j^2(r_j) r_i^2 r_j^2 dr_i dr_j$$

The close and distant electron radii are ' $r_{<}$ & ' $r_{>}$ ', the 4f-radial wave function is ' R ', and the i^{th} & j^{th} electrons are ' i & ' j '. Shortley and Condon reformulated the Slater-Condon parameter (F^k) integrals in terms of reduced integrals (F_k).

$$F_k = \frac{F^k}{D_k}$$

The reduced Slater-Condon integral is provided by an equation that combines the preceding two relations,

$$F_k = \frac{1}{D_k} \int_0^\infty \int_0^\infty \frac{r_{<}^k}{r_{>}^{k=1}} R_i^2(r_i) R_j^2(r_j) r_i^2 r_j^2 dr_i dr_j$$

The linear combinations of F_k are given as the energy interaction parameter Racah E^{ki} ,

$$E^1 = \frac{70F_2 + 231F_4 + 20.02F_6}{9}$$

$$E^2 = \frac{F_2 - 3F_4 + 7F_6}{9}$$

*The text of this chapter has been published as:

¹Juliana Sanchu, Zevivonü Thakro, Chubazenba Imsong and M.I. Devi, "Computation of spectral parameters for the complexation of Pr(III) with L-Histidine through 4f-4f transition spectra: Further analysis of its kinetic and thermodynamic parameters", Chemical Physics Impact, Volume 5 100127 (2022).

$$E^3 = \frac{5F_2 + 6F_4 - 9F_6}{3}$$

The energy (E_{so}) is known to come from a significant magnetic contact, but the spin orbit interactions may be written as,

$$E_{so} = A_{so} \xi_{4f}$$

where the radial integral is ' ξ_{4f} ' and the angular component of spin orbit interaction is ' A_{so} '. By first order approximation, the energy E_j of the j th level is represented as,

$$E_j(F_k, \xi_{4f}) = E_{0j}(F_k^0, \xi_{4f}^0) + \frac{\partial E_j}{\partial F_k} \Delta F_k + \frac{\partial E_j}{\partial \xi_{4f}} \Delta \xi_{4f}$$

where ' E_{0j} ' is the energy of zero-order in j th level. The equations for F_k and ξ_{4f} are given below:

$$F_k = F_k^0 + \Delta F_k$$

$$\xi_{4f} = \xi_{4f}^0 + \Delta \xi_{4f}$$

The difference between the value of zero order ΔE_j and the observed value of E_j is calculated as follows:

$$\Delta E_j = \sum_k 2,4,6 \frac{\partial E_j}{\partial F_k} + \frac{\partial E_j}{\partial \xi_{4f}} \Delta \xi_{4f}$$

The following equation can be solved using the least square approach to determine the values of ΔF_2 & $\Delta \xi_{4f}$. The following is the formula for determining the estimated values of F_4 and F_6 ,

$$\frac{F_4}{F_2} = 0.1380 \text{ and } \frac{F_6}{F_2} = 0.0150$$

5.3.2. Intensity Parameters

A theoretical approach for determining band intensities was developed by Judd [26] and Ofelt [27]. They hypothesised that the transitions are fundamentally electric dipole transitions, and that the oscillator strength corresponding to the induced electric dipole transition $\Psi J \rightarrow \Psi' J'$ as given by

$$\sum_{\lambda=2,4,6} T_{\lambda} \sigma(f^N \psi J \| U^{\lambda} \| f^N \psi' J')^2 \dots \dots \dots (1)$$

The rank matrix element is denoted by $U(\lambda)$. The three values T_2 , T_4 , and T_6 are associated to the radial components of the $4f^N$ wave functions, the closest of which is $4f^{N-1}5d$.

The following equation links measured absorption spectrum intensities to the probability (P) of radiant energy absorption (oscillator strength):

$$P = \frac{2303mc^2}{N\pi e^2} \int \epsilon_i(\sigma) d\sigma$$

$$P = 4.318 \times 10^{-9} \int \epsilon_i(\sigma) d\sigma \dots \dots \dots (2)$$

*The text of this chapter has been published as:

¹**Juliana Sanchu**, Zevivonu Thakro, Chubazenba Imsong and M.I. Devi, "Computation of spectral parameters for the complexation of Pr(III) with L-Histidine through 4f-4f transition spectra: Further analysis of its kinetic and thermodynamic parameters", *Chemical Physics Impact*, Volume 5 100127 (2022).

The experimentally measured oscillator strength (P_{obs}), which is directly proportional to the area under the absorption curve and computed using Gaussian curve analysis, determines the intensity of the absorption band:

$$P = 4.60 \times 10^{-9} \times \epsilon_{max} \times \Delta\nu_{\frac{1}{2}} \dots\dots\dots (3)$$

The molar extinction coefficient is given by ϵ_{max} .

The observed oscillator strength (P_{obs}) of the transition energies was represented using the T_2 , T_4 and T_6 parameters supplied by Judd and Ofelt, which can be calculated using the equation below.

$$\frac{P_{obs}}{\nu} = [(U^2)]^2 T_2 + [(U^4)]^2 T_4 + [(U^6)]^2 T_6 \dots\dots\dots (4)$$

Carnall[23] gave the matrix elements of Pr(III) system as $U^{(\lambda)}$.

5.3.3. Rate of the reactions

On the basis of the concept of the activation energy. Arrhenius described the temperature dependence of the rate constant (k) by the equation,

$$k = A e^{\frac{-E_a}{RT}} \dots\dots\dots (5)$$

This equation is known as Arrhenius rate equation.

Where, A is called frequency factor. The factor $\exp(-E_a/RT)$ is a measure of the probability for the occurrence of a molecule in the activated state.

The activation energy for Praseodymium (III):L-Histidine complex in DMF solvent is determined from the plot of $\log k$ (k = rate constant) against $1/T$ by using Arrhenius rate equation[24,25]

The above equation (5) can be written as

$$\begin{aligned} \ln k &= \ln A - \frac{E_a}{RT} \\ \text{or, } 2.303 \log k &= 2.303 \log A - \frac{E_a}{RT} \\ \text{or, } \log k &= \log A - \frac{E_a}{2.303RT} \dots\dots\dots (6) \end{aligned}$$

where A is the pre-exponential factor or frequency factor.

Thus, a plot of $\log k$ against $1/T$ should give a straight line with negative slope, in which

$$\text{Slope} = \frac{E_a}{2.303R} \text{ and Intercept} = \log A$$

From the slope the activation energy E_a is calculated as

*The text of this chapter has been published as:

¹Juliana Sanchu, Zevivonü Thakro, Chubazenba Imsong and M.I. Devi, "Computation of spectral parameters for the complexation of Pr(III) with L-Histidine through $4f-4f$ transition spectra: Further analysis of its kinetic and thermodynamic parameters", Chemical Physics Impact, Volume 5 100127 (2022).

$$E_a = -\text{Slope} \times 2.303 \times R \dots\dots\dots (7)$$

Where R is the universal gas constant.

The Van't Hoff plot of $\log k$ against $1/T \times 10^3$ were used for determining the thermodynamic parameters of the complexation and is given as:

$$\log k = -\frac{\Delta H^\circ}{R} \left[\frac{1}{T} \right] + \frac{\Delta S^\circ}{R} \dots\dots\dots (8)$$

$$\text{or } \log k = -\frac{\Delta G^\circ}{RT}$$

5.4. Figures and Tables

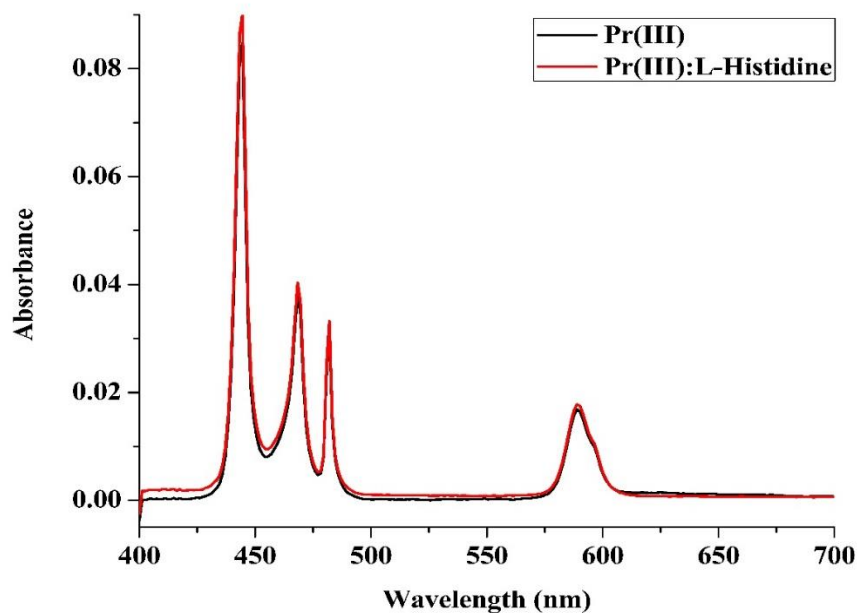


Figure 5.3. The absorption spectra for Praseodymium(III) and Praseodymium(III):L-Histidine complex in aqueous solution.

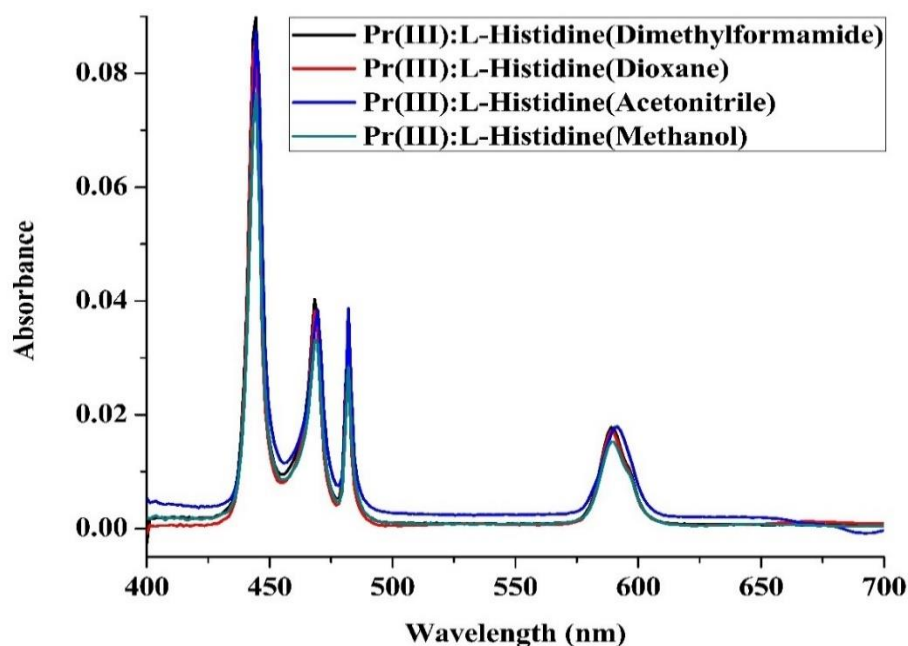


Figure 5.4. The absorption spectra for Praseodymium(III):L-Histidine complex in aqueous solution.

Table 5.1. Comparison of energy interaction values- Slater–Condon (F_k), Lande (ξ_{4f}), Racah energy (E^k), Nephelauxetic ratio (β), bonding ($b^{1/2}$), and covalency (δ) factors of Pr(III) and Pr(III):L-Histidine complex in aqueous solution.

Systems	F_2	F_4	F_6	ξ_{4f}	E^1	E^2	E^3	β	$b^{1/2}$	δ
ACETONITRILE										
Pr(III)	308.471	43.721	5.757	723.62	3515.12	24.782	588.22	0.947	0.1626	5.589
Pr(III)+L-Histidine	308.289	43.697	5.670	723.47	3514.09	24.765	587.86	0.949	0.1629	5.605
DIMETHYLFORMAMIDE										
Pr(III)	308.035	43.655	5.669	721.27	3509.62	24.748	587.38	0.945	0.165	5.754
Pr(III)+ L-Histidine	308.000	43.630	5.659	720.99	3509.49	24.743	587.32	0.947	0.167	5.819
1,4-DIOXANE										
Pr(III)	308.275	43.724	5.677	723.29	3512.75	24.792	588.28	0.947	0.163	5.607
Pr(III)+ L-Histidine	308.144	43.716	5.670	722.74	3512.62	24.770	588.15	0.948	0.165	5.631
METHANOL										
Pr(III)	308.305	43.698	5.678	722.52	3512.85	24.768	587.92	0.944	0.162	5.577
Pr(III)+ L-Histidine	308.263	43.694	5.669	722.30	3511.79	24.763	587.86	0.947	0.164	5.675

Table 5.2. Comparison of energies (cm^{-1}) values as well as RMS values for Pr(III) and Pr(III):L-Histidine complex in aqueous solution.

Systems	$^3\text{H}_4 \rightarrow ^3\text{P}_2$		$^3\text{H}_4 \rightarrow ^3\text{P}_1$		$^3\text{H}_4 \rightarrow ^3\text{P}_0$		$^3\text{H}_4 \rightarrow ^1\text{D}_2$		RMS
	E_{obs}	E_{cal}	E_{obs}	E_{cal}	E_{obs}	E_{cal}	E_{obs}	E_{cal}	
ACETONITRILE									
Pr(III)	22525.06	22469.51	21351.10	21258.39	20741.72	20694.87	16975.33	17146.05	103.56
Pr(III)+ L-Histidine	22524.06	22471.64	21349.73	21258.39	20741.17	20694.39	16974.33	17146.05	103.56
DIMETHYLFORMAMIDE									
Pr(III)	22493.65	22441.63	21293.45	21231.80	20742.15	20674.09	16920.87	17122.77	103.84
Pr(III)+ L-Histidine	22493.14	22441.80	21292.91	21222.58	20741.29	20666.83	16919.61	17121.43	117.09
1,4-DIOXANE									
Pr(III)	22525.06	22470.04	21351.10	21258.39	20741.72	20694.04	16975.33	17146.15	103.56
Pr(III)+ L-Histidine	22524.55	22470.86	21350.19	21257.57	20740.86	20694.54	16974.76	17146.81	103.58
METHANOL									
Pr(III)	22525.16	22470.32	21351.10	21258.39	20741.72	20694.07	16975.33	17146.05	103.56
Pr(III)+ L-Histidine	22524.04	22470.64	21349.73	21258.79	20740.32	20694.87	16974.05	17146.69	103.56

*The text of this chapter has been published as:

¹Juliana Sanchu, Zevivonu Thakro, Chubazenba Imsong and M.I. Devi, "Computation of spectral parameters for the complexation of Pr(III) with L-Histidine through $4f-4f$ transition spectra: Further analysis of its kinetic and thermodynamic parameters", Chemical Physics Impact, Volume 5 100127 (2022).

Table 5.3. Comparison of Oscillator strengths and Judd–Ofelt parameters for Pr(III) and Pr(III):L-Histidine complex in aqueous solution.

Systems	${}^3\text{H}_4 \rightarrow {}^3\text{P}_2$		${}^3\text{H}_4 \rightarrow {}^3\text{P}_1$		${}^3\text{H}_4 \rightarrow {}^3\text{P}_0$		${}^3\text{H}_4 \rightarrow {}^1\text{D}_2$		T_2	T_4	T_6
	P_{obs}	P_{cal}	P_{obs}	P_{cal}	P_{obs}	P_{cal}	P_{obs}	P_{cal}			
ACETONITRILE											
Pr(III)	17.386	17.386	5.559	4.371	3.131	4.299	3.281	3.281	-411.8	11.99	53.83
Pr(III)+ L-Histidine	22.694	22.694	5.952	4.702	3.765	4.625	3.943	3.943	-725.7	12.90	71.08
DIMETHYLFORMAMIDE											
Pr(III)	18.671	18.671	5.797	4.263	2.685	4.193	3.898	3.898	-524.4	11.70	58.12
Pr(III)+ L-Histidine	21.167	21.167	6.118	4.554	2.940	4.479	4.094	4.094	-675.2	12.49	66.10
1,4- DIOXANE											
Pr(III)	16.855	16.855	5.506	3.697	2.871	4.343	3.025	3.025	-356.4	12.12	52.06
Pr(III)+ L-Histidine	20.787	20.787	6.535	5.023	3.886	4.952	4.053	4.053	-476.1	13.82	64.50
METHANOL											
Pr(III)	16.613	16.613	5.551	4.405	1.859	3.639	2.238	2.238	-368.6	10.15	51.80
Pr(III)+ L-Histidine	20.384	20.384	6.104	4.616	2.673	4.538	3.212	3.212	-458.5	12.66	63.47

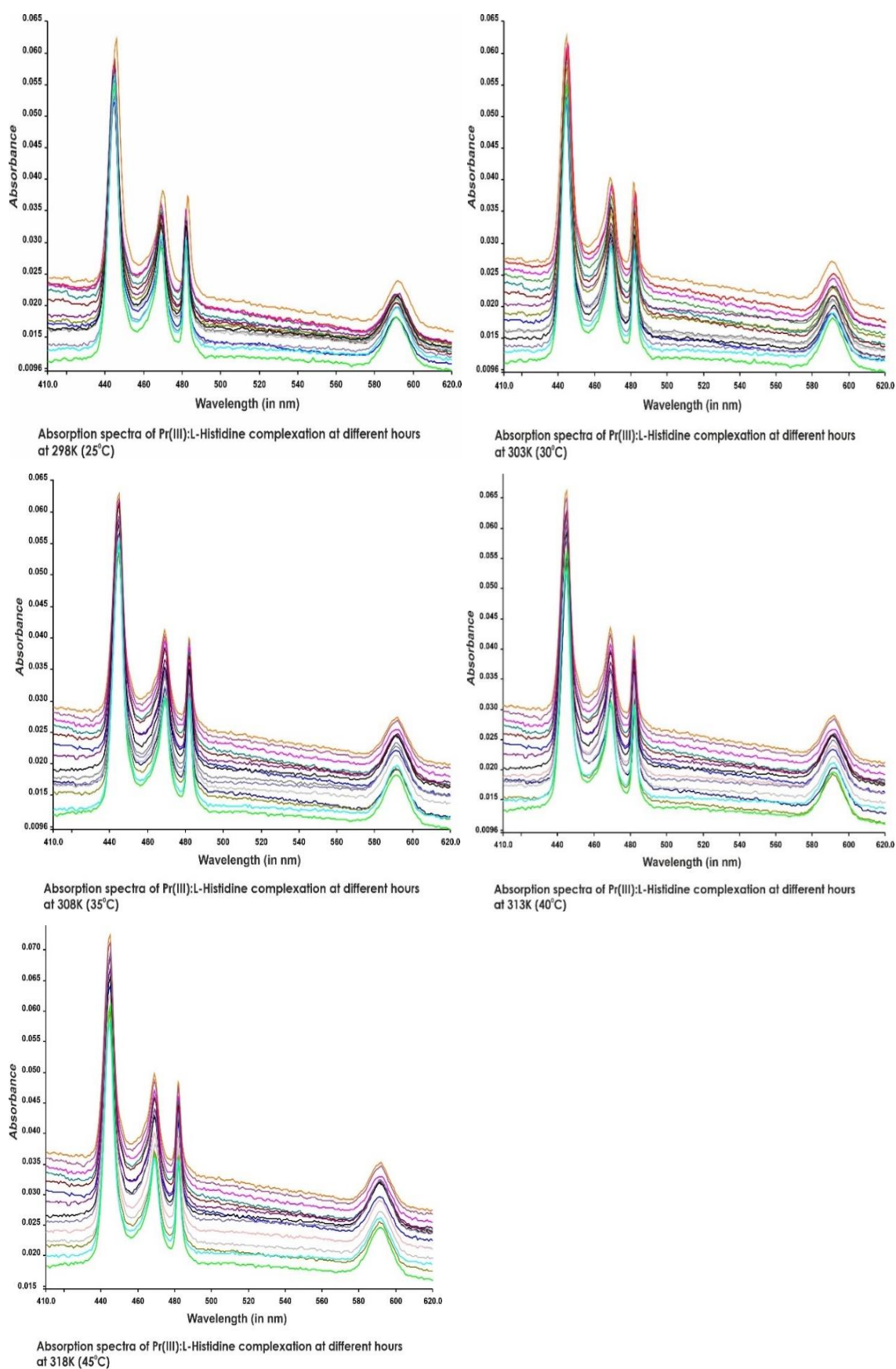


Figure 5.5. Absorption spectra for the complexation of Pr(III):L-Histidine at 298°K, 303°K, 308°K, 313°K and 318°K in aqueous DMF solvent.

*The text of this chapter has been published as:

¹Juliana Sanchu, Zevivonu Thakro, Chubazenba Imsong and M.I. Devi, "Computation of spectral parameters for the complexation of Pr(III) with L-Histidine through $4f-4f$ transition spectra: Further analysis of its kinetic and thermodynamic parameters", Chemical Physics Impact, Volume 5 100127 (2022).

Table 5.4. Observed and calculated oscillator strengths and Judd-Ofelt intensity parameters for the complexation of Pr(III):L-Histidine at 298K (25°C) in various time intervals(hr).

Time (in hour)	${}^3\text{H}_4 \rightarrow {}^3\text{P}_2$		${}^3\text{H}_4 \rightarrow {}^3\text{P}_1$		${}^3\text{H}_4 \rightarrow {}^3\text{P}_0$		${}^3\text{H}_4 \rightarrow {}^1\text{D}_2$		T_2	T_4	T_6
	P_{obs}	P_{cal}	P_{obs}	P_{cal}	P_{obs}	P_{cal}	P_{obs}	P_{cal}			
0	6.252	6.252	3.095	2.286	1.465	2.221	2.832	2.832	235.11	6.281	18.742
2	6.463	6.463	3.107	2.295	1.481	2.229	2.897	2.897	240.05	6.340	18.929
4	6.601	6.601	3.119	2.297	1.498	2.285	2.971	2.971	249.33	6.407	19.015
6	6.643	6.643	3.224	2.304	1.502	2.329	3.023	3.023	255.81	6.483	19.449
8	6.673	6.673	3.257	2.321	1.515	2.374	3.035	3.035	261.45	6.511	19.519
10	6.716	6.716	3.294	2.352	1.520	2.379	3.041	3.041	263.09	6.254	19.914
12	6.843	6.843	3.346	2.398	1.535	2.385	3.049	3.049	269.75	6.582	19.619
14	6.925	6.925	3.381	2.432	1.547	2.389	3.057	3.057	274.48	6.634	19.721
16	6.993	6.993	3.425	2.467	1.562	2.394	3.068	3.068	281.64	6.709	19.832
18	7.008	7.008	3.469	2.490	1.573	2.399	3.073	3.073	289.71	6.764	19.921
20	7.021	7.021	3.501	2.540	1.581	2.407	3.081	3.081	294.55	6.823	20.014
22	7.042	7.042	3.575	2.591	1.593	2.419	3.098	3.098	301.98	6.885	20.127
24	7.059	7.059	3.653	2.671	1.641	2.426	3.112	3.112	307.29	6.971	20.249
26	7.072	7.072	3.712	2.736	1.764	2.439	3.125	3.125	315.09	7.059	20.462
28	7.095	7.095	3.732	2.782	1.827	2.447	3.139	3.139	324.83	7.149	21.164
30	7.125	7.125	3.751	2.864	1.896	2.458	3.151	3.151	333.77	7.221	22.763
32	7.209	7.209	3.774	2.913	1.948	2.470	3.169	3.169	343.95	7.289	21.891
34	7.396	7.396	3.790	2.997	1.991	2.484	3.182	3.182	355.61	7.373	22.992

Table 5.5. Observed and calculated oscillator strengths and Judd-Ofelt intensity parameters for the complexation of Pr(III):L-Histidine at 303K (30°C) in various time intervals (hr).

Time (in hour)	${}^3\text{H}_4 \rightarrow {}^3\text{P}_2$		${}^3\text{H}_4 \rightarrow {}^3\text{P}_1$		${}^3\text{H}_4 \rightarrow {}^3\text{P}_0$		${}^3\text{H}_4 \rightarrow {}^1\text{D}_2$		T_2	T_4	T_6
	P_{obs}	P_{cal}	P_{obs}	P_{cal}	P_{obs}	P_{cal}	P_{obs}	P_{cal}			
0	6.231	6.231	3.091	2.286	1.457	2.251	2.870	2.870	234.51	6.274	18.738
2	6.320	6.320	3.123	2.321	1.471	2.280	2.911	2.911	239.05	6.320	18.932
4	6.398	6.398	3.157	2.347	1.490	2.305	3.012	3.012	247.43	6.397	19.012
6	6.471	6.471	3.191	2.360	1.506	2.324	3.022	3.022	252.80	6.478	19.469
8	6.520	6.520	3.206	2.412	1.519	2.351	3.052	3.052	258.45	6.521	19.501
10	6.590	6.590	3.091	2.286	1.458	2.251	2.870	2.870	210.96	6.274	19.916
12	6.648	6.648	3.231	2.308	1.461	2.275	3.072	3.072	263.09	6.591	19.603
14	6.703	6.703	3.268	2.321	1.472	2.295	3.107	3.107	269.75	6.643	19.711
16	6.775	6.775	3.291	2.359	1.486	2.311	3.148	3.148	274.48	6.701	19.823
18	6.831	6.831	3.301	2.371	1.498	2.338	3.185	3.185	281.64	6.756	19.906
20	6.892	6.892	3.326	2.395	1.507	2.346	3.221	3.221	289.71	6.812	20.008
22	6.951	6.951	3.349	2.419	1.528	2.359	3.276	3.276	294.55	6.893	20.119
24	7.012	7.012	3.364	2.441	1.547	2.376	3.317	3.317	301.98	6.962	20.239
26	7.094	7.094	3.376	2.462	1.561	2.395	3.376	3.376	307.29	7.048	20.452
28	7.172	7.172	3.413	2.518	1.618	2.481	3.491	3.491	315.09	7.132	21.042
30	7.217	7.217	3.450	2.560	1.651	2.598	3.589	3.589	324.83	7.219	22.865
32	7.309	7.309	3.589	2.658	1.701	2.617	3.626	3.626	333.77	7.296	21.998
34	7.669	7.669	3.789	2.807	1.798	2.764	3.777	3.777	343.95	7.706	23.067

*The text of this chapter has been published as:

¹Juliana Sanchu, Zevivonü Thakro, Chubazenba Imsong and M.I. Devi, "Computation of spectral parameters for the complexation of Pr(III) with L-Histidine through $4f-4f$ transition spectra: Further analysis of its kinetic and thermodynamic parameters", Chemical Physics Impact, Volume 5 100127 (2022).

Table 5.6. Observed and calculated oscillator strengths and Judd-Ofelt intensity parameters for the complexation of Pr(III):L-Histidine at 308K (35^oC) in various time intervals (hr).

Time (in hour)	³ H ₄ → ³ P ₂		³ H ₄ → ³ P ₁		³ H ₄ → ³ P ₀		³ H ₄ → ¹ D ₂		T ₂	T ₄	T ₆
	P _{obs}	P _{cal}	P _{obs}	P _{cal}	P _{obs}	P _{cal}	P _{obs}	P _{cal}			
0	6.109	6.109	3.011	2.227	1.431	2.225	2.875	2.875	237.11	6.281	18.741
2	6.225	6.225	3.053	2.278	1.476	2.269	2.981	2.981	236.03	6.342	18.952
4	6.398	6.398	3.097	2.309	1.509	2.295	3.009	3.009	245.43	6.383	19.022
6	6.471	6.471	3.139	2.356	1.555	2.332	3.018	3.018	257.81	6.456	19.465
8	6.590	6.590	3.175	2.399	1.598	2.372	3.027	3.027	259.52	6.513	19.572
10	6.673	6.673	3.091	2.286	1.637	2.399	3.039	3.039	265.09	6.554	19.696
12	6.783	6.783	3.141	2.315	1.672	2.438	3.046	3.046	269.55	6.592	19.713
14	6.891	6.891	3.198	2.327	1.698	2.475	3.057	3.057	272.34	6.641	19.861
16	6.995	6.995	3.239	2.355	1.738	2.499	3.066	3.066	275.81	6.702	19.893
18	7.113	7.113	3.273	2.377	1.773	2.539	3.078	3.078	282.45	6.762	19.926
20	7.231	7.231	3.316	2.399	1.798	2.572	3.089	3.089	288.13	6.814	20.105
22	7.347	7.347	3.345	2.427	1.825	2.602	3.094	3.094	295.55	6.884	20.118
24	7.429	7.429	3.369	2.448	1.876	2.654	3.134	3.134	302.09	6.952	20.261
26	7.555	7.555	3.385	2.482	1.909	2.697	3.194	3.194	308.29	7.062	20.622
28	7.672	7.672	3.419	2.511	1.943	2.734	3.255	3.255	316.32	7.144	21.132
30	7.723	7.723	3.456	2.569	1.993	2.991	3.309	3.309	323.76	7.229	22.234
32	7.817	7.817	3.498	2.608	2.021	3.019	3.387	3.387	335.47	7.353	21.398
34	7.906	7.906	3.549	2.667	2.076	3.065	3.423	3.423	341.61	7.551	23.461

Table 5.7. Observed and calculated oscillator strengths and Judd-Ofelt intensity parameters for the complexation of Pr(III):L-Histidine at 313K (40°C) in various time intervals(hr).

Time (in hour)	${}^3\text{H}_4 \rightarrow {}^3\text{P}_2$		${}^3\text{H}_4 \rightarrow {}^3\text{P}_1$		${}^3\text{H}_4 \rightarrow {}^3\text{P}_0$		${}^3\text{H}_4 \rightarrow {}^1\text{D}_2$		T_2	T_4	T_6
	P_{obs}	P_{cal}	P_{obs}	P_{cal}	P_{obs}	P_{cal}	P_{obs}	P_{cal}			
0	6.115	6.115	3.039	2.165	1.465	2.239	2.889	2.889	239.41	6.291	18.789
2	6.245	6.245	3.087	2.254	1.486	2.272	2.987	2.987	246.05	6.362	18.977
4	6.398	6.398	3.145	2.343	1.512	2.299	3.035	3.035	249.32	6.395	19.053
6	6.485	6.485	3.193	2.446	1.543	2.338	3.087	3.087	256.83	6.476	19.471
8	6.592	6.592	3.235	2.543	1.587	2.377	3.137	3.137	259.21	6.553	19.584
10	6.667	6.667	3.280	2.672	1.617	2.393	3.185	3.185	264.19	6.578	19.698
12	6.754	6.754	3.312	2.753	1.645	2.445	3.246	3.246	268.54	6.592	19.778
14	6.885	6.885	3.356	2.811	1.689	2.482	3.326	3.326	273.46	6.651	19.891
16	6.976	6.976	3.389	2.856	1.718	2.531	3.387	3.387	277.15	6.742	19.978
18	7.109	7.109	3.439	2.898	1.753	2.576	3.413	3.413	283.53	6.798	20.145
20	7.335	7.335	3.555	2.949	1.789	2.602	3.489	3.489	289.12	6.843	20.342
22	7.559	7.559	3.661	2.993	1.829	2.765	3.523	3.523	298.57	6.895	20.521
24	7.746	7.746	3.732	3.117	1.865	2.801	3.591	3.591	308.92	6.972	20.731
26	7.906	7.906	3.845	3.245	1.929	2.897	3.653	3.653	312.25	7.088	20.967
28	8.113	8.113	3.913	3.297	1.943	2.953	3.761	3.761	319.23	7.178	21.132
30	8.326	8.326	3.996	3.321	1.993	2.997	3.837	3.837	326.65	7.267	22.376
32	8.509	8.509	4.124	3.386	2.021	3.076	3.949	3.949	334.72	7.384	21.584
34	8.711	8.711	4.372	3.427	2.076	3.165	4.084	4.084	344.63	7.491	23.789

Table 5.8. Observed and calculated oscillator strengths and Judd-Ofelt intensity parameters for the complexation of Pr(III):L-Histidine at 318K (45^oC) in various time intervals(hr).

Time (in hour)	³ H ₄ → ³ P ₂		³ H ₄ → ³ P ₁		³ H ₄ → ³ P ₀		³ H ₄ → ¹ D ₂		T ₂	T ₄	T ₆
	P _{obs}	P _{cal}	P _{obs}	P _{cal}	P _{obs}	P _{cal}	P _{obs}	P _{cal}			
0	6.198	6.198	3.045	2.187	1.489	2.281	2.891	2.891	241.11	6.295	18.793
2	6.289	6.289	3.098	2.263	1.532	2.325	2.965	2.965	250.53	6.372	18.925
4	6.377	6.377	3.167	2.367	1.591	2.397	3.043	3.043	259.12	6.390	19.065
6	6.463	6.463	3.243	2.454	1.615	2.423	3.095	3.095	260.67	6.469	19.327
8	6.575	6.575	3.319	2.583	1.652	2.496	3.137	3.137	263.15	6.545	19.572
10	6.766	6.766	3.457	2.648	1.697	2.523	3.243	3.243	264.57	6.571	19.692
12	6.981	6.981	3.534	2.761	1.704	2.585	3.355	3.355	267.68	6.598	19.783
14	7.107	7.107	3.654	2.843	1.749	2.618	3.465	3.465	273.86	6.671	19.876
16	7.331	7.331	3.713	2.918	1.794	2.683	3.527	3.527	277.67	6.756	19.982
18	7.563	7.563	3.821	3.014	1.851	2.757	3.631	3.631	282.39	6.792	20.151
20	7.755	7.755	3.943	3.145	1.895	2.843	3.745	3.745	288.62	6.847	20.345
22	7.902	7.902	4.027	3.265	1.939	2.916	3.835	3.835	295.07	6.875	20.537
24	8.125	8.125	4.132	3.372	1.975	2.976	3.946	3.946	307.82	6.792	20.727
26	8.349	8.349	4.243	3.441	2.009	3.004	4.045	4.045	312.51	7.058	20.945
28	8.523	8.523	4.321	3.513	2.066	3.162	4.134	4.134	319.31	7.183	21.165
30	8.735	8.735	4.451	3.635	2.123	3.225	4.253	4.253	329.59	7.273	22.398
32	8.947	8.947	4.580	3.717	2.186	3.361	4.346	4.346	336.92	7.395	22.569
34	9.156	9.156	4.628	3.867	2.245	3.448	4.484	4.484	345.27	7.461	23.761

*The text of this chapter has been published as:

¹Juliana Sanchu, Zevivonu Thakro, Chubazenba Imsong and M.I. Devi, "Computation of spectral parameters for the complexation of Pr(III) with L-Histidine through 4f-4f transition spectra: Further analysis of its kinetic and thermodynamic parameters", Chemical Physics Impact, Volume 5 100127 (2022).

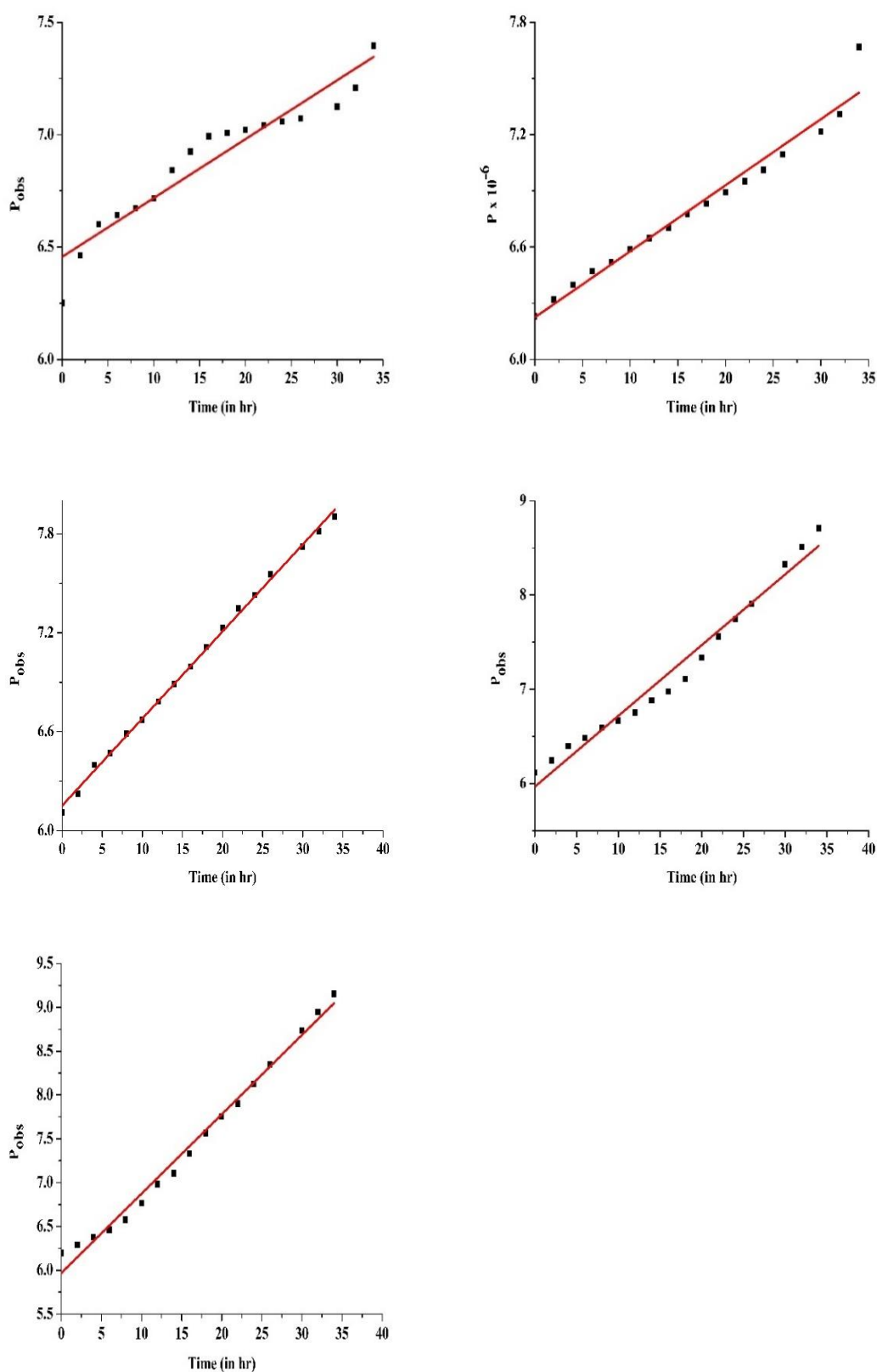


Figure 5.6. Plot of oscillator strength Vs time (in hrs) for ${}^3H_4 \rightarrow {}^3P_2$ transition for Pr(III):L-Histidine complex in aqueous DMF solvent at five different temperatures (i.e., 298°K, 303°K, 308°K, 313°K and 318°K).

*The text of this chapter has been published as:

¹Juliana Sanchu, Zevivonü Thakro, Chubazenba Imsong and M.I. Devi, "Computation of spectral parameters for the complexation of Pr(III) with L-Histidine through 4*f*-4*f* transition spectra: Further analysis of its kinetic and thermodynamic parameters", Chemical Physics Impact, Volume 5 100127 (2022).

Table 5.9. Rate constant k ($\text{Mol L}^{-1} \text{s}^{-1}$) and activation energy, E_a values for the complexation of Pr(III):L-Histidine at various temperatures.

Temp(K)	$1/T \times 10^3$	Rate Constant (k) $\text{Mol L}^{-1}\text{hr}^{-1}$	Rate Constant (k) $\text{Mol L}^{-1}\text{s}^{-1}$	Log k	Pre-exponential factor 'A' $\text{Mol L}^{-1}\text{s}^{-1}$	Activation Energy 'Ea' (kJ mol^{-1})
298	3.3557	0.02619	7.275	0.86183	7.42658	0.05108
303	3.3003	0.03527	9.797	0.99109	9.99776	
308	3.2468	0.05281	14.669	1.16640	14.96455	
313	3.1949	0.07506	20.850	1.31911	21.26336	
318	3.1447	0.09056	25.156	1.40064	25.64662	

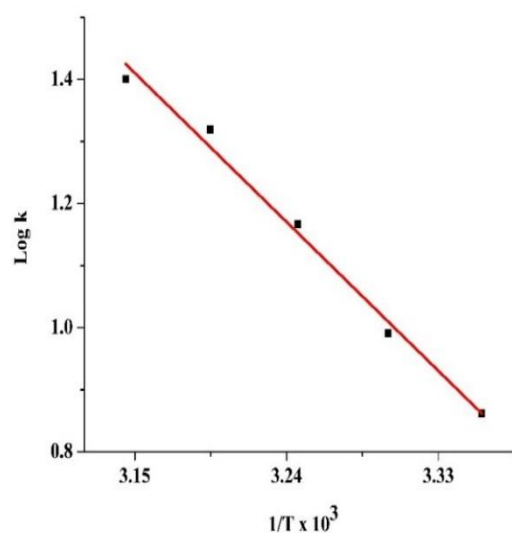


Figure 5.7. Plot of Log k versus $1/T \times 10^3$ for Pr (III): L-Histidine complex in aqueous DMF solvent at different temperatures.

Table 5.10. Thermodynamic parameters for Pr(III):L-Histidine complex at different temperatures and activation energy for the complexation reaction.

Temperature (K)	Rate Constant (k) $\text{Mol L}^{-1}\text{s}^{-1}$	ΔH (kJ mol^{-1})	ΔG (kJ mol^{-1})	ΔS (J K^{-1})	Activation Energy 'Ea' (kJ mol^{-1})
298	7.275	0.05108	-4.91747	16.67	0.05108
303	9.797		-5.74989	19.15	
308	14.669		-6.87863	22.50	
313	20.850		-7.90550	25.42	
318	25.156		-8.52821	26.98	

*The text of this chapter has been published as:

¹Juliana Sanchu, Zevivonü Thakro, Chubazenba Imsong and M.I. Devi, "Computation of spectral parameters for the complexation of Pr(III) with L-Histidine through $4f-4f$ transition spectra: Further analysis of its kinetic and thermodynamic parameters", Chemical Physics Impact, Volume 5 100127 (2022).

5.5. Results and Discussion

The spectroscopic features of the trivalent lanthanide ions are unusual; because the $4f$ subshell is adequately insulated by closed $5s$ and $5p$ subshells, the ligand environment has only a little impact on the lanthanide ion's electronic cloud. This disturbance is responsible for the spectral fine structure, notwithstanding its weakness. The band's line width is modest, and the peak location shows the electrical structure of the $4f^n$ configuration. Judd–Ofelt theory has been used to analyse the absorption spectra of rare earth ions [26,27]; Lanthanide coordination chemistry in solution is becoming increasingly important as lanthanides are used as probes in the discovery of the structural roles of biomolecular processes. [28].

The hypersensitivity of lanthanide trihalides in gaseous form with D_{nh} symmetry may be seen in their absorption spectra. [29]. Jorgenson and Judd [30,31] studied sensitivities and came to the conclusion that such transitions followed selection criteria. The $4f-4f$ transitions of Pr(III), namely $^3H_4 \rightarrow ^3P_2, ^3P_1, ^3P_0$ and 1D_2 do not follow the selection criteria and are thus classified as non-hypersensitive transitions. Experiments have shown that even minor changes in the co-ordination environment around lanthanide ions caused by configuration, density, chelating capability, and co-ordinating power of donor sites of ligand, all of which are related to the coordination number of lanthanide ions, are extremely sensitive to such non-hypersensitive transitions. It's important to emphasize that the current study is only done in the solution state since investigations involving the solution state might give the most relevant data when it comes to human metabolism and the role of L-Histidine. We investigated the coordination of L-Histidine with Pr(III) using comparative and absorption difference spectroscopy involving intra $4f-4f$ transitions as a probe.

Table 5.1. shows the energy interaction parameters: Slater-Condon F_k (cm^{-1}), Lande ζ_{4f} (cm^{-1}), Racah energy E^k (cm^{-1}), nephelauxetic ratio (β), bonding ($b^{1/2}$) and covalency (δ) factor for Pr(III) and Pr(III):L-Histidine complex in various aqueous MeOH, MeCN, DMF and dioxane solvents. The values of energy interaction parameters such as F^k , E^k , and ζ_{4f} for the Pr(III) complex decrease when compared to the free Pr(III) state, indicating a decrease in interelectronic repulsion and spin orbit interaction parameters, resulting in a decrease in the metal-ligand bond distance, allowing complexation. The drop in F^k parameters shows that the ligand has a greater impact on electrostatic repulsion than on spin-orbit coupling. The Slater-Condon parameters are in the following order: $F_2 > F_4 > F_6$. The nephelauxetic effect in all systems is between 0.944 and 0.949, indicating the study's

*The text of this chapter has been published as:

¹Juliana Sanchu, Zevivonu Thakro, Chubazenba Imsong and M.I. Devi, "Computation of spectral parameters for the complexation of Pr(III) with L-Histidine through $4f-4f$ transition spectra: Further analysis of its kinetic and thermodynamic parameters", Chemical Physics Impact, Volume 5 100127 (2022).

validity; and a positive value of β could imply the possibility of a covalent bond formed between the Pr (III) and L-Histidine complex. When Pr(III) and L-Histidine form a complex, the values of nephelauxetic effect, bonding parameter and covalency percentage parameters rises, resulting in a drop in effective nuclear charge and interelectronic repulsion parameters shown by the decrease values of F^k ($k=2,4,6$) and ζ_{4f} . The metal-ligand distance is reduced due to the nephelauxetic effect, thereby increasing interelectronic interaction between the metal and the ligand, which is needed for better covalency.

Except for the ${}^3\text{H}_4 \rightarrow {}^1\text{D}_2$ transition, the observed values of energy for the ${}^3\text{H}_4 \rightarrow {}^3\text{P}_2$, ${}^3\text{P}_1$ and ${}^3\text{P}_0$ transitions of Praseodymium (III) and Praseodymium (III):L-Histidine complex are greater than the estimated values of energies in table 5.2. The root means square deviation (RMS) values demonstrate the accuracy of multiple energy interaction parameters: Slater-Condon (F^k), Lande factor (ζ_{4f}), Racah energy (E^k), Nephelauxetic ratio (β), bonding ($b^{1/2}$), and covalency (δ) factors.

Table 5.3. shows the computed values of ' T_λ ' parameters and ' P ' for pseudohypersensitive transitions of Praseodymium(III) and Praseodymium(III): Ligand complex in various experimental ambiances. When Pr(III) interacts with L-Histidine, the P values and T_λ parameters changes dramatically indicating the possibility of the complexation of Praseodymium (III) with L-Histidine. Because ' T_2 ' is associated to the hypersensitive transition ${}^3\text{H}_4 \rightarrow {}^3\text{F}_3$, which is beyond the UV-Vis. area and has negative values, ' T_2 ' is disregarded. Small variations in the coordination environment, on the other hand, had a considerable impact on the amounts of T_4 and T_6 parameters during complexation, and their values were +ve. The T_4 and T_6 parameters are both related to changes in symmetry features during complexation. As a result, significant variations in T_4 and T_6 detect differences in the symmetry of Pr(III), its complex systems, and the nearby coordination environment. Complexation through the inner-sphere is revealed by large changes in the amounts of ' P ' and ' T_λ ' ($\lambda=2,4,6$), whilst complexation through the outer-sphere is revealed by the small change in the amounts of ' P ' and ' T_λ ' ($\lambda=2,4,6$). Table 5.3. demonstrates how the calculated values of P and T_λ have varied over time, suggesting that the coordination between Praseodymium(III) and L-Histidine occurs through the inner-sphere. As shown in the same table, T_6 is the most significant of the three T_λ ($\lambda=2,4,6$) parameters for the complexation of Pr(III) with L-Histidine, and is in the order: $T_6 > T_4 > T_2$.

*The text of this chapter has been published as:

¹Juliana Sanchu, Zevivonü Thakro, Chubazenba Imsong and M.I. Devi, "Computation of spectral parameters for the complexation of Pr(III) with L-Histidine through 4f-4f transition spectra: Further analysis of its kinetic and thermodynamic parameters", Chemical Physics Impact, Volume 5 100127 (2022).

In comparison to the bands of Pr (III) alone to that when it gets complex with L-Histidine, the absorption band of Praseodymium(III):L-Histidine complex has shifted significantly and the band becomes more intense, demonstrating its sensitivity to small changes in the coordination ambience that causes a wavelength shift towards longer wavelengths (figures 5.3.) i.e., redshift and thereby strengthening the $4f-4f$ transition spectral band. Solvent changes have a considerable impact on the oscillator strengths of the $4f-4f$ bands, resulting in variations in the magnitudes of the intensity parameters ' P ' and ' T_λ ' ($\lambda=2,4,6$). From table 5.3. and figure 5.4., we can say that as compared to the other solvents Acetonitrile shows more preferences for covalent bonding in the formation of Praseodymium(III):L-Histidine complex this might be because Acetonitrile contain 'N' donor atoms [32,33]. Looking into the computed values of the ' P ' and ' T_λ ' parameters, the sensitivity of $4f-4f$ transition of the various aquated organic solvents are in the: $\text{CH}_3\text{CN} > \text{DMF} > \text{C}_4\text{H}_8\text{O}_2 > \text{CH}_3\text{OH}$.

Pr(III) are ionic salt and are hard acceptors, whereas amino acid are hard donors. In aqueous solution, L-Histidine form zwitter-ion at pH 7.6; Since at high pH the complexation occurs between Pr(III) and oxygen and nitrogen donor atom of amino acids.[22,34,35] Praseodymium ion form stable complex with oxygen and nitrogen donor of L-Histidine with 9 coordination number. Figure 5.2. shows the possible chemical reaction for nona-coordinated Pr(III):L- Histidine complex in solution.

Figure 5.5. shows that the intensity of $4f-4f$ transitions increases significantly with time, implying that absorption spectrum investigation might be utilised to study the reaction mechanisms for the present complexation process. The oscillator strengths and ' T_λ ' ($\lambda=2,4,6$) for Praseodymium(III): L-Histidine complex in DMF medium at different temperatures (298°K, 308°K, 308°K, 310°K, and 318°K) are shown in Tables 5.4.-5.8. In comparison to the other ${}^3\text{H}_4 \rightarrow {}^3\text{P}_1$, ${}^3\text{H}_4 \rightarrow {}^3\text{P}_0$, and ${}^3\text{H}_4 \rightarrow {}^1\text{D}_2$ transitions, the pseudohypersensitive transition ${}^3\text{H}_4 \rightarrow {}^3\text{P}_2$ is reported to be the most sensitive $4f-4f$ transition based on changes in the estimated values of P and T_λ ($\lambda=2,4,6$) parameters for the complexation of Pr(III) with L-Histidine. The calculated T_λ data reveals that their values grow proportionally with temperature and time; this tendency indicates that the rate constants for the complexation process of Pr(III) with L-Histidine rise proportionately with time and temperature.

Figure 5.6. illustrates the oscillator strength of ${}^3\text{H}_1 \rightarrow {}^3\text{P}_2$ transitions for the complexation of Pr(III) with L-Histidine vs. time at different temperatures. The slope, pre-exponential factor, and rate of complexation for Pr(III):L-Histidine complexes in DMF medium at

*The text of this chapter has been published as:

¹Juliana Sanchu, Zevivonu Thakro, Chubazenba Imsong and M.I. Devi, "Computation of spectral parameters for the complexation of Pr(III) with L-Histidine through $4f-4f$ transition spectra: Further analysis of its kinetic and thermodynamic parameters", Chemical Physics Impact, Volume 5 100127 (2022).

various temperatures may be measured by graphing the $P_{\text{obs.}}$ with time. The rate of Pr(III) complexation with L-Histidine rises linearly with temperature and time which validates the Arrhenius prediction of the reaction rate. The pre-exponential component (A) also rises as the temperature increases. Because molecules travel faster as temperature rises, they are more likely to clash, increasing the collision number and hence affecting the pre-exponential factor 'A'. The Van't Hoff plot of $\ln k$ against $1/T$ (Figure 5.7.) are used to determine the activation energy (E_a) and further ' E_a ' value is used to evaluate the other thermodynamic parameters. This approach may be applicable to measure the thermodynamic parameters of Pr(III): L-Histidine complexation in DMF medium indirectly. The rate of complexation increases with increasing temperature, as shown in Table 5.9., which is used to compute the rate of reaction and the activation energy 'Ea' of the complexation. Table 5.10. shows that the complexation process is an endothermic, entropy-increasing activity since ΔH° and ΔS° are both positive. Table 5.9. shows that when the temperature rises, the rate of complexation increases, which is used to compute the rate of reaction and the activation energy 'Ea' of the complexation. Table 5.10. show that the values of ΔH° and ΔS° are positive, indicating that the complexation reaction is an endothermic and entropy-increasing activity. Furthermore, the coordination reaction is an entropy-driven process since $T\Delta S^\circ > \Delta H^\circ$. Negative standard Gibbs energy (ΔG°) values imply that the coordination is a spontaneous process as well as favoured one in solution. We may also conclude that the complexation of Pr(III) ions with L-Histidine occurs spontaneously, following the system's randomness as it reaches higher temperatures (increasing S values). Furthermore, the activation energies (E_a) for the Pr(III): L-Histidine complex were found to be 0.05108 kJ. This lower ' E_a ' values support the idea that the reaction is an instantaneous one.

5.6. Conclusion

When compared to the free Pr(III) state, the energy interaction parameters such as F_k , E^k and ξ_{4f} for Pr(III):L-Histidine complex decrease, implying a declines in spin orbit interaction and interelectronic repulsion parameters, indicating the possibility of Pr(III) complexation with L-Histidine. The rise in the values of δ and $b^{1/2}$ implies increase in the complexation and the possibility of covalent bonding between Pr(III) and L-Histidine. The nephelauxetic effect (β) in all systems is between 0.944 and 0.949, revealing the study's validity; and a positive value of β could imply the possibility of a covalent bond formed between the Pr (III) and L-Histidine complex. When Pr(III) and L-Histidine form

*The text of this chapter has been published as:

¹Juliana Sanchu, Zevivonü Thakro, Chubazenba Imsong and M.I. Devi, "Computation of spectral parameters for the complexation of Pr(III) with L-Histidine through 4f-4f transition spectra: Further analysis of its kinetic and thermodynamic parameters", Chemical Physics Impact, Volume 5 100127 (2022).

a complex, the values of nephelauxetic effect (β), bonding parameter ($b^{1/2}$) and percent covalency (δ) parameters rise, resulting in a decrease in effective nuclear charge and interelectronic repulsion parameters shown by the decrease values of F_k and ζ_{4f} . The metal-ligand distance is reduced due to the nephelauxetic effect, thereby increasing interelectronic interaction between Pr (III) and L-Histidine, which is needed for better covalency (δ). When L-Histidine is added to Pr (III), the interaction of $4f$ -orbitals increases, as seen by the intensification of absorption spectrum and the formation of redshift. The reliability of the analyzed data is predicted by the root mean square (RMS) values. In the complexation of Pr(III) with L-Histidine, considerable differences in the calculated values of P and T_λ might lead to the coordination of inner-sphere. Praseodymium ion form stable complex with oxygen and nitrogen donor atom of L-Histidine and form nona-coordination through the inner sphere coordination. The fluctuation in the values of T_4 and T_6 implies that the symmetry of the complex produced has changed. Looking into computed values of the P and T_λ parameters, the sensitivity of $4f$ - $4f$ transition of the various aquated organic solvents are in the:



The findings of the discussions based on the values of intensity parameters for complexation at various time intervals and temperatures clearly demonstrated that, as predicted by Arrhenius, the rate of complexation increased with time and temperature. The fact that the activation energy (E_a) is low indicates that the complexation reaction is instantaneous. The positive values of ΔH^0 denotes an endothermic reaction associated with complexation, whereas the negative value of ΔG^0 denotes the spontaneity of the reaction process as well as its favorability in solution. The current investigation of the reaction is determined to be entropy-driven because $T\Delta S^0 > \Delta H^0$. Depending on the probabilities of how often the molecules collide, the pre-exponential factor (A) values might offer an explicit relation between temperature and reaction rate.

*The text of this chapter has been published as:

¹**Juliana Sanchu**, Zevivonü Thakro, Chubazenba Imsong and M.I. Devi, "Computation of spectral parameters for the complexation of Pr(III) with L-Histidine through $4f$ - $4f$ transition spectra: Further analysis of its kinetic and thermodynamic parameters", *Chemical Physics Impact*, Volume 5 100127 (2022).

References

- [1] M.D.M.C. Ribeiro Da Silva, N.R.M. Araújo, A.L.R. Silva, L.C.M. Da Silva, N.P.S.M. Barros, J.M. Gonçalves, M.A.V. Ribeiro Da Silva, Three N₂O₂ ligands derived from the condensation of 1,2-cyclohexanediamine with salicylaldehyde, acetylacetone and benzoylacetone: AAAAAA new contribution to the energetical characterization of Schiff bases, *J. Therm. Anal. Calorim.* 87 (2007) 291–296. <https://doi.org/10.1007/S10973-006-7808-7>.
- [2] I.P. Kostova, I.I. Manolovi, M.K. Radulova, Stability of the complexes of some lanthanides with coumarin derivatives. II. Neodymium(III)-acenocoumarol, *Acta Pharm.* 54 (2004) 119–131.
- [3] V. Gonzalez, D.A.L. Vignati, C. Leyval, L. Giamberini, Environmental fate and ecotoxicity of lanthanides: are they a uniform group beyond chemistry?, *Environ. Int.* 71 (2014) 148–157. <https://doi.org/10.1016/J.ENVINT.2014.06.019>.
- [4] C.X. Zhang, X.M. Qiao, H.W. Chen, Y.Y. Zhang, Syntheses and Biological Activities of Lanthanide Metal Complexes with Nitronly Nitroxide, <Http://Dx.Doi.Org/10.1080/15533174.2013.819914>. 45 (2014) 145–150. <https://doi.org/10.1080/15533174.2013.819914>.
- [5] P. Caravan, J.J. Ellison, T.J. McMurry, R.B. Lauffer, Gadolinium(III) Chelates as MRI Contrast Agents: Structure, Dynamics, and Applications, *Chem. Rev.* 99 (1999) 2293–2352. <https://doi.org/10.1021/CR980440X>.
- [6] É.T. Andre S. Merbach, Lothar Helm, *The Chemistry of Contrast Agents in Medical Magnetic Resonance Imaging*, 2nd Edition | Wiley, WILEY. (n.d.) 512 Pages. <https://www.wiley.com/enus/The+Chemistry+of+Contrast+Agents+in+Medical+Magnetic+Resonance+Imaging,+2nd+Edition-p-9781119991762> (accessed April 22, 2022).
- [7] X. Qin, J. Wang, Q. Yuan, Synthesis and Biomedical Applications of Lanthanides-Doped Persistent Luminescence Phosphors With NIR Emissions, *Front. Chem.* 8 (2020) 1138. <https://doi.org/10.3389/FCHEM.2020.608578/BIBTEX>.
- [8] J.-C.G. Bünzli, (PDF) *Lanthanides*, Wiley Blackwell. (2013) 44. https://www.researchgate.net/publication/257921324_Lanthanides (accessed April 22, 2022).
- [9] M. Osawa, M. Hoshino, T. Wada, F. Hayashi, S. Osanai, Intra-complex energy transfer of europium(III) complexes containing anthracene and phenanthrene moieties, *J. Phys. Chem. A.* 113 (2009) 10895–10902.
-

*The text of this chapter has been published as:

¹**Juliana Sanchu**, Zevivonü Thakro, Chubazenba Imsong and M.I. Devi, “Computation of spectral parameters for the complexation of Pr(III) with L-Histidine through 4*f*-4*f* transition spectra: Further analysis of its kinetic and thermodynamic parameters”, *Chemical Physics Impact*, Volume 5 100127 (2022).

- <https://doi.org/10.1021/jp905160w>.
- [10] J.C.G. Bünzli, S. V. Eliseeva, Lanthanide NIR luminescence for telecommunications, bioanalyses and solar energy conversion, *J. Rare Earths*. 28 (2010) 824–842. [https://doi.org/10.1016/S1002-0721\(09\)60208-8](https://doi.org/10.1016/S1002-0721(09)60208-8).
- [11] S.N. Misra, M.A. Gagnani, D.M. Indira, R.S. Shukla, Biological and Clinical Aspects of Lanthanide Coordination Compounds, *Bioinorg. Chem. Appl.* 2 (2004) 155–192. <https://doi.org/10.1155/S1565363304000111>.
- [12] L. Zapała, M. Kosińska, E. Woźnicka, Ł. Byczyński, W. Zapała, Synthesis, spectral and thermal study of La(III), Nd(III), Sm(III), Eu(III), Gd(III) and Tb(III) complexes with mefenamic acid, *J. Therm. Anal. Calorim.* 124 (2016) 363–374. <https://doi.org/10.1007/S10973-015-5120-0>.
- [13] R.B. Lauffer, Paramagnetic Metal Complexes as Water Proton Relaxation Agents for NMR Imaging: Theory and Design, *Chem. Rev.* 87 (1987) 901–927. https://doi.org/10.1021/CR00081A003/ASSET/CR00081A003.FP.PNG_V03.
- [14] Y. Marcus, Metal-chloride complexes studied by ion-exchange and solvent-extraction methods. Part I. Non-transition-metal ions, lanthanides, actinides, and d⁰ transition-metal ions, *Coord. Chem. Rev.* 2 (1967) 195–238. [https://doi.org/10.1016/S0010-8545\(00\)80205-2](https://doi.org/10.1016/S0010-8545(00)80205-2).
- [15] G.R. Choppin, Thermodynamics of lanthanide-organic ligand complexes, *J. Less Common Met.* 112 (1985) 193–205. [https://doi.org/10.1016/0022-5088\(85\)90024-4](https://doi.org/10.1016/0022-5088(85)90024-4).
- [16] A.E. (Arthur E. Martell, *Coordination chemistry.*, (1971).
- [17] J. Sanchu, M. Ziekhri, Z. Thakro, M.I. Devi, 4f-4f Transition Spectra of the Interaction of Pr(III) with L-Valine in Solution: Kinetics and Thermodynamic Studies, *Asian J. Chem.* 34 (2022) 2688–2696. <https://doi.org/10.14233/AJCHEM.2022.23911>.
- [18] J. Sanchu, C. Imsong, Z. Thakro, M. Ziekhri, M.I. Devi, Absorption spectral study for the interaction of Pr(III) with L-Aspartic acid in various aquated organic solvents through 4f-4f transition spectra: Analysis of reaction pathways and thermodynamic parameters, *J. Pharm. Negat. Results.* 13 (2022) 860–878. <https://doi.org/10.47750/PNR.2022.13.S01.105>.
- [19] R. Garrett, *Principles of biochemistry: with a human focus*, Harcourt College Publishers, Fort Worth, 2002.
- [20] Thomas M. Devlin, *Textbook of Biochemistry with Clinical Correlations*, 7th

*The text of this chapter has been published as:

¹Juliana Sanchu, Zevivonü Thakro, Chubazenba Imsong and M.I. Devi, “Computation of spectral parameters for the complexation of Pr(III) with L-Histidine through 4f-4f transition spectra: Further analysis of its kinetic and thermodynamic parameters”, *Chemical Physics Impact*, Volume 5 100127 (2022).

- Edition | Wiley, (n.d.). <https://www.wiley.com/en-us/Textbook+of+Biochemistry+with+Clinical+Correlations%2C+7th+Edition-p-9780470281734> (accessed April 22, 2022).
- [21] S. Damodaran, K.L. (Kirk L. Parkin, Fennema's food chemistry, (n.d.) 1107.
- [22] J.C.G. Bünzli, C. Piguet, Lanthanide-containing molecular and supramolecular polymetallic functional assemblies, *Chem. Rev.* 102 (2002) 1897–1928. https://doi.org/10.1021/CR010299J/ASSET/CR010299J.FP.PNG_V03.
- [23] W.T. Carnall, P.R. Fields, B.G. Wybourne, Spectral Intensities of the Trivalent Lanthanides and Actinides in Solution. I. Pr³⁺, Nd³⁺, Er³⁺, Tm³⁺, and Yb³⁺, *J. Chem. Phys.* 42 (2004) 3797. <https://doi.org/10.1063/1.1695840>.
- [24] Keith J Laidler, Chemical Kinetics by Keith J Laidler - PDF Drive, (n.d.). <https://www.pdfdrive.com/chemical-kinetics-e188163536.html> (accessed April 22, 2022).
- [25] P.D. Ross, S. Subramanian, Thermodynamics of Protein Association Reactions: Forces Contributing to Stability, *Biochemistry.* 20 (1981) 3096–3102. https://doi.org/10.1021/BI00514A017/ASSET/BI00514A017.FP.PNG_V03.
- [26] V.K. Rai, S.B. Rai, D.K. Rai, Spectroscopic properties of Pr³⁺ doped in tellurite glass, *Spectrochim. Acta Part A Mol. Biomol. Spectrosc.* 62 (2005) 302–306. <https://doi.org/10.1016/J.SAA.2004.12.043>.
- [27] M. Prasad, V.K. Rai, Thermally stable upconverting Na₃Zr₂(SiO₄)₂PO₄: Er³⁺/Yb³⁺ phosphors for displays and optical thermometry, *J. Alloys Compd.* 911 (2022) 164968. <https://doi.org/10.1016/J.JALLCOM.2022.164968>.
- [28] C.H. Evans, *Biochemistry of the lanthanides*, (1990) 444.
- [29] R.B. Martin, *Structural Chemistry of Calcium: Lanthanides as Probes.*, Wiley, New York.(1983)237–270. https://scholar.google.com/scholar?hl=en&as_sdt=0%2C5&q=Martin%2C+R.B.+%281983%29+Structural+Chemistry+of+Calcium%3A+Lanthanides+as+Probes.+In%3A+Spiro%2C+T.G.%2C+Ed.%2C+Calcium+Biology%2C+Wiley%2C+New+York%2C+237-270.&btnG= (accessed April 25, 2022).
- [30] B.R. Judd, Optical Absorption Intensities of Rare-Earth Ions, *Phys. Rev.* 127 (1962) 750. <https://doi.org/10.1103/PhysRev.127.750>.
- [31] D.M. Gruen, C.W. Dekock, Absorption Spectra of Gaseous NdBr₃ and NdI₃, *J. Chem. Phys.* 45 (2004) 455. <https://doi.org/10.1063/1.1727588>.
- [32] S.N. Misra, S.O. Sommerer, Absorption Spectra of Lanthanide Complexes in

*The text of this chapter has been published as:

¹Juliana Sanchu, Zevivonu Thakro, Chubazenba Imsong and M.I. Devi, "Computation of spectral parameters for the complexation of Pr(III) with L-Histidine through 4*f*-4*f* transition spectra: Further analysis of its kinetic and thermodynamic parameters", *Chemical Physics Impact*, Volume 5 100127 (2022).

-
- Solution, [Http://Dx.Doi.Org/10.1080/05704929108050880](http://dx.doi.org/10.1080/05704929108050880). 26 (2006) 151–202. <https://doi.org/10.1080/05704929108050880>.
- [33] S.N. Misra, S.O. Sommerer, The ligand mediated pseudohypersensitivity of the $3H4 \rightarrow 3P2$, $3H4 \rightarrow 3P1$, $3H4 \rightarrow 3P0$, and $3H4 \rightarrow 1D2$ transitions of praseodymium(III) complexes in solution media, [https://Doi.Org/10.1139/V92-009](https://doi.org/10.1139/V92-009). 70 (2011) 46–54. <https://doi.org/10.1139/V92-009>.
- [34] A.L. Sobolewski, D. Shemesh, W. Domcke, Computational studies of the photophysics of neutral and zwitterionic amino acids in an aqueous environment: Tyrosine-(H₂O)₂ and tryptophan-(H₂O)₂ clusters, *J. Phys. Chem. A.* 113 (2009) 542–550. https://doi.org/10.1021/JP8091754/SUPPL_FILE/JP8091754_SI_001.PDF.
- [35] F. Costanzo, R.G. Della Valle, V. Barone, MD simulation of the Na⁺-phenylalanine complex in water: competition between cation- π interaction and aqueous solvation, *J. Phys. Chem. B.* 109 (2005) 23016–23023. <https://doi.org/10.1021/JP055271G>.

***4f-4f* transition spectral study of the interaction of Pr(III) with L-Valine in solution: Further analysis of its kinetics and thermodynamic parameters**

In this chapter we have investigated the *4f-4f* transition spectra for the interaction of L-Valine with Praseodymium (III) in aquated organic solvents (50 percent v/v) of CH₃CN, DMF, CH₃OH, and C₄H₈O₂. The variation in the theoretically computed values of the absorption spectral parameters: Energy interaction parameters- Spin-orbit interaction (ξ_{4f}), Slater-Condon (F_k), nephelauxetic ratio (β), Racah energy (E_k), bonding parameter ($b^{1/2}$) and percentage covalency (δ) explained the nature of complexation. The values of evaluated intensity parameters: oscillator strengths (P) and Judd-Ofelt parameters T_λ ($\lambda = 2, 4, 6$) were analysed to see the possibility of outer and inner sphere coordination of Pr(III) with L- Valine. Further, reaction pathways for Pr(III) with L-Valine and consequently its thermodynamic parameters have been evaluated through *4f-4f* transition spectra in DMF solvent.

6.1. Introduction

Lanthanide(III) with ligands like amino acids or peptides and their bonding character are being studied within the field of biological chemistry because of their potential utility as structural probes. [1][2][3]. Lanthanides are important in a variety of areas, including organic and bioorganic chemistry, optical sensing technologies (such as luminescence sensors), and medicine (diagnostic and therapy), with medical applications developing rapidly in recent years. The fact that lanthanides, with their unique *4f*-electron configuration, have coordination numbers ranging from 6 to 12 justifies their vast range of uses. Rare earth ions have antibacterial, anticancer, and antiviral properties when combined with organic ligands, and they play a significant role in many essential biological processes [4–6]. Because of their enthralling and important characteristics, such as their capability to attach to nitrogen, oxygen and skeletal probes in biological systems, lanthanide complexes have received a great deal of research interest. A comprehensive analysis of the interactions of several lanthanides with a wide range of proteins, amino acids, and polypeptides has been reported [7]. Because of the lanthanide's paramagnetic properties, which make it spectroscopically active, the lanthanide (III) complex can provide important details regarding how it interacts with amino acids. [8–10]. As lanthanides are utilised more often as probes to examine the structural function of biomolecular processes, their coordinating chemistry in solution is fast emerging [11–13].

Lanthanides favour the donor atoms O>N>S and F>Cl in the complexation. This shows a high preference for 'O' donor atoms by the lanthanide. As long as the side chains (-R group) of amino acids are present, their functional groups (-COOH & -NH₂) can be employed to change the shape and size of positive materials [14]. Peptides and amino acids are frequent macromolecules that function as efficient metal binding sites in physiological conditions. Simple amino acid building blocks make up peptides, which have a wide spectrum of biological significance. Due to its therapeutic qualities, peptide research is one of the most popular areas of study [15]. The relationship between Ln (III) ions and amino acids is well known; the lanthanide ion is attached to

the oxygen atom of the carboxylate group and the nitrogen atom of the amine group [16]. When amino acids are solid, they are in a state of neutrality. They exist as zwitterions in an aqueous solution if their isoelectric point is maintained [17,18], as seen in figure 6.1.

*The text of this chapter has been published as:

¹Juliana Sanchu, Mhasiriekho Ziekhri, Zevivonü Thakro and M. Indira Devi, "4f-4f Transition Spectra of the Interaction of Pr(III) with L-Valine in Solution: Kinetics and Thermodynamic Studies", Asian Journal of Chemistry, 34(10):2688-2696 (2022).

Thus, using a probe ($4f-4f$ spectra) of Praseodymium (III) to understand the interaction of the ligand with the metal ion would be a fascinating scope to investigate in detail.

By employing the $4f-4f$ spectra of praseodymium (III) as a probe, the current study explores the complexation between the praseodymium (III) ion and L-Valine in the binary mixtures of water and organic solvents (CH_3CN , DMF, $\text{C}_4\text{H}_8\text{O}_2$, and CH_3OH). The fluctuations in the theoretically determined values of the energy parameters—Slater-Condon (F_k), Spin-orbit interaction (ζ_{4f}), Racah energy (E_k), Nephelauxetic ratio (β), bonding parameter ($b^{1/2}$) and percentage covalency (δ) were used to investigate the complexity of the complexation. The oscillator strengths (P) and Judd-Ofelt parameters T_λ ($\lambda=2, 4, 6$) used to measure intensity were analysed. The variations in P and T_λ ($\lambda = 2, 4, 6$) values show a specific correlation between relative intensities, ion behaviour toward solvents, ligand structures, and complexation nature. By calculating the parameters such as rate constant (k), ΔH^0 , ΔS^0 , ΔG^0 and frequency factor (A), it is possible to analyse the thermodynamic behaviour as well as the pathways of the reaction.

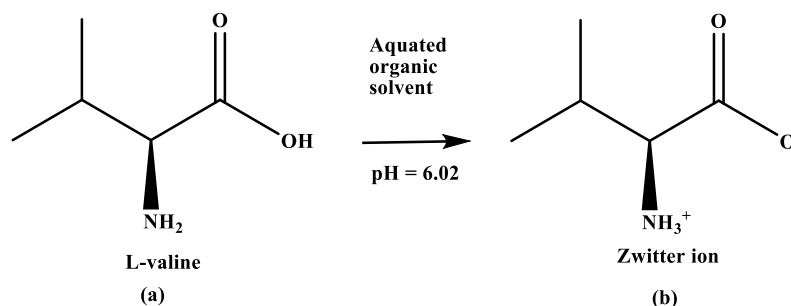


Figure 6.1. Structure of L-Valine in its free state and zwitterion form.

6.2. Materials and methods:

Pr(III) chloride hydrate [$\text{PrCl}_3 \cdot x\text{H}_2\text{O}$] of 99.9% purity was purchased from Alfa Aesar, and the ligand i.e. L-Valine was purchased from HIMEDIA. The solvents used are DMF, acetonitrile, methanol and 1,4-dioxane are of AR grade. The concentration of solutions for recording spectra is maintained at 10^{-2} M and the instrument used is a Perkin Elmer 35 UV-Vis spectrophotometer in the 400-700 nm region.

For kinetic investigations, a 10^{-2} M concentration of Pr (III) and L-Valine combination was prepared in DMF solvent. At various temperatures, all spectra were recorded from 400-700 nm using a temperature-controlled Perkin Elmer Lambda-35 UV-Visible spectrophotometer with related kinetic assembly. Using a water-circulating HAAKE DC 10 Thermostat, all of the observations are kept at the same temperature. The energy bands are determined using Judd [19] and Ofelt [20] theoretical treatment.

*The text of this chapter has been published as:

¹Juliana Sanchu, Mhasiriekho Ziekhri, Zevivonu Thakro and M. Indira Devi, "4f-4f Transition Spectra of the Interaction of Pr(III) with L-Valine in Solution: Kinetics and Thermodynamic Studies", Asian Journal of Chemistry, 34(10):2688-2696 (2022).

6.3. Theoretical

6.3.1. Energy interaction and Intensity parameters

For Pr (III) complexes, the values of interelectronic parameters, i.e., F_2 , F_4 , F_6 and ξ_{4f} were determined by using the technique developed by Mishra et al.[21]

$$E_{obs} = E_{oj} + \frac{\delta E_j}{\delta F_2} \Delta F_2 + \frac{\delta E_j}{\delta \xi_{4f}} \Delta \xi_{4f} \dots \dots \dots (1)$$

The partial regression approach is then used to obtain estimated F_2 and ξ_{4f} values. The following relationship yields approximate F_4 and F_6 values:

$$\frac{F_4}{F_2} = 0.13805 \text{ and } \frac{F_6}{F_2} = 0.0151 \dots \dots \dots (2)$$

Nephelauxetic ratio ' β ' measures the change in F_k w.r.t free ion, which is defined as:

$$\beta_1 = \frac{F_k^c}{F_k^f}; \beta_2 = \frac{\xi_{4f}^c}{\xi_{4f}^f} \text{ and } \beta = \left[\frac{\beta_1 + \beta_2}{2} \right] \dots \dots \dots (3)$$

Where F_k^c and F_k^f refer to parameters in free ion and complex respectively.

Another bonding measure, $b^{1/2}$, related to the nephelauxetic effect, can be used to determine the degree of mixing between the 4f-orbital and the ligand orbital:

$$b^{1/2} = \left[\frac{1-\beta}{2} \right]^{1/2} \dots \dots \dots (4)$$

Sinha[22] introduced another parameter known as the percentage covalency parameter ($\delta\%$) which is defined as:

$$\delta\% = \left[\frac{1-\beta}{\beta} \right] \times 100 \dots \dots \dots (5)$$

The area under the absorption curve and the oscillator strength (P) are directly related. It is given by:

$$P = 4.6 \times 10^{-9} \left[\frac{9\eta}{(\eta^2 + \eta)^2} \right] \int \varepsilon_{max} \bar{\nu} d\bar{\nu} \dots \dots \dots (6)$$

Where ε_{max} = molar extinction coefficient, $\bar{\nu}$ = transition energy in wave number and η = refractive index of the medium

The experimental value of oscillator strengths (P_{obs}) of absorption band determined via Gaussian Curve analysis is

$$P_{obs} = 4.6 \times 10^{-9} \times \varepsilon_{max} \times \bar{\nu}^{1/2} \dots \dots \dots (7)$$

The transition energies' observed oscillator strength (P_{obs}) was expressed in terms of T_2 , T_4 and T_6 parameters provided by Judd[19] and Ofelt[20], which are supplied:

$$\frac{P_{obs}}{\nu} = [(U^2)]^2 T_2 + [(U^4)]^2 T_4 + [(U^6)]^2 T_6 \dots \dots \dots (8)$$

Where U^λ is the matrix element given by Carnall et al.[23] and the transition energy is ' ν '.

6.3.2. Evaluation of thermodynamic parameters

Using the Arrhenius rate equation[24] by graphing $\log k$ versus $1/T$, and is used to calculate the activation energy for the complexation of Praseodymium (III) and L- Valine.

$$\log k = \log A - \frac{E_a}{2.303R} \times \frac{1}{T} \dots\dots\dots (9)$$

From the slope, the activation energy E_a is given by:

$$E_a = - 2.303 \times R \times \text{Slope} \dots\dots\dots (10)$$

Where R = universal gas constant

The thermodynamic features for Praseodymium (III): L-Valine complex is evaluated using Van't Hoff [29] equation of $\log k$ Vs. $1/T \times 10^3$

$$\log k = -\frac{\Delta H^\circ}{R} \left[\frac{1}{T} \right] + \frac{\Delta S^\circ}{R}$$

$$\text{or } \log k = -\frac{\Delta G^\circ}{RT} \dots\dots\dots (11)$$

*The text of this chapter has been published as:

¹**Juliana Sanchu**, Mhasiriekho Ziekhri, Zevivonu Thakro and M. Indira Devi, "4f-4f Transition Spectra of the Interaction of Pr(III) with L-Valine in Solution: Kinetics and Thermodynamic Studies", Asian Journal of Chemistry, 34(10):2688-2696 (2022).

6.4. Figures and tables

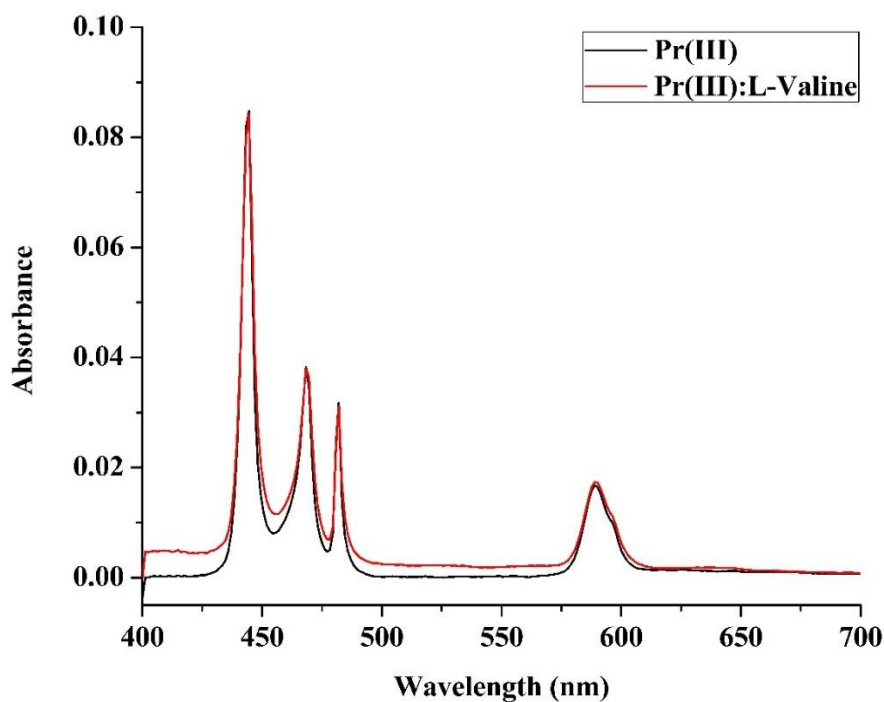


Figure 6.2. Absorption spectra of Pr(III) and Pr(III): L-Valine complex in aqueous DMF solvent.

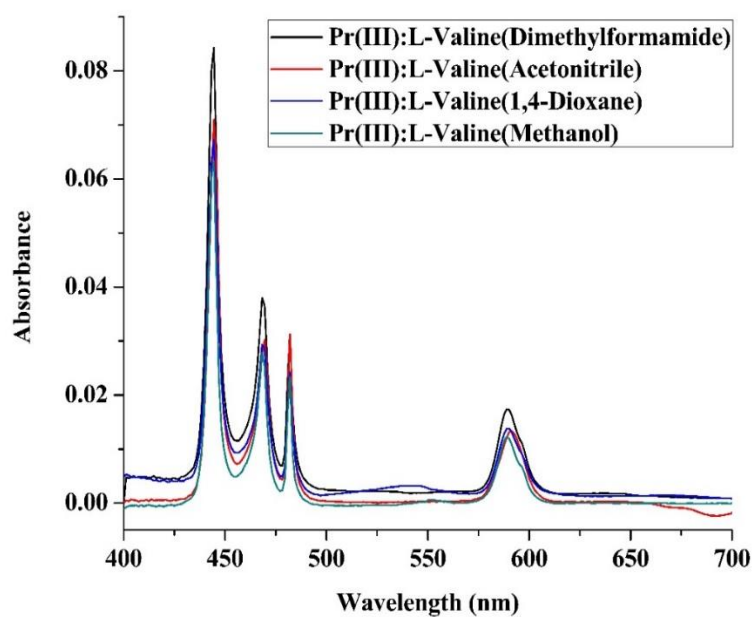


Figure 6.3. Absorption spectra of Pr(III) and Pr(III): L-Valine complex in various aqueous organic solvents.

*The text of this chapter has been published as:

¹Juliana Sanchu, Mhasiriekho Ziekhri, Zevivonu Thakro and M. Indira Devi, "4f-4f Transition Spectra of the Interaction of Pr(III) with L-Valine in Solution: Kinetics and Thermodynamic Studies", Asian Journal of Chemistry, 34(10):2688-2696 (2022).

Table 6.1. Comparison of energy interaction values- Slater–Condon (F_k), Lande (ξ_{4f}), Racah energy (E^k), Nephelauxetic ratio (β), bonding ($b^{1/2}$), and covalency (δ) factors of Pr(III) and Pr(III): L- Valine complex in different aquated solvents.

Systems	F_2	F_4	F_6	ξ_{4f}	E^1	E^2	E^3	β	$b^{1/2}$	δ
ACETONITRILE										
Pr(III)	308.471	43.721	5.757	723.62	3515.12	24.782	588.22	0.946	0.163	5.589
Pr(III)+Valine	308.303	43.698	5.678	723.60	3514.99	24.768	587.89	0.947	0.164	5.593
DIMETHYLFORMAMIDE										
Pr(III)	308.035	43.655	5.669	721.27	3509.62	24.748	587.38	0.945	0.165	5.754
Pr(III)+Valine	308.029	43.650	5.665	720.21	3509.58	24.746	587.35	0.947	0.165	5.778
1, 4 – DIOXANE										
Pr(III)	308.275	43.724	5.677	723.29	3512.75	24.792	588.28	0.946	0.163	5.607
Pr(III)+Valine	308.270	43.722	5.674	723.22	3512.69	24.786	588.22	0.947	0.163	5.588
METHANOL										
Pr(III)	308.305	43.698	5.678	722.52	3512.85	24.768	587.92	0.944	0.162	5.577
Pr(III)+Valine	308.301	43.697	5.675	722.49	3511.81	24.767	587.88	0.945	0.163	5.590

*The text of this chapter has been published as:

¹Juliana Sanchu, Mhasiriekho Ziekhri, Zevivonu Thakro and M. Indira Devi, “4f-4f Transition Spectra of the Interaction of Pr(III) with L-Valine in Solution: Kinetics and Thermodynamic Studies”, Asian Journal of Chemistry, 34(10):2688-2696 (2022).

Table 6.2. Comparison of energies (cm^{-1}) values as well as RMS values for Pr(III) and Pr(III): L- Valine in different aquated solvents.

Systems	$^3\text{H}_4 \rightarrow ^3\text{P}_2$		$^3\text{H}_4 \rightarrow ^3\text{P}_1$		$^3\text{H}_4 \rightarrow ^3\text{P}_0$		$^3\text{H}_4 \rightarrow ^1\text{D}_2$		RMS
	E_{obs}	E_{cal}	E_{obs}	E_{cal}	E_{obs}	E_{cal}	E_{obs}	E_{cal}	
ACETONITRILE									
Pr(III)	22525.06	22469.51	21351.10	21258.39	20741.72	20694.87	16975.33	17146.05	103.56
Pr(III)+ Valine	22524.55	22470.19	21350.36	21257.21	20740.43	20693.66	16974.76	17145.28	103.44
DIMETHYLFORMAMIDE									
Pr(III)	22493.65	22441.63	21293.45	21231.80	20742.15	20674.09	16920.87	17122.77	103.84
Pr(III)+ Valine	22493.64	22441.69	21293.36	21222.04	20742.11	20666.31	16920.47	17122.07	117.21
1, 4 – DIOXANE									
Pr(III)	22525.06	22470.04	21351.10	21258.39	20741.72	20694.04	16975.33	17146.15	103.56
Pr(III)+ Valine	22524.76	22470.30	21350.64	21258.42	20741.29	20694.29	16975.25	17146.51	103.60
METHANOL									
Pr(III)	22525.16	22470.32	21351.10	21258.39	20741.72	20694.07	16975.33	17146.05	103.56
Pr(III)+ Valine	22525.06	22470.47	21351.05	21258.45	20740.59	20694.35	16974.76	17145.54	103.68

*The text of this chapter has been published as:

¹**Juliana Sanchu**, Mhasiriekho Ziekhri, Zevivonu Thakro and M. Indira Devi, "4f-4f Transition Spectra of the Interaction of Pr(III) with L-Valine in Solution: Kinetics and Thermodynamic Studies", Asian Journal of Chemistry, 34(10):2688-2696 (2022).

Table 6.3. Comparison of Oscillator strengths and Judd–Ofelt parameters for Pr(III) and Pr(III): L- Valine complex in different aquated solvents.

Systems	$^3H_4 \rightarrow ^3P_2$		$^3H_4 \rightarrow ^3P_1$		$^3H_4 \rightarrow ^3P_0$		$^3H_4 \rightarrow ^1D_2$		T ₂	T ₄	T ₆
	Pobs	Pcal	Pobs	Pcal	Pobs	Pcal	Pobs	Pcal			
ACETONITRILE											
Pr(III)	18.671	18.671	5.797	4.263	2.685	4.193	3.898	3.898	-524.4	11.697	58.123
Pr(III) Valine	19.29	19.29	5.865	4.405	2.897	4.333	3.98	3.98	-595.4	12.086	60.044
DIMETHYLFORMAMIDE											
Pr(III)	17.386	17.386	5.559	4.371	3.131	4.299	3.281	3.281	-411.8	11.992	53.831
Pr(III)+Valine	20.879	20.879	5.571	4.595	3.216	4.520	3.435	3.435	-492.1	12.608	65.049
1, 4 – DIOXANE											
Pr(III)	16.855	16.855	5.506	3.697	2.871	4.343	3.025	3.025	-356.4	12.116	52.055
Pr(III)+Valine	18.022	18.022	5.861	4.639	3.674	4.574	3.883	3.883	-378.3	12.759	58.872
METHANOL											
Pr(III)	16.613	16.613	5.551	4.405	1.859	3.639	2.238	2.238	-368.6	10.149	51.796
Pr(III)+Valine	18.437	18.437	5.898	4.134	2.367	4.066	2.418	2.418	-400.2	11.341	55.741

*The text of this chapter has been published as:

¹Juliana Sanchu, Mhasiriekho Ziekhri, Zevivonu Thakro and M. Indira Devi, “4f-4f Transition Spectra of the Interaction of Pr(III) with L-Valine in Solution: Kinetics and Thermodynamic Studies”, Asian Journal of Chemistry, 34(10):2688-2696 (2022).

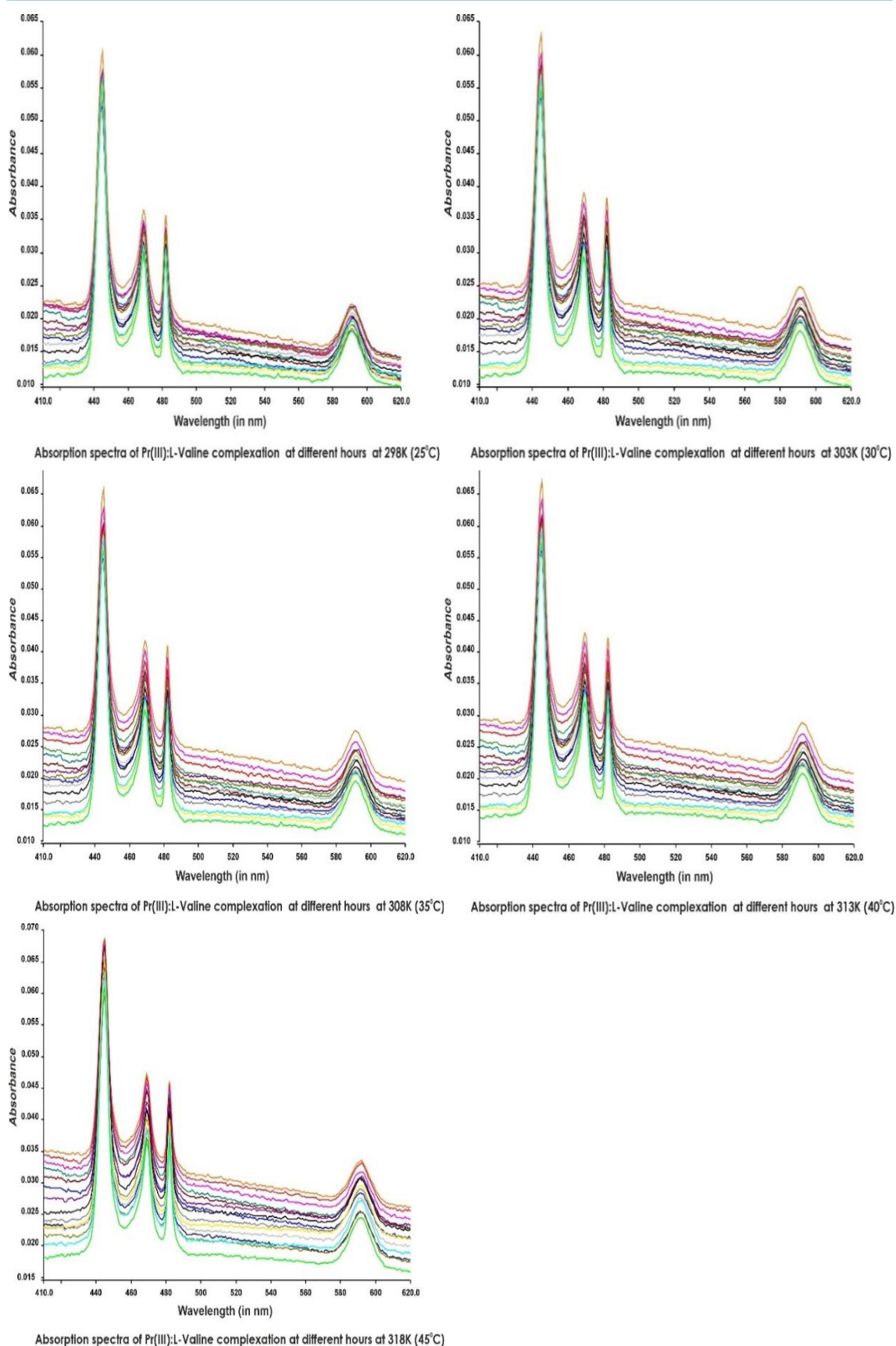


Figure 6.4. Absorption spectra for the interaction of Pr(III): L-Valine at various temperatures 298°K, 303°K, 308°K, 313°K and 318°K in DMF solvent.

*The text of this chapter has been published as:

¹Juliana Sanchu, Mhasirikho Ziekhri, Zevivonu Thakro and M. Indira Devi, "4f-4f Transition Spectra of the Interaction of Pr(III) with L-Valine in Solution: Kinetics and Thermodynamic Studies", Asian Journal of Chemistry, 34(10):2688-2696 (2022).

Table 6.4. Computed oscillator strengths and Judd-Ofelt intensity parameter for Pr(III): L-Valine complex at 298^oK (25^oC) in various time (hr) intervals.

Time	³ H ₄ → ³ P ₂		³ H ₄ → ³ P ₁		³ H ₄ → ³ P ₀		³ H ₄ → ¹ D ₂		T ₂	T ₄	T ₆
	P _{obs}	P _{cal}	P _{obs}	P _{cal}	P _{obs}	P _{cal}	P _{obs}	P _{cal}			
0	6.636	6.636	2.745	1.765	0.634	1.656	1.122	1.122	-180.23	4.731	20.412
2	6.678	6.678	2.915	1.913	0.755	1.787	1.357	1.357	-179.55	4.965	20.545
4	6.734	6.734	3.164	2.072	0.872	1.986	1.406	1.406	-179.87	5.342	20.672
6	6.855	6.855	3.243	2.098	0.897	2.023	1.628	1.628	-79.36	5.578	20.819
8	6.918	6.918	3.356	2.106	0.909	2.091	1.849	1.849	-39.78	5.731	21.223
10	7.116	7.116	3.361	2.142	0.949	2.126	1.884	1.884	-43.99	5.827	21.674
12	7.207	7.207	3.378	2.192	0.995	2.145	1.906	1.906	-45.78	5.965	22.123
14	7.296	7.296	3.391	2.204	1.003	2.159	1.975	1.975	-41.67	6.055	22.356
16	7.367	7.367	3.433	2.219	1.016	2.191	2.104	2.104	-134.36	6.097	22.543
18	7.475	7.475	3.482	2.271	1.042	2.213	2.338	2.338	39.05	6.173	22.812
20	7.654	7.654	3.567	2.338	1.066	2.276	2.434	2.434	48.56	6.359	23.256
22	7.734	7.734	3.712	2.456	1.096	2.341	2.543	2.543	68.02	6.534	23.786
24	8.012	8.012	3.821	2.465	1.118	2.431	2.589	2.589	49.45	6.717	24.423
26	8.094	8.094	3.872	2.572	1.135	2.487	2.641	2.641	68.78	6.856	24.876
28	8.211	8.211	3.976	2.624	1.145	2.532	2.731	2.731	87.76	6.967	25.512
30	8.376	8.376	4.199	2.687	1.231	2.631	2.897	2.97	93.67	7.234	25.854
32	8.521	8.521	4.295	2.791	1.362	2.708	3.013	3.013	102.45	7.441	26.398
34	8.889	8.889	4.387	2.867	1.456	2.829	3.201	3.201	100.67	7.653	26.875

*The text of this chapter has been published as:

¹Juliana Sanchu, Mhasiriekho Ziekhri, Zevivonu Thakro and M. Indira Devi, "4f-4f Transition Spectra of the Interaction of Pr(III) with L-Valine in Solution: Kinetics and Thermodynamic Studies", Asian Journal of Chemistry, 34(10):2688-2696 (2022).

Table 6.5. Computed oscillator strengths and Judd-Ofelt intensity parameter for Pr(III): L-Valine complex at 303^oK (30^oC) in various time (hr) intervals.

Time	³ H ₄ → ³ P ₂		³ H ₄ → ³ P ₁		³ H ₄ → ³ P ₀		³ H ₄ → ¹ D ₂		T ₂	T ₄	T ₆
	P _{obs}	P _{cal}	P _{obs}	P _{cal}	P _{obs}	P _{cal}	P _{obs}	P _{cal}			
0	4.629	4.629	2.519	1.857	1.153	1.834	1.717	1.717	78.187	5.145	13.841
2	4.864	4.864	2.591	1.919	1.227	1.896	1.794	1.794	78.385	5.268	14.574
4	5.055	5.055	2.623	1.959	1.259	1.912	1.822	1.822	70.866	5.373	15.162
6	5.178	5.178	2.644	1.967	1.278	1.986	1.915	1.915	89.827	5.436	15.387
8	5.439	5.439	2.765	2.065	1.341	2.025	1.997	1.997	90.855	5.663	16.319
10	5.585	5.585	2.918	2.138	1.366	2.116	2.356	2.356	170.46	5.872	16.655
12	5.667	5.667	2.935	2.163	1.389	2.122	2.523	2.523	201.66	5.965	16.786
14	5.772	5.772	2.958	2.193	1.412	2.166	2.576	2.576	207.45	6.059	17.512
16	5.954	5.954	2.987	2.214	1.462	2.191	2.646	2.646	209.76	6.182	18.154
18	6.172	6.172	3.056	2.294	1.523	2.242	2.782	2.782	210.87	6.271	18.587
20	6.287	6.287	3.178	2.379	1.577	2.383	3.009	3.009	269.76	6.545	18.842
22	6.345	6.345	3.352	2.482	1.634	2.462	3.045	3.045	272.66	6.739	19.063
24	6.456	6.456	3.467	2.639	1.701	2.571	3.095	3.095	267.52	7.179	19.267
26	6.531	6.531	3.681	2.744	1.795	2.683	3.187	3.187	283.12	7.461	19.396
28	6.569	6.569	3.782	2.798	1.804	2.725	3.298	3.298	309.69	7.673	19.544
30	6.672	6.672	3.863	2.859	1.813	2.784	3.495	3.495	346.31	7.791	19.683
32	6.723	6.723	3.887	2.946	1.967	2.855	3.565	3.565	360.88	8.158	19.881
34	6.881	6.881	4.123	3.106	2.245	2.983	3.884	3.884	410.59	8.374	20.218

*The text of this chapter has been published as:

¹Juliana Sanchu, Mhasiriekho Ziekhri, Zevivonu Thakro and M. Indira Devi, "4f-4f Transition Spectra of the Interaction of Pr(III) with L-Valine in Solution: Kinetics and Thermodynamic Studies", Asian Journal of Chemistry, 34(10):2688-2696 (2022).

Table 6.6. Computed oscillator strengths and Judd-Ofelt intensity parameter for Pr(III): L-Valine complex at 308^oK (35^oC) in various time (hr) intervals.

Time	³ H ₄ → ³ P ₂		³ H ₄ → ³ P ₁		³ H ₄ → ³ P ₀		³ H ₄ → ¹ D ₂		T ₂	T ₄	T ₆
	P _{obs}	P _{cal}	P _{obs}	P _{cal}	P _{obs}	P _{cal}	P _{obs}	P _{cal}			
0	5.355	5.355	1.183	1.189	1.003	1.056	2.467	2.467	219.55	2.475	16.854
2	5.767	5.767	1.372	1.156	1.072	1.155	2.574	2.581	209.52	3.431	18.571
4	6.605	6.605	3.168	2.187	1.155	2.147	1.116	1.116	-185.21	5.459	20.712
6	6.679	6.679	3.247	2.233	1.204	2.246	1.187	1.187	-173.65	6.234	20.129
8	6.706	6.706	2.756	1.997	1.235	1.969	1.248	1.248	-166.36	5.493	20.621
10	6.735	6.735	2.764	2.008	1.251	1.993	1.317	1.329	-148.51	5.542	20.682
12	6.787	6.787	2.767	2.041	1.285	2.007	1.383	1.381	-138.23	5.651	20.843
14	6.951	6.951	2.789	2.113	1.336	2.182	1.406	1.406	-141.59	5.771	21.273
16	7.046	7.046	3.143	2.236	1.407	2.248	1.875	1.875	-136.26	6.243	21.345
18	7.187	7.187	3.245	2.366	1.449	2.308	1.961	1.961	-37.83	6.461	21.783
20	7.276	7.276	3.316	2.451	1.494	2.427	2.083	2.083	-16.67	6.726	22.082
22	7.437	7.437	3.455	2.570	1.584	2.490	2.121	2.121	-22.83	6.969	22.813
24	7.609	7.609	3.527	2.553	1.636	2.576	2.195	2.195	-9.39	7.183	23.126
26	7.716	7.716	3.617	2.642	1.656	2.631	2.491	2.491	43.91	7.327	23.648
28	7.878	7.878	3.727	2.732	1.689	2.685	2.578	2.578	57.19	7.464	23.838
30	8.339	8.339	4.445	3.134	1.715	3.123	2.623	2.623	65.57	8.531	25.118
32	8.549	8.549	5.423	3.284	1.786	3.405	2.787	2.787	66.26	9.562	25.339
34	8.637	8.637	5.905	3.845	1.855	3.806	3.099	3.099	122.59	7.937	25.981

*The text of this chapter has been published as:

¹Juliana Sanchu, Mhasiriekho Ziekhri, Zevivonu Thakro and M. Indira Devi, "4f-4f Transition Spectra of the Interaction of Pr(III) with L-Valine in Solution: Kinetics and Thermodynamic Studies", Asian Journal of Chemistry, 34(10):2688-2696 (2022).

Table 6.7. Computed oscillator strengths and Judd-Ofelt intensity parameter for Pr(III): L-Valine complex at 313^oK (40^oC) in various time (hr) intervals.

Time	³ H ₄ → ³ P ₂		³ H ₄ → ³ P ₁		³ H ₄ → ³ P ₀		³ H ₄ → ¹ D ₂		T ₂	T ₄	T ₆
	P _{obs}	P _{cal}	P _{obs}	P _{cal}	P _{obs}	P _{cal}	P _{obs}	P _{cal}			
0	6.545	6.545	1.856	1.663	1.456	1.657	2.765	2.765	203.34	4.545	20.167
2	6.667	6.667	1.967	1.847	1.612	1.723	2.824	2.824	211.23	5.123	20.567
4	6.834	6.834	2.135	1.945	1.678	1.865	3.167	3.167	234.12	5.245	20.978
6	7.143	7.143	2.255	1.989	1.734	1.967	3.264	3.264	253.53	5.476	21.698
8	7.367	7.367	2.354	2.076	1.785	2.007	3.312	3.312	263.56	5.672	22.543
10	7.545	7.545	2.513	2.231	1.813	2.089	3.398	3.398	266.78	5.895	23.276
12	7.788	7.788	3.624	2.651	1.667	2.654	2.491	2.491	47.45	7.653	23.645
14	7.945	7.945	2.383	2.176	1.925	2.234	3.541	3.372	243.65	5.954	24.521
16	8.097	8.097	3.765	2.454	1.168	2.482	2.685	2.685	66.164	6.734	24.634
18	8.234	8.234	3.945	2.564	2.018	2.234	3.576	3.576	271.56	6.324	25.321
20	8.347	8.347	4.056	2.676	2.148	2.567	3.661	3.661	93.76	7.543	25.865
22	8.564	8.564	4.067	2.686	2.216	2.573	3.765	3.765	276.38	6.989	26.182
24	8.672	8.672	4.112	2.645	2.292	2.587	3.812	3.812	316.31	8.143	26.586
26	8.784	8.784	4.256	2.731	2.307	2.671	3.883	3.883	-210.12	6.563	26.889
28	8.865	8.865	4.354	2.784	2.421	2.741	3.945	3.945	100.06	7.632	26.955
30	9.463	9.463	4.472	2.921	2.572	2.838	4.046	4.046	-298.34	4.731	29.987
32	9.651	9.651	4.512	3.029	2.463	2.678	4.134	4.134	-152.45	7.464	30.408
34	10.089	10.089	4.634	3.231	2.678	2.992	4.263	4.263	258.65	7.534	31.519

*The text of this chapter has been published as:

¹Juliana Sanchu, Mhasiriekho Ziekhri, Zevivonu Thakro and M. Indira Devi, "4f-4f Transition Spectra of the Interaction of Pr(III) with L-Valine in Solution: Kinetics and Thermodynamic Studies", Asian Journal of Chemistry, 34(10):2688-2696 (2022).

Table 6.8. Computed oscillator strengths and Judd-Ofelt intensity parameter for Pr(III): L-Valine complex at 318^oK (45^oC) in various time (hr) intervals.

Time	³ H ₄ → ³ P ₂		³ H ₄ → ³ P ₁		³ H ₄ → ³ P ₀		³ H ₄ → ¹ D ₂		T ₂	T ₄	T ₆
	P _{obs}	P _{cal}	P _{obs}	P _{cal}	P _{obs}	P _{cal}	P _{obs}	P _{cal}			
0	6.134	6.134	1.745	1.543	1.321	1.456	2.524	2.524	202.56	4.321	20.123
2	6.345	6.345	1.881	1.673	1.387	1.515	2.637	2.637	209.23	5.112	20.654
4	6.543	6.543	1.964	1.733	1.398	1.567	2.721	2.721	231.12	5.267	20.862
6	6.767	6.767	2.015	1.890	1.406	1.589	2.798	2.798	243.52	5.321	21.701
8	6.911	6.911	2.165	1.947	1.435	1.625	2.835	2.835	254.61	5.546	22.683
10	7.058	7.058	2.223	2.001	1.487	1.664	2.905	2.905	258.07	5.786	23.465
12	7.286	7.286	2.299	2.104	1.502	1.697	3.023	3.023	46.56	7.543	23.870
14	7.457	7.457	2.383	2.156	1.563	1.722	3.112	3.112	241.52	5.872	24.324
16	7.631	7.631	2.523	2.266	1.599	1.776	3.234	3.234	64.124	6.931	24.701
18	7.886	7.886	2.741	2.198	1.627	1.855	3.345	3.345	270.61	6.573	25.253
20	8.049	8.049	2.956	2.564	1.709	1.902	3.427	3.427	91.62	7.497	25.907
22	8.278	8.278	2.989	2.645	1.785	1.996	3.491	3.491	271.33	6.831	26.342
24	8.542	8.542	3.009	2.667	1.831	2.045	3.532	3.532	314.55	8.432	26.671
26	8.781	8.781	3.078	2.692	1.891	2.098	3.589	3.589	-217.16	6.231	26.967
28	8.959	8.959	3.111	2.712	1.935	2.157	3.665	3.665	99.16	7.751	27.563
30	9.258	9.258	3.156	2.761	1.986	2.231	3.712	3.712	-297.84	4.645	29.675
32	9.573	9.573	3.179	2.795	2.021	2.354	3.755	3.755	-150.75	7.573	30.617
34	9.813	9.813	3.213	2.816	2.188	2.406	3.803	3.803	256.71	7.470	31.456

*The text of this chapter has been published as:

¹Juliana Sanchu, Mhasiriekho Ziekhri, Zevivonu Thakro and M. Indira Devi, "4f-4f Transition Spectra of the Interaction of Pr(III) with L-Valine in Solution: Kinetics and Thermodynamic Studies", Asian Journal of Chemistry, 34(10):2688-2696 (2022).

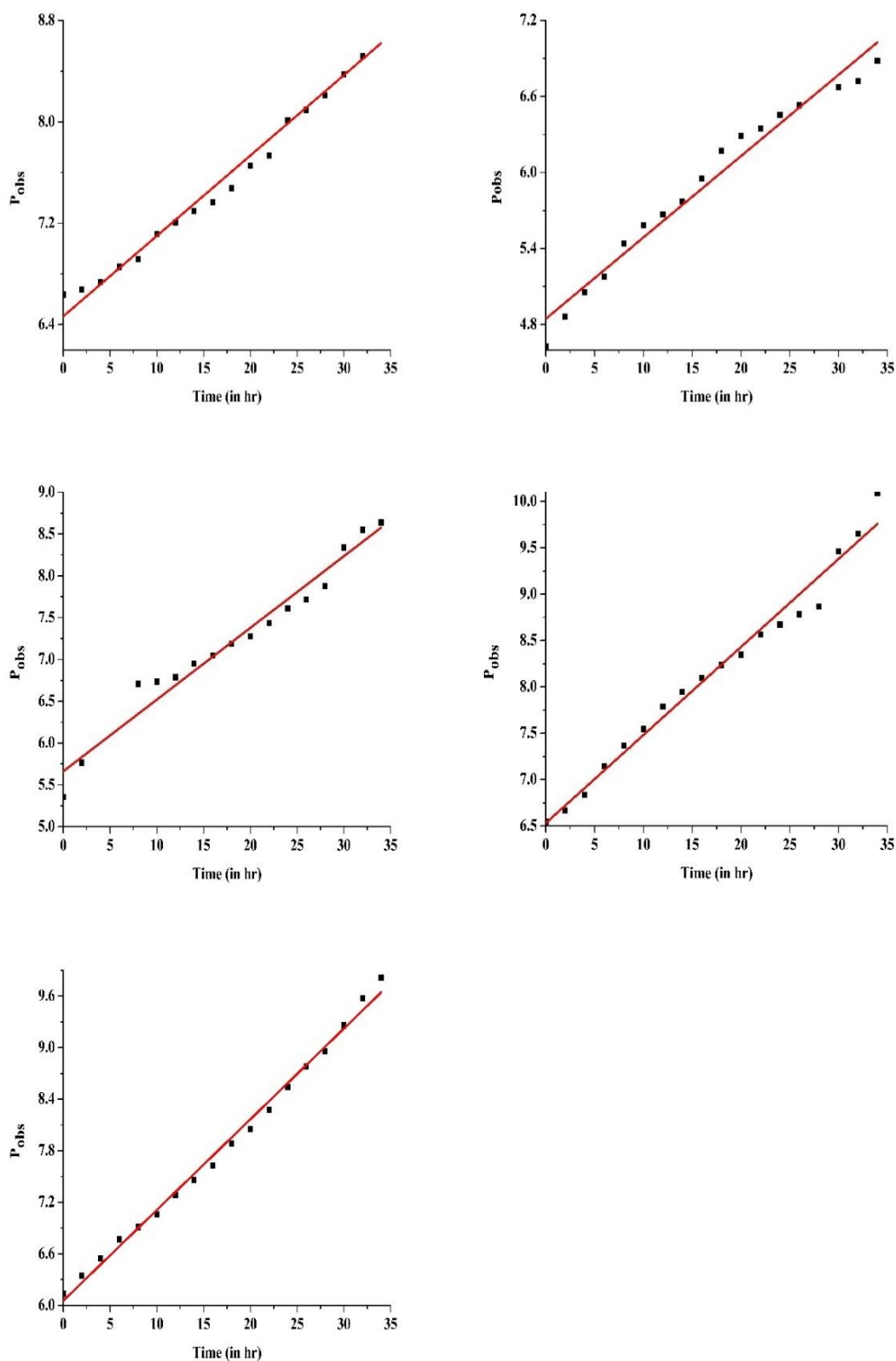


Figure 6.5. Plot of oscillator strength vs. time (in hrs) for ${}^3\text{H}_4 \rightarrow {}^3\text{P}_2$ transition for Pr (III): L-Valine complex in DMF solvent at different temperatures 298°K, 303°K, 308°K, 313°K and 318°K.

*The text of this chapter has been published as:

¹Juliana Sanchu, Mhasiriekho Ziekhri, Zevivonu Thakro and M. Indira Devi, "4f-4f Transition Spectra of the Interaction of Pr(III) with L-Valine in Solution: Kinetics and Thermodynamic Studies", Asian Journal of Chemistry, 34(10):2688-2696 (2022).

Table 6.9. Rate constant and activation energy for the complexation of Pr(III): L-Valine at various temperatures.

Temp(K)	1/T x 10 ³	Rate Constant	Rate Constant (k)	Log k	ln k	Frequency factor (A)	Activation Energy
298	3.3557	0.06341	17.614	1.24586	2.86869	17.98173	0.05119
303	3.3003	0.06418	17.828	1.25110	2.88077	18.19407	
308	3.2468	0.08573	23.814	1.37683	3.17027	24.29479	
313	3.1949	0.09494	26.372	1.42114	3.27230	26.89593	
318	3.1447	0.10556	29.322	1.46719	3.37834	29.89539	

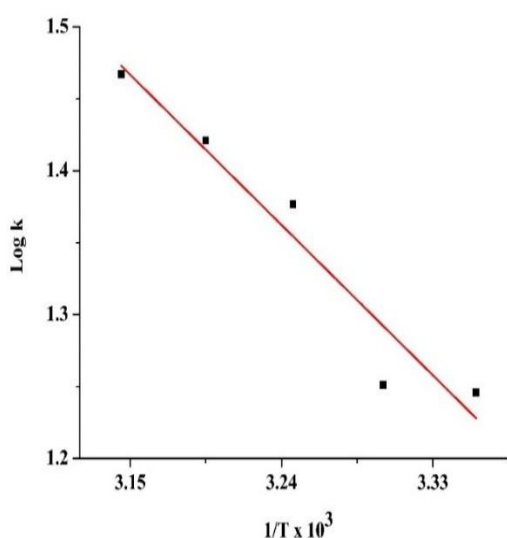


Figure 6.6. Graph of Log k versus $1/T \times 10^3$ for the complexation of Pr (III): L-Valine in DMF at various temperatures

Table 6.10. The activation energy and thermodynamic features for Pr(III): L-Valine complex at various temperatures.

Temperature (K)	Rate Constant (k)	ΔH	ΔG	ΔS	Activation Energy 'Ea'
298	17.614	0.05119	-7.13859	0.02402	0.05119
303	17.828		-7.34724	0.02413	
308	23.814		-7.98780	0.02653	
313	26.372		-8.65303	0.02737	
318	29.322		-8.79295	0.02826	

*The text of this chapter has been published as:

¹Juliana Sanchu, Mhasiriekho Ziekhri, Zevivonu Thakro and M. Indira Devi, "4f-4f Transition Spectra of the Interaction of Pr(III) with L-Valine in Solution: Kinetics and Thermodynamic Studies", Asian Journal of Chemistry, 34(10):2688-2696 (2022).

6.5. Results and discussion

Deep within the metal's core cell, non-hypersensitive transitions are assumed to be insensitive to the coordination environment [29]. The hypersensitive transitions, on the other hand, are extremely receptive to changes in their coordination sphere and conform to the selection criteria, when Ln(III) complexes with ligand [25]. Studies have shown that some Pr(III) transition intensities ($^3H_4 \rightarrow ^3P_2, ^3P_1, ^3P_0$ and 1D_2) do not follow the selection criteria but are extraordinarily sensitive to even the smallest variations in their coordinating surroundings. Because of how their coordinated environment affects their sensitivity, these pseudoquadrupole transitions are also known as Ligand Mediated Pseudohypersensitive Transitions [26,27][28]. To study the structural conformations and interactions of Pr(III) with ligand, this pseudohypersensitive transition has been widely exploited in solution absorption studies [29].

Table 6.1. shows the calculated values for Pr(III) and Pr(III): L-Valine complex for the following energy interaction parameters: Spin-orbit interaction (ζ_{4f}), Racah energy (E_k), nephelauxetic ratio (β), Slater-Condon (F_k), bonding ($b^{1/2}$) and covalency factor (δ) in all systems. Table 6.1. shows that when L-Valine is added to Pr(III), the Slater-Condon 'F_k' (k = 2,4,6) and Spin-Orbit interaction ' ζ_{4f} ' decreases, indicating a decrease in both spin-orbit interaction and coulombic parameters, resulting in an expansion of the central metal ion orbital and a decrease in the metal-ligand bond distance, allowing complexation. The nephelauxetic effect (β) in all systems ranges between 0.944-0.947, which is less than unity, indicating the validity of the computed data. The values of bonding parameters ($b^{1/2}$) are positive, with increasing values of Sinha's parameter (δ) indicating the possibility of covalent bonding. It is based on the earlier stated notion of $f-f$ transition[30]. Table 6.2. shows the calculated and observed values of energy for the different bands, and the value of root mean square deviation (RMS) indicates how close to the accuracy of the the evaluated data.

The intensity parameters ' P ' and ' T_λ ' ($\lambda = 2, 4, 6$) for the transitions ($^3H_4 \rightarrow ^3P_2, ^3P_1, ^3P_0$, and 1D_2) of free Pr(III) and Pr(III): L-Valine complex in various aquated organic solvents were evaluated. The remarkable increases in the ' P ' values as shown in table 6.3. suggest the possibility of Pr(III) and L-Valine interaction. When complexation occurs between Pr(III) and L-Valine in solution, the readings of ' T_λ ' parameters increases significantly, the possibility of binding of L-Valine to Pr (III). T_4 and T_6 are significantly affected, and their values are +ve, allowing them to be used in the Judd-Ofelt hypothesis.

Large fluctuations in the magnitudes of the T_4 and T_6 parameters suggest the possible

*The text of this chapter has been published as:

¹Juliana Sanchu, Mhasiriekho Ziekhri, Zevivonu Thakro and M. Indira Devi, "4f-4f Transition Spectra of the Interaction of Pr(III) with L-Valine in Solution: Kinetics and Thermodynamic Studies", Asian Journal of Chemistry, 34(10):2688-2696 (2022).

modifications of the coordination spheres that surround them and also the possible influence how Pr(III) interacts with its ligands. Both T_4 and T_6 parameters are connected to changes in the symmetry characteristics of complex species [36]. Although the transitions ${}^3H_4 \rightarrow {}^3F_3$ and T_2 are associated with the hypersensitive transition, T_2 is disregarded because the transition ${}^3H_4 \rightarrow {}^3F_3$ has readings that are negative and is outside of the Ultraviolet-Visible zone [31]. While modest fluctuations of P and T_λ parameters show the outer-sphere complexation, whereas large variations in the readings of P and T_λ parameters indicate inner-sphere complexation. The significant changes in the calculated values of P and T_λ give strong support for the involvement of L-Valine in the inner-sphere coordination of Pr(III).

The comparative absorption spectra of Pr(III) and Pr(III): L-Valine complex in aqueous DMF solvent are shown in figure 6.2. All of the energy bands experience a red shift when a ligand like L-Valine is added, however, the changes in the intensity data are brought by the strengthening of the $4f-4f$ transition bands. Band intensification is thought to be diligent from increased interaction between ligand orbitals and $4f$ -metal orbitals. A reduction in the coordination number and the metal-ligand bond length may be connected to the intensification of bands, notably the ${}^3H_4 \rightarrow {}^3P_2$ transition. As seen in figure 6.3., the development of the Pr (III): L-Valine complex reveals the sensitivities of solvent shown by the varied intensities of the bands of the four transitions and the order of the sensitivity of the solvent is DMF > CH₃CN > Dioxane > CH₃OH. DMF often binds through oxygen rather than nitrogen when it coordinates to hard acids, such as lanthanide ions, whereas CH₃CN binds through nitrogen. The increased intensification in the DMF medium also reveals that oxygen and nitrogen can form stronger bonds than nitrogen, that why DMF could show the maximum intensification and hence is the best solvent. Methanol is a poor donor. The coordination numbers and geometries are dictated largely by ligand properties such as ion generation, donor atoms, sizes, and solvation effects. Lanthanide aqueous solution has a coordination number of 9 and 8, which may be increased to 12 with the addition of a ligand. Praseodymium ions produce weak complexes when goes complexation with monodentate ligands, but stronger complexes when complexed with chelated ligands due to the chelate effect [32]. When an amino acid's isoelectric point is maintained, it exists in solution as a zwitterion. Praseodymium (III) is an ionic salt that is a hard acceptor, whereas amino acids are hard donors. At low pH, complexation occurs between Pr(III) and the oxygen atom of the amino acid, but at high pH, the metal ion bonds to the oxygen and nitrogen atoms of the amino acid, respectively. Praseodymium

*The text of this chapter has been published as:

¹Juliana Sanchu, Mhasiriekho Ziekhri, Zevivonu Thakro and M. Indira Devi, "4f-4f Transition Spectra of the Interaction of Pr(III) with L-Valine in Solution: Kinetics and Thermodynamic Studies", Asian Journal of Chemistry, 34(10):2688-2696 (2022).

ions form stable complexes with oxygen and nitrogen donor ligands, resulting in nona-coordinating complex. Figure 6.7. depicts a reaction pathway for the nona-coordinated Pr (III): L-Valine complex in an aquated organic solvent.

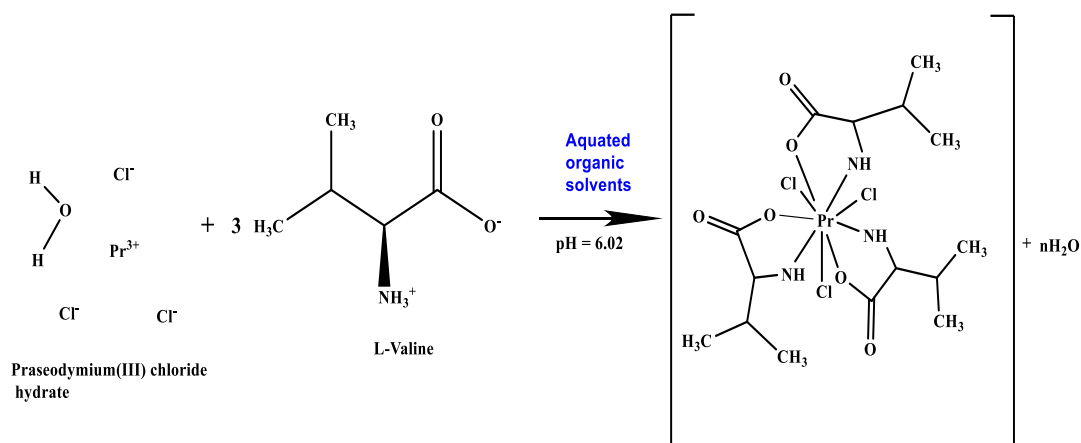


Figure 6.7. The reaction pathway for nona-coordinated Pr(III): L-Valine complex in an aquated organic solvent.

To explore the kinetics of the complexation of Pr(III) with L-Valine, the absorption spectra for the complexation of Pr(III) with L-Valine were recorded at various temperatures (298°K, 303°K, 308°K, 313°K, and 318°K) and time intervals in aquated DMF solvent (figure 6.3). Based on changes in the observed and calculated values of oscillator strength and Judd Ofelt parameters at various temperatures for Pr(III): L-Valine complex as shown in tables 6.4., 6.5., 6.6., 6.7. and 6.8. it is observed that the pseudohypersensitive transition ${}^3H_4 \rightarrow {}^3P_2$ is the most sensitive transition in comparison to the other ${}^3H_4 \rightarrow {}^3P_1$, 3P_0 , and 1D_2 transitions. The plot of P_{obs} vs time for the transition ${}^3H_4 \rightarrow {}^3P_2$ at various temperatures is shown in figure 6.5. The rate constants were calculated using the values of slope derived from the graph, as given in table 6.9. Following the Arrhenius theoretical prediction, complexation rates grow with a rise in temperature as shown in tables 6.4.-6.8. Additionally, the Pre-exponential Factor (A) values increasing with temperature suggests an increase in molecules colliding. The extremely low activation energy (E_a) value suggests that the reaction is a fast one. Figure 6.6. also shows the graph of $\log k$ versus $1/T \times 10^3$, the values of ΔH^0 , ΔG^0 and ΔS^0 as given in table 6.10. were determined from the graph. The +ve values of ΔH^0 demonstrate that the reaction is an endothermic reaction, whereas the -ve value of ΔG^0 represents the spontaneity of the reaction process. According to the positive values of ΔS^0 , the complexation process is entropy-driven and the complex is well-formed. Additionally, it was discovered that the Pr(III): L-Valine complex's activation energies (E_a) were 0.05119 kJ. These kinetic

*The text of this chapter has been published as:

¹Juliana Sanchu, Mhasiriekho Ziekhri, Zevivonu Thakro and M. Indira Devi, "4f-4f Transition Spectra of the Interaction of Pr(III) with L-Valine in Solution: Kinetics and Thermodynamic Studies", Asian Journal of Chemistry, 34(10):2688-2696 (2022).

studies, based on an investigation through absorption spectrum are used as an alternate method to explore the reaction kinetics theoretically and to forecast potential thermodynamic behaviour related to the complexation of Pr(III): L-Valine.

6.6. Conclusion

The reduction in the values of ζ_{4f} , E^k , F_k and the increase in the values of β , $b^{1/2}$ and δ reveals the complexation of praseodymium (III) with L-Valine. When the ligand is introduced to praseodymium (III), the band intensifies showing the interaction in the ligand orbital and the 4f-orbital of the metal which is also substantiated by the sharpening of the absorption bands and the appearance of the redshift. The decrease in the coordination number and the metal-ligand bond length of the complex formed are both related to the rise in absorption bands of the Pr(III): L-Valine complex. The bonding parameter being positive and the growing value of Sinha's parameters (δ) implies the likelihood of covalent bonding in all situations where the nephelauxetic effect (β) value ranges from 0.944 to 0.947, which is less than unity. The correctness of the calculated data is predicted by the root mean square (RMS) values. The strong binding effect as well as the development of inner-sphere complexation in Pr(III): L-Valine complex could be provided by the large fluctuations in the estimated readings of P and T_λ . With the oxygen and nitrogen donor ligands of L-Valine, praseodymium ions form a stable complex, and through the inner sphere coordination, a nona-coordinated complex is formed. According to the assessed values of P and T_λ parameters for the various organic solvents used, their sensitivity to the $4f-4f$ transition is in the following order:



According to the Arrhenius reaction rate, the rate of complexation calculated from the intensity parameters rises with increasing time and temperature. The low activation energy (E_a) measurement indicates a fast reaction, the low readings of ΔG^0 illustrate the favourability and spontaneity of the reaction, whereas +ve readings of ΔH^0 imply that the reaction is an endothermic reaction. $T\Delta S^0 > \Delta H^0$ reveals that the current research of complexation reaction is entropy-driven. Depending on how frequently molecules collide, the frequency factor (A) values show the important correlation between reaction rate and temperature.

*The text of this chapter has been published as:

¹Juliana Sanchu, Mhasiriekho Ziekhri, Zevivonu Thakro and M. Indira Devi, "4f-4f Transition Spectra of the Interaction of Pr(III) with L-Valine in Solution: Kinetics and Thermodynamic Studies", Asian Journal of Chemistry, 34(10):2688-2696 (2022).

References

- [1] A.M. Măciucă, A.C. Munteanu, V. Uivarosi, Quinolone complexes with lanthanide ions: An insight into their analytical applications and biological activity, *Molecules*. (2020). <https://doi.org/10.3390/molecules25061347>.
- [2] J.A. Cotruvo, *The Chemistry of Lanthanides in Biology: Recent Discoveries, Emerging Principles, and Technological Applications*, *ACS Cent. Sci.* 5 (2019) 1496–1506. https://doi.org/10.1021/ACSCENTSCI.9B00642/ASSET/IMAGES/LARGE/OC9B00642_0005.JPEG.
- [3] R.B. Martin, F.S. Richardson, Lanthanides as probes for calcium in biological systems, *Q. Rev. Biophys.* 12 (1979) 181–209. <https://doi.org/10.1017/S0033583500002754>.
- [4] K.B. Gudasi, V.C. Havanur, S.A. Patil, B.R. Patil, Antimicrobial study of newly synthesized lanthanide(III) complexes of 2-[2-hydroxy-3-methoxyphenyl]-3-[2-hydroxy-3-methoxybenzylamino]-1, 2-dihydroquinazolin-4(3H)-one, *Met. Based. Drugs*. 2007 (2007). <https://doi.org/10.1155/2007/37348>.
- [5] S. Alghool, M.S. Zoromba, H.F.A. El-Halim, Lanthanide amino acid Schiff base complexes: synthesis, spectroscopic characterization, physical properties and in vitro antimicrobial studies, *J. Rare Earths*. 31 (2013) 715–721. [https://doi.org/10.1016/S1002-0721\(12\)60347-0](https://doi.org/10.1016/S1002-0721(12)60347-0).
- [6] M.P. Cabral Campello, E. Palma, I. Correia, P.M.R. Paulo, A. Matos, J. Rino, J. Coimbra, J.C. Pessoa, D. Gambino, A. Paulo, F. Marques, Lanthanide complexes with phenanthroline-based ligands: insights into cell death mechanisms obtained by microscopy techniques, *Dalt. Trans.* 48 (2019) 4611–4624. <https://doi.org/10.1039/c9dt00640k>.
- [7] J.V. Kuntal Prajapati, Pravin Prajapati, Manish Brahmhatt, a Review: Lanthanide Complexes and Their Biological Importance, *Res. J. Life Sci. Bioinformatics, Pharm. Chem. Sci.* 4 (2018) 803–813. <https://doi.org/10.26479/2018.0405.56>.
- [8] E.M. Stephens, S. Davis, M.F. Reid, F.S. Richardson, Empirical Intensity Parameters for the $4f \rightarrow 4f$ Absorption Spectra of Nine-Coordinate Neodymium(III) and Holmium(III) Complexes in Aqueous Solution, *Inorg. Chem.* (1984). <https://doi.org/10.1021/ic00194a040>.
- [9] S.N. Misra, M.I. Devi, The synthesis and determination of the octacoordinated structure of Pr(III) and Nd(III) complexes with β -diketones and diols in non aqueous solutions: evidence of some participation of π -electron density of diols with Pr(III) and Nd(III) in complexation, *Spectrochim. Acta Part A Mol. Biomol. Spectrosc.* 53 (1997) 1941–1946.

*The text of this chapter has been published as:

¹Juliana Sanchu, Mhasiriekho Ziekhri, Zevivonu Thakro and M. Indira Devi, “4f-4f Transition Spectra of the Interaction of Pr(III) with L-Valine in Solution: Kinetics and Thermodynamic Studies”, *Asian Journal of Chemistry*, 34(10):2688-2696 (2022).

[https://doi.org/10.1016/S1386-1425\(97\)00064-4](https://doi.org/10.1016/S1386-1425(97)00064-4).

- [10] X.M. Qiao, C.X. Zhang, Y.K. Kong, Y.Y. Zhang, A Mononuclear Lanthanide Metal Compounds Based on the Nitronyl Nitroxide Radicals: Synthesis, Crystal Structure, and Magnetic Properties, <Http://Dx.Doi.Org/10.1080/15533174.2014.989594>. 46 (2016) 841–846. <https://doi.org/10.1080/15533174.2014.989594>.
- [11] S.N. Misra, G. Ramchandriah, M.A. Gagnani, R.S. Shukla, M.I. Devi, Absorption Spectral Studies Involving 4f–4f Transitions as Structural Probe in Chemical and Biochemical Reactions and Compositional Dependence of Intensity Parameters, <Http://Dx.Doi.Org/10.1081/ASR-120026330>. 38 (2006) 433–493. <https://doi.org/10.1081/ASR-120026330>.
- [12] N. Bendangsenla, T. Moaienla, T. David Singh, C. Sumitra, N. Rajmuhon Singh, M. Indira Devi, Evaluation of intensity and energy interaction parameters for the complexation of Pr(III) with selected nucleoside and nucleotide through absorption spectral studies, *Spectrochim. Acta. A. Mol. Biomol. Spectrosc.* 103 (2013) 160–166. <https://doi.org/10.1016/J.SAA.2012.11.011>.
- [13] T.D. Singh, C. Sumitra, N. Yaiphaba, H.D. Devi, M.I. Devi, N.R. Singh, Comparison of energy interaction parameters for the complexation of Pr(III) with glutathione reduced (GSH) in absence and presence of Zn(II) in aqueous and aquated organic solvents using 4f-4f transition spectra as PROBE, *Spectrochim. Acta. A. Mol. Biomol. Spectrosc.* 61 (2005) 1219–1225. <https://doi.org/10.1016/J.SAA.2004.06.044>.
- [14] Y. Martínez, X. Li, G. Liu, P. Bin, W. Yan, D. Más, M. Valdivié, C.A.A. Hu, W. Ren, Y. Yin, The role of methionine on metabolism, oxidative stress, and diseases, *Amino Acids.* 49 (2017) 2091–2098. <https://doi.org/10.1007/S00726-017-2494-2>.
- [15] K.K. Gangu, S. Maddila, S.N. Maddila, S.B. Jonnalagadda, Nanostructured Samarium Doped Fluorapatites and Their Catalytic Activity towards Synthesis of 1,2,4-Triazoles, *Mol.* 2016, Vol. 21, Page 1281. 21 (2016) 1281. <https://doi.org/10.3390/MOLECULES21101281>.
- [16] F. Costanzo, R.G. Della Valle, V. Barone, MD simulation of the Na⁺-phenylalanine complex in water: competition between cation- π interaction and aqueous solvation, *J. Phys. Chem. B.* 109 (2005) 23016–23023. <https://doi.org/10.1021/JP055271G>.
- [17] A.L. Sobolewski, D. Shemesh, W. Domcke, Computational studies of the photophysics of neutral and zwitterionic amino acids in an aqueous environment: Tyrosine-(H₂O)₂ and tryptophan-(H₂O)₂ clusters, *J. Phys. Chem. A.* 113 (2009) 542–550. https://doi.org/10.1021/JP8091754/SUPPL_FILE/JP8091754_SI_001.PDF.

*The text of this chapter has been published as:

¹Juliana Sanchu, Mhasiriékho Ziekhri, Zevivonü Thakro and M. Indira Devi, “4f-4f Transition Spectra of the Interaction of Pr(III) with L-Valine in Solution: Kinetics and Thermodynamic Studies”, *Asian Journal of Chemistry*, 34(10):2688-2696 (2022).

- [18] M.F. Bush, J. Oomens, R.J. Saykally, E.R. Williams, Effects of alkaline earth metal ion complexation on amino acid zwitterion stability: Results from infrared action spectroscopy, *J. Am. Chem. Soc.* 130 (2008) 6463–6471. https://doi.org/10.1021/JA711343Q/SUPPL_FILE/JA711343Q-FILE002.PDF.
- [19] B.R. Judd, Optical Absorption Intensities of Rare-Earth Ions, *Phys. Rev.* 127 (1962) 750. <https://doi.org/10.1103/PhysRev.127.750>.
- [20] G.S. Ofelt, Intensities of Crystal Spectra of Rare-Earth Ions, *J. Chem. Phys.* 37 (2004) 511. <https://doi.org/10.1063/1.1701366>.
- [21] S.N. Misra, S.O. Sommerer, Absorption Spectra of Lanthanide Complexes in Solution, <Http://Dx.Doi.Org/10.1080/05704929108050880>. 26 (2006) 151–202. <https://doi.org/10.1080/05704929108050880>.
- [22] S.P. Sinha, Structure and bonding in highly coordinated Lanthanide complexes, (1977) 69–149. https://doi.org/10.1007/3-540-07508-9_3.
- [23] W.T. Carnall, P.R. Fields, B.G. Wybourne, Spectral Intensities of the Trivalent Lanthanides and Actinides in Solution. I. Pr³⁺, Nd³⁺, Er³⁺, Tm³⁺, and Yb³⁺, *J. Chem. Phys.* 42 (2004) 3797. <https://doi.org/10.1063/1.1695840>.
- [24] P.D. Ross, S. Subramanian, Thermodynamics of protein association reactions: forces contributing to stability, *Biochemistry.* 20 (2002) 3096–3102. <https://doi.org/10.1021/BI00514A017>.
- [25] M. Ziekhri, Z. Thakro, C. Imsong, J. Sanchu, M. Indira Devi, Computation of energy interaction and intensity parameters for the complexation of Pr(III) with glutathione at different pH in the presence/absence of Mg²⁺: 4f-4f transition spectra as a probe, *Polyhedron.* 200 (2021) 115099. <https://doi.org/10.1016/J.POLY.2021.115099>.
- [26] J.B. Gruber, G.W. Burdick, S. Chandra, D.K. Sardar, Analyses of the ultraviolet spectra of Er³⁺ in Er₂O₃ and Er³⁺ in Y₂O₃, *J. Appl. Phys.* 108 (2010) 023109. <https://doi.org/10.1063/1.3465615>.
- [27] R.D. Peacock, The intensities of lanthanide transitions, *Rare Earths.* (1975) 83–122. <https://doi.org/10.1007/BFB0116556>.
- [28] W.T. Carnall, P.R. Fields, B.G. Wybourne, Spectral Intensities of the Trivalent Lanthanides and Actinides in Solution. I. Pr³⁺, Nd³⁺, Er³⁺, Tm³⁺, and Yb³⁺, *J. Chem. Phys.* 42 (2004) 3797. <https://doi.org/10.1063/1.1695840>.
- [29] Comparative 4f-4f absorption spectral study for the interactions of Pr(III) with selected urea and thiourea: Energy and electric dipole intensity parameters, (n.d.). https://www.researchgate.net/publication/288225649_Comparative_4f-

*The text of this chapter has been published as:

¹Juliana Sanchu, Mhasiriekho Ziekhri, Zevivonu Thakro and M. Indira Devi, “4f-4f Transition Spectra of the Interaction of Pr(III) with L-Valine in Solution: Kinetics and Thermodynamic Studies”, *Asian Journal of Chemistry*, 34(10):2688-2696 (2022).

4f_absorption_spectral_study_for_the_interactions_of_PrIII_with_selected_urea_and_t
hiourea_Energy_and_electric_dipole_intensity_parameters (accessed May 14, 2022).

- [30] S.N. Misra, K. John, Difference and Comparative Absorption Spectra and Ligand Mediated Pseudohypersensitivity for 4f-4f Transitions of Pr(III) and Nd(III), *Http://Dx.Doi.Org/10.1080/05704929308018115*. 28 (2006) 285–325. <https://doi.org/10.1080/05704929308018115>.
- [31] T. Moaienla, N. Bendangsenla, M.I. Devi, A Probe into the Kinetics of the Interaction of Pr(III) Ions with Some Selected Amino Acids: A 4f-4f Transition Spectral Study, *Adv. Mater. Sci. Appl.* 3 (2014) 157–163. <https://doi.org/10.5963/AMSA0303007>.
- [32] J. Burgess, *Metal ions in solution*, Ellis Horwood;;Distributed by Halsted Press, Chichester ;New York, 1978.

*The text of this chapter has been published as:

¹**Juliana Sanchu**, Mhasiriekho Ziekhri, Zevivonü Thakro and M. Indira Devi, “4f-4f Transition Spectra of the Interaction of Pr(III) with L-Valine in Solution: Kinetics and Thermodynamic Studies”, *Asian Journal of Chemistry*, 34(10):2688-2696 (2022).

Synthesis, spectral and antimicrobial studies of Praseodymium (III): Isonicotinic acid complex.

In this chapter, Praseodymium (III): isonicotinic acid complex was synthesized and characterised by elemental analysis, molar conductance, FT-IR, X-ray powder diffraction, Fluorescence, UV-vis spectroscopy and Thermogravimetric studies. Also, their antimicrobial properties were observed. The ligand isonicotinic acid contained carbonyl oxygen atom and nitrogen atom of the pyridine ring as potential donor sites. On coordination, deprotonation occurred and as a result, ligand isonicotinic acid acted as bidentate ligands. A coordination number of 9 was assigned to the praseodymium (III) ion in this complex with monoclinic structure. The complex was thermally stable and shows photochemical and antimicrobial properties.

7.1. Introduction

Over the past few decades, research in the field of lanthanide chemistry has risen in both interest and scope. These efforts focus in large part on the creation of complexes with novel structural features for the production of advanced materials as well as the use of their unique spectroscopic properties in the development of biological probes and sensors in the fields of molecular biology and clinical chemistry. The wide range of applications for lanthanide compounds in biology and medicine has made lanthanide coordination chemistry an increasingly significant part of contemporary chemistry. The low toxicity and exceptional magnetic and luminous capabilities of lanthanide compounds make them particularly attractive for prospective uses¹¹. There is a great deal of interest in the interactions of rare earths with enzymes and proteins and their application as luminous probes in physiologically significant systems. In biological systems, lanthanide ions are frequently employed as spectroscopic Ca^{2+} probes and as diagnostic tools in clinical research². The bonding mechanism between the lanthanide and the ligand is extremely interesting and significant since these applications require the interaction of the lanthanide ion with biological ligands³.

An essential heterocyclic substance found in many natural products is pyridine. To treat a variety of human illnesses, there are numerous medications on the market that contain the pyridine ring system. One of the active inorganic chemistry research areas is lanthanide coordination chemistry. According to the research that has been published, lanthanides are able to create stable complexes with Schiff bases and many other newly synthesized compounds or its derivatives⁴. A significant percentage of these described complexes have pharmaceutical uses. The lanthanide complexes have also been revealed to possess anticancer, antibacterial, antifungal, and several other diverse therapeutic characteristics⁵. All Lanthanide complexes displayed stronger antibacterial activity than lanthanide ions and radicals, according to the research of antibacterial activity⁶.

It has been proven that utilization of absorption spectrophotometry, a newly developed method for researching the chemistry of lanthanides, particularly in solutions can provide an insight into complexes with intricate *f*-electron transitions, and sensitivity of lanthanide to the complex's shape and coordination environment, has made it a viable tool for investigating the chemistry of lanthanides⁷⁻⁹. The strength of the metal-ligand bond, coordination geometry, shape of the complex produced, and interaction of chelate-solvent can be determined by the absorption spectra for the *4f-4f* transitions of lanthanide ions¹⁰.

In this paper we have synthesized Praseosmium(III):Isonicotinic acid complex and have characterized them with the following techniques elemental analysis, IR, powdered XRD, Fluorescence studies, UV-Vis spectroscopy and TGA. The molar conductance was measured, solubility and antimicrobial properties of the Pr (III): Isonicotinic acid complex was also observed.

7.2. Materials and methods

Praseodymium (III) nitrate hexahydrate $[\text{Pr}(\text{NO})_3 \cdot 6\text{H}_2\text{O}]$ of 99.9% purity was purchased from Sigma Aesar and the ligand i.e, Isonicotinic acid was purchased from HIMEDIA. Nutrient Agar, Nutrient Broth and Sabouraud dextrose agar was purchased from HIMEDIA. Elemental analysis for C, H, O and N were analyzed using Elemental Analyzers CHNS-O EuroVector. The metal content was estimated by the oxalate-oxide method. Molar conductance measurements were carried out by using 10^{-3} M solutions of the complexes in a suitable solvent at room temperatures using a Systronic direct reading conductometer. The infrared spectra were recorded using KBr pellets on the Perkin Elmer FT-IR spectrophotometer (Spectrum two) over the range of $400\text{-}4000\text{ cm}^{-1}$. Luminescence studies was carried out using fluorescence spectrophotometer SHIMADZU model no. RF – 6000. Powder X-Ray diffraction studies were carried out using the X-Ray Diffraction Rigaku Ultima IV using $\text{Cu}_{\text{K}\alpha}$ radiation of wavelength $\lambda = 1.5406\text{ \AA}$ from 10° to 80° (2θ) at room temperature. With a heating rate of 20° C/min and nitrogen environment, thermal analysis was performed using the SDT Q600V20.9 Build 20 thermal analyzer..

7.2.1. Synthesis of Pr(III):Isonicotinic acid complex

Praseodymium(III):Isonicotinic acid complex was synthesized using the general method outlined below. 20 ml of 0.01 mol aquted solution of the ligand was added to 20 ml of hot alcoholic solution of praseodymium(III) nitrate hexahydrate and refluxed. The refluxing procedure was carried out for 24-36 hours while the pH of the solution was kept at its isoelectric point. The solution was taken and kept in a water bath until it had been concentrated to half of its original volume. The solution was allowed to cool, filtered and the filtrate was kept. After few days, the crystals were collected at the bottom of the beaker which was washed with modest amounts of distilled water, alcohol and ether. The collected crystals were dried in a desiccator

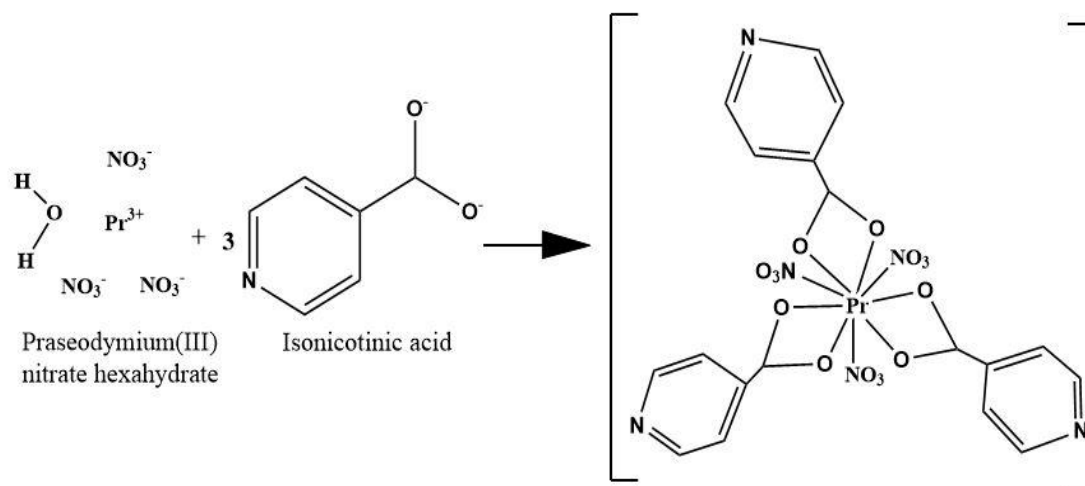


Figure 7.1. Probable Chemical Reaction for the synthesized Praseodymium (III): Ligands (Isonicotinic acid) complex

7.2.2. Biological Activity

Source of Microorganism: For the purpose of evaluating the antimicrobial activities, organisms such as Gram-positive *Staphylococcus aureus* and *Bacillus subtilis* were utilised in addition to Gram-negative *Escherichia coli* and *Klebsiella pneumoniae*. The fungal culture *Fusarium oxysporum*, *Penicillium italicum*, *Aspergillus niger* and *Candida albicans* were used.

Preparation of Bacterial Pathogens: The overnight cultures (0.2ml) of each bacterium were divided into 20ml of sterile nutrient broth and incubated for around 3-5 hours in order to standardise the culture. The standard cultures were employed in a loop for the antibacterial test.

Antibacterial Assay: Nutrient Agar was sterilised and prepared. In Petriplates, 20 ml of medium were added and left to solidify. The sterile cotton swab used to create the bacterial grass culture was labelled. With the use of a metallic borer with centres at least 24 mm in diameter, the wells were drilled into the medium. 50 μ l of the test sample, diluted to the necessary concentration of 1 mg/ml, were added to the appropriate wells. Reference antimicrobial medication is added to additional wells¹⁰. The plates are immediately incubated for 24 hours at 37°C. By measuring the diameter of zones exhibiting total inhibition, activity was calculated (mm). The medication was contrasted with growth inhibition.

Minimum Inhibitory Concentration: The minimum inhibitory concentration was determined using the tube dilution method by preparing different concentration of metal complex solution (i.e., 300 $\mu\text{g/ml}$, 500 $\mu\text{g/ml}$, 600 $\mu\text{g/ml}$, 800 $\mu\text{g/ml}$ and 1 mg/ml)¹¹. Cleaned test tubes were taken and different concentration of metal complex such as 300 $\mu\text{l/ml}$, 500 $\mu\text{l/ml}$, 600 $\mu\text{l/ml}$, 800 $\mu\text{l/ml}$ and 1 mg/ml was poured in the cleaned test tubes respectively and the volume of the medium was made upto 2 ml with nutrient broth. 2ml of the prepared control was put into the test tubes and autoclave at 121°C temperature and 15 lbs pressure for 15 minutes. After sterilization, the medium was allowed to cool and 0.2ml of overnight cultures of each organism was dispensed into sterile medium and incubated for 24 hours. The activity was measured by turbidity in the broth¹².

Antifungal Assay: The antifungal activity of metal complex was studied against four fungal cultures, *Aspergillus niger*, *Penicillium italicum*, *Candida albicans* and *Fusarium oxysporum*. Sabouraud dextrose agar was prepared and sterilized. The culture plates were prepared with the same method as that of the antibacterial assay. After the media was solidified, respective fungal spore suspensions were transferred in the petri plates. With the help of a sterile metallic borer, the wells were made in the centers at least 24 mm of the media. Recommended concentration 50 μl of the test sample 1 mg/ml in water was introduced in the wells. The plates were incubated at 30°C for 72 hours. The results were recorded as zones of inhibition in mm ¹³.

7.3. Results and discussion

Analytical data indicates that praseodymium:Isonicotinic acid complex was formed with 1:3 metal-ligand stoichiometry and it possess good keeping qualities. The complex is non-hygroscopic solids and is soluble in common organic solvents, such as methanol, ethanol, ACN and DMF. The analytical values of the complex are in good agreement with their formation and the elemental analysis and metal composition of the complex are given in table 7.1. The molar conductance value of the complex, as given was in the range of 11.9 $\Omega \text{ cm}^{-2} \text{ mol}^{-1}$ in DMF solution at room temperature. This value indicated that the complex was non-electrolytes in nature¹⁴.

Table 7.1. Analytical data and other details of the Praseodymium (III):Isonicotinic acid complex; calculated values are given in brackets

Sl. No.	Complex	%Yield	Colour	M	C	H	N	O	Molar conductance (DMF) $\Omega \text{ cm}^{-2} \text{ mol}^{-1}$
1	$\text{Pr}(\text{INA})_3(\text{NO}_3)_3$	91	Greenish	19.06 (19.01)	34.11 (34.16)	3.01 (2.96)	11.37 (11.46)	32.45 (32.40)	11.9

IR Spectra

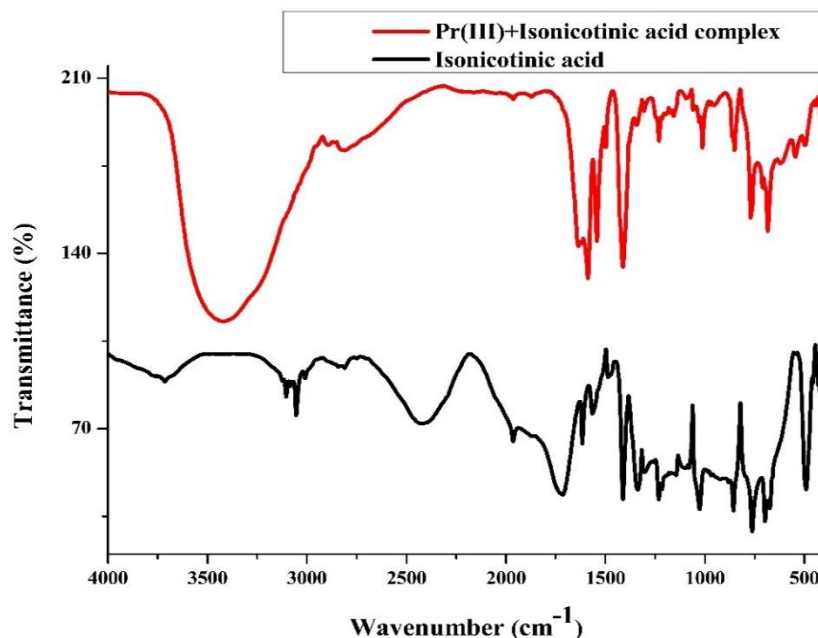


Figure 7.2. The FT-IR spectra of the ligand (Isonicotinic acid) and Pr(III): Ligand complex. *Red is the complex and black is the ligand.

The infrared spectra of Pr(III):Isonicotinic acid complex and pure ligand is shown in figure 7.2. the characteristic infrared absorption frequencies of the complex in solid state is tabulated in table 7.2. analysing the characteristic infrared absorption in frequencies of the Isonicotinic acid complex with Pr(III) ion, we could observe the intense peaks at 1644.98 cm^{-1} correspond to the asymmetric stretching vibrations of the carboxyl group as observed for the coordinated carboxylate ligands¹⁵. When a carboxylic acid is protonated, the stretching frequency shifts to 1700 cm^{-1} and when it is deprotonated the frequency shifts towards 1600 cm^{-1} . The $-(\text{C}=\text{O})$ vibration observed in the IR spectrum of the complex at 1644.98 cm^{-1} is absent in the spectrum of the ligand suggesting the deprotonation of the carboxyl group⁶. Absorption bands at 3414.92 , 1231.62 , 1021.06 and 690.70 cm^{-1} is assigned to $-(\text{C}=\text{N})$ and $-(\text{C}=\text{C})$ modes of the pyridine ring. The C-H bending vibration appears at 1409.47 cm^{-1} . The peaks at around 491.99 cm^{-1} and 419.62

cm^{-1} may lead to coordinating sites such as oxygen and nitrogen; M-O and M-N, respectively^{16,17}. The presence of asymmetric stretching vibration of -N-O was seen in 1539.49 which was absent in the ligand spectra.

Table 7.2. FT-IR wavenumbers with functional groups assigned to the Pr:Isonicotinic acid complex.

Sl. No.	Assignments (Functional groups)	Wavenumber (cm^{-1})
		Pr(III):Isonicotinic acid complex
1	-HC=CH stretching (aromatic compound)	3414.92
2	-O-H (carboxylic acid)	2889.95(s), 2797.96(b)
3	-C=O (Carboxylic acid)	1644.98
4	-COO stretching	1589.78,
5	-N-O asymmetric stretching (nitro compound)	1539.49
6	-C-H bending (aromatic compound)	1409.47
7	-C-N stretching (aromatic compound)	1231.62
8	-CH=CH bending (aromatic compound)	1021.06, 690.70
9	Ring	851.38, 766.75

Luminescence Studies

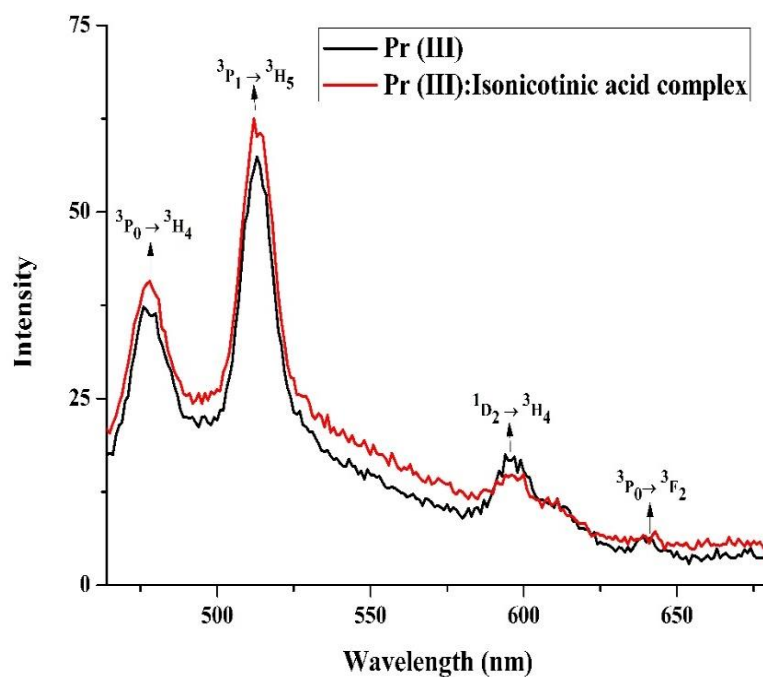


Figure 7.3. (a) Emission spectra of Praseodymium(III) and Praseodymium(III):Isonicotinic acid complex.

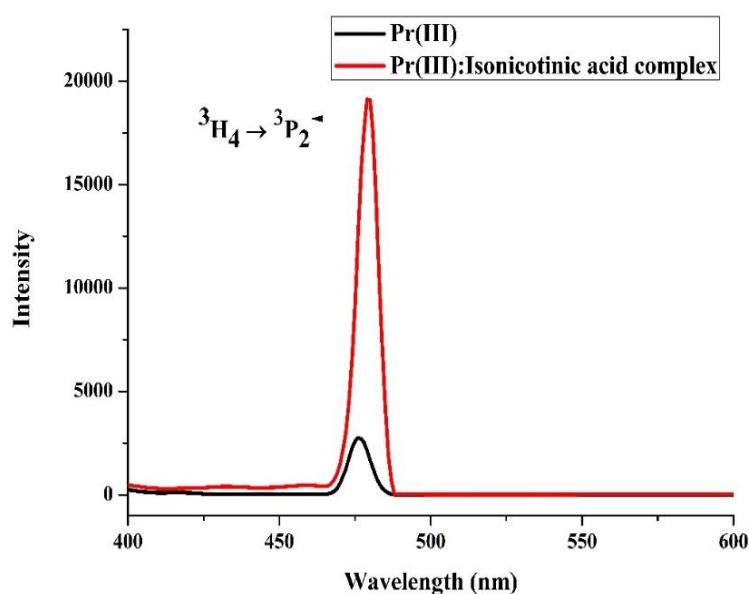


Figure 7.3. (b) Excitation spectra of Praseodymium(III) and Praseodymium(III):Isonicotinic acid complex.

Figure 7.3. (a) and (b) shows the emission spectra of Pr^{3+} ions and $\text{Pr(III):Isonicotinic acid complex}$ in the spectral region 430–680 nm obtained by 444 nm excitation corresponding to the ${}^3\text{H}_4 \rightarrow {}^3\text{P}_2$ transition. The emission bands centred at 477, 512, 595 and 640 nm are assigned to ${}^3\text{P}_0 \rightarrow {}^3\text{H}_4$, ${}^3\text{P}_1 \rightarrow {}^3\text{H}_5$, ${}^1\text{D}_2 \rightarrow {}^3\text{H}_4$ and ${}^3\text{P}_0 \rightarrow {}^3\text{F}_2$ transitions, respectively. Upon 444 nm excitation, the excited Pr^{3+} ion decay non-radiatively from the ${}^3\text{P}_J$ and ${}^1\text{D}_2$ excited state to the lower lying ${}^3\text{H}_4$, ${}^3\text{H}_5$ and ${}^3\text{F}_4$ energy states^{18,19}. The luminescence intensity of the emission transitions depends on the population of the complexes and Pr ion in the excited levels. However, the intensity of the ${}^3\text{P}_0 \rightarrow {}^3\text{H}_4$ transition is high due to the fast nonradiative decay from the higher lying ${}^3\text{P}_{2,1,0}$ levels. The inset of Figure 7.3. describes the emission channels of Pr^{3+} ions in $\text{Pr(III):isonicotinic acid complex}$. From the emission spectra it is clear that the emission intensity of the ${}^3\text{P}_0 \rightarrow {}^3\text{H}_4$ transition is almost constant for the $\text{Pr(III):Isonicotinic acid complex}$ due to the increase in the energy transfer among the excited Pr(III) ions. Moreover, the free metal ion and praseodymium(III) complex of the emission bands ${}^3\text{P}_0 \rightarrow {}^3\text{F}_4$ and ${}^1\text{D}_2 \rightarrow {}^3\text{H}_4$ transition overlap each other whereas for ${}^3\text{P}_0 \rightarrow {}^3\text{H}_4$, ${}^3\text{P}_1 \rightarrow {}^3\text{H}_5$ are well resolved. Significant red shift has been observed for all the emission transition ${}^3\text{P}_0 \rightarrow {}^3\text{H}_4$, ${}^3\text{P}_1 \rightarrow {}^3\text{H}_5$, ${}^1\text{D}_2 \rightarrow {}^3\text{H}_4$ and ${}^3\text{P}_0 \rightarrow {}^3\text{F}_4$. This red shift may be due to the distribution of excited ions in the vicinity of ligand fields at complexation²⁰. The intensities of all the observed emission bands

increase with complexation. This may be mainly due to the phenomenon of quenching through the energy transfer between the excited state of the Pr(III) ion. The emission dominates from the 3P_0 state which is populated by fast multiphonon non-radiative relaxation from the higher lying $^3P_{2,1,0}$ levels. As the complexation of the Pr^{3+} ion with the ligands takes place, the energy transfer process becomes more predominant and fast quenching in emission intensity takes place²¹. At lanthanide (III): Ligands complexes red emission quenches significantly. The lanthanide complexes show enhancement in the emission intensity compared to that of the metal ion. The enhancement of the emission intensity of the metal complex shows clear evidence of metal-ligand complexation. The quantum yield for Pr(III):Isonicotinic acid complex was 0.0575. Compared to the metal ion, which served as their precursor, the metal complexes displayed significant fluorescence intensities. The addition of a metal ion to the complex may have made the ligand more rigid in its conformation, which would have raised the fluorescence intensities of the complexes. These findings indicate that the created complexes could be useful in photochemical applications²²⁻²⁴.

X-Ray Diffraction

Praseodymium (III):Isonicotinic acid complex X-ray diffraction pattern was observed (figure 7.4.). The unit cell parameters and Miller indices were used to connect the Bragg angles and the set of interplanar spacing to these values, which were then applied to the individual reflections using formulas using $\sin 2\theta$ ²⁵. The reflections between 2θ in the diffractogram of the complexes ranged from 10 to 80°, with a maxima at $2\theta = 16.69$.

However, the lattice parameters calculated for the unit cell value of Pr (III):Isonicotinic acid complex are; $a = 7.2391$ (Å), $b = 7.4661$ (Å), $c = 6.3910$ (Å) and cell volume of cell : 275.03 (Å)³. The observed diffraction pattern corresponds to Anorthic crystal system which match with the JCPDS PDF No. 00-038-1885. The presence of possible phase such as PrO_3 is not observed. This confirms the lattice substitution of Pr^{3+} in $(C_6H_5NO)_3^-$ site. The crystal size was estimated using the Scherrer formula's,

$$d_{XRD} = \frac{\kappa\lambda}{\beta \cos \theta'}$$

where κ is the shape factor (≈ 0.9), β is the full width at half maximum of the reflection peak, θ is Bragg's angle, and λ is the wavelength of Cu k_α radiation. The average crystal size (d_{XRD}) is found to be 27.32 nm.

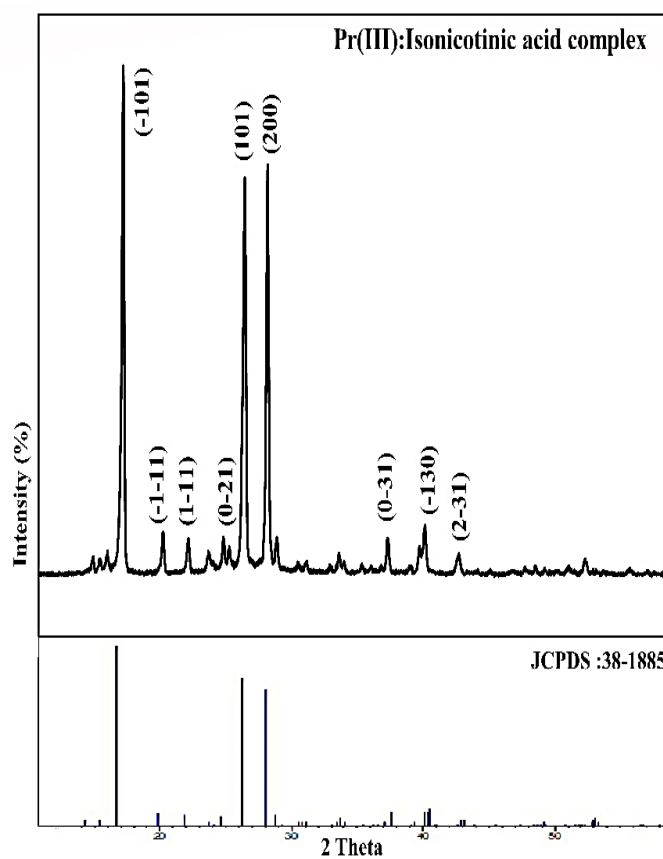


Figure 7.4. XRD spectrum of Praseodymium:Isonicotinic acid complex.

Thermal analysis

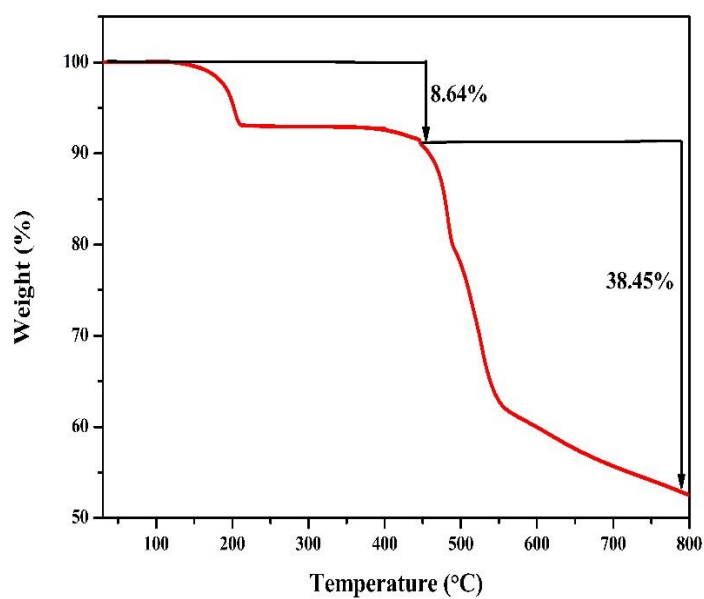


Figure 7.5. TGA of the the synthesized Praseodymium: Isonicotinic acid complex.

The TGA measurements for Pr(III): Isonicotinic acid complex was measured in dynamic air while being heated at a rate of 20°C/min. As shown in figure 7.5., It has been found that the Praseodymium (III):Isonicotinic acid complex decomposes thermally in two stages, in the first stage a single molecule of pyridine decomposes and in the second stage two molecules of the Isonicotinic acid and methanoic acid was decomposed thus leaving Pr(NO₃)₃ as the final residue. The stages of decomposition were in good agreement when compared with the elemental analysis result. The praseodymium (III): Isonicotinic acid complex starts decomposition at a temperature higher than 470°C which shows that the complex is thermally stable at room temperature.

Table 7.3. Antibacterial activity of Pr(III):Isonicotinic acid complex, metal ion as negative control, commercial drug as positive control.

Sl. No.	Name of bacterial pathogens	Zone of inhibition(mm)		
		Pr(III):Isonicotinic acid complex	Negative control	Positive control (Ampicillin)
1	<i>Escherichia coli</i>	28	No zone	25
2	<i>Klebsiella pneumonia</i>	21	No zone	28
3	<i>Staphylococcus aureus</i>	22	No zone	26
4	<i>Bacillus subtilis</i>	23	No zone	19

Table 7.4. Minimum Inhibitory Concentration assay of Pr(III):Isonicotinic acid complex against bacterial pathogens.

Sl. No.	Name of the bacterial pathogens	Observation of Growth				
		300 µg/ml	500 µg/ml	600 µg/ml	800 µg/ml	1 mg/ml
[Pr(Aspartic acid) ₃ (NO ₃) ₃]						
1	<i>Escherichia coli</i>	+	-	-	-	-
2	<i>Bacillus subtilis</i>	+	+	-	-	-
[Pr(Histidine) ₃ (NO ₃) ₃]						
1	<i>Escherichia coli</i>	+	+	-	-	-
2	<i>Bacillus subtilis</i>	+	-	-	-	-
[Pr(Valine) ₃ (NO ₃) ₃]						
1	<i>Escherichia coli</i>	+	+	-	-	-
2	<i>Bacillus subtilis</i>	+	-	-	-	-

Note: + = Growth of bacteria, - = No growth of bacteria

Table 7.5. Antifungal Activity of Pr(III):Isonicotinic acid complex.

Sl. No.	Name of Fungal Pathogens	Zone of inhibition (mm)
1	<i>Candida albicans</i>	38
2	<i>Aspergillus niger</i>	29
3	<i>Penicillium italicum</i>	17
4	<i>Fusarium oxysposum</i>	14

Antibacterial Activity of Lanthanide (III) Complex: Antibacterial activity of Pr(III):Isonicotinic acid complex with positive control commercial drugs (Ampicillin) and negative control metal ion¹⁵ were studied against four bacterial pathogens such as *Escherichia coli*, *Klebsiella pneumonia*, *Staphylococcus aureus* and *Bacillus subtilis*. Pr(III):Isonicotinic acid complex has shown better result in the form, zone of inhibition in culture plates rather than commercial drugs against two pathogens such as *Escherichia coli* and *Bacillus subtilis*. The zone of inhibition (mm) of Pr(III):Isonicotinic acid complex in the culture plate was 28 mm against *Escherichia coli* and 23 mm against *Bacillus subtilis* respectively. Whereas negative control (metal ion) did not show any zone of inhibition (Table 7.5.). The present finding shows the antibacterial activity of the Pr(III):Isonicotinic acid complex.

Minimum Inhibitory Concentration Assay: *Escherichia coli* and *Bacillus subtilis* were checked for the Minimum inhibitory concentration. Minimum inhibitory concentrations of bacterial pathogens were observed such as *Bacillus subtilis* (300 µg/ml) and *Escherichia coli* (500 µg/ml) (Table 7.6.). This result is similar to the finding of Chohan *et al*²⁶.

Antifungal Activity of Praseodymium (III) Complex: The inhibitory activity of Pr(III):Isonicotinic acid complex was observed in fungal pathogens. Among the three fungal pathogens *Candida albicans* was highly susceptible (38 mm) followed by *Aspergillus niger* (29 mm), *Penicillium italicum* (17 mm) and *Fusarium oxysposum* (14 mm). The results are presented in Table 7.7.

UV-Vis spectroscopy studies

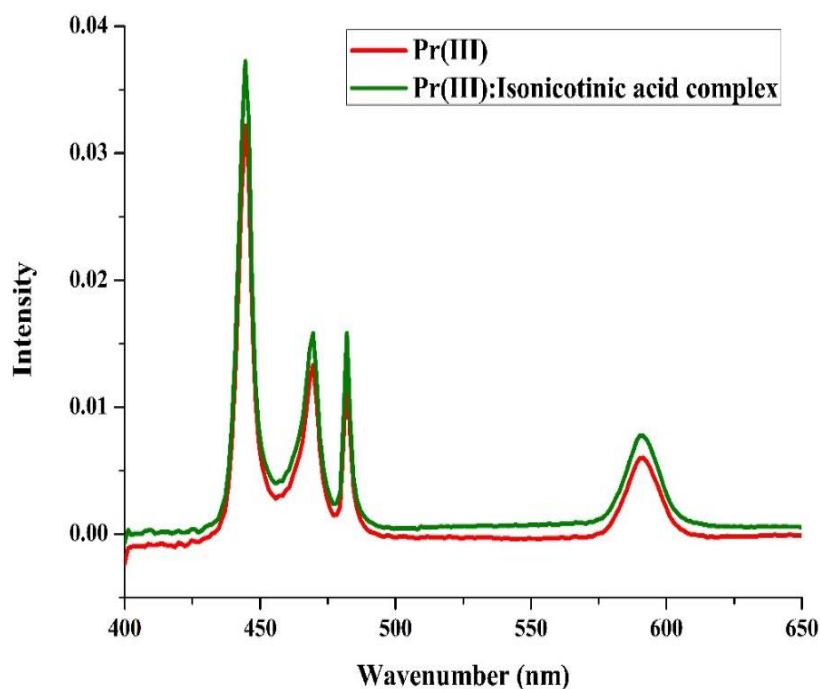


Figure 7.6. Absorption spectra of Pr(III) and Pr(III):Isonicotinic acid complex in aquated DMF (50% v/v)

Table 7.6. Computed value of energy interaction parameters Slater-Condon F_k (cm^{-1}), Spin Orbit Interaction ζ_{4f} (cm^{-1}), Nephelauxetic ratio (β), bonding ($b_{1/2}$), and covalency (δ) parameters of Pr(III) and Pr(III) with Isonicotinic acid in aquated (N,N Dimethylformamide) solvent.

System	F_2	F_4	F_6	ζ_{4f}	E_1	E_2	E_3	β	$b^{1/2}$	δ	RMS
DMF:Water											
Pr(III)	308.895	42.643	4.664	719.965	3507.395	23.735	614.104	0.944	0.166	5.856	122.50
Pr(III):Isonicotinic acid	308.592	42.601	4.649	719.767	3503.955	23.712	613.502	0.943	0.167	5.921	121.20

Table 7.7. Observed and calculated P and T_λ (T_λ , $\lambda = 2, 4, 6$) intensity parameter of Pr(III) with Isonicotinic acid in aquated DMF solvent.

System	${}^3\text{H}_4 \rightarrow {}^3\text{P}_2$		${}^3\text{H}_4 \rightarrow {}^3\text{P}_1$		${}^3\text{H}_4 \rightarrow {}^3\text{P}_0$		${}^3\text{H}_4 \rightarrow {}^1\text{D}_2$		T_2	T_4	T_6
	Pobs	Pcal	Pobs	Pcal	Pobs	Pcal	Pobs	Pcal			
DMF:Water											
Pr(III)	5.355	5.355	1.826	1.288	0.739	1.270	0.915	0.915	-147.4	3.544	16.62
Pr(III):Isonicotinic acid	7.838	7.838	2.991	2.038	1.071	2.010	1.125	1.125	-265.5	5.614	24.24

The presence of a highly detailed internal f-electron transition, as well as Lanthanide's sensitivity to the coordination environment and geometry of the complex formed with various ligands in easily accessible spectral regions, have paved the way for a broad approach to using absorption spectrophotometry as an important tool for studying lanthanide chemistry, especially in solutions in both aqueous and non-aqueous solvents^{27,28}. The absorption spectra for the $4f$ - $4f$ transitions of the Ln^{3+} ions are used to determine the strength of Ln^{3+} with ligand interaction coordination geometry, structure of metal-ligand complex formed and chelate-solvent interactions²⁹⁻³¹.

$4f$ - $4f$ transitions of lanthanide ions occur deep within the metal's core cell and they are generally insensitive to the coordination environment and are referred to as non-hypersensitive. The hypersensitive transitions, on the other hand, follow the selection rules, $\Delta S = 0$, $\Delta L \leq 2$ and $\Delta J = \leq 2$ and are highly sensitive to changes in their coordination environment and their band intensities become more intensified when a lanthanide ion gets complexed with ligands³².

Through investigations it is revealed that some transition intensities of Pr(III) (${}^3\text{H}_4 \rightarrow {}^3\text{P}_2$, ${}^3\text{H}_4 \rightarrow {}^3\text{P}_1$, ${}^3\text{H}_4 \rightarrow {}^3\text{P}_0$ and ${}^3\text{H}_4 \rightarrow {}^1\text{D}_2$) do not follow the selection rule but they could exhibit an exceptionally sensitive character towards minor changes in their coordination environment. Such transitions, pseudoquadrupole in character are known as Ligand Mediated Pseudohypersensitive transitions since their sensitivity is the inducing result of their coordination environment. This Pseudohypersensitive transition has been used extensively for the absorption study to understand the nature of bonding and structural conformations of Pr(III) with ligand in solution study. The interaction of Pr(III) with the

ligand and their sensitivity towards the formation of the complex is shown vividly by the corresponding intensification of the pseudo hypersensitive transitions³³.

Table 7.8. shows the computed values of the various energy interaction parameters: F_k ($k=2,4,6$), ζ_{4f} , E^k ($k=1,2,3$), β , $b^{1/2}$, δ and RMS values. From the variation in the values of Pr(III) and Pr(III):Isonicotinic acid complex in aqueous DMF solutions, the detailed nature of bonding could be studied. It was found that there was a decrease in the computed values of the energy interaction parameters β , ζ_{4f} and F_k for Pr(III):Isonicotinic acid complex as compared to the metal ion Pr(III) revealing the possibility of formation of complexes. The increase of percent covalency (δ) and the bonding parameter ($b^{1/2}$) followed by the nephelauxetic ratio (β) values, which were found to be less than unity, implies the possibility of the formation of covalent bond in the complexation of Pr(III) with isonicotinic acid. The decreased value of (β) explained the expansion of the orbital of central metal ion thereby shortening the metal-ligand distance known as the nephelauxetic effect. The decrease in the values of β also conveys its correlation to the intensification of the various transitions bands of Pr(III) (3P_2 , 3P_1 , 3P_0 , and 1D_2) as shown in figure 7.6. The root mean square (RMS) values predict the accuracy of the estimated values of energy interaction parameters.

The intensity parameters; Judd-Ofelt parameters (T_λ) and Oscillator strength (P) for the ligand-mediated pseudohypersensitive transitions (${}^3H_4 \rightarrow {}^3P_2$, ${}^3H_4 \rightarrow {}^3P_1$, ${}^3H_4 \rightarrow {}^3P_0$, and ${}^3H_4 \rightarrow {}^1D_2$) for Pr(III) ion and Pr(III): isonicotinic acid complex was evaluated. The remarkable changes in the P values of $4f-4f$ bands shown in table 7.2. implies the possibility of the interaction between Pr(III) with isonicotinic acid. When Pr(III) interacts with the ligand in solution the magnitude of T_λ ($\lambda = 2, 4, 6$) parameters increase significantly; this validates the possibility of the binding of isonicotinic acid to Pr(III). The T_4 and T_6 are affected significantly and their values are positive thus can be applied in the Judd-Ofelt theory of $4f-4f$ transitions. Both T_4 and T_6 parameters are related to changes in symmetry properties of the complex species thus, the significant changes in the values of T_4 and T_6 suggest possible changes in their immediate coordination environment which induces to the changes in the complexation of Pr(III) with Isonicotinic acid. On the other hand, though the transition ${}^3H_4 \rightarrow {}^3F_3$ and T_2 are correlated to the hypersensitive transition, since ${}^3H_4 \rightarrow {}^3F_3$ transition is beyond the UV-Visible region and its values are negative, thereby T_2 is ignored^{31,34}. When the values of P and their corresponding T_λ have significant variations, it indicates inner-sphere complexation while

slight changes in the values of P and T_λ parameters indicate outer-sphere complexation of the metal with the ligand³⁵. The significant changes in computed values of P and T_λ provide substantial evidence of the involvement of isonicotinic acid in the nona-inner-sphere coordination of Pr(III).

7.4. Conclusions

Pr(III):Isonicotinic acid complex was synthesized which is verified by the characterization and they were non-hydroscopic solid and soluble in water and most of the organic solvents. Their molar conductance was found to be $11.9 \Omega^{-1}\text{cm}^2\text{mol}^{-1}$ in DMF solution at room temperature which indicated that the complex were non-electrolytes in nature. Isonicotinic acid coordinates with Praseodymium (III) by its oxygen anion of deprotonated carboxyl group and the nitrogen atom of the pyridine ring. The metal to oxygen and metal to nitrogen coordination has been justified by our IR data. The synthesized complexes were crystalline in nature and they match the JCPDS PDF No. 00-038-1885 and average crystal size (d_{XRD}) was found to be 27.32 nm. However, the lattice parameters calculated for the unit cell value of Pr (III): Isonicotinic acid complex are; $a = 7.2391$ (Å), $b = 7.4661$ (Å), $c = 6.3910$ (Å) and cell volume of cell: 275.03 (Å)³.

From the variation in the computed energy interaction and intensity parameters, it was found that there was complexation between Pr(III) and isonicotinic acid. It was also found that there was formation of nona-inner sphere coordination between Pr(III) and isonicotinic acid. The synthesized complexes possess high thermal stability in air at room temperature as they start decomposition above 470°C. The metal ion and the complexes were excited at 444 nm and the excited metal ion and complexes decay non-radiatively from the 3P_1 and 1D_2 excited state to the lower lying 3H_4 , 3H_5 and 3F_4 energy states. The quantum yield was found to was 0.0575. The synthesized complex was found to exhibit good photochemical properties and antimicrobial properties; this finding indicates that it can be useful for photochemical and therapeutic applications.

REFERENCES

1. Lin, L. R. *et al.* Functionalized Lanthanide(III) Complexes Constructed from Azobenzene Derivative and β -Diketone Ligands: Luminescent, Magnetic, and Reversible Trans-to-Cis Photoisomerization Properties. *Inorg. Chem.* **56**, 3889–3900 (2017).
2. Evans C.H. *Biochemistry of the Lanthanides*. (Plenum Press, 1990).
3. Evans, C. H. The Interaction of Lanthanides with Amino Acids and Proteins. *Biochem. Lanthanides* 85–172 (1990) doi:10.1007/978-1-4684-8748-0_4.
4. Balogh, E. *et al.* Pyridine- and phosphonate-containing ligands for stable Ln complexation. Extremely fast water exchange on the GdIII chelates. *Inorg. Chem.* **45**, 8719–8728 (2006).
5. Ali Altaf, A. *et al.* A Review on the Medicinal Importance of Pyridine Derivatives. <http://www.sciencepublishinggroup.com> **1**, 1 (2015).
6. Nazir, M., Naqvi, I. I., Nazir, M. & Naqvi, I. I. Synthesis, Spectral and Electrochemical Studies of Complex of Uranium(IV) with Pyridine-3-Carboxylic Acid. *Am. J. Anal. Chem.* **4**, 134–140 (2013).
7. Ahmed, Z. & Iftikhar, K. Synthesis and visible light luminescence of mononuclear nine-coordinate lanthanide complexes with 2,4,6-tris(2-pyridyl)-1,3,5-triazine. *Inorg. Chem. Commun.* **11**, 1253–1258 (2010).
8. Zhao, Y. F. *et al.* Synthesis, crystal structure, luminescent property and antibacterial activity of lanthanide ternary complexes with 2,4,6-tri(2-pyridyl)-s-triazine. *J. Organomet. Chem.* **716**, 167–174 (2012).
9. Sorace, L., Benelli, C. & Gatteschi, D. Lanthanides in molecular magnetism: old tools in a new field. *Chem. Soc. Rev.* **40**, 3092–3104 (2011).
10. Sumitra, C., Singh, T. D., Devi, M. I. & Singh, N. R. Absorption spectral studies of 4f-4f transitions for the complexation of Pr(III) and Nd(III) with glutathione reduced (GSH) in presence of Zn(II) in different aquated organic solvents and kinetics for the complexation of Pr(III):GSH with Zn(II). *J. Alloys Compd.* **451**, 365–371 (2008).
11. Balasankar, T., Gopalakrishnan, M. & Nagarajan, S. Synthesis and antibacterial activity of some 5-(4-biphenyl)-7-Aryl[3,4-d]-1,2,3-benzoselenadiazoles. <http://dx.doi.org/10.1080/14756360601051365> **22**, 171–175 (2008).
12. Mohanan, K., Aswathy, R., Nitha, L. P., Mathews, N. E. & Kumari, B. S. Synthesis, spectroscopic characterization, DNA cleavage and antibacterial studies

- of a novel tridentate Schiff base and some lanthanide(III) complexes. *J. Rare Earths* **32**, 379–388 (2014).
13. Kadam, M. S., Khiste, S. A., Dake, S. A. & Khade, B. C. Studies on X-Ray Diffraction, Thermogravimetric Stability, Antibacterial- Antifungal Activity of Fe(II), Ni(II), Cu(II) Metal Chloroquine Complexes Against Bacterial Strains and Fungal Spore. *Anti-Infective Agents* **18**, 339–351 (2019).
 14. Geary, W. J. The use of conductivity measurements in organic solvents for the characterisation of coordination compounds. *Coord. Chem. Rev.* **7**, 81–122 (1971).
 15. Omar, M. M., Abd El-Halim, H. F. & Khalil, E. A. M. Synthesis, characterization, and biological and anticancer studies of mixed ligand complexes with Schiff base and 2,2'-bipyridine. *Appl. Organomet. Chem.* **31**, e3724 (2017).
 16. Devi, P. P., Chipem, F. A. S., Singh, C. B. & Lonibala, R. K. Complexation of 2-amino-3-(4-hydroxyphenyl)-N'-[(2-hydroxyphenyl) methylene] propane hydrazide with Mn(II), Co(II), Ni(II), Cu(II) and Zn(II) ions: Structural characterization, DFT, DNA binding and antimicrobial studies. *J. Mol. Struct.* **1176**, 7–18 (2019).
 17. Nazir, M. & Naqvi, I. I. Synthesis and characterization of uranium (IV) complexes with various amino acids. *J. Saudi Chem. Soc.* **14**, 101–104 (2010).
 18. Herrera, A. & Balzaretto, N. M. Effect of High Pressure in the Luminescence of Pr³⁺-Doped Ge₂O-PbO Glass Containing Au Nanoparticles. *J. Phys. Chem. C* **122**, 27829–27835 (2018).
 19. Liu, C. *et al.* Excitation wavelength dependent luminescence of LuNbO₄:Pr³⁺- Influences of intervalence charge transfer and host sensitization. *J. Phys. Chem. C* **120**, 26044–26053 (2016).
 20. Rajesh, D., Balakrishna, A., Seshadri, M. & Ratnakaram, Y. C. Spectroscopic investigations on Pr³⁺ and Nd³⁺ doped strontium–lithium–bismuth borate glasses. *Spectrochim. Acta Part A Mol. Biomol. Spectrosc.* **97**, 963–974 (2012).
 21. Jamalayah, B. C. *et al.* Optical absorption, fluorescence and decay properties of Pr³⁺-doped PbO–H₃BO₃–TiO₂–AlF₃ glasses. *J. Lumin.* **129**, 1023–1028 (2009).
 22. Liu, C. *et al.* Host-sensitized luminescence of Dy³⁺ in LuNbO₄ under ultraviolet light and low-voltage electron beam excitation: energy transfer and white emission. *J. Mater. Chem. C* **5**, 9012–9020 (2017).
 23. Kamal, R. & Hafez, H. Novel Down-converting single-phased white light Pr³⁺-doped BaWO₄ Nanophosphors material for DSSC applications. *Opt. Mater.*

- (*Amst*). **121**, 111646 (2021).
24. Sasi Kumar, M. V *et al.* Thermal, structural and spectroscopic properties of Pr³⁺-doped lead zinc borate glasses modified by alkali metal ions. <https://doi.org/10.1016/j.jtusci.2016.04.004> **11**, 593–604 (2018).
 25. Mathews, S., Kumari, B. S., Rijulal, G. & Mohanan, K. Synthesis, Characterization and Antibacterial Activity of Some Transition Metal Complexes of 2-N-(isatinamino)-3-carboxyethyl-4,5,6,7-tetrahydrobenzo[b]thiophene. <http://dx.doi.org/10.1080/00387010802007981> **41**, 154–161 (2008).
 26. Chohan, Z. H., Supuran, C. T., Ben Hadda, T., Nasim, F. U. H. & Khan, K. M. Metal based isatin-derived sulfonamides: Their synthesis, characterization, coordination behavior and biological activity. <http://dx.doi.org/10.1080/14756360802447636> **24**, 859–870 (2009).
 27. Carnall, W. T., Eieids, P. R. & Rajnak, K. Electronic energy levels of the trivalent lanthanide aquo ions. II. Gd³⁺. *J. Chem. Phys.* **49**, 4407–4411 (1968).
 28. Gruber, J. B., Burdick, G. W., Chandra, S. & Sardar, D. K. Analyses of the ultraviolet spectra of Er³⁺ in Er₂O₃ and Er³⁺ in Y₂O₃. *J. Appl. Phys.* (2010) doi:10.1063/1.3465615.
 29. Sanchu, J., Imsong, C., Thakro, Z. & Indira, D. M. Absorption spectral study for the interaction of Pr(III) with L-Aspartic acid in various aquated organic solvents through 4f-4f transition spectra: Analysis of reaction pathways and thermodynamic parameters. *J. Pharm. Negat. Results* **13**, (2022).
 30. Sanchu, J., Ziekhru, M., Thakro, Z. & Devi, M. I. 4f-4f Transition Spectra of the Interaction of Pr(III) with L-Valine in Solution: Kinetics and Thermodynamic Studies. *Asian J. Chem.* **34**, 2688–2696 (2022).
 31. Bendangsenla, N., Moainla, T., Sanchu, J. & Devi, M. I. Computation of Energy, Intensity and Thermodynamic Parameters for the Interaction of Ln(III) with Nucleic Acid: Analysis of Structural Conformations, Chemical Kinetics and Thermodynamic Behaviour through 4f-4f Transition Spectra as Probe. *J. Mater. Sci. Chem. Eng.* **06**, 169–183 (2018).
 32. Misra, S. N. & John, K. Difference and Comparative Absorption Spectra and Ligand Mediated Pseudohypersensitivity for 4f-4f Transitions of Pr (III) and Nd (III) Difference and Comparative Absorption Spectra and Ligand Mediated Pseudo hypersensi tivi ty for 4f-4f Transitions o. **4928**, (2016).
 33. Klixbüll Jørgensen, C., Judd, B. R., Klixbüll Jørgensen, C. & Judd, B. R.

-
- Hypersensitive pseudoquadrupole transitions in lanthanides. *MolPh* **8**, 281–290 (1964).
34. Moaienla, T., Singh, T. D., Singh, N. R. & Devi, M. I. Computation of energy interaction parameters as well as electric dipole intensity parameters for the absorption spectral study of the interaction of Pr(III) with l-phenylalanine, l-glycine, l-alanine and l-aspartic acid in the presence and absence of Ca²⁺. *Spectrochim. Acta Part A Mol. Biomol. Spectrosc.* **74**, 434–440 (2009).
35. Moaienla, T. *et al.* Comparative 4f-4f absorption spectral study for the interactions of Nd(III) with some amino acids: Preliminary thermodynamics and kinetic studies of interaction of Nd(III):glycine with Ca(II). *Spectrochim. Acta - Part A Mol. Biomol. Spectrosc.* (2012) doi:10.1016/j.saa.2011.11.028.

Summary and Conclusion

This chapter presents the overall summary and conclusions of the thesis. The future scope of the work is also highlighted in this chapter.

In the present study, we synthesized Praseodymium (III) with some selected ligands (L-Aspartic acid, L-Histidine and L-Valine and Isonicotinic acid) and were characterized through various physicochemical, spectral and TGA studies. The elemental and IR studies revealed that the ligand is coordinated to the Praseodymium(III) ion in a bidentate fashion through the oxygen atom of the carboxylic acid and nitrogen atom of the amine/heterocyclic group. The powder XRD of Praseodymium (III) complexes was studied. The photoluminescent properties of the metal ion and the metal complexes were evaluated, and it was observed that the metal complexes show significant enhancement of intensities compared to the free metal ion. TGA studies show that all the complexes were thermally stable in air at room temperatures. The antimicrobial and photochemical properties of the complexes could also be detected.

We have also used absorption difference and comparative absorption spectrophotometry as PROBE to follow the simultaneous co-ordination of Pr(III) with the ligands (L-Aspartic acid, L-Histidine and L-Valine and Isonicotinic acid) in different solvents. It has been found that significant information can be obtained which can be of direct chemical interest such as co-ordination number, structure, geometry, nature of complex species as well as in following a number of biochemical reactions.

We have evaluated intensity parameters: Oscillator strength 'P' and Judd-Ofelt ' T_{λ} ' ($\lambda = 2,4,6$) and energy interaction parameters such as Slater Condon F_k 's ($k = 2,4,6$), Lande factor (ξ_{4f}), Racah energy (E^k), nephelauxetic effect (β), bonding ($b^{1/2}$) and percent covalency (δ) by employing partial multiplet regression method using least square fit procedure. The quantitative analysis of 4f-4f spectral transitions through the computation of various spectral parameters gives as useful information regarding symmetry, coordination number, nature and strength of bonding of the co-ordinating ligand from the energies, intensities of transition and spectral pattern itself.

Literature suggests that, only a little attempt has been made to follow the kinetics of lanthanide complexation with biomolecules using 4f-4f transition spectra. The present thesis describes a systematic approach for determining the rate of the metal complexation of some selected amino acids and pyridine as ligands using comparative absorption and absorption difference spectroscopy. Since it was observed that the intensity of 4f- 4f transitions showed substantial increase with Time, therefore absorption spectral analysis of 4f- 4f transitions have been employed to explore the kinetics of the formation of the complexes. The Rate constants (k), Activation energy (E_a), ΔH^0 , ΔS^0 and ΔG^0 of the complexation of Pr(III): amino acids/pyridine in DMF medium has been evaluated. The

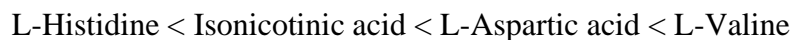
observed values of reaction rate constant (k) were evaluated in terms of the complex formed during the progress of the reaction and the same has been evaluated from the plots of oscillator strength of ${}^3\text{H}_4 \rightarrow {}^3\text{P}_2$ transition of Pr(III) complex versus time (in hour). The values of activation energy (E_a) and thermodynamic parameters, ΔH^0 , ΔS^0 and ΔG^0 are evaluated from the Van't Hoff plot of $\log K$ against $1/T \times 10^3$. This technique provided the means to determine indirectly the thermodynamic parameters of the complexation of Pr(III) in DMF medium. It was observed that the rate of complexation increases with increase in temperature and from which the activation energy E_a of the complexation was evaluated.

From our study it has been observed that:

- All the synthesized complexes were 1:3 metal-ligand stoichiometry, non-hydroscopic solids and soluble in common organic solvents, such as methanol, ethanol, Dioxane, ACN and DMF.
- The molar conductance values of the synthesized complexes were in the range of 10-13.1 $\Omega^{-1}\text{cm}^2\text{mol}^{-1}$ in DMF solution at room temperature. These values indicated that the complexes were non-electrolytes in nature.
- Amino acid coordinates with Praseodymium(III) by its oxygen anion of deprotonated carboxyl group and the nitrogen atom of NH_2 group. Pyridine coordinates with Praseodymium(III) by its oxygen anion of deprotonated carboxyl group and the nitrogen atom of heterocyclic group. The metal to oxygen and metal to nitrogen coordination has been justified by the enclosed IR data.
- Compared to the metal ion, which served as their precursor, the metal complexes displayed significant fluorescence intensities. The addition of a metal ion to the complex may have made the ligand more rigid in its conformation, which would have raised the fluorescence intensities of the complexes. These findings indicate that the synthesized complexes could be useful in photochemical applications.
- From powdered XRD, the four observed diffraction pattern for Pr:L-Aspartic acid, Pr(III):L-Histidine, Pr(III):L-Valine and Pr(III):Isonicotinic acid complexes corresponds to monoclinic, orthorhombic, monoclinic and anorthic phases which matches with the JCPDS PDF No. 00-023-1519, 00-051-2290, 00-022-1930 and 00-038-1885 respectively. The average crystal size (d_{XRD}) was found to be 40.11 nm, 15.78 nm, 25.20 nm and 27.32 nm respectively.

-
- All the synthesized complexes were found to be thermally stable in air at room temperature as they all start decomposition at a high temperature. All the synthesized complexes were found to have better antimicrobial activities as compared to that of the metal ion and ligands alone.
 - The presence of internal 4f electron transition spectra in the accessible spectral region for most of the lanthanides and the sensitivities of such transitions towards coordination environment makes quantitative absorption spectroscopy, involving 4f-4f transitions a powerful tool in the investigation of coordination chemistry and biochemistry of lanthanides especially in solution. The 4f-4f transition of Pr(III) can be used to investigate the nature of binding of some biologically important ligands even though they are non-hypersensitive.
 - On complexation red shift is observed leading to the phenomena of nephelauxetic effect. Nephelauxetic effect brings about the shortening of metal-ligand bond distance resulting in the intensification of the 4f-4f bands showing the binding of ligands to the metal ions.
 - The decrease in the values of F_k and ξ_{4f} on addition of ligands as compared to those of the free metal ion indicates the decrease in the inter-electronic repulsion and spin orbit interaction. This can be attributed to the complexation of Pr(III) with ligand present in the surrounding environment and which in turn indicates the expansion of the central metal ion orbital. This information is further supplemented more clearly by increase in the observed value of oscillator strengths 'P' and Judd-Ofelt parameter ' T_λ ' ($\lambda = 2, 4, 6$) when ligands are added to metal ions.
 - In all the system the values of nephelauxetic ratio (β) are less than unity and the values of bonding parameters ($b_{1/2}$) are positive which indicates the possibility of the covalent bonding.
 - The variation of solvent has significant effect on the oscillator strengths of the 4f-4f bands and this leads to variation in the magnitude of Judd-Ofelt (T_λ) parameters. When the ligands are added to the metal ion in different solvents, we find maximum intensities and marked variation in the magnitudes of intensity parameters in case where DMF is the solvent. This is due to their ability to donate oxygen donor atoms. The order of sensitivities of the solvents in the formation of complexes of both Pr (III) ion with the ligands was found to be in the order:
$$\text{DMF} > \text{CH}_3\text{CN} > \text{Dioxane} > \text{CH}_3\text{OH}$$
 - The magnitude of T_2 is found to be negative in case of Pr(III) so it is meaningless. Hence T_6 is most significant followed by T_4 .
-

-
- The sensitivity of the binding of different amino acids and pyridine ligands to Pr(III) is in the order:



- The positive enthalpy and entropy in Pr(III) indicates that the complexation reaction is endothermic and entropy increasing process. Since $T\Delta S^0 > \Delta H^0$, the coordination reaction is entropy driven process, spontaneous one and favoured in solution.
- Negative values of ΔG^0 predicts that the complex formation is favourable and also a spontaneous one.
- We can further justify that the simultaneous complexation reaction between Pr(III) ions with amino acids/pyridine occurs at a spontaneous pace, following the randomness of the system when it approaches higher temperatures (increasing ΔS^0 values). The lower values of E_a give further evidence that the reaction is a fast reaction.



NAGALAND UNIVERSITY

(A Central University Estd. By the Act of Parliament No. 35 of 1989)

Headquarters: Lumami – 798627, Nagaland, India

Ph.D. Thesis Certificate on Plagiarism check

Name of the Research Scholar	Juliana Sanchu
Ph.D. Registration Number	788/2017
Title of Ph.D. thesis	Synthesis and spectral studies of the lanthanide complexes with pyridine and some amino acids: kinetic and thermodynamic approach.
Name & Institutional Address of the Supervisor	Prof. M.Indira Devi Department of Chemistry, Nagaland University, Lumami
Name of the Department and School	Department of Chemistry, School of Sciences
Date of submission	15-12-2022
Date of plagiarism check	15-12-2022
Percentage of similarity detected by the URKUND software	1 %

I hereby declare that/certify that the Ph.D. thesis submitted by me is complete in all respect as per guidelines of Nagaland University (NU) for this purpose. I also certify that the Thesis (soft copy) has been checked for plagiarism using URKUND similarity checked software. It is also certified that the contents of the electronic version of the thesis are the same as the final hardcopy of the thesis. Copy of the report generated by the URKUND software is also enclosed.

Place:

Date:

(Name & Signature of the Scholar)

Name & Signature of the Supervisor



Document Information

Analyzed document	Julia Ph.D. Thesis.docx (D153449033)
Submitted	2022-12-15 07:31:00
Submitted by	Indira Devi
Submitter email	indira@nagalanduniversity.ac.in
Similarity	1%
Analysis address	indira.naga@analysis.orkund.com

Sources included in the report

SA	Chapter 1. corrected.pdf Document Chapter 1 corrected.pdf (D21075389)	3
SA	9. Km-Chapter I- urkund.docx Document 9. Km-Chapter I- urkund.docx (D36870039)	1
SA	Research Paper 1 sent to IOSR Erbium Neodymium Alanine Urea.docx Document Research Paper 1 sent to IOSR Erbium Neodymium Alanine Urea.docx (D63179213)	1
W	URL:https://kundoc.com/pdf-physical-and-optical-properties-of-dy3-pr3-co-doped-lithium-borate-glas... Fetched: 2022-12-15 07:14:02	3
SA	ddd.docx Document ddd.docx (D100483400)	2
SA	ADLIN HELEN-MPHIL-STRUCTURAL AND OPTICAL PROPERTIESCO-DOPED BORO-PHOSPHATEGLASSES FOR.docx Document ADLIN HELEN-MPHIL-STRUCTURAL AND OPTICAL PROPERTIESCO-DOPED BORO-PHOSPHATEGLASSES FOR.docx (D40434763)	2
SA	Urkund Report - Chapter-4 - Results and Discussion.pdf (D62056997).pdf Document Urkund Report - Chapter-4 - Results and Discussion.pdf (D62056997).pdf (D62062906)	1
SA	Nagaland University, Kohima / 1spectral study of pr ph-mhasi.docx Document 1spectral study of pr ph-mhasi.docx (D76603225) Submitted by: indira@nagalanduniversity.ac.in Receiver: indira.naga@analysis.orkund.com	2



NAGALAND UNIVERSITY

(A Central University Estd. By the Act of Parliament No. 35 of 1989)
Headquarters: Lumami – 798627, Nagaland, India

Ph.D. Thesis Certificate on Plagiarism check

Name of the Research Scholar	Juliana Sanchu
Ph.D. Registration Number	788/2017
Title of Ph.D. thesis	Synthesis and spectral studies of the lanthanide complexes with pyridine and some amino acids: kinetic and thermodynamic approach.
Name & Institutional Address of the Supervisor	Prof. M. Indira Devi Department of Chemistry, Nagaland University, Lumami
Name of the Department and School	Department of Chemistry, School of Sciences
Date of submission	15-12-2022
Date of plagiarism check	15-12-2022
Percentage of similarity detected by the URKUND software	1 %

I hereby declare that/certify that the Ph.D. thesis submitted by me is complete in all respect as per guidelines of Nagaland University (NU) for this purpose. I also certify that the Thesis (soft copy) has been checked for plagiarism using URKUND similarity checked software. It is also certified that the contents of the electronic version of the thesis are the same as the final hardcopy of the thesis. Copy of the report generated by the URKUND software is also enclosed.

Place: Lumami,

Juliana
(JULIANA SANCHU)

Date: 19/12/2022

(Name & Signature of the Scholar)

Indira Devi
Prof. M. Indira Devi
Name & Signature of the Supervisor

LIST OF PUBLICATIONS

1. **Juliana Sanchu**, Mhasirikho Ziekhru, Zevivonu Thakro and M. Indira Devi, “4f-4f Transition Spectra of the Interaction of Pr(III) with L-Valine in Solution: Kinetics and Thermodynamic Studies”, Asian Journal of Chemistry, 34(10):2688-2696 (2022).
 2. **Juliana Sanchu**, Chubazenba Imsong, Zevivonu Thakro, Mhasirikho Ziekhru and M. Indira Devi, “Absorption spectral study for the interaction of Pr(III) with L-Aspartic acid in various aquated organic solvents through 4f-4f transition spectra: Analysis of reaction pathways and thermodynamic parameters”, Journal of Pharmaceutical Negative Results, Volume 13(S01) (2022).
 3. **Juliana Sanchu**, Zevivonu Thakro, Chubazenba Imsong and M.I. Devi, “Computation of spectral parameters for the complexation of Pr(III) with L-Histidine through 4f-4f transition spectra: Further analysis of its kinetic and thermodynamic parameters”, Chemical Physics Impact, Volume 5 100127 (2022).
 4. **Juliana Sanchu** and M. Indira Devi, “Kinetic Studies of the Interaction of Pr(III) with some amino acids in Aqueous Medium using pH meter: Evaluation of Pre-exponential Factor and Activation Energy”, International Journal of Scientific Research in Science and Technology, 9(4):583-591 (2022).
 5. Mhasirikho Ziekhru, **Juliana Sanchu**, Zevivonu Thakro, Chubazenba Imsong and M. Indira Devi, “Computational study of multimetal complexation of Nd(III) with GSH and Mg(II) in solution at different pH through 4f-4f transition spectra”, Chemical Physics Impact, Volume 5 100090 (2022).
 6. Zevivonu Thakro, **Juliana Sanchu**, Chubazenba Imsong and M. Indira Devi, “Complexation of Pr³⁺ with L-methionine in the presence/absence of Mg²⁺ : Their reaction dynamics and thermodynamic properties”, Chemical Physics Impact, Volume 4 100078 (2022).
 7. N. Bendangsenla, T. Moainla, **Juliana Sanchu** and M. Indira Devi, “Computation of Energy, Intensity and Thermodynamic Parameters for the Interaction of Ln(III) with Nucleic Acid: Analysis of Structural Conformations, Chemical Kinetics and Thermodynamic Behaviour through 4f-4f Transition Spectra as Probe”, Journal of Materials Science and Chemical Engineering 06(07):169-183 (2018).
-

-
8. Mhasirikho Ziekhri, Zevivonu Thakro, Chubazenba Imsong, **Juliana Sanchu** and M. Indira Devi, “Computation of energy interaction and intensity parameters for the complexation of Pr(III) with glutathione at different pH in the presence/absence of Mg²⁺: 4f-4f transition spectra as a probe”, *Polyhedron* 200:115099 (2021).
 9. Zevivonu Thakro, T. Moainla, Chubazenba Imsong, **Juliana Sanchu**, Mhasirikho Ziekhri and M. Indira Devi, “Absorption spectral and thermodynamic analysis for the complexation of Pr³⁺ with L-phenylalanine in the presence/absence of Mg²⁺ using 4f–4f transitions spectra as probe”, *European Physical Journal Plus* 137(5):608 (2022).
 10. Chubazenba Imsong, Mhasirikho Ziekhri, Zevivonu Thakro, **Juliana Sanchu** and M. Indira Devi, “Theoretical study of the heterometal complexation of Pr(III) with L-isoleucine in the presence/absence of Mg(II) in solution: 4f-4f transition spectra as probe”, *Chemical Physics Impact*, 5 (2022).

BOOK CHAPTER PUBLISHED

1. **Juliana Sanchu**, Yenwang Konyak and M. Indira Devi, “Analysis of Physio-chemical Properties and the Microbial Contamination of Water in Lumami, Zunheboto – Nagaland”, *SCIENG Publications*; Volume III, ISBN: 978-81-955557-8-9; 17(2022).
-

CONFERENCES/SEMINARS/WORKSHOPS PRESENTED/ATTENDED

1. **Poster presented** at National Seminar on “*Chemistry in Interdisciplinary Research-2017*” (NSCIR-2017), Nagaland University, Lumami.
 2. **Poster presented** at Conference on Recent Advances in Nano Science and Technology (RANST-2017) organized by Institute of Nano Science and Technology, Mohali, Punjab [December 19th – 21st, 2017].
 3. **Paper presented** at *National Seminar on Chemistry in Interdisciplinary Research*, Department of Chemistry, Nagaland University, Lumami, 9-10 November 2018.
 4. **Paper presented** at International E-Conference on Sustainable and Futuristic Materials (SFM-2021) organized by International Research Centre and Department of Chemistry, Kalasalingam Academy of Research and Education, Krishnankoil, Department of Chemistry, J.M. Patel Arts, Commerce and Science College, Bhandara & Department of Chemistry, Kamla Nehru Mahavidyalaya, Nagpur [29th – 30th November 2020].
- International Conference on Emerging Trends in Nanomaterials and Technology (ICETNMST-2017) organized by Department of Science and Humanities, National Institute of Technology, Dimapur, Nagaland [January 4th – 6th, 2017].
 - National Seminar on Chemistry in Interdisciplinary Research (NSCIR-2017) organized by Department of Chemistry, Nagaland University, Nagaland [March 16th – 17th, 2017].
 - Conference on Recent Advances in Nano Science and Technology (RANST-2017) organized by Institute of Nano Science and Technology, Mohali, Punjab [December 19th – 21st, 2017].
 - Workshop on Advanced Techniques in Nano Science and Technology organized by Institute of Nano Science and Technology, Mohali, Punjab [December 13th – 16th, 2017].
-

-
- Participant in Short term course on “*Analytical Techniques for Physical, Chemical & Bioinspired Materials*”, National Institute of Technology, Chumukedima, Nagaland [July 23^t – 27th, 2018].
 - National Seminar on Chemistry in Interdisciplinary Research (NSCIR-2018) organized by Department of Chemistry, Nagaland University, Nagaland [November 9th – 10th, 2018].
 - One-day Workshop on “Importance of IPR in Academic Institutions” organized by IPR Cell, Nagaland University, Nagaland [May 29th, 2019].
 - National Webinar on Opportunities in Chemical Sciences post Covid-19 Scenario organized by Department of Chemistry of Smt. G.G.Khadse College, Muktainagar, Dist. – Jalgaon (M.H.) [June 26th, 2020]
 - National Webinar on Scintillating Chemistry (SC-2020) organized by ACT, Homi Bhabha Centre for Science Education (HBCSE), Mumbai [June 28th, 2020].
 - Webinar on Advanced Nanotechnology, Versatile Molecule & Spectroscopy organized by Department of Chemistry, Sikkim Manipal Institute of Technology in Collaboration with Association of Chemistry Teachers (ACT) C/O Homi Bhabha Centre for Science Education, Mumbai [July 3rd & 4th July 2020]
 - International Virtual Conference on Modern Instrumental and Characterization Techniques in Applied Sciences (MICTAS – N2020) organized by MIET Kumaon Haldwani & Department of Chemistry, H.N.B. Govt. P.G. College, Khatima, Uttarakhand in collaboration with USERC DST Dehradun & Department of Chemistry, R.H. Govt. P.G. College, Kashipur, Uttarkhand [July 5th-6th, 2020]
 - International E-Conference on Sustainable and Futuristic Materials (SFM-2021) organized by International Research Centre and Department of Chemistry, Kalasalingam Academy of Research and Education, Krishnankoil, Department of Chemistry, J.M. Patel Arts, Commerce and Science College, Bhandara & Department of Chemistry, Kamla Nehru Mahavidyalaya, Nagpur [29th – 30th November 2020].
 - International Webcon on Recent Advances in Chemistry Education and Chemical Research (IWRACECR – 2020) organized by Association of Chemistry Teachers C% Homi Bhabha Centre of Science Education (TIFR) Mumbai and Department of Chemistry, MLSM College, Darbhanga, Bihar, India [November 29th, 30th & December 01, 2020].
-

-
- International Webinar on Innovations in Science & Technology (IWIST-2021) organized by Department of Chemistry, Smt. Narsamma Arts, Commerce and Science College, Kiran Nagar, Amravati and Association of Chemistry Teachers, Mumbai [February 27th 2021].
 - TEQIP – III sponsored Five days online workshop on “Recent Advances in Organic and Biomolecular Chemistry 2021”, (RAOBC – 21) organized by the Department of Chemistry, NIT Sikkim [March 22nd – 26th, 2021].
 - Two-day Workshop on “Quality Enhancement in Research” organized by IQAC, Nagaland University, Nagaland [March 22nd – 23rd, 2021].
 - International E-Conference on Recent Trends on Advanced Materials & Environment (RTAME -2020) organized by the Department of Chemistry, IQAC and Research & Development Cell [August 5th, 2022].
-